Multimodal magnetic resonance investigation of childhood metabolic neurodegenerative disease

by

JAMES EDWARD DAVISON

A thesis submitted to the University of Birmingham
for the degree of DOCTOR OF PHILOSOPHY

School of Clinical and Experimental Medicine
College of Medical and Dental Sciences
University of Birmingham
April 2012

Abstract

Background: The central nervous system is frequently affected in children with inherited metabolic disorders (IMD). The causes of the brain insult are incompletely understood, and novel methods are required for disease diagnosis and monitoring response to novel therapies.

Aims & Methods: The study aimed to improve understanding of the pathogenesis of IMD-related neurodegeneration, and to identify potential disease biomarkers in specific IMD, by directly investigating alterations in brain tissue metabolite profiles using non-invasive *in vivo* magnetic resonance spectroscopy (MRS) in conjunction with conventional MRI brain scans.

Results: MRI/MRS studies were performed on over 300 children. Normal brain metabolite profiles were established from a standard comparator cohort. A detailed quality analysis enabled combination of data from different scanner systems. Non-standard brain metabolites were detected in 2.3% of children. Metabolite-based methods of disease progression monitoring were evaluated in Hunter Syndrome. Mechanisms leading to strokes in patients with propionic acidaemia and to learning difficulties and epilepsy in argininosuccinic aciduria were explored using brain tissue metabolite profiling.

Conclusions: Non-invasive *in vivo* brain tissue metabolite profiling is achievable using quantitative magnetic resonance spectroscopy in the routine clinical paediatric setting, and has utility in disease diagnostics, in monitoring disease progression and in investigating disease pathogenesis.

Dedication

For my wife Joy,

without whose steadfast love and support this would not have been possible;

and for my sons Samuel and Timothy,

who have brought so much happiness and of whom I am very proud.

Soli Deo gloria

Declaration

I confirm that this thesis and the work described therein are my own.

The following aspects of the study were undertaken as part of collaboration:

1. The standardised magnetic resonance spectroscopy protocol for inherited metabolic disorder patients was originally devised by Dr Andrew Peet and Dr Paul Gissen.
2. MRI and MRS investigations were acquired from patients in the Radiology Department at Birmingham Children's Hospital. MRS data transfer and processing was performed by the Peet Brain Tumour Research Group.
3. Dr Martin Wilson developed and provided programming scripts used in the analysis of *in vitro* NMR experiments as described in Chapter 3.
4. Dr Nigel Davies and Dr Eleni Orphanidou contributed to the development of Matlab programming scripts used in the analysis of *in vivo* MRS experiments.
5. Dr Nigel Davies, Sim Gill and Dr Jan Novak assisted with the test solution clinical scanner spectroscopy experiments described in Chapter 5.
6. All clinical biochemical assays were performed by the clinical biochemistry department at the Birmingham Children's Hospital.
7. Qualitative reporting of magnetic resonance imaging was performed by Consultant Radiology staff at the Birmingham Children's Hospital, in particular Dr Lesley Macpherson and Dr Katharine Foster.
8. The photomicrographs of the muscle biopsy histology examination described in Chapter 5 were provided by Dr Marie-Anne Brundler.
9. The Mitochondrial Research Group at the Newcastle University (Prof R Taylor) undertook the assay of mitochondrial respiratory chain complexes and associated succinate dehydrogenase gene studies described in Chapter 5.

Acknowledgements

I would like to thank my research supervisors Dr Paul Gissen and Dr Andrew C Peet for their tireless support, advice and encouragement throughout the time of this study. (Andrew also provided a steady supply of ground *Coffea arabica*).

The members of the Peet Brain Tumour Research Group have provided computing and laboratory technical support as well as entertainment and copious biscuits along the way; thanks in particular to Martin Wilson, Nigel Davies, Rachel Grazier, Xiaoyan Pan, Eleni Orphanidou, Yu Sun, Sim Gill, and Jan Novak.

The work described relied on the Radiology Department at the Birmingham Children's Hospital. I am grateful in particular to Dr Lesley Macpherson and Dr Katharine Foster who have been generous with their time and expertise. I also wish to record thanks to the radiographers who have undertaken the MRS studies described.

The Inherited Metabolic Diseases Unit at Birmingham Children's Hospital provided the clinical base for the research, and I am grateful to the clinical staff on the team including Evangeline Wassmer, Chris Hendriksz, Anupam Chakrapani, Saikat Santra, Suresh Vijay, Louise Simmons and Catherine Stewart. From the clinical laboratories, Tim Hutchin, Alison Armitage, Sarah Ball, Ian Surplice and Mary Anne Preece have all offered advice and technical support and contributed to discussions relating to this research.

At the Henry Wellcome Building for NMR Spectroscopy I would like to thank in particular Sara Whittaker, Sue Rhodes and Christian Ludwig for helping me learn the theory, and the ropes, of NMR spectroscopy.

I am also especially grateful to those who have provided the funding that has made possible this project and the clinical research training that I have received. Thanks therefore to the Birmingham Children's Hospital Charities Research Foundation for the Springboard Fellowship; to the BCH IMD Department for the Bridging Clinical Fellowship, and to Sparks: The Children's Medical Research Charity for the Clinical Research Training Fellowship.

Table of Contents

List of Figures

List of tables

Abbreviations

ADC	Apparent diffusion coefficient
AGAT	L-arginine:glycine amidinotransferase
AGC1	Aspartate-glutamate carrier isoform 1
Ala	Alanine
ANOVA	Analysis of variance
ASA	Argininosuccinic aciduria
ASL	Argininosuccinate lyase
Asp	Aspartate
ASPA	Aspartoacylase
ASS	Argininosuccinate synthase
ATP	Adenosine triphosphate
a.u.	Arbitrary units
BCAA	Branch chain amino acid
BCH	Birmingham Children's Hospital
BPSU	British Paediatric Surveillance Unit
CEST	Chemical exchange saturation transfer
CHESS	Chemical shift selective pulse sequence
CNS	Central nervous system
CPS	Carbamoyl phosphate synthase
Cr	Creatine (total Creatine + phosphocreatine)
CSF	Cerebrospinal fluid
CT	Computed tomography
CVVH	Continuous veno-venous haemofiltration
DAG	1,2-diacylglycerol
DTI	Diffusion tensor imaging
DWI	Diffusion weighted imaging
ECC	Eddy current correction
ERT	Enzyme replacement therapy
FAD	Flavin adenine dinucleotide

FID	Free induction decay
FWHM	Full width at half maximum
GABA	Gamma-amino butyric acid
GAG	Glycosaminoglycans
GALNS	N-acetylgalactosamine 6 sulfatase
GAMT	Guanidinoacetate methyltransferase
Gln	Glutamine
Gln+Glu	Total glutamine+glutamate
Glu	Glutamate
GPC	Glycerophosphocholine
Gua	Guanidinoacetate
HOS	Hunter Outcome Survey
I2S	Iduronate-2-sulfatase
IMD	Inherited metabolic disease
Ins	Myo-inositol
IP_3	Inositol trisphosphate
ISIS	Image selected in vivo spectroscopy
Lac	Lactate
Lip	Lipid
LSD	Lysosomal storage disease
MM	Macromolecule
MPS	Mucopolysaccharidosis
MR	Magnetic resonance
MRI	Magnetic resonance imaging
MRS	Magnetic resonance spectroscopy
NAA	N-acetylaspartate
NAAG	N-acetylaspartyl glutamate
NAD	Nicotinamide adenine dinucleotide
NMDA	*N*-methyl D-aspartic acid
NMR	Nuclear magnetic resonance
NO	Nitric oxide
NOS	Nitric oxide synthase

OTC	Ornithine transcarbamoylase
PA	Propionic acidaemia
PACS	Picture archiving and communication system
PCA	Principal component analysis
PCC	Propionyl CoA carboxylase
PCh	Phosphocholine
PCr	Phosphocreatine
PET	Positron emission tomography
PIND	Progressive Intellectual and Neurological Deterioration
PKU	Phenylketonuria
ppm	parts per million
PRESS	Point resolved spectroscopy sequence
PVS	Perivascular spaces
RF	Radiofrequency
ROC	Receiver operator characteristic
ROI	Region of interest
Scy	Scyllo-inositol
SNR	Signal to noise ratio
STEAM	Stimulated echo acquisition mode
Tau	Taurine
tCho	Total cholines
TE	Echo time
tNAA	Total N-acetylaspartate and N-acetylaspartyl glutamate
TSP	3-(trimethylsilyl)propionic-2,2,3,3-d_4 acid sodium salt
UCD	Urea cycle disorder
vCJD	Variant Creutzfeldt-Jakob Disease

Chapter One

1. An Introduction to Childhood Metabolic Neurodegenerative Disease

The developing and maturing brain is vulnerable to damage from a wide range of causes and this damage frequently manifests as developmental delay. Where there is an ongoing active process causing injury to the brain, there can be progressive loss of developmental skills, i.e. developmental regression. Developmental delay is a common paediatric clinical problem, affecting up to 3-5% of the UK paediatric population [1]. In a substantial number of these children there is a genetic or inherited basis for the disease causing the brain insult, including the inherited metabolic disorders [2]. Children with inherited metabolic disorders are vulnerable to chronic brain degeneration, developmental delay/regression, epilepsy and also sudden acute episodes of brain damage including strokes. Understanding of the mechanisms underlying the processes causing brain damage in the metabolic diseases is far from complete, and in a substantial number of children with presumed metabolic neurodegenerative disease no specific diagnosis is reached. Although clinically invaluable, current neuroimaging techniques are limited to detecting visible structural changes in the brain late in the disease process, and are inadequate for diagnosing and monitoring these conditions. In this work a novel functional imaging technique for probing brain metabolism directly is investigated.

In this chapter a brief introduction is given to the inherited metabolic disorders, with a particular focus on their direct and secondary effects on the central nervous system. Potential methods for investigating brain pathological processes are outlined, and functional neuroimaging techniques are introduced. The aims and objectives of this thesis are then described.

1.1. Inherited metabolic disorders

The inherited metabolic disorders (IMD) are a heterogeneous group of monogenic diseases caused by defects in diverse metabolic pathways. Sir Archibald Garrod is widely held as the father of the study of metabolic disorders, describing in a lecture to the Royal College of Physicians in 1908 several diseases that

> *"...apparently result from failure of some step or other in the series of chemical changes which constitute metabolism"* [3].

Each step of a metabolic pathway is facilitated by an enzyme, a protein capable of catalysing a specific chemical conversion [4]. In general terms, a single defective or deficient enzyme step in a pathway results in disease by one of several mechanisms: accumulation of a proximal metabolite that is in someway deleterious (e.g. phenylalanine in phenylketonuria; dermatan and heparan sulfates in Hunter Syndrome); deficiency of a required product of the pathway (e.g. adenosine triphosphate (ATP) in mitochondrial respiratory chain defects); accumulation of an alternative and toxic metabolite (e.g. galactitol in galactosaemia; methylcitrate in propionic acidaemia); or various secondary metabolic effects (e.g.

hyperammonaemia in methylmalonic and propionic acidaemia due to secondary urea cycle inhibition) [3].

IMDs variably affect all organ systems and many result in multi-organ system dysfunction, commonly including hepatic, endocrine, renal, cardiac, muscular or neurologic systems. Involvement of the central nervous system (CNS) can be particularly devastating and is a feature of many IMD [5], either in isolation or conjunction with other organ system involvement, and either as an acute or chronic process. The "neurologic syndrome" is a common mode of initial presentation of the IMDs, often in the neonatal period but potentially at any stage during childhood or even adult life [5].

Although individually rare, inherited metabolic disorders together constitute an important disease group. One recent retrospective study in the West Midlands found an overall birth prevalence of 1 in 784 live births [6], generating by extrapolation around 800 new cases annually in the United Kingdom. The expanding newborn screening programme is testament to the clinical importance of these disorders [7].

1.1.1. Classification of inherited metabolic diseases

In clinical practice, a classification system of the numerous IMD based on clinical presenting features assists in the recognition and diagnosis of these disorders. A taxonomy based on pathophysiological characteristics is useful, however, in providing an overview of the wide range of metabolic pathways that may be affected by an IMD. One such pathophysiological classification divides the IMDs into three broad categories: firstly disorders involving

metabolic intoxication, secondly disorders of energy metabolism, and thirdly disorders of complex molecules [8].

The intoxicating disorders are due to abnormalities of intermediary metabolism, whereby the pathology arises due to accumulation of a metabolite proximal to the metabolic block. Diverse metabolic pathways can be affected, including amino acid metabolism (e.g. tyrosinaemia, phenylketonuria), organic acid catabolism (e.g. propionic acidaemia), the urea cycle (e.g. citrullinaemia), sugar metabolism and neurotransmitter metabolism [3, 8]. Jean-Marie Saudubray highlights some of the key characteristics of this group, including the protection of the foetus *in utero* afforded by placental "dialysis", and the classical symptom-free interval after birth, followed by either an acute or progressive intoxication phenotype [8].

The disorders of energy metabolism manifest signs and symptoms due to failure in energy production or utilisation, with prominent features seen in the organs and tissues with high metabolic energy demands such as cardiac and skeletal muscle and brain. These may be subdivided into mitochondrial disorders including the congenital lactic acidaemias due to pyruvate metabolism or Krebs cycle defects, disorders of the electron transport chain, disorders of fatty acid oxidation or ketone body metabolism, and defects of cytoplasmic energy production including disorders of glycolysis, glycogen metabolism and creatine metabolism [8].

The third category of IMD, i.e. those involving complex molecules, arise due to the disrupted synthesis or catabolism of complex molecules, often due to dysfunction in the various subcellular organelles including the endoplasmic reticulum and lysosomal system [9]. This

group includes the diverse lysosomal storage disorders (e.g. the mucopolysaccharidoses, neuronal ceroid lipofuscinoses and sphingolipidoses), disorders of peroxisomal function, and other disorders of intracellular trafficking. These disorders usually present with chronic insidious symptoms rather than an acute or fluctuating phenotype.

1.2. The neurology of inherited metabolic disease

As already noted, the CNS is frequently affected in IMDs, and neurologic features are found in IMDs from each of the three pathophysiological categories described [3]. The nature of the CNS involvement, however, covers a wide spectrum from acute encephalopathy and acute stroke or stroke-like episodes to a chronic neurodegenerative phenotype (chronic encephalopathy). Encephalopathy is a clinical description of global brain dysfunction, and may be an acute phenomenon such as that seen due to hyperammonaemia in the urea cycle defects, or a chronic process as seen in many of the lysosomal storage disorders.

The differential diagnosis for a child presenting with an acute encephalopathy includes trauma, CNS infection, and exogenous intoxication, as well as metabolic causes. Metabolic causes of acute encephalopathy include secondary features of diabetic ketoacidosis or multiorgan dysfunction, as well as the specific IMDs. Such acute CNS dysfunction is a feature of the metabolic crises seen in many IMDs, resulting from intoxication with accumulating metabolites including ammonia, and organic or amino acids.

Stroke and stroke-like phenomena are seen in many IMDs, including Fabry disease. Acute basal ganglia infarction or dysfunction is seen in the organic acidaemias, in particular

propionic acidaemia [10] and glutaric aciduria [11] as well as in the mitochondrial disorders [12].

Chronic encephalopathy is a feature of many IMDs that result in neurodegeneration, i.e. the progressive structural and/or functional loss of CNS neuronal and glial cells. The clinical hallmarks of neurodegenerative disorders include developmental delay and regression, namely the failure to acquire, or loss of previously acquired, developmental milestones or skills. The clinical features depend on which brain areas are predominantly affected. Disorders predominantly affecting gray matter (poliodystrophies) manifest with seizures, psychomotor retardation and progressive dementia, and impairment of the special senses notably visual dysfunction. Clarke notes that the cognitive impairment seen in many IMDs is often global, i.e. affecting all domains of development, and is frequently associated with severe irritability or aggressiveness as seen, for example in Krabbe or Sanfilippo disease [3]. Disorders predominantly affecting white matter (leukoencephalopathies) manifest with mainly motor features, e.g. progressive spastic paraparesis, and other extra-pyramidal signs [13].

In addition to the neurodegeneration seen in known IMDs, there is a large cohort of children with neurodegeneration and neurodevelopmental regression in whom a diagnosis of neurometabolic disease is suspected but no formal diagnosis reached despite extensive investigation. The recently reported British Paediatric Surveillance Unit (BPSU) Progressive Intellectual and Neurological Deterioration (PIND) of Childhood Study was established to gather epidemiological data on variant Creutzfeldt-Jakob Disease (vCJD), but concurrently studied all children with progressive deteriorating developmental and neurological function

based on the BPSU monthly surveillance card system [14]. This study identified 1558 children who fulfilled the criteria for progressive intellectual and neurological deterioration; 6 had vCJD, 293 are still being analysed, 1114 had a diagnosis other than vCJD, and 145 remained undiagnosed despite full investigation. Of the 1114 with a formal diagnosis, the commonest disease groups were the leukoencephalopathies, neuronal ceroid lipofuscinoses, mitochondrial diseases, mucopolysaccharidoses and peroxisomal disorders. The undiagnosed cohort represented just fewer than 10% of reported cases in this study. However, the percentage of children with global developmental delay or neurological regression in whom no formal diagnosis is reached may be much higher than this figure suggests [1, 15].

Thus involvement of the central nervous system is a feature of many known IMDs, resulting in debilitating neurological impairment [3, 5, 16]. Reaching a conclusive diagnosis in many children with a suspected neurometabolic disorder presents an ongoing clinical challenge. In many IMDs the pathogenesis of the neurological insult is poorly understood, even when the fundamental biochemical enzymatic defect has been well characterised. Treatment strategies for many IMDs are successful at controlling the metabolic derangement, for example dietary control and supplementation in phenylketonuria (PKU), and yet even in PKU subtle neurologic dysfunction is common [17]. In other disorders current treatment strategies do not prevent or reverse central nervous system damage, for example enzyme replacement therapy in Hunter Syndrome has limited effect on the central nervous system as it does not significantly penetrate the blood-brain barrier [18]. For many disorders such as the mitochondrial cytopathies or leukodystrophies such as Alexander Disease there are no effective treatments. In propionic acidaemia best current practice does not prevent acute

metabolic crises and the associated neurological insult; the propensity for basal ganglia infarction in this and associated disorders is incompletely explained [10, 19].

There are, therefore, a number of current clinical challenges for which novel research is required. These include improving diagnostic methods for clinical investigation of the undiagnosed neurometabolic disorder cohorts, improving the understanding of the pathogenesis and pathophysiology of neurodegeneration in known IMDs, and identifying disease biomarkers that are required in evaluating the effect of novel therapies [20].

Clearly given the diversity of IMDs, and the different metabolic pathways that each affects, such research needs to be specific for each group of disorders. That said, the complex interaction of metabolic pathways means that many disorders have overlapping features, both clinically and biochemically, and insights gained in one disorder may provide valuable insight in to other disorders. Furthermore, insights derived from the study of patients with rare IMDs can aid understanding of the normal role and function of specific metabolic pathways that may have implications in common diseases affecting the wider population.

1.3. Approaches to investigating human brain pathology

Biochemical analysis of body fluids, enzyme assays and genetic analyses provide the cornerstones of diagnosis and disease monitoring of the IMDs. Routine clinical biochemical analyses measure a wide variety of intermediary metabolites, including amino and organic acids, small molecule carbohydrates and lipids. However, alterations in blood or urinary metabolites may not reflect tissue-level metabolism in the brain and provide only indirect and remote information about CNS pathophysiology.

1.3.1. Cerebrospinal fluid analysis

Cerebrospinal fluid (CSF) surrounds the brain and spinal cord, providing mechanical suspension for the central nervous system. CSF is synthesised and secreted by the choroid plexus, prior to circulation and subsequent absorption by the arachnoid granulations. In addition to its mechanical function, "*CSF also has a function in circulating nutrients and chemicals filtered from the blood along with waste management by removing organic acids either by active transport or bulk flow from the extracellular fluid in the brain to the subarachnoid compartment, and ultimately into the venous blood stream and the lymphatic system*" [21]. Analysis of CSF can therefore provide specific insights into pathologic mechanisms affecting brain function, for example quantification of CSF metabolites has a particular role in the evaluation of disorders of monoamine neurotransmitters [22] and in pyridoxal phosphate metabolism [23]. Profiling of the full range of metabolites found within CSF (metabolomics) has been proposed as a means of disease diagnosis and monitoring, either with targeted metabolite evaluation or global profiling of the entire "metabolome" [21].

1.3.2. Brain micro-dialysis

The metabolite profile of CSF is, however, only an indirect reflection of brain tissue metabolites, being an excretory/ secretory product of the choroid plexus. Direct measurement of brain tissue metabolites is possible using microdialysis techniques, a method employed in clinical practice in neurointensive care, for example in the management of traumatic brain injury or acute stroke, and may provide insight into disease mechanisms [24-26]. Similar techniques are employed in experimental animal model work [27]. Due to the invasive nature of the procedure, however, it is only tenable in human patients in the context of disease

requiring intensive care support with invasive intracerebral monitoring, and is not widely used in UK paediatric intensive care practice (B Scholefield, personal communication).

1.3.3. Direct brain tissue analysis

Brain biopsy is a routine part of clinical evaluation of brain tumours, and indeed could also have an important role to play in the diagnosis of neurodegenerative disease, having a diagnostic yield of 48.5% in one series [26]. Material obtained at biopsy can be subjected to numerous analyses, primarily histological, but also including the evaluation of tissue metabolite profiles [28, 29]. Similarly in experimental animal models, brain tissue metabolite profiles are of significant value in investigating disease processes [30]. In the United Kingdom, however, brain biopsy is not a common investigation in the evaluation of paediatric neurodegenerative disease, due to the associated potential risk of morbidity and mortality. *Post mortem* pathological examination can yield useful information about disease processes, but the rate of consent for such examinations is very low, and the rapid *post mortem* changes in tissue metabolites need careful interpretation.

1.3.4. Neuroimaging

Since the discovery of the nuclear magnetic resonance phenomenon and the development of magnetic resonance imaging by Lauterbur, Damadian and Mansfield [31-33], magnetic resonance imaging (MRI) of the CNS *in vivo* has revolutionised the investigation of neurologic disorders. MRI plays a key role in the evaluation of neurologic disease, giving exquisitely detailed images of brain structures by a safe, non-invasive technique. MRI-based diagnostics are now fundamental in many areas of medicine, not least neuro-oncology and neurodegenerative diseases [33, 34]. These methods are invaluable in the diagnostic process

and in monitoring disease progression, and yet they are limited to detecting potentially late and irreversible brain damage. Thus MRI-visible abnormalities may reflect relatively late, often irreversible, structural CNS damage.

1.3.5. Functional Imaging Techniques

Functional imaging techniques go beyond the macroscopic appearance to probe tissue metabolism, blood supply, and micro-architecture [34, 35]. Magnetic resonance based functional imaging techniques include magnetic resonance spectroscopy (MRS), diffusion weighted and diffusion tensor imaging (DWI, DTI). MRS provides data on a range of tissue metabolites, while DWI/DTI detects alterations in water diffusivity magnitude and directionality giving insight in to alterations in tissue micro-architecture not detectable with conventional MRI.

These techniques have the potential to augment current clinical and research approaches to IMD-related neurodegeneration, and their use has been reported in a number of IMDs. The ability to profile *in vivo* brain tissue metabolites using MRS is particularly attractive in the study of the IMDs, where abnormalities and alterations at the metabolite level are present.

MRS and DWI/DTI can be readily obtained using standard clinical magnetic resonance (MR) scanner hardware. Standard MR scanner software includes the facility for these modalities. They do not require administration of additional contrast agents, and as with all MR-based modalities do not expose the subject to ionising radiation. It is therefore feasible to incorporate these modalities of investigation in to routine clinical investigations, the only

requirement being the additional scan time to complete the studies (approximately 15 minutes for MRS).

1.4. Aims and objectives

The long-term clinical aim of this work is to contribute to improved clinical outcome for children affected by neurodegeneration in the context of inherited metabolic disorders.

1.4.1. Aims

The aims of the project were to employ multimodal magnetic resonance imaging, particularly *in vivo* magnetic resonance spectroscopy-based brain metabolite profiling, in order to:

(a) Identify potential novel biomarkers of disease with utility in disease diagnosis and in monitoring of disease progression and response to therapy, and

(b) Improve the understanding of the pathogenesis of neurological damage in specific inherited metabolic disorders.

1.4.2. Objectives

The objectives of the project designed to achieve these aims were:

(a) To establish methods for analysing *in vivo* MR spectroscopy data for neurometabolic patients and evaluate the reliability of data acquired in a standard clinical paediatric setting.

(b) To investigate regional and age-dependent variation in standard brain metabolite profiles, and to establish normal baseline brain metabolite profile datasets to provide utilisable background comparator data for subsequent analysis of specific disease cohorts and individual cases.

(c) To investigate the occurrence of non-standard brain metabolites that may have specific diagnostic value.

(d) To combine information from *in vivo* MR spectroscopy with other MR imaging modalities including conventional anatomical imaging and diffusion-based imaging, and with clinical parameters including biochemical and neurocognitive data.

(e) To apply the methodologies developed to the investigation of specific disease cohorts.

Chapter Two of the thesis provides an introduction to the theory and implementation of magnetic resonance spectroscopy including a discussion of the metabolites detected in brain using this method. The thesis then presents methods and data relating to each of the objectives outlined above. Chapter Three gives details of the general methods developed and Chapter Four describes the evaluation of the data quality, and addresses the development of standard baseline brain metabolite profiles. Chapter Five presents data on the identification of non-standard brain metabolites.

Chapters Six to Eight give examples of how the methodologies have been applied to the study of cohorts of children with three specific IMDs: firstly (Chapter Six) a disorder of complex molecule metabolism (mucopolysaccharidosis type II, Hunter Syndrome) where boys affected have an aggressive neurodegenerative disease for which the evaluation of novel therapies requires the identification of novel disease biomarkers; secondly (Chapter Seven) a disorder of amino acid catabolism (propionic acidaemia) where patients have a high rate of strokes affecting the basal ganglia; and thirdly (Chapter Eight) a disorder of the urea cycle (argininosuccinic aciduria) which has unique neurological manifestations.

Chapter Two

2. An Introduction to Magnetic Resonance Spectroscopy

Magnetic resonance imaging and spectroscopy are based on the nuclear magnetic resonance phenomenon. This section provides a brief introduction to nuclear magnetic resonance theory, and how it is applied to achieve *in vivo* MR imaging and detection of metabolites by spectroscopy.

2.1. Overview of the Nuclear Magnetic Resonance Phenomenon

The MR-based functional imaging modalities are all based upon the phenomenon of nuclear magnetic resonance (NMR), discovered in the 1940s, whereby certain nuclei when placed in a strong magnetic field resonate at radio-frequencies that are characteristic for that nucleus (the Larmor frequency) [36]. The Larmor frequency depends on the strength of the external magnetic field and an intrinsic property of the nucleus, the gyromagnetic ratio. The decay rate of the signal detected from a sample depends on the relaxation time constants T_1 and T_2.

Conventional MR imaging is concerned with detection of this signal predominantly from hydrogen nuclei in water molecules (which constitutes some 70% of body weight) with imaging contrast being detected by localised variation in the tissue relaxation time constants. The use of additional magnetic field gradients is required to allow spatial localisation of the signal detected, i.e. in order to obtain spatial information required for reconstruction of images across two (or three) dimensions. These additional magnetic field gradients alter the

Larmor frequency of water molecules depending on their spatial position in the field thereby allowing spatial encoding.

Magnetic resonance spectroscopy is based on the dispersion of chemical shifts. The local chemical environment of a proton will alter the magnetic field that the nucleus experiences. This leads to a small change in the Larmor frequency for that nucleus, thus the signals from protons in different molecules (and hence different local chemical environments) can be differentiated, allowing detection of different metabolites. Different metabolites appear as distinct metabolite peaks on the MR spectrum that is generated. The chemical shift is reported in units of parts per million (ppm), and for a typical *in vivo* proton spectrum ranges from 0.5 ppm to 9.0 ppm. Water itself resonates at around 4.65ppm. The downfield region (5 to 9.0ppm) includes peaks from aromatic compounds such as phenylalanine, but is not usually included in the standard output from a clinical MRS study as the signal in this region is much weaker compared to the up-field region.

2.2. Nuclear magnetic resonance theory

Protons possess fundamental properties including electric charge ($e=1.6x10^{-19}C$), mass ($m_p=1.67x10^{-27}kg$) and spin ($I=\pm$ ½). A spinning electric charge generates a magnetic field, thus protons possess a magnetic moment. The behaviour of protons placed in a strong external magnetic field (B_0) can be described by both classical or quantum mechanics.

The classical description states that when placed in a strong magnetic field, protons tend to align with the magnetic field. However, the interaction of the magnetic moment of the proton

with the external field causes the proton to precess (circular rotary motion) around the magnetic field (figure 2.1) [37].

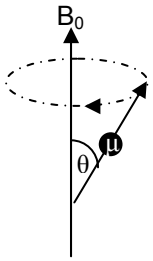

Figure 2.1: Precession of a proton placed in a strong magnetic field. θ is the angle between the spinning magnetic moment (μ) and the external magnetic field (B_0).

The speed of rotation (precession) is given by the Larmor equation

Equation (1) $\upsilon_0=\gamma B_0/2\pi$

where υ_0 is the Larmor frequency (Hz), γ is the gyromagnetic ratio of the nucleus (2.675×10^8 rad $s^{-1}T^{-1}$ for proton), and B_0 is the external magnetic field strength. The magnetic energy (E) associated with a magnetic moment rotating in the external magnetic field is

Equation (2) $E=-\mu B_0 \cos\theta$

where θ is the angle between the spinning magnetic moment μ and the external magnetic field, giving minimum energy when the magnetic moment is parallel with B_0 (since $\theta = 0^o$, and $\cos 0^o = 1$) and maximum when the magnetic moment is lying antiparallel with B_0 (since $\theta = 180^o$, and $\cos 180^o = -1$) [36].

The quantum model dictates that protons are able to occupy one of two quantum states. In the absence of an external magnetic field these states have equal energy. In an external magnetic field one state is a lower energy state than the other (the lower energy state corresponding to the proton aligned parallel with the magnetic field, and the higher energy state corresponding to the proton aligned antiparallel to the magnetic field), the energy gap proportional to the magnetic field strength B_0. Provision of a quantum of energy in the form of a photon that equals the energy gap ΔE to a proton in the lower energy state will promote it to the higher energy state:

Equation (3) $$\Delta E = h \upsilon_0$$
$$= h\gamma B_0 / 2\pi$$

where h is Planck's constant. Note that in both the classical and quantum descriptions the Larmor frequency υ_0 is proportional to the gyromagnetic ratio and the strength of the external field.

If radiofrequency (RF) energy of the correct frequency is applied to the system, protons can move from the lower energy state to the higher energy state. This frequency is the Larmor frequency as given by both the classical and quantum mechanical models.

A sample, be it a test tube of serum or *in vivo* brain, contains many more than one proton. The net (macroscopic) magnetisation is the *"resultant of the sum over all the individual magnetic moments"* [36] in a sample. Using the classical description, and assuming that all the spins lie at the same point in space, the distribution of the many spins can be depicted by adjoining two

cones with the upper cone representing the protons lying in the lower energy (α) parallel state and the lower cone representing protons lying in the higher energy (β) antiparallel state, all precessing (rotating) around the external magnetic field B_0 (figure 2.2).

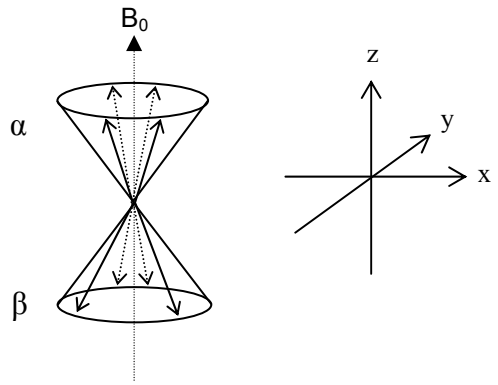

Figure 2.2: Protons lying in external magnetic field B_0. (α – lower energy parallel state, β – higher energy antiparallel state).

The net magnetisation is the net effect of all the magnetic moments and is represented by a single vector **M**. Consider first the component of **M** in the horizontal x-y plane at equilibrium ($\mathbf{M_{xy}}$): the individual magnetic moments are randomly distributed around the cones, and thus the horizontal components cancel out and at equilibrium there is no horizontal component to **M**. The net magnetisation is therefore proportional to the difference between the number of spins in the low energy state (upper cone) and the high energy state (lower cone). This population ratio is given by the Boltzmann distribution:

Equation (4) $$(n_\beta - n_\alpha)/(n_\beta + n_\alpha) = \tanh (\hbar\gamma B_0/2kT)$$

where n_α is the number of protons in the low energy state, n_β is the number of protons in the high energy state, ħ is the reduced Planck constant, γ is the gyromagnetic ratio, B_0 the applied magnetic field, k is the Boltzmann constant ($1.38\text{x}10^{-23}\text{JK}^{-1}$), and T is the absolute

temperature. For B_0=1 T and at room temperature (T=300K), the population ratio between the two states is equivalent to a few parts per million. Although only a small difference, this equilibrium magnetisation $\mathbf{M}_0$ is detected by the NMR experiment.

However, to detect $\mathbf{M}_0$ it must be rotated onto the transverse x-y plane, which is achieved by using a second magnetic field (B_1 field) applied to the sample perpendicular to the main B_0 external field. This is accomplished using a radiofrequency pulse at the resonance frequency of the proton. This results firstly in an equal distribution of spins in the α and β states by providing quanta of energy that promote protons from the low energy α state to the higher energy β state and secondly phase coherence of the spins, i.e. all the spins are at the same "position" on the cone (i.e. they precess in phase), with the net effect that the net magnetisation then lies in the transverse plane, with $\mathbf{M}_0$ precessing around the z-axis (figure 2.3) [36].

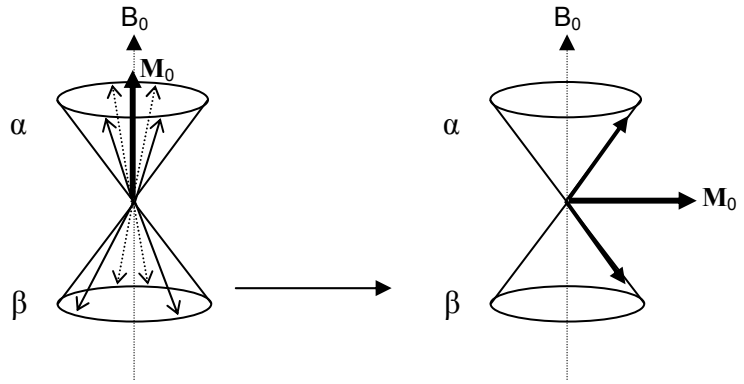

Figure 2.3: Net magnetisation M_0 at equilibrium (left) and after application of perpendicular B_1 field (right).

After the B_1 pulse is switched off the net magnetisation will precess (rotate) in the transverse plane generating an oscillating signal in the receiver coil. However the excited protons will gradually return to their equilibrium state and as they do so the emitted radiofrequency signal

decays. This is detected as the “free induction decay” or FID, and is the basis of the signal detected by the NMR experiment and consequently by MRS and MR imaging.

Fourier Transform of the FID converts the signal from the time domain to the frequency domain, i.e. from a plot of signal intensity against time to a plot of signal intensity against frequency, resulting in a peak for each resonance frequency of nuclei in the sample (figure 2.4).

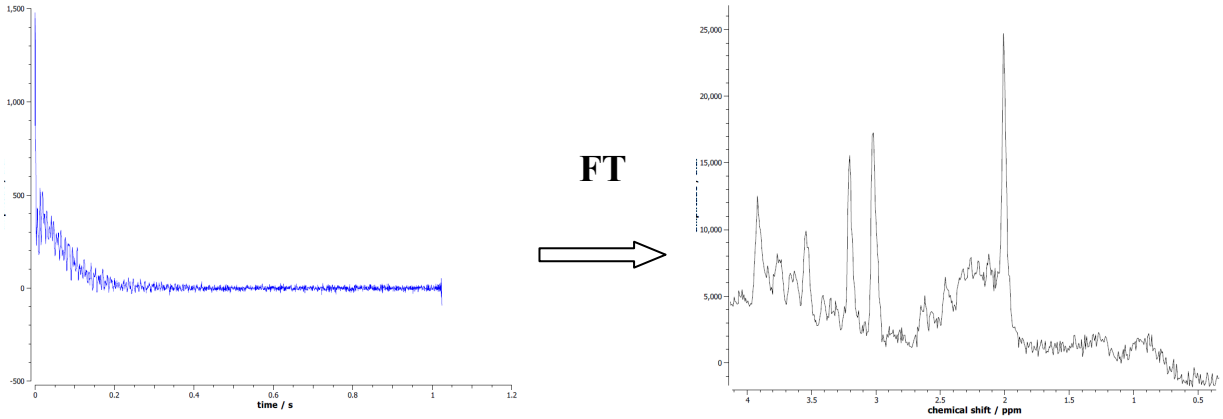

Time domain free induction decay
(x-axis: time (s))

Frequency domain spectrum
(x-axis: chemical shift (ppm))

Figure 2.4: Plots of time domain free induction decay (left) and frequency domain spectrum (right) after Fourier Transform (FT)

The return to the equilibrium ($\mathbf{M}_0$) state following perturbation by the B_1 radiofrequency pulse is described by the relaxation constants T_1 and T_2. T_1 (longitudinal or spin-lattice) relaxation is caused by loss of energy from proton spins to the “lattice” or bulk structure of the sample, and depends on both B_0 and the properties of the tissue. T_2 (transverse or spin-spin) relaxation is caused by interactions between adjacent spins, resulting in loss of phase coherence of spins.

Equation (5) $\mathbf{M}_z = \mathbf{M}_0[1-\exp(-t/T_1)]$

Equation (6) $\mathbf{M}_{xy} = \mathbf{M}_0 \exp(-t/T_2)$

where $\mathbf{M}_z$ is the component of the net vector **M** on the z-axis and $\mathbf{M}_{xy}$ the component of the net vector **M** on the x-y plane. It can be seen from equations (5) and (6) that $\mathbf{M}_{xy}$ decays exponentially with time while $\mathbf{M}_z$ increases back to $\mathbf{M}_0$ (figure 2.5).

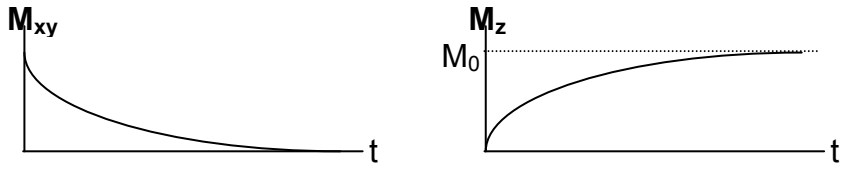

Figure 2.5: Plots of M_{xy} and M_z components of net magnetisation against time showing exponential decay and increase.

T_2 is constant with varying B_0 and is characteristic of the sample. Differences in relaxation constants between different tissues and between normal and diseased tissues generate the image contrast seen in MRI.

2.3. Magnetic resonance spectroscopy

2.3.1. Chemical Shift Phenomenon

Thus far the description has considered only a standard proton experiencing a uniform external magnetic field B_0. Hence MR imaging relies on the signal from protons in water molecules. However, protons in different chemical (molecular) environments will experience a slightly different applied magnetic field, since the surrounding electron cloud of its chemical environment will generate a small local magnetic field that will either augment or subtract

from the main B_0 field. Protons in different molecules will therefore experience different local field alterations:

Equation (7) $B_{local}=B_0(1-\sigma)$

where σ is the shielding effect of local electrons. From the Larmor equation (1) ($\upsilon_0=\gamma B_0/2\pi$), varying the actual magnetic field experienced by the proton will alter the Larmor frequency υ_0 of that proton, altering the signal detected by the NMR experiment. This is known as the chemical shift effect, and is the basis for NMR spectroscopy [37]. The FID will contain information about the different proton resonances within the sample, and Fourier Transform of the FID will generate a spectrum of signal intensity against frequency. Peaks at different frequencies correspond to protons in different chemical environments, i.e. different molecules.

The chemical shift is reported in parts per million, where

Equation (8) $\upsilon_{act} = (1.0 + \delta \times 10^{-6})/ \upsilon_0$

and thus

Equation (9) $\delta = [(\upsilon_{act}/ \upsilon_0)-1] \times 10^6]$

where υ_{act} is the actual Larmor frequency of the proton in its unique chemical environment, and δ is the chemical shift.

By convention spectra are plotted with the chemical shift (x) axis inverted, so that a typical brain MRS spectrum has 4ppm on the left running to 0ppm on the right. Different chemicals will therefore produce peaks at characteristic positions on the spectrum allowing their identification, while the amplitude of the signal relates to the relative concentration of the metabolite.

2.3.2. J-coupling

While chemical shift describes the effect of chemical bonds (electron clouds) on the local magnetic field experienced by a nucleus, J-coupling describes the effect of other close nuclei (i.e. 3 or less bonds away) on the experienced magnetic field [37]. Consider one proton H_a: another nearby proton nucleus H_b may be aligned in either the α or β state, and will consequently either augment or subtract from the magnetic field experienced by the H_a. As approximately 50% of the nuclei will be in each of the two states, the resonant frequency of H_a will be split in to two (nearby) peaks, separated by the coupling constant J (in Hz). This phenomenon is seen in *in vivo* brain MRS where lactate is seen as a "doublet" at around 1.3ppm[38].

In molecules where there is more than one near proton the resultant splitting patterns are more complicated as there are increasing possible combinations of parallel/anti parallel alignment of the spins, with the number of peaks and intensity ratios given by Pascal's triangle (figure 2.6).

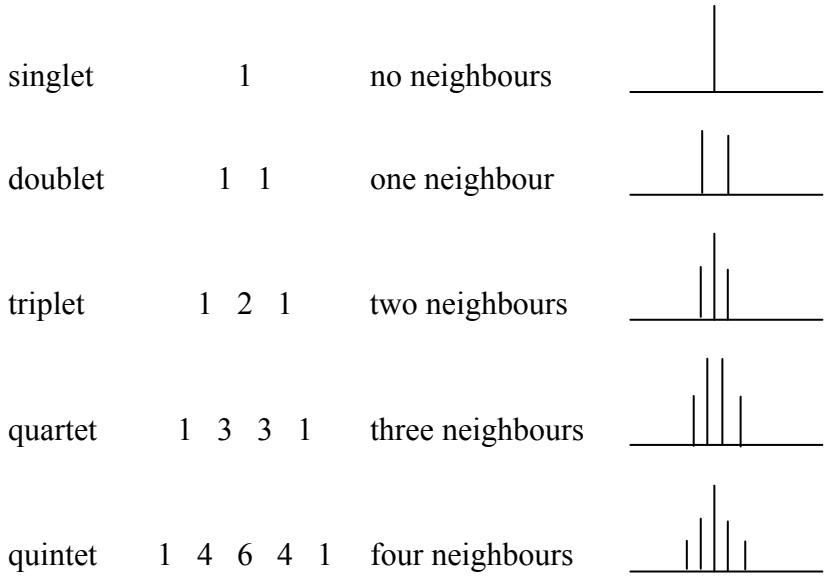

Figure 2.6: J-coupling: effect of increasing numbers of near protons. (Adapted from figure 1.5, [37])

2.4. *In vivo* spectroscopy considerations

The same NMR phenomenon provides the basis for both *in vitro* NMR and *in vivo* MRS. *In vivo* MRS however has additional requirements and challenges, notably the need to select signal from a volume of interest only (and not for example the whole brain), the need to suppress the overwhelming signal from water that is the main constituent of most tissues, and to optimise detection of the relatively low concentration metabolite signal

2.4.1. Volume selection

There are a number of techniques available for volume selection, including Point Resolved Spectroscopy (PRESS) [39], Stimulated Echo Acquisition Mode (STEAM) [40] and Image Selected In Vivo Spectroscopy (ISIS) [41]. PRESS is the technique in clinical use at the Birmingham Children's Hospital and will be briefly described.

In order to detect signal from a volume of interest, pulse sequences are used in conjunction with magnetic field gradients to selectively excite only protons within the volume of interest.

Thus when the signal is obtained it will originate only from molecules within the volume of interest.

Application of a linear magnetic gradient will alter the Larmor frequencies of protons relative to their position along x (figure 2.7). Application of a pulse with a narrow range of υ_0 frequencies will therefore only excite protons in the spatial position corresponding to the frequencies of the RF pulse. Application of slice selection gradients in each plane x, y, and z will generate a signal only from the cuboid volume of interest (i.e. the intersection of 3 excited "slabs").

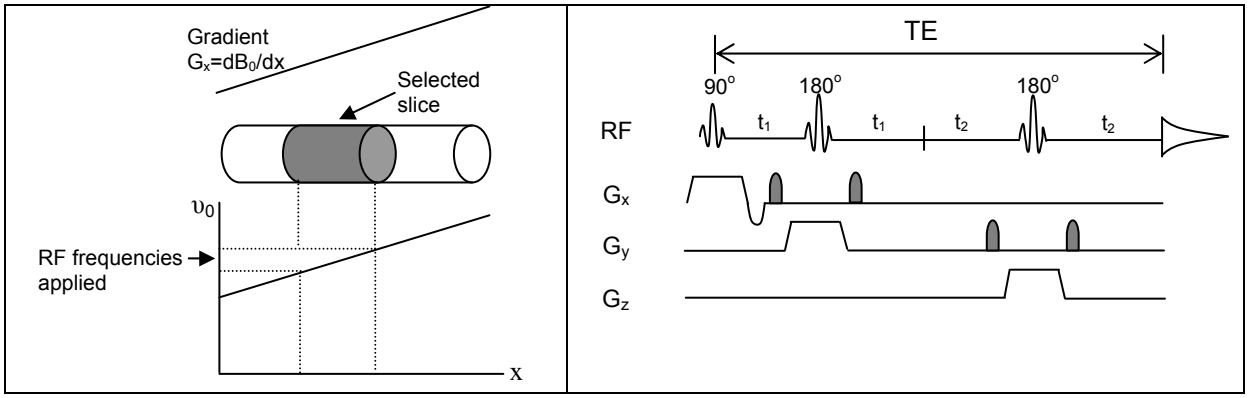

Figure 2.7: Simplified PRESS pulse sequence. Three slice-selective gradients applied during sequence on each axis G_{x-z}. Initial 90° soft pulse places $\mathbf{M}_0$ onto transverse plane. The two 180° pulses refocus the spins, the first generating a spin-echo at $2t_1$. The second 180° pulse refocuses to generate a second spin-echo at $2t_2$. The two 180° pulses also aid in the slice-selection. Two pairs of crusher gradients (shaded) in orthogonal directions around 180° pulses assist selection of coherences. The final signal is detected at a time $2(t_1+t_2)$ (the echo time, TE). (Adapted from figure 6.13, [36].)

Variation of the echo time (TE) generates different spectra, due to the differing relaxation constants of each metabolite. A greater number of metabolites are seen at short echo time (e.g. 30ms), whereas at longer echo time (e.g. 135ms) certain metabolites, notably lipids and

macromolecules, are no longer seen in the spectrum, as the signal from these metabolites has already diminished to zero during the echo time, due to short relaxation time constants.

2.4.2. Water suppression

Since metabolites of interest in brain are usually present in millimolar concentration, and water is around 50-100M, methods to suppress the water signal are required. Methods such as the Chemical Shift Selective (CHESS) pulse sequence selectively excite water molecules by use of a narrow band radiofrequency pulse, and then apply a "spoiler" gradient to dephase the excited spins. This water suppression is required both to aid the identification of very small metabolite peaks adjacent to the very much larger water peak, and also to enable optimal detection of these peaks by avoiding swamping of the analogue to digital converter by the very large water signal.

Due to the relative insensitivity of the NMR experiment, further exacerbated by *in vivo* low concentrations of metabolites of interest compared to the concentration of water, the signal to noise ratio (SNR) is low for MRS compared to MRI. Subsequently to improve the SNR multiple repeated acquisitions are required and summed together, thereby allowing peak signal to summate while random baseline noise will cancel out. Typically for *in vivo* acquisition 128 repetitions are acquired for each voxel of interest.

2.5. Spectral post-processing and metabolite quantification

The FID acquired by the clinical MR scanner can be displayed as a basic spectrum after Fourier Transform, a functionality available on clinical MR systems. This unprocessed spectrum is useful for immediate clinical review by the radiologist. Some systems also

provide a basic metabolite identification and fitting algorithm, such as that on the Siemens system (figure 2.8).

For detailed analysis, metabolite fitting and quantification, however, further offline processing is undertaken. This section gives a generic overview of the techniques involved in post-processing, and introduces the standard software used in the current study.

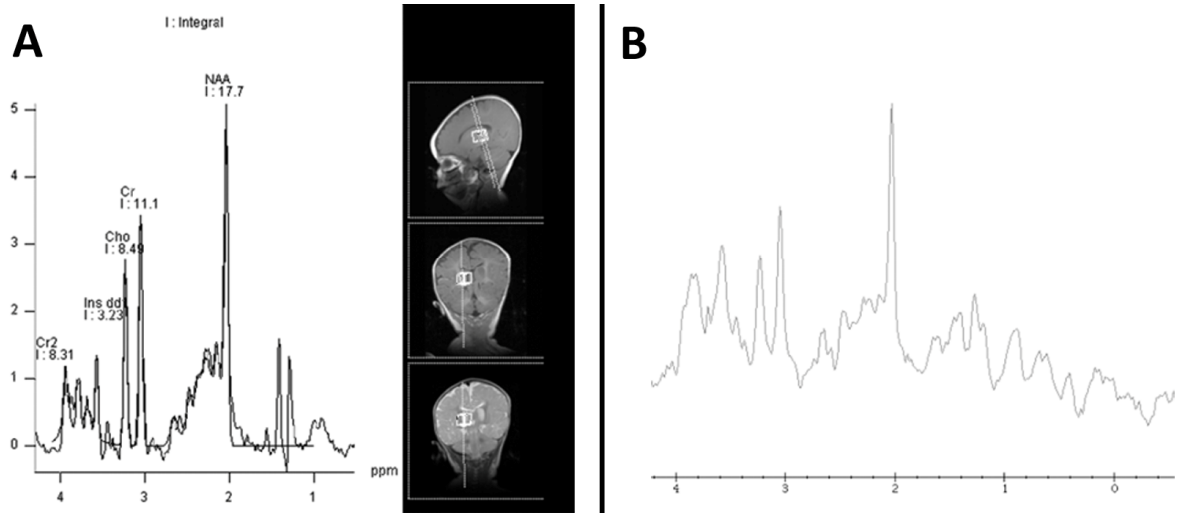

Figure 2.8: Example MR scanner unprocessed spectrum output. (A) Output from Siemens system including 3-plane images for voxel localisation. (B) Output from GE system.

2.5.1. Post-processing

The quality and appearance of the spectrum from the measured signal can be enhanced by a variety of post-processing techniques that aim to overcome some of the specific problems inherent in *in vivo* spectroscopy. While these techniques can improve the accuracy of metabolite quantification there is a risk of altering the FID parameters such that the accuracy is in fact decreased [42].

The post-processing steps described here are carried out automatically by many processing software programmes, including LCModel™ which is the software used here. However an understanding of these steps is required in the appraisal of spectral quality and of factors that may impinge on the reliability of metabolite quantification.

2.5.1.1. Eddy current correction

Eddy currents are currents induced within the MR scanner system components by the numerous rapidly switching magnetic field gradients applied during signal acquisition. Since a flowing electric current generates a magnetic field, eddy currents generate additional varying magnetic fields within the system. These result in time-dependent phase shifts within the FID and subsequent lineshape distortions in the post-Fourier transform spectrum, which restrict the accuracy of metabolite quantification.

Eddy current correction (ECC) techniques overcome this by use of a reference FID acquired without water suppression. When the water signal is not suppressed, and assuming that the reference frequency Ω is set to the water frequency, the FID acquired will not have any components caused by the chemical shift of water since it is on resonance and the signal from the much lower concentration metabolites is negligible. Any phase evolution seen in this water unsuppressed FID/spectrum will therefore be due to the presence of eddy currents. This phase evolution data can then be used to correct the water suppressed (metabolite) FID. This makes the assumption that the two FIDs are acquired from exactly the same location, and with no change in the acquisition parameters except that water suppression is switched off, and only a single acquisition repetition is required for the water unsuppressed FID. It has also been noted for many newer MR scanners that have active gradient shielding that eddy current distortions are a less frequent problem [42].

2.5.1.2. Zero filling

The signal detected by the receiver coil is sampled at a finite number of time points by an analogue-digital converter. If the time interval is too great between sampled points the definition of peaks in the spectrum may be inadequate resulting in inaccurate metabolite fitting. Zero filling can improve the digital resolution of a spectrum by appending zeros to the end of the FID in the time domain and thereby allowing interpolation of the spectral signal. This can improve the digital resolution of the spectrum, allowing more accurate signal analysis as well as better visual presentation [42].

2.5.1.3. Phase Correction

The lineshapes of metabolite peaks in the spectrum may be distorted due to phase changes, including first order changes arising from the time delay in FID acquisition. To overcome this a phase correction must be applied, either manually or automatically, by observing the effect of altering the phase factor θ to restore the peak to an absorptive shape [42]. The phase factor is made up of two components, the zero order phase θ_0 which is independent of the frequency and the first order phase θ_1 which varies with frequency, and phase correction techniques have to account for both of these with zero and first order corrections.

2.5.1.4. Baseline correction

It is commonly observed that the peaks in a spectrum do not arise from a zero intensity baseline. A baseline that deviates significantly from a zero intensity flat line can arise due to the presence of signal from macromolecules and lipids with short T_2* values, and also due to hardware factors. (T_2* refers to decay of transverse magnetisation due to spin-spin interactions and inhomogeneities in the magnetic field). Baseline correction concerns the

removal of this baseline. The inclusion of macromolecular and lipid signal parameters in metabolite fitting models significantly improves the modelling of the baseline [42].

2.5.2. Spectral fitting algorithms

Having acquired the FID using optimal parameters and then applied specific post-processing techniques, the next stage in analysis is to identify and quantify the metabolite signals present within the spectrum. While manual identification of peaks is possible by consideration of peak chemical shifts and evident J-couplings, the spectrum acquired from a typical *in vivo* MRS study is complicated by the presence of multiple overlapping resonances and so automated methods of metabolite identification are required.

The approach used here is an example of fitting a linear combination of metabolite spectra, whereby a model is derived composed of a linear combination of the different individual metabolite spectra that together make up the complex total measured spectrum. The library of expected metabolite resonance profiles is referred to as the "basis set". Linear combination modelling algorithms then derive the best fit to the actual spectrum by altering the amplitudes, frequencies, phases and linewidths of the basis set [36].

The software programme employed in the current work is LCModel^{TM}, which has been widely employed in many research settings [43, 44]. The programme automates the post-processing steps discussed above including lineshape, eddy current correction and baseline functions, and zero and first-order phase corrections. It employs a constrained least squares analysis method to provide the best fit from a basis set containing seventeen metabolite and nine macromolecular and lipid spectra. The basis set spectra are adjusted to take account of

additional line spectral broadening and chemical shift referencing errors. The inclusion of the macromolecular and lipid components allows effective derivation of the baseline function.

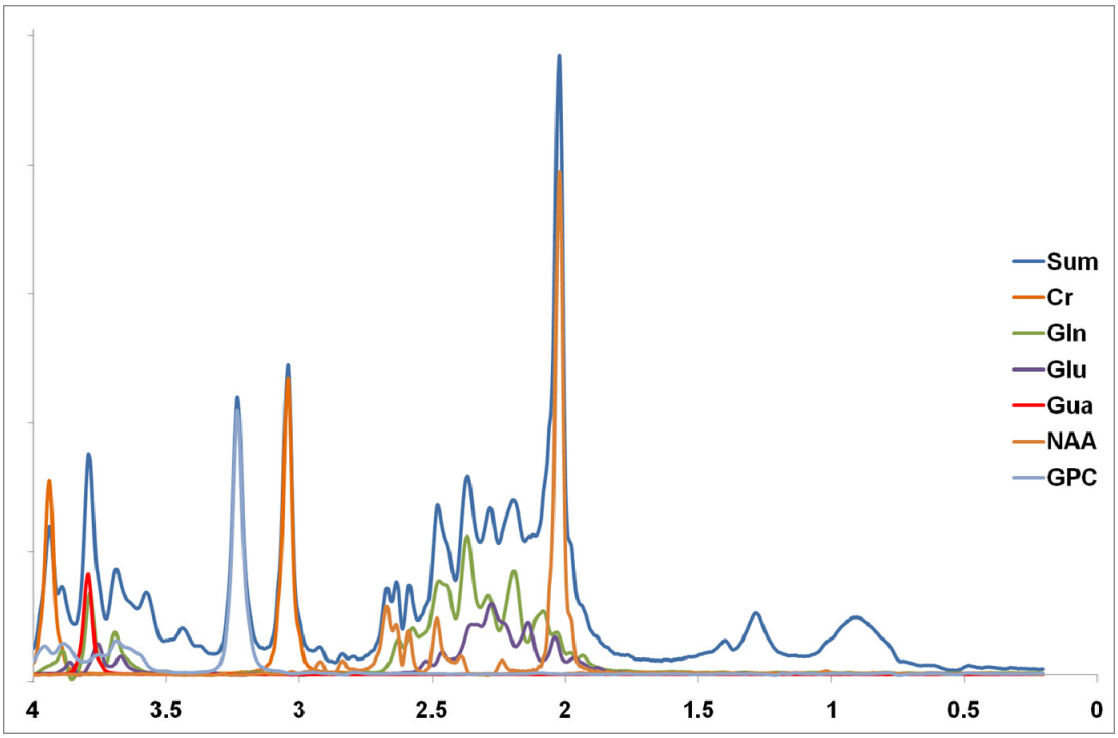

Figure 2.9: Example of linear combination metabolite fitting demonstrating contribution of different individual metabolite spectra to overall fitted combination. Blue line: sum of all metabolites (fitted linear combination). Other lines: individual spectra from different metabolite that sum together to create the fitted combination. (Not all metabolites shown for clarity).

2.5.3. Metabolite quantification

The concentration of each metabolite present in a spectrum is proportional to the peak integral, i.e. the area under the peaks that constitute the individual metabolite spectrum. Relative metabolite concentrations can be established by comparing the area under peaks from different metabolites. It is, however, possible to derive an absolute quantification of the metabolite concentration by normalization to the area of the water peak from the non-water

suppression FID. Thus the acquisition of an additional spectrum without water suppression while keeping all other parameters constant is used to provide a standard reference for calculating metabolite concentrations as well as for eddy current corrections [45].

This method requires an assumption as to the brain water concentration. The default water concentration used by LCModel is 35880mM, based on data from Ernst *et al* [46]. Variation in the water content of different brain tissues would need to be considered to enable direct comparison of metabolite concentrations between regions, and furthermore variation in water concentration in different pathological states could invalidate the assumptions made.

LCModel generates two outputs, one with and one without the application of eddy current correction steps. In addition to values for the estimated metabolite concentration it also generates estimates of the standard deviation of each concentration, expressed in percent of the estimated concentration (the Cramér-Rao lower bounds).

2.6. Scanner hardware elements

A full discussion of the hardware and component design of MR systems is beyond the scope of this thesis, but a brief description of the hardware components of MR system is required particularly to inform analysis of inter-scanner data variability [47]. A typical MR scanning system has several key components: Firstly, a constant magnetic field is generated by a superconducting magnet (the B_0 field). This strong field (typically 1.5 – 3 Tesla) provides the constant magnetic field lying parallel to the bore of the magnet, required to initially align proton magnetic spins. Secondly, gradient coils are required to generate magnetic field gradients required for the localisation of MR signal, and also the generation of diffusion

weighting. Three sets of coils are required, one for each orthogonal axis. Thirdly, radiofrequency transmit and receiver coils are required to generate excitatory radiofrequency pulses and to detect the NMR signal. A body coil is built in to the scanner "doughnut", though body-part specific coils may be used such as a head-coil which fit around the anatomical structure of interest and increase signal to noise ratio. Some such coils are "arrays", i.e. have multiple coil elements. Fourthly a computer control system is required to operate the scanner, and finally the entire system must be enclosed within a Faraday cage to isolate the MR scanner from external RF interference.

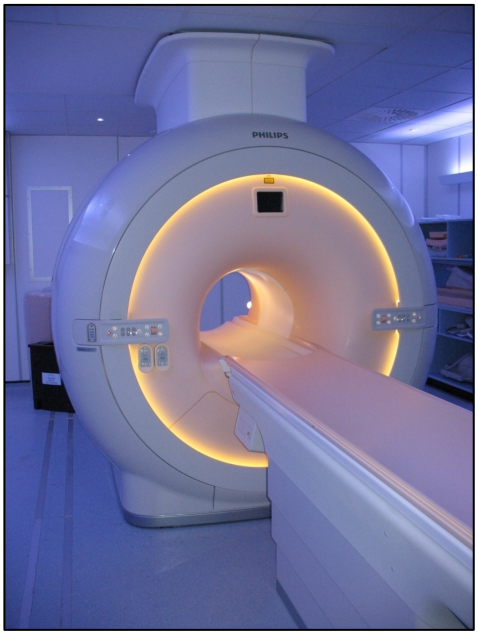

Figure 2.10: Photograph of 3T Magnetic Resonance scanning system (Philips), 3T Magnetic Resonance Suite, Birmingham Children's Hospital.

2.7. An Introduction to the Metabolites Detected by *In Vivo* proton MR Spectroscopy of Brain

The purpose of this section is to provide an introduction to the main metabolites that may be detected in the brain using *in vivo* proton MR spectroscopy. For each metabolite, salient spectroscopic features are mentioned, and the clinical relevance of the metabolite is described. Selected metabolic pathways to which the metabolite contributes are also described, since perturbations in metabolite concentrations detected will have implications for these pathways.

A typical brain MR spectrum (figure 2.11) contains several major prominent metabolite peaks. In general the limit of detection of metabolites by *in vivo* MRS is around 0.5-1mM. Table 2.1 provides specific chemical shift parameters and approximate normal brain concentrations for each metabolite.

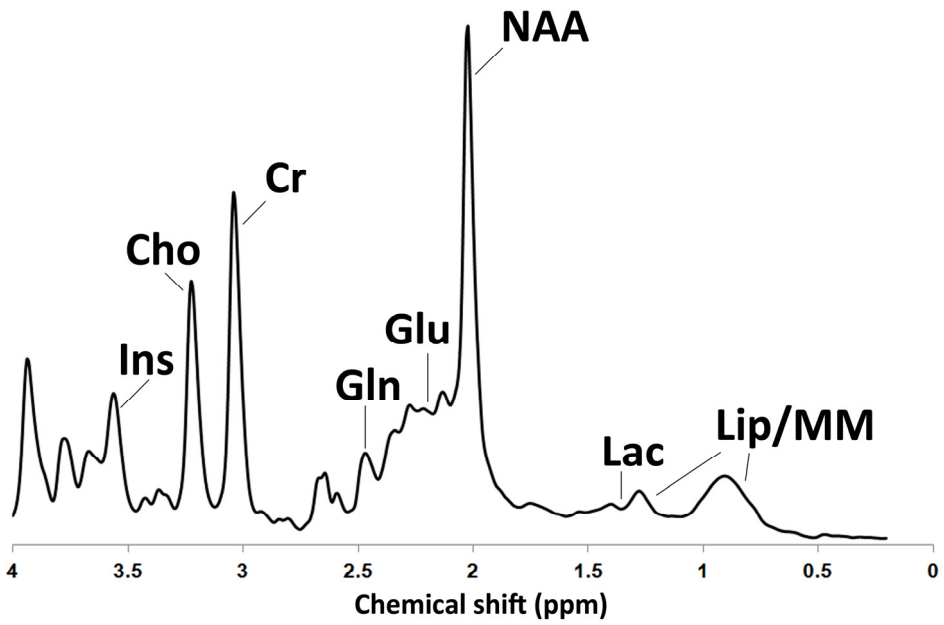

Figure 2.11: Example of *in vivo* brain MR spectrum with major metabolite peaks identified. (Ins, myo-inositol; Cho, choline; Cr, creatine; Gln, glutamine; Glu, glutamate; NAA, *N*-acetylaspartate; Lac, lactate; Lip, lipid; MM, macromolecule.

Metabolite (abbreviation)	Molecular groups	Chemical shift (ppm)	Multiplicity	Human brain mmol/L
N-acetylaspartate (NAA)	Acetyl $^{2}CH_3$	2.008	s	7.5
	Aspartate ^{2}CH	4.382	m	
	$^{3}CH_2$	2.673	dd	
		2.486	dd	
	NH	7.820	d	
N-acetylaspartyl glutamate (NAAG)	Acetyl $^{2}CH_3$	2.042	s	0.5
	Aspartate ^{2}CH	4.607	dd	
	$^{3}CH_2$	2.721	dd	
		2.519	dd	
	Glutamate ^{2}CH	4.128	dd	
	$^{3}CH_2$	1.881	m	
		2.049	m	
	$^{4}CH_2$	2.190	m	
		2.180	m	
Creatine (Cr)	CH_3	3.027	s	4.5
	CH_2	3.913	s	
	NH	6.650	s	
Glycerophosphocholine (GPC)	Glycerol $^{1}CH_2$	3.605	dd	0.5
		3.672	dd	
	^{2}CH	3.903	m	
	$^{3}CH_2$	3.871	m	
		3.946	m	
	Choline $(CH_3)_3$	3.212	s	
	$^{7}CH_2$	4.312	m	
	$^{8}CH_2$	3.659	m	
Phospho(ryl)choline (PCh)	$(CH_3)_3$	3.209	s	0.2
	$^{1}CH_2$	4.282	m	
	$^{2}CH_2$	3.643	m	
Phosphocreatine (PCr)	CH_3	3.029	s	3.0
	$^{2}CH_2$	3.930	s	
	NH	6.58	s	
	NH	7.30	s	
Myo-inositol (Ins)	^{1}CH	3.522	dd	4.0
	^{2}CH	4.054	dd	
	^{3}CH	3.522	dd	
	^{4}CH	3.614	dd	
	^{5}CH	3.269	dd	
	^{6}CH	3.614	dd	

Table 2.1: (See also next page) Chemical shifts and peak multiplicity of metabolites detectable with MR spectroscopy in human brain. (Data from [36]. s, singlet; d, doublet; t, triplet; q, quartet; m, multiplet; dd, double doublet).

Metabolite (abbreviation)	Molecular groups	Chemical shift (ppm)	Multiplicity	Human brain mmol/L
Scyllo-inositol (Scy)	$^{1\text{-}6}CH$	3.340	s	0.2
Glutamine (Gln)	^{2}CH	3.757	dd	3.0
	$^{3}CH_2$	2.135	m	
		2.115		
	$^{4}CH_2$	2.434	m	
		2.456		
Glutamate (Glu)	^{2}CH	3.746	dd	6.0
	$^{3}CH_2$	2.042	m	
		2.120		
	$^{4}CH_2$	2.336	m	
		2.352		
Lactate (Lac)	^{2}CH	4.097	q	0.2
	$^{3}CH_3$	1.313	d	
Alanine (Ala)	^{2}CH	3.775	q	0.1
	$^{3}CH_3$	1.467	d	
Aspartate (Asp)	^{2}CH	3.891	dd	1.0
	$^{3}CH_2$	2.801	dd	
		2.653	dd	
γ-aminobutryic acid (GABA)	$^{2}CH_2$	2.283	t	1.0
	$^{3}CH_2$	1.889	m	
	$^{4}CH_2$	3.012	d	
Taurine (Tau)	$^{1}CH_2$	3.420	dd	2.0
	$^{2}CH_2$	3.246	dd	

Table 2.1: (See also previous page) Chemical shifts and peak multiplicity of metabolites detectable with MR spectroscopy in human brain. (Data from [36]. s, singlet; d, doublet; t, triplet; q, quartet; m, multiplet; dd, double doublet).

2.7.1. N-acetylaspartate (NAA)

The largest peak in a typical brain MR spectrum at 2.01ppm is assigned to N-acetylaspartate (NAA), particularly the methyl group of its acetyl moiety. Subsidiary peaks are seen at 2.49ppm, 2.67ppm and 4.38ppm originating from protons in the CH_2 and CH groups.

NAA is found in very high (~10mM) concentrations in the brain [48]. NAA is mainly though not exclusively located in neuronal cells, axons and dendrites [49], and has been widely used in MRS studies as a marker of neuronal density and viability. However more recent data suggest that NAA is also found in other non-neuronal cell types within the central nervous system, notably within oligodendrocytes [49, 50].

NAA is synthesised within neurons from L-aspartate by the L-aspartate N-acetyltransferase (EC 2.3.1.17, see figure 2.12) [51]. This enzyme is active in both the mitochondrial matrix and within the cytosol, potentially within the endoplasmic reticulum [52]. NAA is transported by transaxonal transfer to oligodendrocytes, where it is catabolised by aspartoacylase (ASPA, EC 3.1.5.15) releasing acetate and L-aspartate. The acetate groups are subsequently utilised in the synthesis of fatty acids and myelin lipids [52], while the L-aspartate enters the Krebs cycle. Thus NAA has a vital role in myelination of the developing brain.

Two IMDs shed light on the function and biochemistry of NAA, Canavan disease and aralar deficiency. Canavan disease (OMIM #271900) is a progressive leucodystrophy due to deficiency of ASPA, the enzyme which catabolises NAA within oligodendrocytes. Patients have significantly elevated concentrations of brain NAA detectable by MRS, and impaired

ability to properly myelinate the CNS [53]. Whether NAA also has a direct toxic effect is a moot point [52].

The mitochondrial malate-aspartate shuttle transports malate, glutamate, aspartate and α-ketoglutarate across the mitochondrial outer membrane [54]. One of the transporters involved is the aspartate-glutamate carrier isoform 1 (aralar, AGC1, encoded by *SLC25A12*), which is the only isoform expressed in the CNS and solely in neurons [54]. In a knockout animal model and human patients with AGC1 deficiency there is widespread lack of CNS myelination, and very low NAA concentrations detected by MRS, indicating that AGC1 plays an important role in providing aspartate for NAA synthesis [54], also supporting the cytosolic localisation of NAA synthesis.

In addition to the important role in providing acetate groups for myelin synthesis, NAA is also the immediate precursor for N-acetyl aspartyl glutamate (NAAG, see below). NAA may also act as an organic osmolyte, and potentially facilitates some aspects of glutamate derived mitochondrial energy production [52].

Alterations in NAA, as detected by MRS, have been reported in a wide range of disorders including ischaemic stroke, epilepsy, and Alzheimer's disease, and monitoring serial variation in NAA suggested as a means to monitor disease progression [52]. Decreased NAA is also seen in a wide range of metabolic brain disorders, and while therefore not disease-specific, is a means to monitor the effect a given disease has on brain neurochemistry [55]. NAA also varies significantly between brain regions and with developmental stage, in particular relating

to the degree of myelination [56], factors which must be taken into account when studying the impact of disease states.

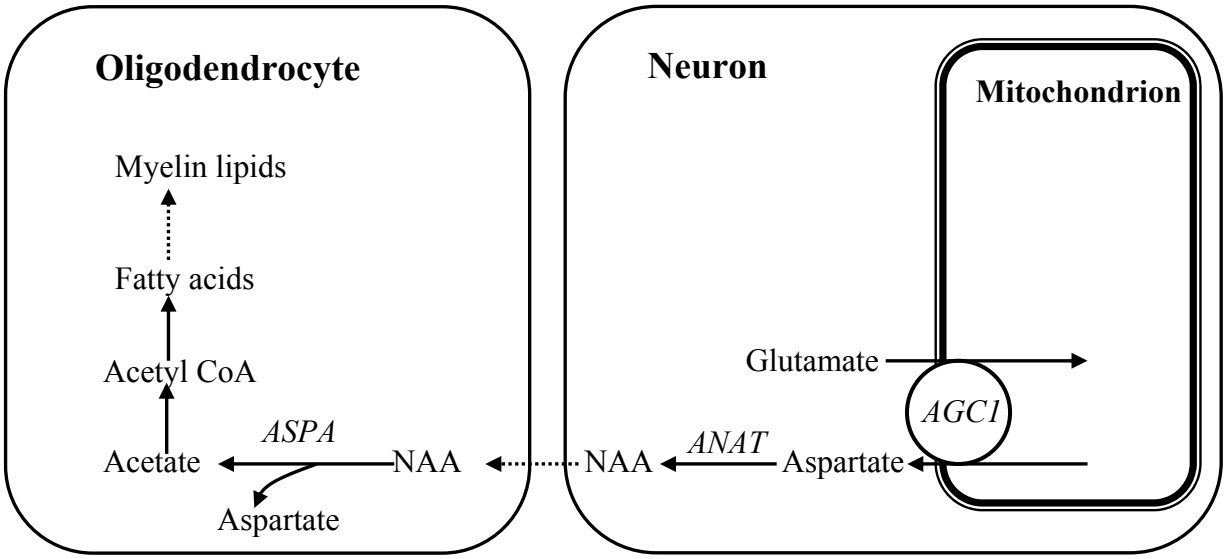

Figure 2.12: Neuronal/oligodendrocytic interactions in the metabolic pathways of *N*-acetylaspartate. ASPA: aspartoacylase; ANAT, aspartate *N*-acetyltransferase; AGC1, aspartate-glutamate carrier isoform 1; NAA, *N*-acetylaspartate. (Adapted from [54]).

2.7.2. N-acetyl aspartyl glutamate (NAAG)

N-acetyl aspartyl glutamate (NAAG) contributes to the peak seen *in vivo* at 2.01ppm from NAA, as its largest resonance is at 2.04ppm. NAAG is reported to be a neuronal glutamate storage pool [56], and may represent up to 20% of the total NAA signal. Differentiation between NAA and NAAG at 1.5 T is not robust, and therefore is usually reported as a value for the total NAA + NAAG (tNAA) as an indicator of the total peak concentration.

NAAG is the most abundant brain neuropeptide [57], synthesised by an incompletely characterised NAAG synthase [58] by the ATP-dependent condensation of glutamate and NAA, primarily within neurons. NAAG is catabolised by various peptidases including glutamate carboxypeptidase II (EC 3.4.17.21), a membrane-bound enzyme found in neurons

and glial cells [59]. NAAG is an active agonist at various receptors including the metabotropic glutamate receptor 3, and is a partial antagonist of the N-methyl D-aspartic acid (NMDA) receptor [59]. It is purported to have a role in neuron to astrocyte signalling [60].

Elevated levels of NAAG have been reported in a number of hypomyelinating disorders, including in the CSF of children with Pelizaeus-Merzbacher like-diseases [60, 61] and free sialic acid storage diseases who also had hypomyelination [59]. Corresponding elevations in the total NAA+NAAG peak has been reported using *in vivo* MRS in these conditions [62].

2.7.3. Creatine and Phosphocreatine

Creatine (Cr) and phosphocreatine (PCr) have resonances at 3.01ppm and 3.9ppm and are not distinguishable at low field strengths *in vivo*, and are reported as total Creatine + phosphocreatine. (In this thesis, Cr represents the total creatine + phosphocreatine concentration).

The creatine-phosphocreatine-creatine kinase system (figure 2.13) plays a central role in maintaining adequate ATP supplies for the high-energy demands of the active brain, particularly in facilitating the transport of high energy compounds from the site of production within the mitochondria to the sites of consumption such as at the synapse [63, 64], thereby providing *"temporal and spatial energy buffering"* [65]. Mitochondrial creatine kinase (mtCK) phosphorylates creatine to phosphocreatine; phosphocreatine thus formed is transported to sites of energy consumption, where cytosolic creatine kinases are coupled to, or associated with, glycolysis, ATP-dependent or ATP-gated processes, ion pumps and other energy consuming processes [65].

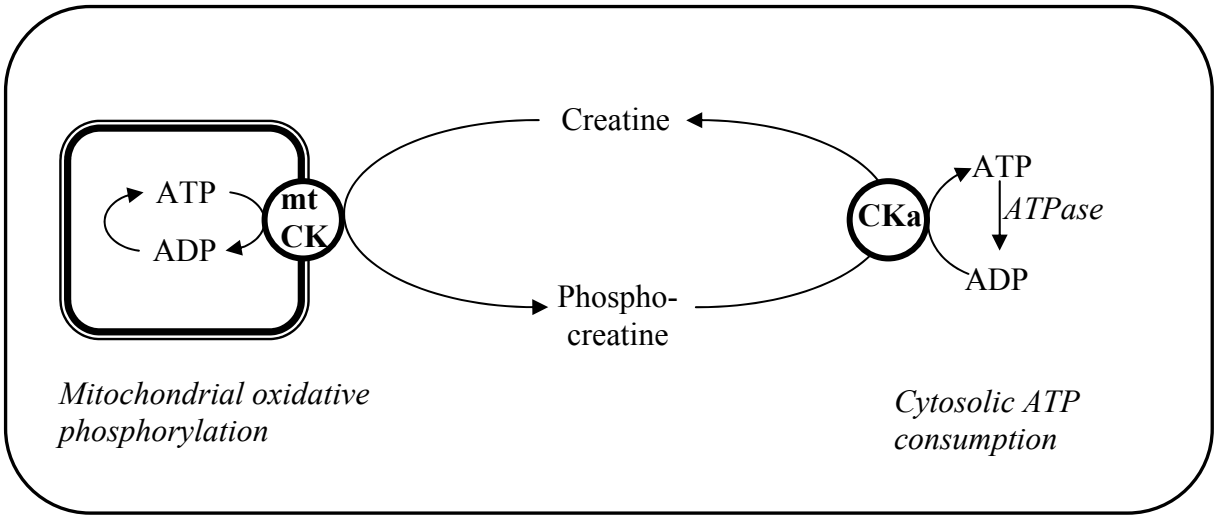

Figure 2.13: The creatine/phosphocreatine/creatine kinase system: high energy phosphate shuttling. mtCK, mitochondrial creatine kinase; CKa, cytosolic creatine kinase associated with ATPase. (Adapted from [65]).

The crucial role of the creatine system in the CNS is highlighted by another group of IMDs, the creatine deficiency syndromes, which again provide "human knockout models" that have helped in the understanding of the physiological roles of the system. These include disorders of creatine synthesis due to deficiencies of the synthetic enzymes L-arginine:glycine amidinotransferase (AGAT; EC 2.1.4.1; OMIM #602360) or guanidinoacetate methyltransferase (GAMT; EC 2.1.1.2; OMIM #601240), and disorders of creatine transport due to deficiency of the creatine transporter SLC6A8 (X-linked; OMIM #300036). Patients have a near-total lack of brain creatine detected by MRS, and have severe developmental delay and usually severe epilepsy [65, 66]. The disorders of synthesis are at least partially treatable by oral creatine supplements, whereas the phenotype of the transporter defect is not ameliorated by oral supplementation as the CNS is unable to import creatine [64].

Studied by *in vivo* MRS, the highest concentrations of Cr are reported in cerebellum, basal ganglia and thalamus, with lower levels in white matter [67], and developmental changes are

limited to the first year of life. Since concentrations were considered to not vary significantly between individuals or with pathology, Cr has been used widely as a denominator for comparing other metabolite ratios. This assumption, however, may not be valid, as Cr may alter in pathology as illustrated by the creatine deficiency syndromes, and elevated Cr has been reported in certain white matter disorders (leukodystrophies) and Sjogren-Larsson syndrome (OMIM #270200) [55].

2.7.4. Choline containing compounds

The prominent peak at 3.2ppm is assigned to the methyl group of glycerophosphocholine (GPC) and phospho(ryl)choline (PCh); free choline contributes only a small amount to this resonance and is individually below the limit of detection by MRS [36]. The sum of these signals is reported as the total choline (tCho) concentration.

These compounds are found in the phospholipid metabolic pathways and variation in the tCho signal is reported as a marker of membrane function. The phospholipids are the major constituents of the cellular bilayer membrane, in particular phosphatidylcholine and phosphatidylethanolamine; phosphocholine is required for the synthesis of phosphatidylcholine and is also generated by its degradation [68]. Choline-phospholipid metabolism requires numerous synthetic enzymes as well as active choline transporters (figure 2.14). Choline is also required in the synthesis of the neurotransmitter acetylcholine, and as a source of methyl groups that feed in to the synthesis of S-adenosylmethionine, which is an important methyl group donor in various transmethylation reactions [69].

Thus increased tCho is reported to reflect membrane disruption or cellular proliferation with alterations seen in various white matter disorders [13] and demyelinating disorders [70]. Alterations in GPC and PCh are important markers in malignant cells, and have been widely investigated in this context both *in vivo* and *in vitro* [68].

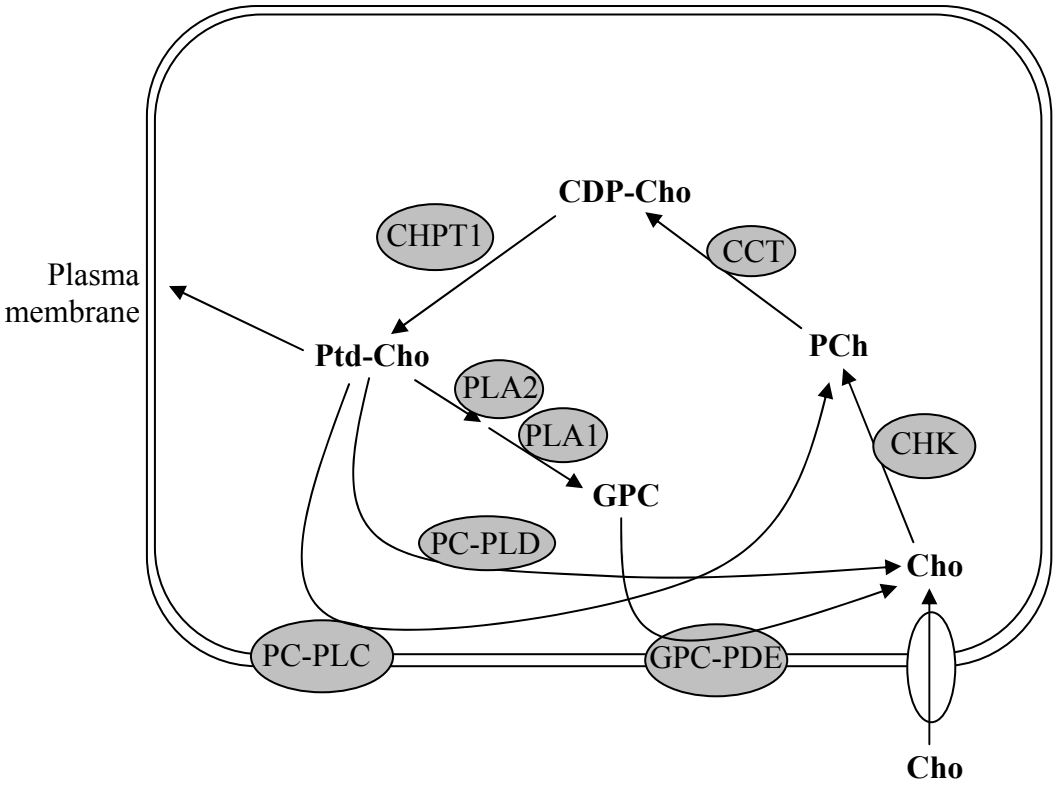

Figure 2.14: Outline metabolic pathways in choline phospholipid metabolism. Metabolites: Cho, choline; PCh, phosphocholine; CDP-Cho, cytidine diphosphate choline; PtdCho, phosphatidylcholine; GPC, glycerophosphocholine. Enzymes: CHK, choline kinase; CCT, cholinecytidyltransferase; CHPT1, diacylglycerol cholinephosphotransferase 1; PLA2, phospholipase A2; PLA1, phospholipase A1; PC-PLD, phosphatidylcholine-specific phospholipase D; PC-PLC, phosphatidylcholine-specific phospholipase C; GPC-PDE, glycerophosphocholine phosphodiesterase.(Adapted from [68]).

2.7.5. Myo-Inositol (Ins) and scyllo-inositol (Scy)

The peak present in the typical brain MR spectrum at around 3.55ppm is assigned to myo-inositol [36]. Myo-inositol is the predominant isoform of the 6-carbon sugar inositol (hexahydroxy-cyclohexane), present at particularly high concentrations within the brain [71].

Myo-inositol is a precursor for the phosphoinositides important in second messenger signal transduction systems. The ubiquitous phosphoinositide second messenger system operates via the conversion by phospholipase C of phosphatidylinositol 4,5-bisphophate to inositol trisphosphate (IP_3) and 1,2-diacylglycerol (DAG), both of which then initiate numerous intracellular cascades [72].

Myo-inositol also has an important role in osmoregulation within the central nervous system [71]. Osmoregulatory homeostatic mechanisms are required to maintain neuronal cell volume; while acute alterations in tonicity are counteracted by the rapid transport of electrolytes including sodium and potassium, chronic alterations are balanced by the shift of "organic osmolytes", principally myo-inositol [71]. The osmoregulatory role of myo-inositol is facilitated by the presence within the CNS of specific transporters including sodium-myo-inositol and hydrogen-myo-inositol transporters [73]. The expression of these is altered by osmotic stress, such that expression is increased by hyperosmolar conditions. Conversely in the context of hypotonic stress, myo-inositol efflux from the cell is mediated via a voltage-sensitive organic osmolyte anion channel [71]. Astrocytes in particular have a central role in CNS osmoregulation, actively altering in volume to maintain and control extracellular fluid osmolarity [74].

Within the MRS literature, myo-inositol is reported to be a "glial marker" as it is predominantly located in glial cells, although as with NAA this is not exclusive, being found in a range of other neuronal cell types [36]. Thus in diseases with prominent glial expansion such as gliosis or tumours of glial origin, the myo-inositol signal is increased [75, 76]. Elevated myo-inositol has been investigated as an early marker of Alzheimer's disease [77].

The physiological role of the isoform scyllo-inositol is not well described and unlike myo-inositol may not be incorporated into inositol-lipids [78]. Elevated scyllo-inositol has been reported in mitochondrial disease, brain tumours and in Alzheimer's disease [77], and scyllo-inositol is a potential therapy in Alzheimer's disease [78]. As scyllo-inositol has molecular symmetry, its protons give rise to an NMR signal at the single resonance of 3.34ppm and thus appears as a singlet peak visible separate from the complex myo-inositol signal [36].

2.7.6. Glutamine and Glutamate (Gln+Glu)

Although the resonances of glutamine (Gln) and glutamate (Glu) overlap significantly in *in vivo* spectra acquired at 1.5 T (table 2.1) there is evidence that they can be distinguished (see Chapter 7). The two amino acids are closely linked in several metabolic pathways, and within brain a glutamine-glutamate cycle operates between neurons and glial cells (figure 2.15). Glutamate is synthesised from glutamine within neurons by glutaminase (EC 3.1.5.2), or from α-ketoglutarate by glutamate dehydrogenase (EC 1.4.1.2). Glutamate is the major excitatory neurotransmitter acting on several fast and metabotropic glutamate receptors [79]. It is released into the synaptic cleft from the pre-synaptic bouton, and subsequently initiates post-synaptic signalling cascades via specific glutamate receptors. Glutamate is cleared from the synapse by rapid uptake into astrocytes which surround the synapse, maintaining the low

glutamate concentration within the synapse required for efficient synaptic signalling. This uptake is mediated by a specific Na^+-glutamate transporter, resulting in an elevated astrocytic intracellular Na^+ concentration which activates astrocytic Na^+/K^+ ATPase resulting in stimulation of glycolysis and hence glucose consumption [80].

Glutamate within astrocytes is converted to glutamine by incorporation of NH_4^+ by ATP-dependent glutamine synthetase (EC 6.3.1.2). This enzyme is found only in astrocytes. The glutamine is then released by astrocytes and transported to neurons, where it can be converted again to glutamate, constituting the "glutamine-glutamate cycle".

Some of the glutamate taken up into astrocytes is converted to α-ketoglutarate by transamination of oxaloacetate or pyruvate with the formation of aspartate or alanine respectively, or via nicotinamide adenine dinucleotide (NAD)-requiring oxidative deamination by glutamate dehydrogenase, with the release of ammonium. The α-ketoglutarate is transported to the neuron, where it can re-enter the Krebs cycle, and is also consumed to generate glutamate. Since α-ketoglutarate is therefore consumed, proximal Krebs cycle metabolites must be replenished; this is achieved in part by pyruvate carboxylase (EC 6.4.1.1) which generates oxaloacetate from pyruvate. Pyruvate carboxylase is predominantly found in astrocytes, indicating the important energy metabolism role played by these glial cells [74].

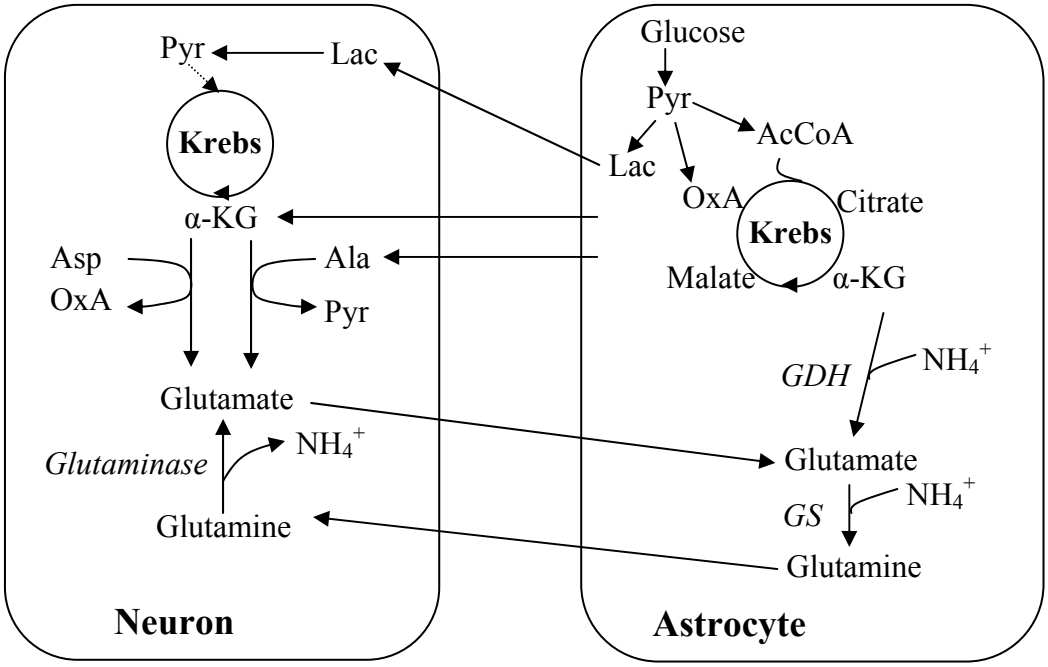

Figure 2.15: Glutamate-glutamine cycle and anaplerotic supply of neuron by astrocytes. Lac, lactate; Pyr, pyruvate; AcCoA, acetyl Coenzyme A; α-KG, α-ketoglutarate; OxA, oxaloacetate; NH_4^+, ammonium; Ala, alanine; asp, aspartate; GDH, glutamate dehydrogenase; GS, glutamine synthase; Krebs, Krebs cycle. (Adapted from [74] and [80].)

2.7.7. Lactate (Lac)

Due to the J-coupling effect lactate appears as a doublet at around 1.31ppm. Acquired at 1.5 T with short echo time (30-35ms) the doublet is upright, but at longer echo times (135-144ms) the doublet is inverted. This is a useful phenomenon facilitating the detection of lactate and differentiation from lipid and macromolecular signals that resonate in the same region.

The brain has high energy requirements, responsible for some 25% of glucose and 20% of oxygen total body utilisation [80]. Glucose is the predominant brain energy substrate, and is also required for biosynthesis of glycolipids, glycoproteins and the major neurotransmitters glutamate, GABA and acetylcholine. The high energy requirement of the brain is due to the numerous energetic mechanisms required for maintaining neuronal membrane potentials and

propagating action potentials, for the action of ionic pumps notably the Na^+/K^+ ATPase, as well as for biosynthetic pathways and axonal transport [80].

Plasma glucose is transported across the blood brain barrier by specific transporters, predominantly GLUT1 (SLC2A1). Inherited deficiency of this transporter results in significant neuroglycopaenia and low CSF glucose concentrations manifest with microcephaly, infantile seizures and developmental delay [81]. GLUT1 is predominantly expressed by astrocytes, the foot-processes of which surround brain capillaries and form the blood brain barrier. Glucose is transported into neurons by the GLUT3 (SLC2A3) [82], found in both axons and dendrites. Thus astrocytes have an important role in regulating the entry of glucose in to the brain.

Furthermore, the supply of energy (glucose) is coupled to the local activity of the brain, such that activated regions receive increased blood flow and glucose uptake. The glial cells, notably astrocytes, play a key role in regulating this coupling, and the astrocytes are also crucial in supplying neuronal energy substrates [80]. Glucose is metabolised by glycolysis in astrocytes with the generation of lactate; lactate is then transported to neurons where it is converted to pyruvate and can enter oxidative phosphorylation with the generation of ATP.

Thus glycolysis is the principal pathway of glucose metabolism; the end product is the synthesis of pyruvate [83]. During glycolysis ATP is generated. In aerobic conditions and in the presence of functional mitochondrial systems, pyruvate is further oxidised and ATP generated via the Krebs cycle and mitochondrial electron transport chain. However in anaerobic situations, or in the absence of mitochondria (such as in erythrocytes), oxidative

phosphorylation does not occur, and there is a shift towards the conversion of pyruvate to lactate by lactate dehydrogenase (EC 1.1.1.27). Thus elevated lactate concentrations are detectable in brain tissue both in hypoxic/ischaemic conditions [84] and in some mitochondrial cytopathies [38, 85]. Indeed there is evidence that a transient rise in tissue lactate is a normal physiological event, for example following the activation of the visual cortex [86].

2.7.8. Other metabolites

A number of other small molecular metabolites may also be detected, including alanine (Ala), aspartate (Asp), gamma-amino butyric acid (GABA), glucose, taurine (Tau), and guanidinoacetate (Gua). Many of these metabolites are usually at or below the limit of detection by MRS, and this together with the complexity of their resonance peaks means that advanced techniques are required to achieve robust identification and quantification. Such spectral editing techniques have been applied to several metabolites including GABA [87].

Some of these metabolites may be robustly quantified when present in elevated concentrations since their NMR resonances do not significantly overlap other metabolites, such as taurine which is detectable in young infants, or alanine in some cases with lactic acidosis.

2.7.9. Macromolecules (MM) and lipids (Lip)

A substantial proportion of the signal detected by *in vivo* MRS is derived from "macromolecular resonances". The macromolecular signal originates from proteins and amino acids and result in broad resonances. These have short T_2 relaxation constants and so are not seen at longer echo time acquisitions [37, 88].

Contributions from CH_3 and CH_2 groups of NMR-visible lipids are also detected, with characteristic peaks at 1.3ppm and 0.9ppm [89, 90], which have significant changes in various brain pathologies including brain tumours [76].

2.7.10. Developmental & Age Variation in Metabolites

It is expected that brain metabolites will vary according to brain development and maturation. This is reflected in the age-related variation in the MRS detectable brain metabolites. This must be taken in to consideration when evaluating MRS alterations seen in pathology, and also generates the requirement for age-specific control groups for different metabolites.

Pouwels *et al* reported metabolite data from MRS studies in 97 children [67]. The most significant period of variation is in the first year of life, with in particular a rapid rise in tNAA seen in the first 6 months of life in most brain regions. In white and gray matter, taurine levels were highest in infancy and then fell, suggesting a specific role in brain development. Within white matter and basal ganglia glutamate and glutamine decreased with age, while Cr and myo-inositol levels were generally stable (figure 2.16).

This data also highlights the regional variation in metabolite concentrations, notably the higher tNAA in gray matter regions (both parietal and deep basal ganglia), where Cr, glutamine and glutamate were also higher than in parietal white matter.

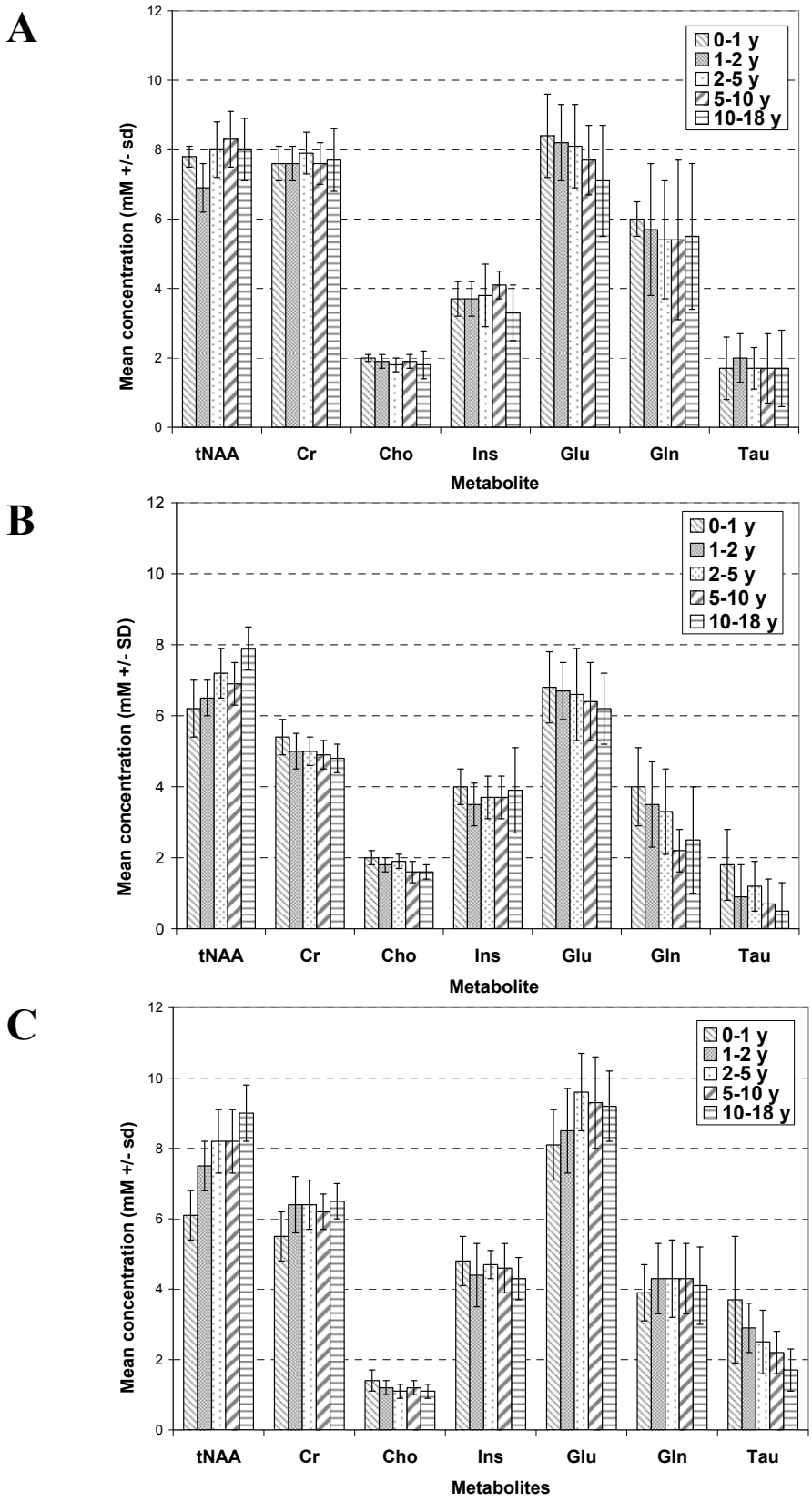

Figure 2.16: Regional and age variation in brain metabolites determined by MR spectroscopy. (A) basal ganglia, (B) parietal white matter, (C) parietal gray matter.(Data from [67]).

2.8. The Use of Magnetic Resonance Spectroscopy in Inherited Metabolic Disorders

MRS has the potential to be a powerful tool in both clinical and research applications in particular with regard to the inherited metabolic diseases [55, 56, 91, 92]. Alterations in MRS-visible brain metabolites reflect both non-specific alterations in cellular function or integrity that could be the common end point of several disease processes, and specific alterations in metabolic pathways that may have direct relevance to inherited disorders of these pathways. However, for most IMDs only case reports or small case series utilising MRS have been reported.

2.8.1. Specific Disease Biomarkers

MRS may provide a specific diagnosis when there is a qualitative alteration in the major metabolite peaks detected, either the absence of an expected peak, or the presence of an unusual peak representing a metabolite not normally seen in brain at levels detectable by MRS. Table 2.2 gives examples of IMDs that have specific qualitative brain metabolite alterations detectable using MRS.

Absence of the expected creatine peak is the preferred method for diagnosing the creatine deficiency syndromes and MRS is also of value in monitoring the response to treatment with supplementary creatine [93].

Sjogren-Larsson syndrome (OMIM #270200) [94-97] may be detected by the presence of a characteristic lipid peak at 1.3ppm, while adenylosuccinate lyase deficiency (OMIM #103050) may be detected by the observation of a peak at 8.28ppm corresponding to succinyladenosine [98]. It should be noted that standard MRS software typically analyses the

region between 0.5 to 4.0ppm only, and does not analyse downfield of the water peak. In theory this is a region that could yield further important diagnostic information.

MRS has been extensively used as a tool in evaluating potential mitochondrial disease, and the presence of detectable levels of lactate used as a marker of possible mitochondrial dysfunction [38, 99] although the sensitivity and specificity of lactate detection may not be high. As noted previously, Canavan disease has a characteristic MRS finding of very high levels of NAA caused by deficiency of the enzyme aspartoacylase [53].

2.8.2. Non-disease specific metabolite alterations

As already noted in most IMDs disease-specific metabolite alterations detectable by MRS do not appear. The limitations to the sensitivity of the technique in detecting low concentration metabolites means that a metabolite must reach significant concentration levels in brain tissue before it could be detected. In many disease states alterations in the standard metabolites detected give a secondary reflection of the brain tissue pathological processes such as demyelination, neuronal loss or ischaemia, and therefore the pattern of alterations may still provide useful information as to the nature of the brain pathology and in known diseases may be a means to monitoring disease progression. MRS has been incorporated in to a few disease/therapy monitoring trials involving IMD, usually monitoring brain NAA levels [100].

Metabolic Disease/ Enzyme deficiency	OMIM #	Metabolite	Ref
Ribose-5-phosphate isomerase deficiency	608611	Arabinitol/ ribitol	[101, 102]
Mitochondrial Complex II deficiency (succinate dehydrogenase deficiency)	252011	Succinic acid	[101]
HMG Co-enzyme A lyase deficiency	246450	Uncertain	[103]
Phenylketonuria (phenylalanine hydroxylase deficiency)	261600	Phenylalanine	[104]
Canavan (aspartoacylase deficiency)	271900	High NAA	[53]
Aralar deficiency (AGC1)	612949	Absent NAA	[54]
Creatine deficiency (GAMT deficiency)	601240	Absent Cr High GAA	[93]
Creatine deficiency (AGAT or SLC6A8 deficiency)	602360 300036	Absent Cr	
Maple syrup urine disease (branch chain ketoacid dehydrogenase deficiency)	248600	Branch chain amino acids	[105]
Sjogren-Larsson (Fatty aldehyde dehydrogenase deficiency)	270200	Fatty alcohol	[94, 96]
Succinic semialdehyde dehydrogenase deficiency	271980	GABA	[106]
3-methylglutaconic aciduria type I	250950	3-hydroxyiso-valeric acid	[107]
Adenylosuccinate lyase (ADSL) deficiency	103050	Succinyl-adenosine	[98]
Non ketotic hyperglycinaemia (glycine cleavage system defect)	605899	Glycine	[101]
Pyruvate dehydrogenase deficiency	312170	Lac & alanine	[55]
Galactosaemia	230400	Elevated galactitol	[55]

Table 2.2: Disease-specific biomarkers of inherited metabolic disorders identified using *in vivo* brain MR spectroscopy

An extensive review of the case series and reports of MRS derived brain metabolite patterns in numerous IMD is available [55]. This review highlights some of the challenges in applying the MRS technique to the study of rare diseases. As well as the paucity of individual patients with a given disease, the case reports of neuroimaging and MRS have often sampled only one time point in the disease process. This coupled with the normal age-dependent alterations in brain metabolite profiles means that often *"we are tracking moving targets"* [55]. When numbers being studied are small, the impact of non-biological causes of data variability becomes more important, such as the discrepancies between different data acquisition protocols and post-processing techniques.

This thesis demonstrates that it is possible to overcome some of these obstacles, with the use of standard acquisition and processing protocols, the combination of data from multiple scanner systems, and with the use of large comparator datasets, and that progress towards "tracking the moving targets" has been made.

Chapter Three

3. General Methods

3.1. Research Ethical Approval

Magnetic resonance spectroscopy was established initially at Birmingham Children's Hospital (BCH) in the context of diagnosis and evaluation of paediatric brain tumours. Approval for this study included extension to facilitate the acquisition of MRS data on children with other neurological disorders. ("A comparison of magnetic resonance spectroscopy and tumour genetics in childhood brain tumours." Dr A Peet, Dr R Grundy. Reference: LREC 5512M[B].)

Subsequently further Research Ethics Committee approval for continuation and extension of the project was obtained. ("Multimodal investigation of childhood metabolic neurodegenerative disease". REC Reference: 09/H1206/112, Birmingham, East, North and Solihull Research Ethics Committee, National Research Ethics Service). This includes provision for the acquisition of *in vivo* functional imaging data (including MRS and DTI) from patients with metabolic and neurological disorders, and also from patients undergoing imaging for other indications as a putative control cohort. The approval also includes obtaining body fluid samples for *in vitro* analysis. MRS and diffusion studies are also undertaken in some children under clinical indications (including investigation of possible mitochondrial disorder or possible creatine deficiency). Consent for access to medical records in these cases was also sought prior to accessing this information.

3.2. *In vivo* Magnetic resonance spectroscopy methods

3.2.1. Standard *in vivo* MRS Acquisition

A standard protocol for MRS acquisitions from non-oncological cases has been employed in this study (table 3.1). Single voxel spectroscopy was performed concurrently with MRI scans by clinical radiographers. Research-based MRS acquisitions were performed after other clinically indicated imaging sequences were completed. General anaesthesia or oral sedative drugs were used to facilitate MRI/MRS as indicated according to the Birmingham Children's Hospital policies.

MR scanner field strength	1.5 Tesla
MR scanners	Siemens Avanto Siemens Symphony Magnetom NUM4 GE Signa Excite & HDx
Voxel dimensions	2x2x2cm ($8cm^3$)
Voxel positions	Left basal ganglia Right parietal white matter
Volume selection method	Point RESolved Spectroscopy (PRESS) sequence
Water suppression	Chemical Shift Selective (CHESS)
Echo time (TE)	30ms & 135ms
Repetition time	1500ms
Number of repetitions	128

Table 3.1: Standard MRS acquisition parameters employed in the present study.

A water unsuppressed FID was also obtained from each voxel to enable subsequent eddy current corrections and metabolite concentration quantification by scaling to the water peak.

3.2.2. Voxel positioning

Voxels were placed in two standard positions, one sited within the left basal ganglia and the second in right parieto-occipital white matter. Standard positioning of the voxels in these areas was selected as these regions are frequently involved in neurometabolic disease. A standard position with well defined landmarks also facilitated the independent acquisition of data by radiographers without need to consult clinicians on the selection of position. Use of a standard voxel position across all cases and controls allowed direct comparison between cases without need to consider the effects of differing anatomical positions. The standard voxel positioning protocol did mean, however, that in some cases the MRS was acquired from normal appearing brain regions rather than over other abnormal regions.

Voxels were manually positioned on the MR scanner control station by reference to the standard three-plane anatomical (T_1 and T_2) image sequences. A composite 3 plane image view (Siemens) or screen capture images and spectrum protocol tagging (GE) were stored to allow subsequent re-examination and verification of the voxel localisation.

3.2.3. Spectral Processing

Raw data from the MR scanner were transferred for subsequent offline post-processing. The FID raw data was automatically processed using LCModel^{TM} software as described above. LCModel^{TM} automates the post-processing steps discussed above including lineshape and baseline corrections, and zero and first-order phase corrections. It employs a constrained least squares analysis method to provide the best fit from a basis set containing seventeen metabolite and nine macromolecular and lipid spectra. LCModel generated two outputs, one with and one without the application of an eddy current correction. Metabolite quantification

was achieved by normalization to the water reference peak area, with an assumption made that the water concentration is constant (35880mM).

The outputs generated by LCModel include a portable document file (pdf) with images of the original data spectrum, fitted spectrum, unfitted residual and the baseline applied (figure 3.1) together with listings of the metabolite concentrations derived and the Cramér-Rao lower bounds. The file also documents the linewidth of the spectrum expressed as the full width at half maximum (FWHM) and the signal to noise ratio. A separate text file also contains the metabolite concentrations, Cramér-Rao lower bounds as well as coordinate points for the original data spectrum, fitted spectrum, baseline function and the constitutive component spectra for each metabolite fitted.

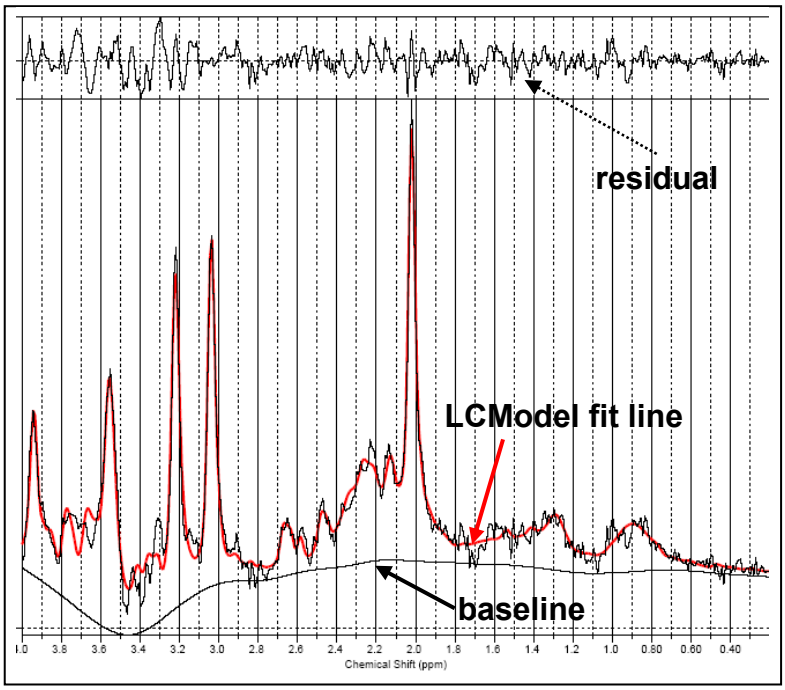

Figure 3.1: Example LCModel spectrum output. Original data spectrum line (black), LCModel fitted line (red), fitted baseline (arrow), and residual (i.e. difference between original data spectrum and LCModel fitted line, dotted arrow).

3.3. Data Quality Assessment

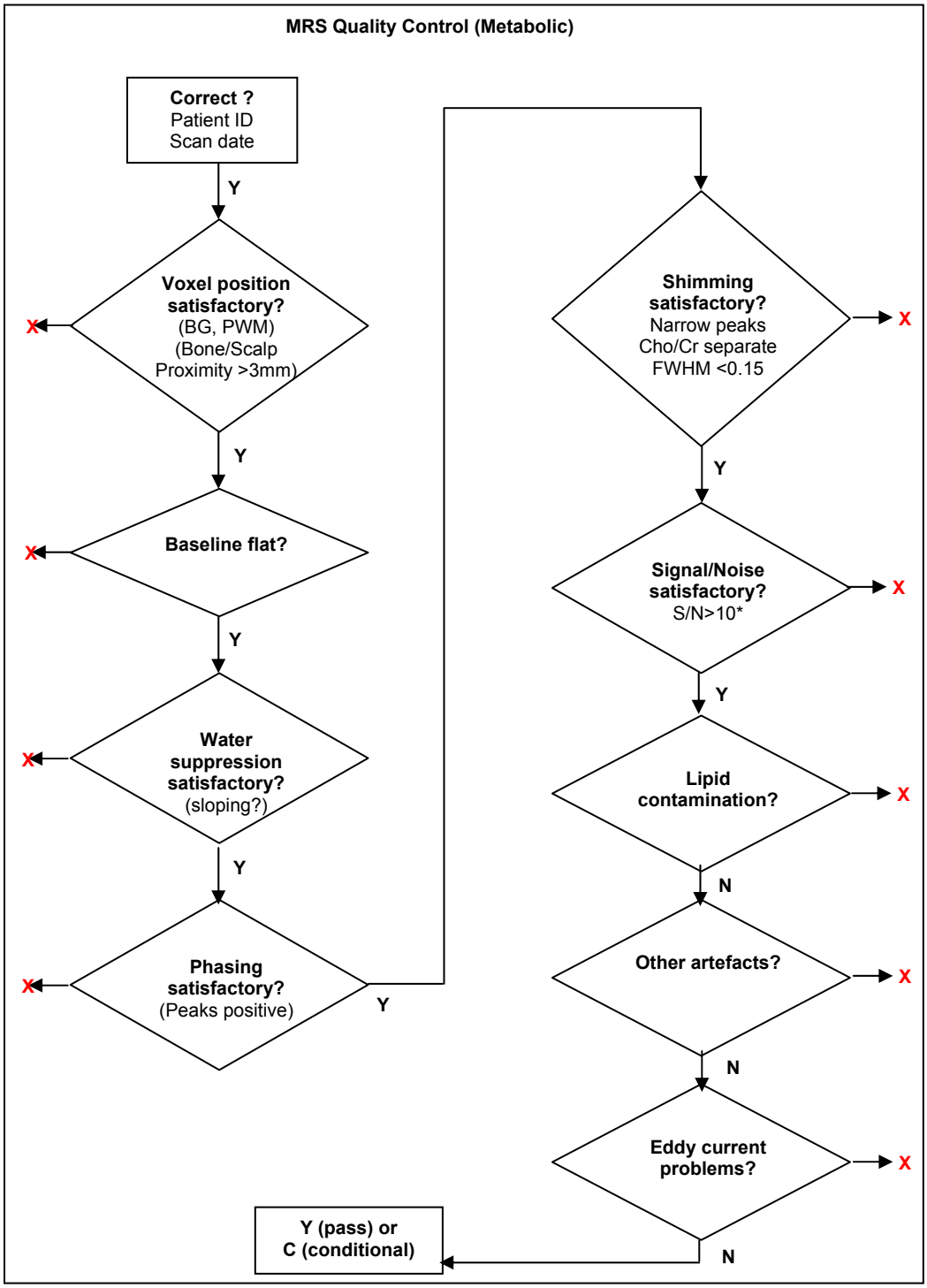

Figure 3.2: Quality assessment evaluation flowchart for MRS studies

Each individual MRS acquisition was quality assessed as outlined in figure 3.2 by inspection of the LCModel™ spectral output (pdf file). The quality assessment process was adapted

from the procedure applied at Birmingham Children's Hospital in the assessment of spectra acquired from brain tumours. The quality assessment process initially ensured correct patient demographics, and then assessed the voxel position by examination of the three-plane images of the voxel position. This evaluates the contents of the voxel as well positioning factors that could adversely affect the signal detected. As two standard locations were acquired, proximity to scalp and bone was not expected to be a significant issue unlike for brain tumours when the location was determined by the location of the tumour. Having evaluated voxel position, several parameters were evaluated including visual inspection of the baseline, water suppression, phasing, lipid contamination, eddy current and other artefacts. LCModel output includes two objective measures of quality, namely the FWHM which reflects adequacy of shimming, and is an estimate of the linewidth of the *in vivo* spectrum, and the signal to noise ratio (SNR). For brain tumour spectra, an SNR >5 is considered adequate, for metabolic cases a higher SNR is required because of the need to observe more subtle alterations in lower concentration metabolites.

3.4. Metabolite and Spectral Data Processing

Metabolite concentrations for defined groups of patients were exported from the LCModel™ text file to a standard spreadsheet package (Excel, Microsoft) using a specifically developed software programme script (developed in Matlab 7.1, The Mathworks Inc. by JED, N.Davies and E.Orphanidou). Metabolite concentrations from GE spectroscopy studies were adjusted by a specific factor derived from the analysis of the inter-compatibility of data from the different scanner systems used (see Chapter 4). The programme also extracted the coordinate points for the original data spectrum, fitted spectrum, and baseline function. The spectral output from LCModel binned each spectrum from the Siemens scanner in to 496 data points,

whereas GE spectra were binned in to 399. An interpolation technique was applied to the spectral coordinate points to convert the GE spectra to 496 points to allow direct comparison of GE and Siemens spectra.

Mean spectra for specified cohorts were then generated by combination of each fitted spectrum after subtraction of the specific baseline function from each individual spectrum, and the mean and standard deviation of the spectra derived for each point. GE spectra were further adjusted by a specific calculated factor (see Chapter 4).

3.5. Statistical Methods

Statistical analysis was performed using SPSS Statistics 17.0 (SPSS Inc.). Concentrations of metabolites were compared between cohorts by use of either Student's t-test or the non-parametric Mann-Whitney U-test. Test of significance of trends between multiple groups was performed using analysis of variance (ANOVA).

Principal component analysis (PCA) performed using SPSS Statistics was employed to reduce dimensions in complex datasets with large numbers of variables (such as plasma quantitative amino acid profiles). PCA was also implemented in the analysis of body fluid metabolite profiles as described below.

3.6. Clinical Information

Relevant clinical information pertaining to study subjects was obtained from the medical records and from clinical databases held at the Birmingham Children's Hospital. Data

included past medical history, qualitative radiological reports of previous and current MRI studies, and biochemical assays.

Biochemical results from clinical investigations were extracted from the medical records or from the clinical pathology results reporting system and tabulated in a standard spreadsheet (Excel, Microsoft). This included in particular quantitative assays of plasma amino acids determined using a standard method (cation exchange chromatography and photometric detection following derivatization with ninhydrin) in a single NHS service laboratory. Normal quoted control ranges were also obtained for all biochemical parameters extracted.

3.7. *In vitro* NMR Spectroscopy

One dimensional proton NMR spectroscopy of metabolite test solutions and a number of body fluid samples (urine and cerebrospinal fluid) from the patients was undertaken at the Henry Wellcome Building for NMR Spectroscopy, University of Birmingham.

3.7.1. Sample Preparation

3.7.1.1. Metabolite Test Solutions

Test solutions of (a) 20mM succinic acid plus 20mM creatine and (b) 50mM glycerol plus 20mM creatine (all reagents Sigma-Aldrich Ltd, Dorset, UK) were made. 100μL/L gadolinium contrast agent (dimeglumine gadopentetate, 'Magnevist', Bayer, Berkshire UK) was added to shorten the T_1 component.

The pH of the solution was measured using a standard calibrated pH electrode (Mettler Toledo). The pH of 800µL aliquots of the succinate-creatine test solution was adjusted by addition of NaOH (1M) to give a series of pH values (pH 4 to 11).

To 560µL of the test solution were added 40µL of deuterium oxide (D_2O) to provide a lock signal, and 5µL of 50mM 3-(trimethylsilyl)propionic-2,2,3,3-d_4 acid sodium salt (TSP) to provide a chemical shift reference (0ppm).

3.7.1.2.Body fluid samples

Random collection midstream samples of urine were collected into sterile universal containers. Cerebrospinal fluid samples were collected into sterile universal containers at the time of clinical indicated lumbar puncture by sterile technique. All samples were transferred immediately to the clinical biochemistry laboratory and then aliquoted and frozen at minus 80^{o}C prior to transfer for analysis. Samples were defrosted to room temperature immediately prior to analysis.

3.7.1.2.1. Urine samples

A standard phosphate buffer solution (pH 7.4) was made (1.44g Na_2HPO_4, 0.26g NaH_2PO_4 added to 10mL D_2O made up to total volume of 50ml with sterile distilled water), after the method described by Beckonert *et al* [108] to provide stabilisation of the urinary pH.

To 400µL of urine was added 200µL of phosphate buffer solution and 5µL of 50mM TSP. The pH of the sample was documented.

3.7.1.2.2. CSF Samples

To 400µL of CSF was added 200µL of D_2O and 5µL of 50mM TSP. The pH of the sample was documented.

3.7.2. NMR Spectroscopy Acquisition

Samples were transferred to Wilmad 7" length, 5mm diameter glass NMR tubes (Sigma Aldrich Ltd) for NMR experiments. NMR spectroscopy experiments were performed on a vertical bore Bruker Avance 500MHz spectrometer fitted with an HCN cryoprobe, using Topspin software. A standard pulse-acquire sequence with water presaturation was used with an acquisition of 16K complex points with bandwidth of 7200Hz.

The sample tube was loaded into the spectrometer and the sample temperature set to 298K. Iterative tuning and matching was performed on the proton nucleus channel. The sample was automatically locked to the deuterium signal and lock gain adjusted. Optimal shimming was achieved by initial loading of a standard shim set followed by use of an automatic shimming algorithm and also further manual shimming if required. The 90^{o} pulse was automatically calibrated and receiver gain automatically set. An initial brief acquisition with n=4 scans was performed and if satisfactory a full acquisition with n=32, 128 or 256 scans performed. FID data files and associated acquisition parameter files were transferred to a separate work station for subsequent analysis.

3.7.3. Metabolite identification and fitting

The one dimensional proton spectra were processed and viewed using Chenomx NMR Suite (v7.1, Chenomx Inc. 2011). The FID was imported into the Chenomx Processor module. Chemical shift was automatically calibrated to the TSP peak and the documented pH of the sample entered. Automatic zero filling, 0.5Hz line broadening, phase correction and baseline corrections were applied. The processed spectrum was exported to the Chenomx Profiler module.

This enabled visual inspection of the spectrum and identification of metabolite peaks seen. Metabolite fitting was performed by automated fitting of the standard Chenomx metabolite library (302 compounds) and the metabolite fits subsequently inspected. Alternatively targeted fitting of expected metabolites was performed.

Metabolite peaks not accounted for by expected/ standard metabolite spectra were putatively identified by reference to, and comparison with, chemical shift parameters and experimental spectra from the Human Metabolome Database (HMDB, www.hmdb.ca, [109]).

3.7.4. Principal component analysis

To examine differences in body fluid spectral profiles between different cohorts of patients and controls an unsupervised principal component analysis (PCA) was employed. This obviated the requirement for specific metabolite identification prior to analysis, but enabled key differences in metabolite profiles to be identified. The identity of metabolites contributing to the differentiation of groups could then be established from the PCA loadings plots.

FID files from the Bruker spectrometer were imported into the 1D NMR visualisation and processing application Dangerplotpy (http://www.pipegrep.co.uk/dangerplotpy/, M.Wilson). Spectra were manually phase corrected and chemical shift referenced to the TSP peak at 0ppm. Processed spectra were saved and grouped into relevant cohorts.

A software script (M.Wilson) executed in R (v2.13.0, The R Foundation for Statistical Computing) was used to further process the cohorted spectra. This applies automatic water filtering, line-broadening and baseline correction to each spectrum. Chemical shift regions

were selected to include as appropriate 0.4-4.5ppm plus/minus 6-10ppm with removal of the water peak region. The signal was normalised to the total integral of peaks and spectral binning applied.

The script then executed a principal component analysis on the processed spectra generating principal component scores plot and loadings plots for first and second principal components. Loadings plots could then be visually examined to identify spectral regions and specific metabolite peaks that distinguished clusters of cases seen on the scores plot.

Chapter Four

4. Preparatory Technical Development.

4.1. Patient Cohort Investigated with MRS

350 MRS studies with good quality data were available from 307 children who had studies performed for non-oncological indications at Birmingham Children's Hospital. 58% of children were male. The distribution of age at time of the MRS investigation (figure 4.1) showed a positive skew indicating that the majority of MRS are undertaken in younger children but with a smaller number having the study throughout later childhood up to mid-teenage years. The mean age at time of MRS study was 4.6 years, median 3.3years, range 0.0-17.4 years.

A wide range of diseases was represented by the cases acquired (figure 4.2). A specific diagnosis of an IMD was known in 104 (34%); 28 (9%) had a known specific non-IMD diagnosis; 175 (57%) did not have a known diagnosis at time of the MRS. Specific diseases identified with substantial cohorts of MRS data available included organic acidaemias (propionic acidaemia, methylmalonic aciduria, glutaric aciduria), urea cycle disorders, mucopolysaccharidoses and the mitochondrial disorders.

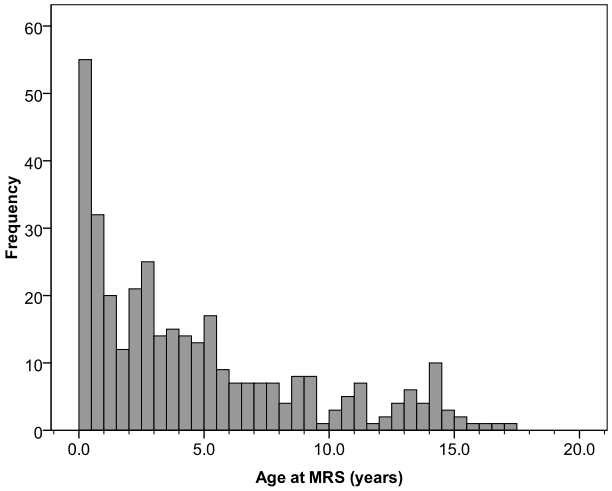

Figure 4.1: Histogram of age at time of MRS examination (6 month bins).

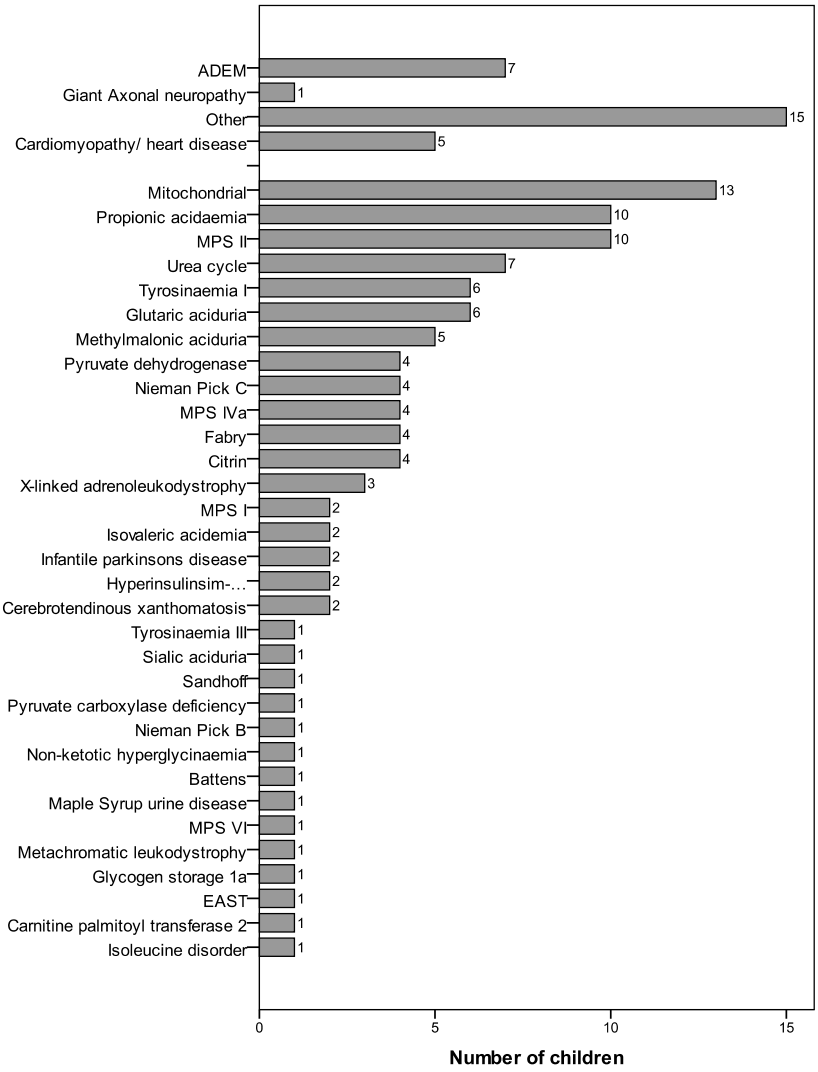

Figure 4.2: Bar chart of numbers of children with specific known diagnoses in whom MRS was performed.

4.2. Data Quality Assessment

It was important to establish that metabolite data generated were reliable. Several components of data fidelity were assessed, including (a) case-by-case spectral quality control analysis, (b) post-processing technique analysis and (c) inter-scanner data compatibility (i.e. could data from two different MRI systems be combined and directly compared).

4.2.1. Spectral quality assessment analysis

To evaluate the ability of the research protocol to generate a high rate of good quality MRS data, a detailed quality assessment was undertaken. 204 studies from the Siemens scanner and 52 studies from the GE scanner were evaluated according to the quality assessment protocol (figure 3.2).

4.2.1.1.Siemens quality assessment analysis

Data from 204 separate studies completed on Siemens scanner were analysed. 370 voxel acquisitions (echo time 30ms) were analysed. Both the non-eddy current and eddy current corrected data sets were analysed.

Of the 370 voxel acquisitions assessed, only 18 (4.9%) failed quality assessment analysis of both non-eddy current corrected and eddy-current corrected data sets (table 4.1). Of these cases, 10 were due to missing data, two due to inadequate signal to noise ratio, and four due to problems with phasing, baseline or water suppression. Two failed because of inappropriate voxel localisation (one in cerebrospinal fluid (CSF) completely, one unclear from stored images if in cerebellum). In a further 19 acquisitions there was some concern over voxel

location, mainly encroachment onto ventricle and therefore CSF contamination of voxel; these cases were not excluded at this stage.

4.2.1.2.GE quality assessment analysis

Data from 52 cases acquired using the GE scanner were analysed. Of these, 8 were excluded because of an incorrect echo time parameter (TE 35ms) or missing data. Of the 44 acquisitions assessed 93.2% had useable data; in all cases that passed the quality assessment analysis the eddy-current corrected data was useable, and it was also observed that in many cases the quality of the spectrum produced was substantially higher in eddy-current corrected data (for example see figure 4.3) even though an eddy current correction should not significantly alter the SNR *per se*.

Thus overall good quality spectral data was obtained in 93-95% of cases.

Siemens Scanner System	*n = 370*	**Reasons**
Both ECC and non-ECC	271	
Non-ECC only	74	
ECC only	7	phasing/ baseline/ water suppression (5), SNR (1), other (1)
Neither	18	Voxel location (2). No data (6), SNR (2), phasing/ baseline/ water suppression (4), no water unsuppressed file (4)

GE Scanner System	*n = 44*	**Reasons**
Both ECC and non-ECC	36	
Non-ECC only	0	
ECC only	5	SNR and water suppression (1), SNR (4)
Neither	3	SNR (3) and baseline/ water suppression (3)

Table 4.1: Results of quality assessment analysis of MRS studies on Siemens and GE scanner systems

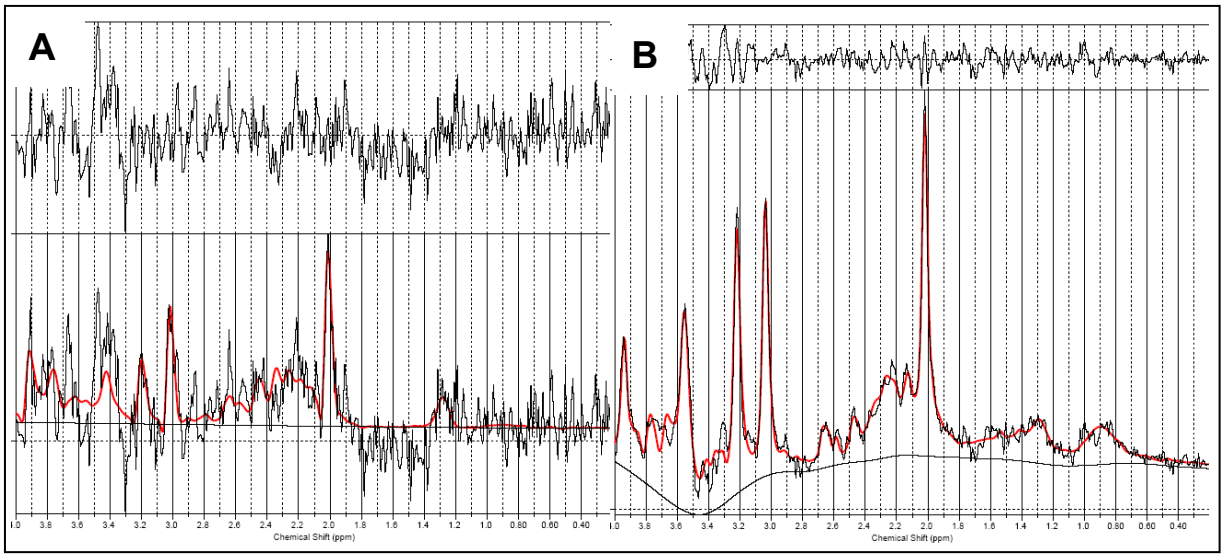

Figure 4.3: Example of LCModel spectrum output from GE system scanner showing improved SNR with eddy current correction. (A) Non-eddy current corrected, (B) Eddy current corrected. In (A) and (B) upper panel is the fitting residual, lower panel original data spectrum line (black), and LCModel fitted line (red).

4.2.2. Post-processing technique analysis

As described above, post-processing of raw spectroscopy data was performed using LCModel^{TM} software [44]. The software processes the raw data using two methods, with and without eddy current correction, generating two output files. As demonstrated above, for an individual study one or other of these outputs may not pass the quality control filter, and so it was necessary to evaluate whether the two methods were inter-changeable, producing directly comparable metabolite values. To make this evaluation, data from cases where both the eddy-current corrected (ECC) and non-eddy current corrected (non-ECC) outputs met the quality assessment criteria were selected, and a paired-sample analysis applied to compare concentration estimates of the major metabolites detected, namely total creatine, myo-inositol, total choline, total N-acetylaspartate and glutamine+glutamate. At this stage consideration of anatomical position of voxels was not included in the analysis.

4.2.2.1.Siemens data

299 studies acquired using the Siemens system were analysed (figures 4.4 and 4.5). For most of the major metabolites with the exception of choline and glutamine+glutamate there was only a small (although consistently statistically significant) difference in metabolite values as evaluated by paired sample t-test. There was no difference detected in choline concentrations. The ECC method gave a higher estimate of glutamine+glutamate.

The quality assessment process had highlighted that in many cases the application of the ECC method by LCModel generated artefacts such that the data did not meet the quality assessment criteria, whereas the corresponding non-ECC method data did meet the quality assessment criteria. It was therefore decided that Siemens data should be solely processed using the non-ECC method, except in the few cases where the non-ECC method data did not meet the quality assessment criteria but the ECC method did (circa 1.9%).

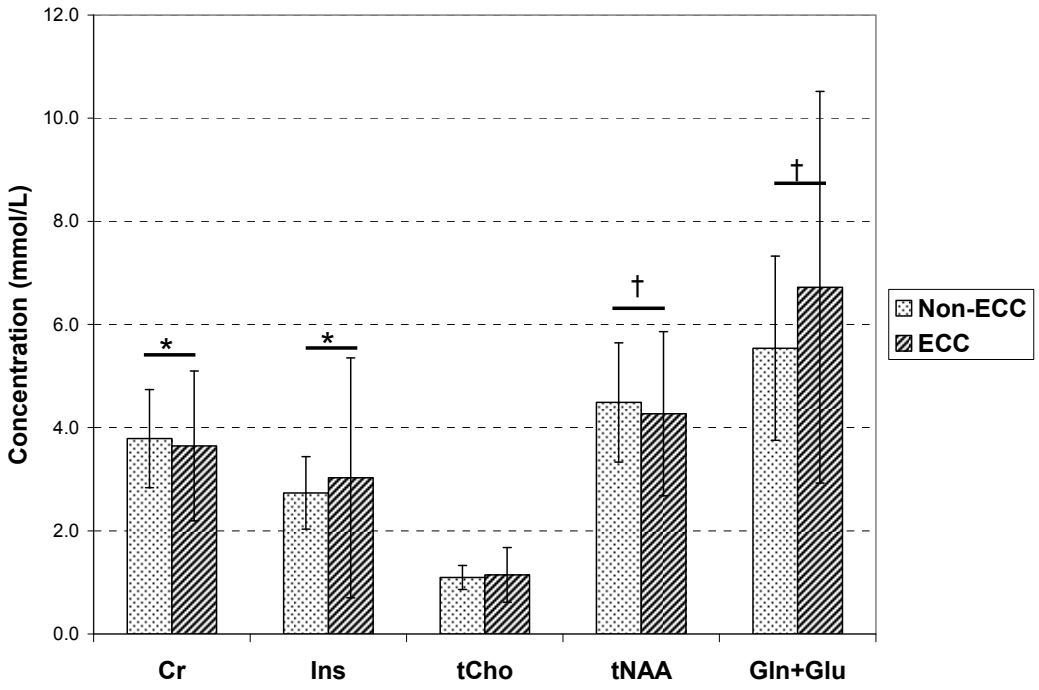

Figure 4.4: Bar chart of mean brain metabolite concentrations determined for Siemens MRS data with and without eddy current correction. (n=299 studies. Paired sample t-test, * $p<0.05$, † $p<0.01$. Error bars indicated standard deviation).

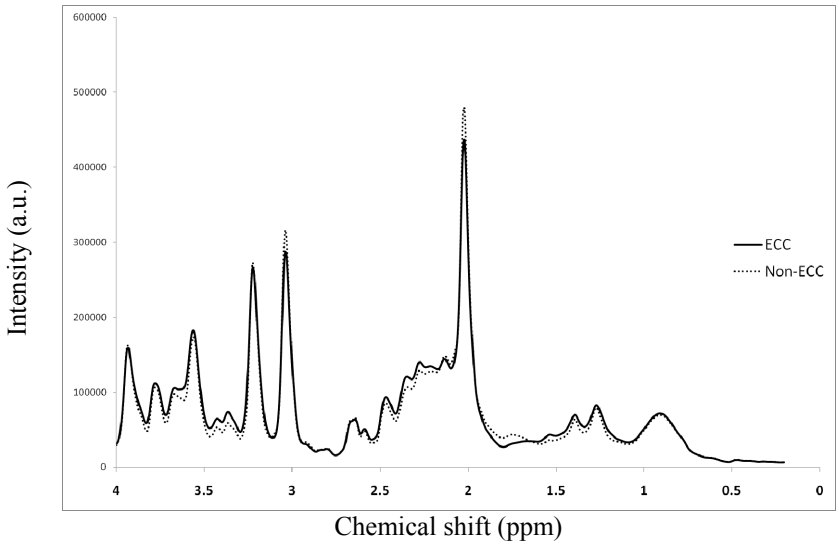

Figure 4.5: Plot of mean spectra for Siemens *in vivo* MRS data from brain of n=299 studies processed with and without eddy current correction.

4.2.2.2.GE Data

118 studies acquired using the GE system were analysed (figures 4.6 and 4.7). In this case, the ECC method generated significantly ($p<0.001$ by paired sample t-test) higher metabolite concentrations for all of the major metabolites.

These data indicate that metabolite concentration values derived from the GE scanner using ECC and non-ECC processing methods were not directly comparable. Since the quality assessment process found that for the GE scanner in the majority of cases the ECC data met the quality assessment criteria, it was decided that data from the GE scanner should be processed by the ECC method.

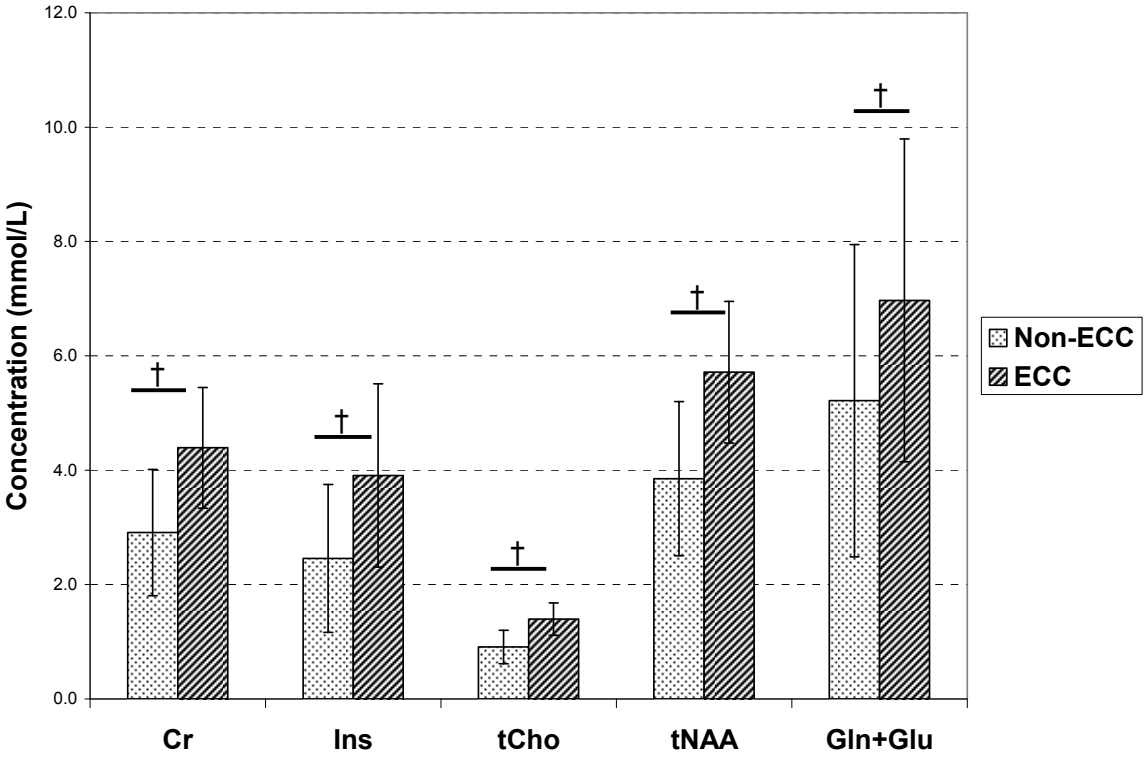

Figure 4.6: Bar chart of mean brain metabolite concentrations determined for GE MRS data with and without eddy current correction. (n=118 studies. Paired sample t-test, * $p<0.05$, † $p<0.01$. Error bars indicated standard deviation).

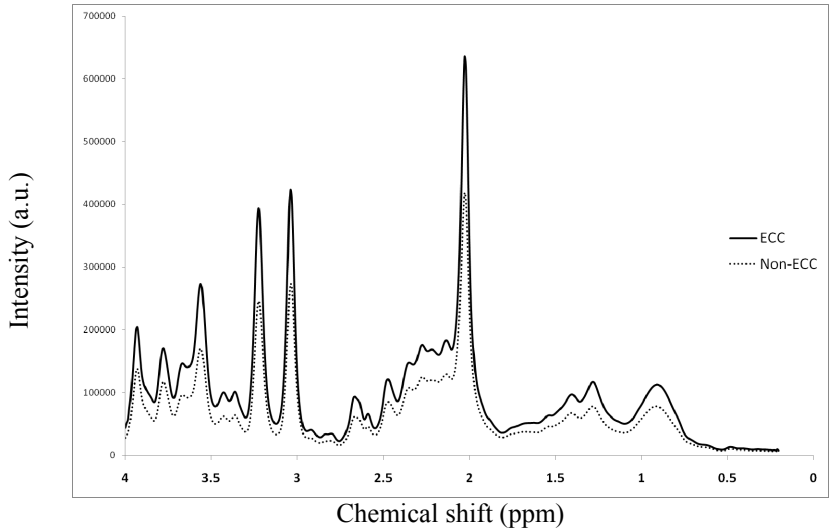

Figure 4.7: Plot of mean spectra for GE *in vivo* MRS data from brain of n=118 studies processed with and without eddy current correction.

4.2.3. Inter-scanner data compatibility

The potential contribution of different scanner systems to "instrumental variation" in the metabolite data was assessed.

4.2.3.1. Initial inter-scanner analysis

Comparison of the mean spectra generated above was undertaken (figure 4.8). By visual inspection, data generated by the non-ECC method from the GE system corresponded with the non-ECC method data from the Siemens system, whereas the GE ECC data gave significantly higher spectral peaks. This was confirmed by comparison of the mean metabolite concentrations for each group (figure 4.9): the absolute difference in metabolite concentration was smaller between GE non-ECC and SM non-ECC than between GE ECC and SM non-ECC data, although differences remained statistically different.

As a first approximation, data from studies on the GE scanner could be processed using the ECC method, and then scaled to approximate to the values obtained using the non-ECC method which is comparable to the data obtained using the Siemens system. A scaling factor applied to the major metabolites was derived from the average ratio of ECC:non-ECC values from the dataset (ratio applied to ECC data, ~0.65).

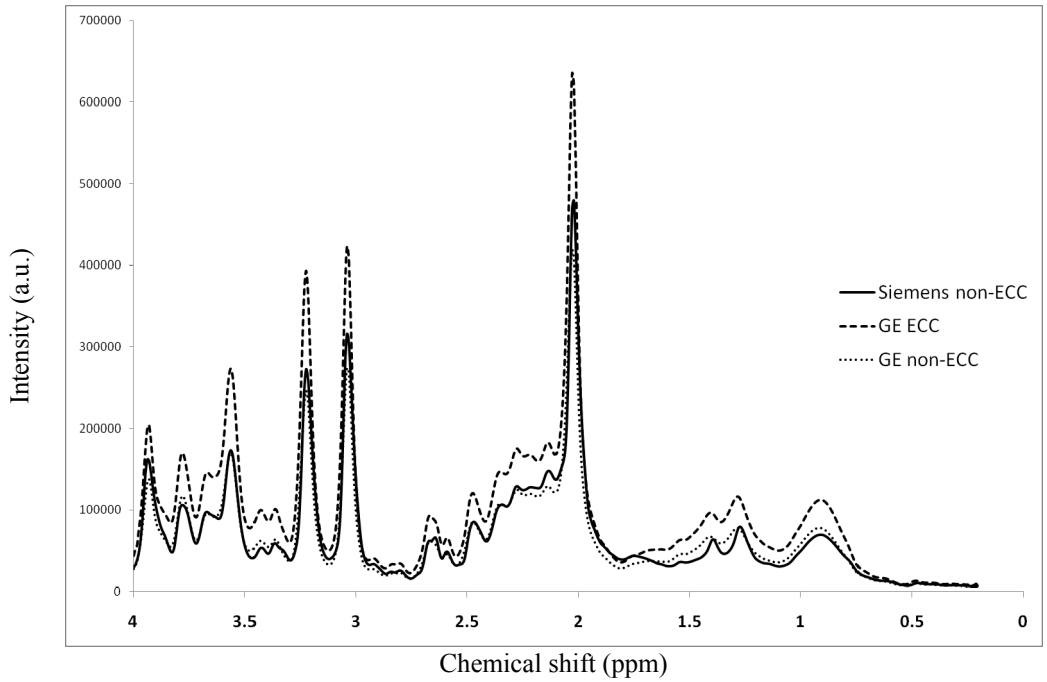

Figure 4.8: Overlay plots of mean *in vivo* brain MR spectra for Siemens (n=299) non-eddy current corrected, and GE (n=118) eddy current corrected and non-eddy current corrected datasets.

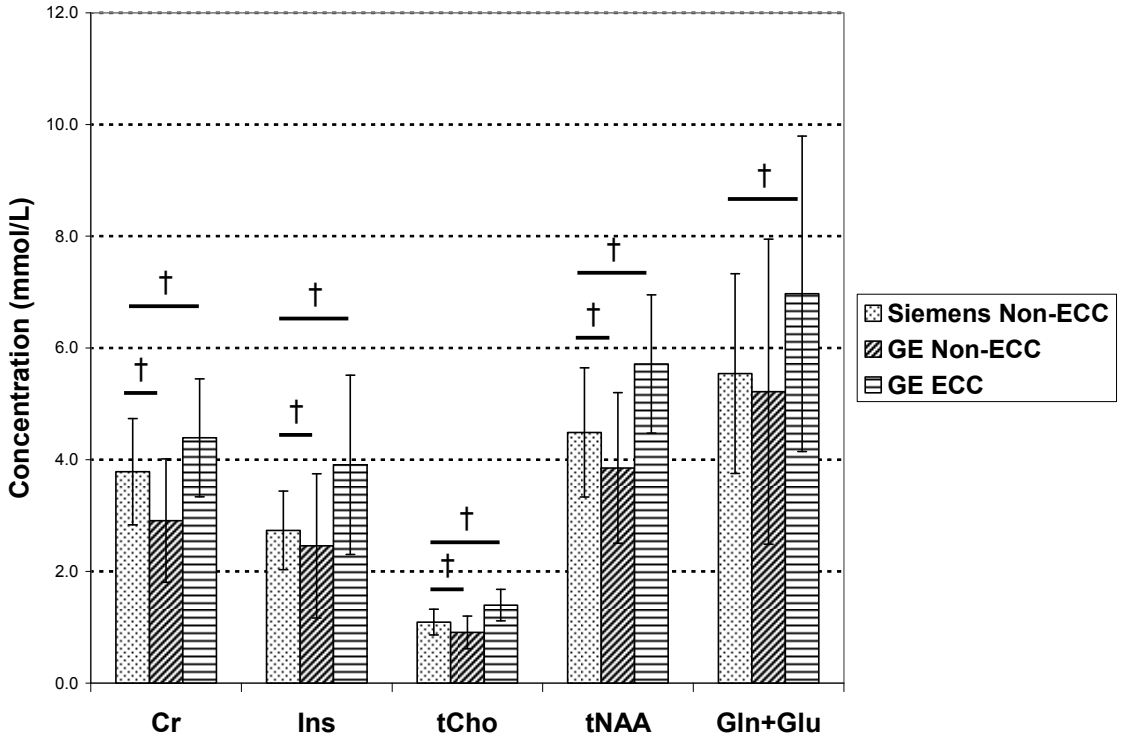

Figure 4.9: Bar chart of mean brain metabolite concentrations for Siemens non-eddy current corrected, and GE eddy current corrected and non-eddy current corrected datasets. Independent sample t-test, † $p<0.01$. Error bars indicated standard deviation).

4.2.3.2.Detailed inter-scanner analysis

A further detailed analysis of inter-scanner compatability was then undertaken, this time taking account of the different anatomical regions being analysed.

4.2.3.2.1. Basal ganglia

215 basal ganglia voxel acquistions from the Siemens scanner were compared with 104 basal ganglia voxel acquistions from the GE system, combining both those with and without MRI abnormalities. In line with the previous analysis, all data from the GE system were processed using the ECC method. The metabolite concentrations were compared by independent sample t-test (figure 4.10). As seen in the prior analysis, all major metabolite values were significantly different, with all except lactate significantly higher for GE system with the ECC method. The lactate was significantly lower ($p<0.05$) for the GE system ECC method than Siemens system data, but there was a correspondingly significantly higher concentration of macromolecules/lipids at 1.3ppm in the GE data suggesting that the signal at ~1.3ppm was being assigned more to macromolecule/lipids than lactate. Glutamine was higher for GE data but not significantly different from Siemens data.

A plot of mean metabolite value for Siemens and GE systems was generated (figure 4.11). A linear regression line fitted to the data points demonstrated a very strong linear correlation ($R^2 = 0.989$); the regression coefficient derived from the linear regression fit of 1.26 could be applied to the metabolite data from GE scanner (ECC method) to approximate to the Siemens scanner data set.

4.2.3.2.2. White matter:

The analysis was repeated for data from the white matter voxel. Thus 183 white matter voxel acquistions from the Siemens scanner were compared with 92 white matter voxel acquistions from the GE system, combining both those with and without MRI abnormalities. Again all data from the GE system were processed using the ECC method. The metabolite concentrations were compared by independent sample t-test (figure 4.10). Again, all major metabolite concentrations were signicantly higher from GE system. Glutamine and taurine concentrations were higher in GE dataset but not significantly different from Siemens data.

A plot of mean metabolite value for Siemens and GE systems was generated (figure 4.11). Here the linear regression line fitted to the data points again demonstrated a strong linear correlation (R^2 = 0.987); the regression coefficient derived from the linear regression fit of 1.25 could be applied to the metabolite data from GE scanner (ECC method) to approximate to the Siemens scanner data set.

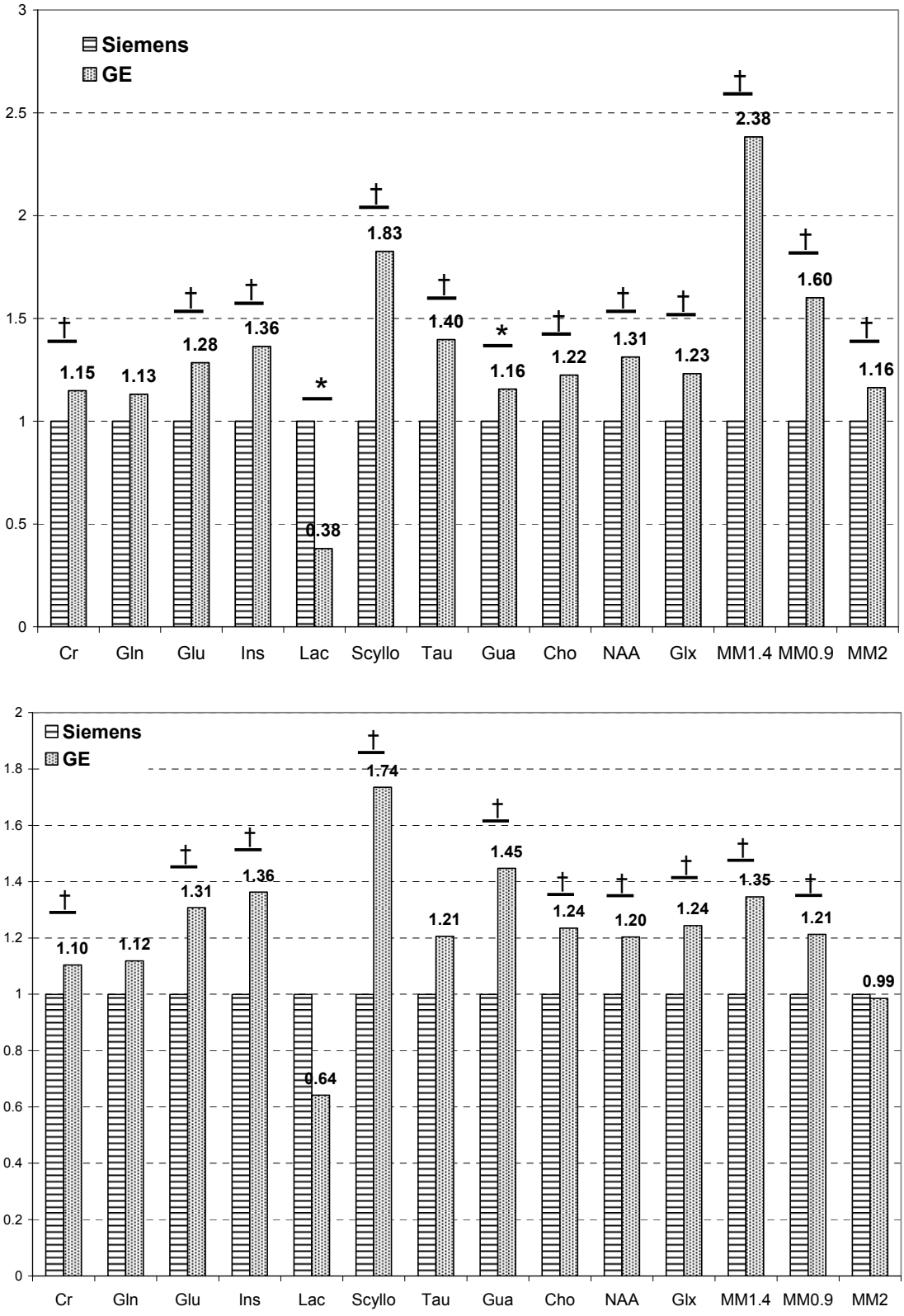

Figure 4.10: Bar charts of ratio mean metabolite concentration in (top) basal ganglia and (bottom) white matter for Siemens (normalised to 1) and GE systems. Independent sample t-test, * $p<0.05$, † $p<0.01$.

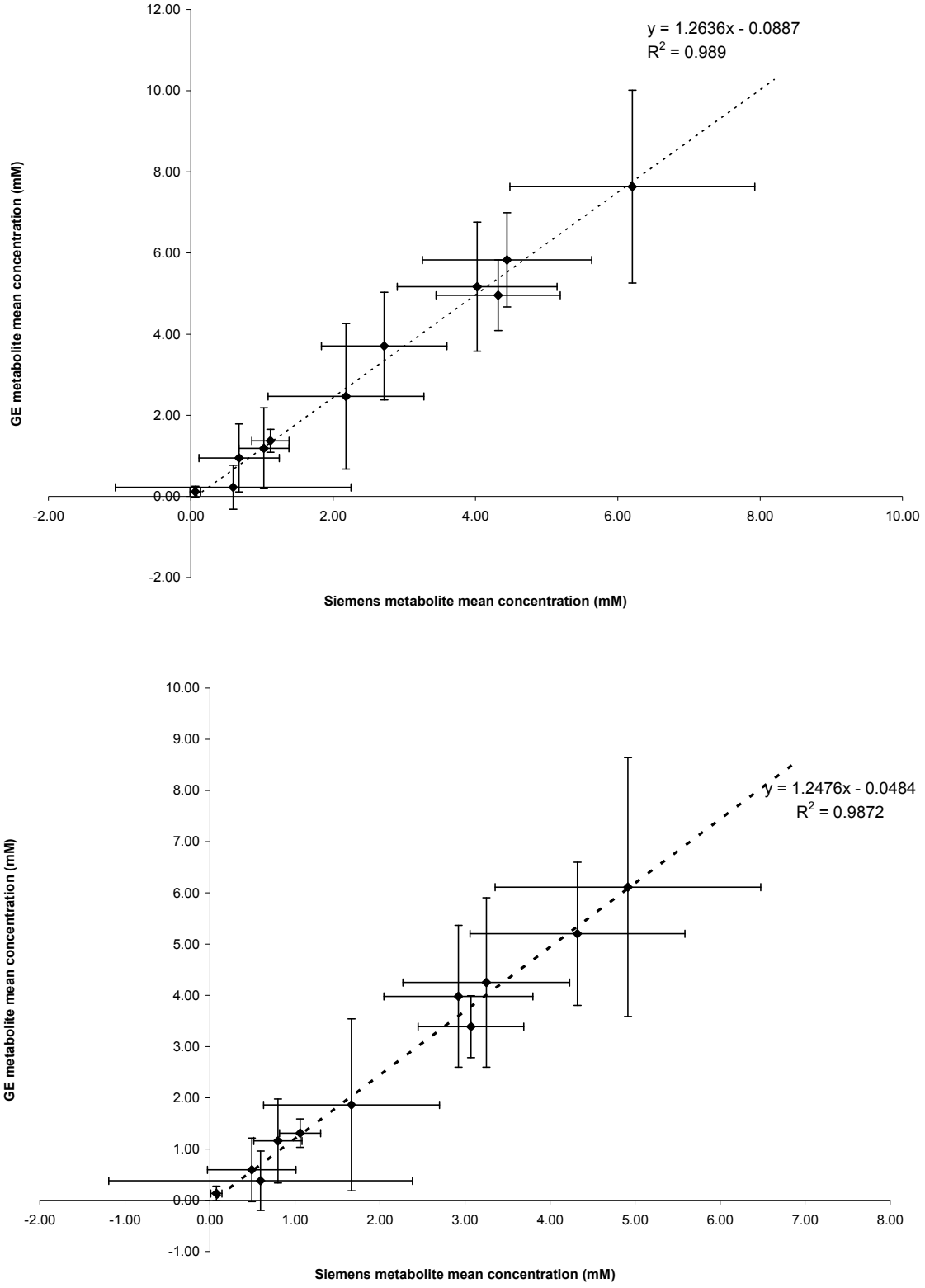

Figure 4.11: Plot of mean metabolite concentration in (top) basal ganglia and (bottom) white matter from two scanner systems and linear regression analysis. Each point represents a different metabolite. Error bars: horizontal (Siemens) and vertical (GE) standard deviation of metabolite concentrations. Dotted line: linear regression line.

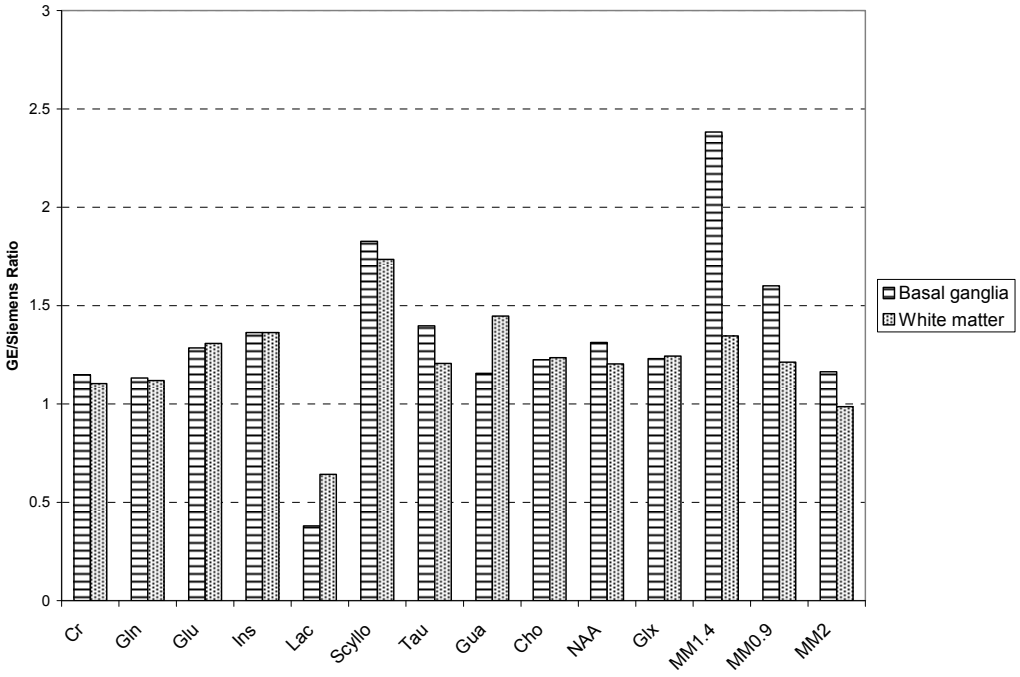

Figure 4.12: Bar chart of GE:Siemens ratio for mean metabolite concentration comparing basal ganglia and white matter.

4.2.4. Discussion – quality assessment

The variability in metabolite data obtained by MRS is generated from several sources. The "biological variation" in metabolite data is that which is of interest in answering clinical research questions, i.e. alterations in metabolite concentrations due to pathological or physiological reasons. However, variability may also be generated by "instrumental variation" and "acquisition variation". Minimising acquisition variation requires a set standard pulse sequence for acquisiton, such that all acquistion parameters remain the same between cases. Furthermore, voxel positioning should be standard and relies on radiographer input. This factor can be further explored by *post hoc* analysis using recorded voxel localisation images.

Instrumental variation arises when different hardware systems are used to obtain data, which may have different configurations and designs that result in systematic differences in data. The analysis above demonstrates that data from the two scanner systems pertaining to the

current work are systematically different. It should be noted that the data presented are not a direct comparison of the two scanners, as the datasets being compared are from different cohorts of children. That said, the cohorts being compared are large, with no overt systematic differences in age, gender or disease characteristics, and so should provide a representative spread of data.

A number of factors may contribute to this instrumental variation. Firstly, the two systems have differing water suppression modules, with the GE system considered to have a more "aggressive" water suppresion system that may affect the integrity of metabolites signals in proximity to the water peak (i.e. close to 4.0ppm). Secondly, the radiofrequency coils have different technical specifications, in particular the GE system RF coil is composed of an array of coils, each of which receives and collects an individual FID, whereas the Siemens systems operate in an effective single channel (CP) mode. Thus the post-processing software (e.g. LCModel^{TM}) has to handle the combination of this data, and there may be limitations in how that is performed regarding differences in phasing between coil elements.

Further variability may be introduced by post-processing methodologies. In particular, this analysis has demonstrated the systematic differences in data generated by use of ECC and non-ECC methods. It is important, therefore, that a single methodology is applied as far as possible to eliminate this systematic source of data variability. The analysis above dictates that for data from Siemens scanner, the non-ECC method is used, and the ECC method for data from the GE scanner. Importantly it has been observed that for newer generation MR systems eddy currents may not represent a significant issue, and this is observed for the

Siemens data here where the systematic application of a post-processing eddy current correction did not improve data quality [42].

Methods have been proposed to enable comparison of data acquired from different scanner systems. These are based upon the concept of using known conversion factors to translate data from the GE system to be comparable to Siemens system data. The first approach made the assumption that GE non-ECC data was comparable to Siemens non-ECC data, and applied a conversion factor to GE ECC data (where this needed to be used if the non-ECC data was not available) to convert it to the GE non-ECC data ranges. Later analysis found that this method provided only an approximation. The second approach entailed systematic usage of GE ECC data, and applied a conversion method to this data to translate it to be comparable to the Siemens non-ECC data using a static ratio applied to all metabolite data acquired from the GE system.

While it would be ideal to use one scanner system for all data acquisition, different clinical settings have differing scanner systems, and even within one institution more than one scanner system may be present. Thus for single centre studies, and more so for multi-centre studies, data from differing systems is likely to be encountered. Given the importance of multi-centre studies, particularly for rare diseases such as those under consideration in the present work, approaches to combining data from different systems must be considered, although the potential problems from acquisition and instrumental variation in the data must be accounted for before biological conclusions drawn from the data. To this end, "reproducibility studies" are required to evaluate the ability to generate combinable data from

different studies. This could include the use of static test objects (phantoms) loaded with known concentrations of metabolites, as well as by scanning volunteers on multiple scanners.

4.3. Metabolite concentration age variation analysis

Previous studies have established that MRS-detectable brain metabolites vary with age (see Chapter 2, [67]). To assess the variation in metabolites within the current cohort, metabolite data from studies that had passed quality assessment were analysed. To remove potential confounding from inter-scanner variability, only data acquired using the Siemens system were included here. This analysis included 215 voxel acquisitions from basal ganglia and 183 from white matter. All studies were included irrespective of diagnosis or MR imaging features. Studies were analysed first in age cohorts (0-3m, 3m-1y, 1-2y, 2-5y, 5-10y, >10y; table 4.2 and figure 4.13) with differences between age cohorts evaluated by one-way analysis of variance (ANOVA). Data were then evaluated with age as a continuous variable (figure 4.14), with correlation between age and metabolite concentration evaluated by calculation of the Pearson correlation coefficient. Mean spectra for each age cohort were generated for basal ganglia and white matter (figure 4.15). As previously reported, the most significant alterations in metabolites occurred during the first year of life, particularly the first 6 months.

4.3.1. Total N-acetylaspartate + N-acetylaspartylglutamate

The concentration of tNAA increased with age in both basal ganglia and white matter, as determined both by ANOVA analysis of age cohorts and by correlation analysis (Pearson coefficient 0.34 and 0.62 for basal ganglia and white matter respectively, indicating moderate to high correlation). Previous studies have demonstrated a similar finding [67]. The biggest increase was seen during the first year of life but the trend continued throughout childhood.

4.3.2. Creatine

Creatine did not alter significantly with age in the basal ganglia, although there did appear to be a trend towards increasing with age, but creatine did increase with age in white matter ($r=0.30$, $p<0.01$). As with tNAA, the largest increase was seen in the first 6 months of life. Pouwels *et al* reported a similar finding in basal ganglia, but found a trend towards falling creatine concentration with age in white matter, albeit based on a smaller cohort of children [67].

4.3.3. Choline compounds

Total choline was seen to decrease with age in both white matter and basal ganglia, though once again the biggest changes were demonstrated in the first year of life, consistent with previous studies [67].

4.3.4. Inositol (Ins)

Myo-inositol showed a weak correlation with age, with decreasing concentration with age in basal ganglia ($r=-0.18$). This trend was again similar to that previously reported.

4.3.5. Glutamate & Glutamine

Analysis of the composite result for glutamate+glutamine demonstrated no significant change in concentration with time, although inspection of the cohort trends suggests an increase in both white matter and basal ganglia in the first year of life. Evaluating the separate concentrations of glutamate and glutamine found that glutamate increased with age in both basal ganglia and white matter ($r=0.20$ and 0.23 respectively), while glutamine decreased with age in white matter but did not alter significantly with age in basal ganglia ($r=-0.19$ and -0.07 respectively). Pouwels *et al* found that glutamate decreased with age in both white matter and basal ganglia in contradiction to the current data, but they found that glutamine showed a strong trend to decrease with increasing age in white matter consistent with the data presented

here [67]. They also demonstrated a strong trend to decreasing total glutamine+glutamate with age in both regions.

4.3.6. Taurine

As has been reported previously, taurine concentrations fell with increasing age in both brain regions analysed. It is thought that taurine may have specific functions in early neuronal development since it is detected at much higher concentrations in the neonatal period [67].

4.3.7. Lactate

No specific trend was seen in lactate concentration (figure 4.14) as it is not normally detected. It was evident that most of the cases with high lactate levels were in the youngest patients, reflecting the occurrence of both aggressive early onset mitochondrial disease and also the propensity of this age group to suffer hypoxic ischaemic insults, both of which cause elevated brain lactate. The age cohort mean spectra (figure 4.15) have wide standard deviations around the lactate peak indicating the occurrence of cases with significantly increased levels on a background of most cases having no detectable lactate.

4.3.7.1.Lactate in mitochondrial disorders

A specific comment on the detection of lactate in mitochondrial disease is warranted, since the detection of elevated brain lactate by MRS is reported to be suggestive of mitochondrial disease, caused by the shift from oxidative phosphorylation to glycolysis [110-112]. The mitochondrial diseases are a group of disorders caused by inherited abnormalities of the electron transport chain [12, 113]. However, the sensitivity of lactate may not be high [114], and its detection can vary during the course of the disease process and across anatomic regions within the brain [115-117].

15 MRS studies were available from patients with mitochondrial disorders confirmed on the basis of electron transport chain complex activity assay or genetic abnormality, all of whom had evidence of cerebral involvement evidenced by either neurologic symptoms or MR imaging abnormalities. A cut-off of 0.6mM lactate was used since this was the concentration above which the Cramér-Rao lower bounds were less than 30%. Using this definition, elevated brain lactate was detected in 4/15 patients in basal ganglia and 6/15 in white matter, corresponding to a test sensitivity of only 27-30% for the identification of mitochondrial disease, confirming previous reports of the limited sensitivity of MRS-detected brain lactate as a stand-alone test [114]. (See Appendix D for preliminary results evaluating the use of a multivariate statistical analysis approach to improving the diagnostic power of MRS in this context).

Mean metabolite concentration (mM (standard deviation))							
Basal ganglia							
	n	Cr	Ins	tNAA	Gln+Glu	tCho	Tau
0-3m	20	3.90 (0.89)	3.54 (0.92)	2.93 (0.90)	5.39 (2.12)	1.32 (0.31)	1.33 (0.54)
3m-1y	37	4.14 (1.02)	2.77 (1.33)	3.87 (1.31)	5.97 (1.95)	1.20 (0.32)	0.91 (0.59)
1y-2y	19	4.50 (0.80)	2.70 (0.82)	4.41 (1.09)	6.31 (1.51)	1.19 (0.19)	0.85 (0.41)
2y-5y	62	4.51 (0.85)	2.63 (0.62)	4.79 (0.94)	6.28 (1.62)	1.10 (0.22)	0.75 (0.47)
5y-10y	44	4.36 (0.83)	2.61 (0.71)	4.75 (1.07)	6.53 (1.68)	1.08 (0.24)	0.41 (0.42)
>10y	33	4.27 (0.73)	2.48 (0.64)	4.96 (0.83)	6.32 (1.47)	0.94 (0.16)	0.15 (0.29)
ANOVA p-value		0.07	0.00	0.00	0.22	0.00	0.00
White matter							
	n	Cr	Ins	tNAA	Gln+Glu	tCho	Tau
0-3m	17	2.16 (0.83)	3.67 (1.36)	1.97 (1.22)	4.06 (1.98)	1.00 (0.40)	1.14 (0.75)
3m-1y	26	3.09 (0.56)	3.19 (0.93)	3.52 (0.90)	5.06 (1.51)	1.15 (0.20)	1.04 (0.51)
1y-2y	14	2.99 (0.78)	2.70 (1.23)	4.02 (0.76)	5.11 (1.96)	1.11 (0.37)	0.62 (0.35)
2y-5y	56	3.16 (0.38)	2.74 (0.50	4.57 (0.63)	5.08 (1.50)	1.06 (0.21)	0.42 (0.31)
5y-10y	37	3.11 (0.54)	2.69 (0.65)	4.64 (0.87)	4.89 (1.37)	1.08 (0.21)	0.22 (0.24)
>10y	33	3.36 (0.49)	2.99 (0.86)	5.52 (0.85)	4.92 (1.44)	0.98 (0.12)	0.10 (0.21)
ANOVA p-value		0.00	0.00	0.00	0.29	0.09	0.00

Table 4.2: Variation in mean MRS derived metabolite concentrations across different age cohorts.

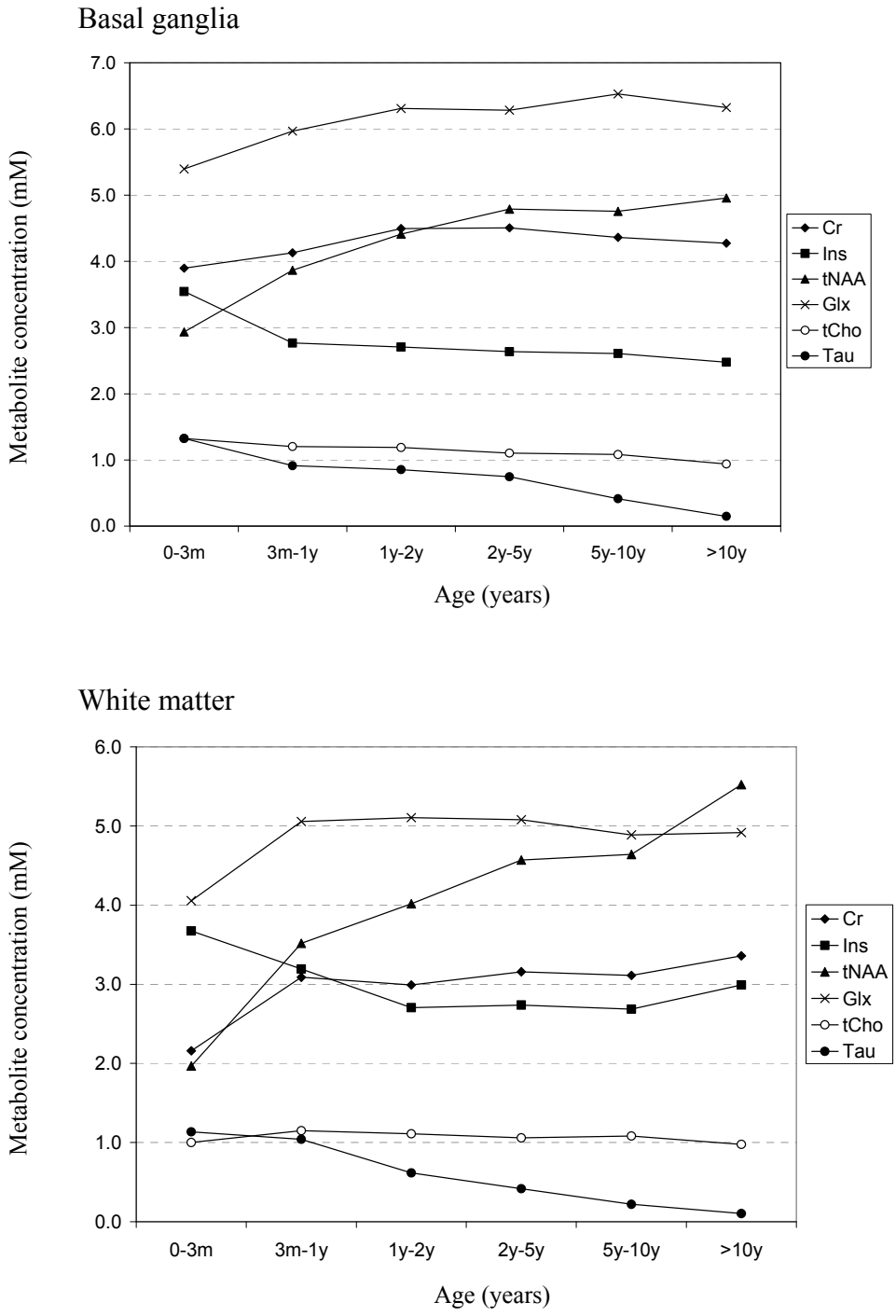

Figure 4.13: Line chart showing age variation in mean metabolite concentrations in basal ganglia (upper panel) and white matter (lower panel). (Here Glx represents Gln+Glu)

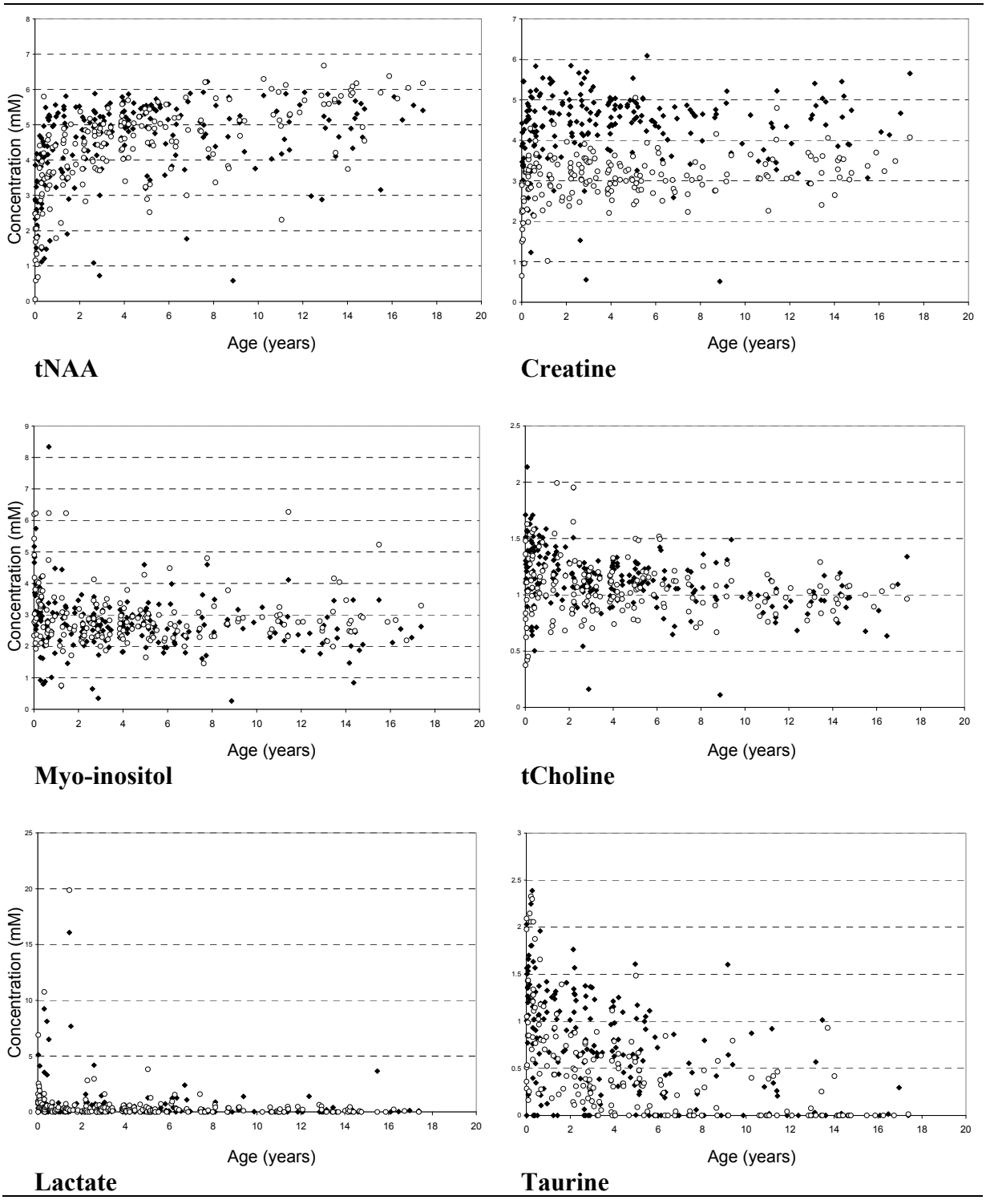

Figure 4.14: **(**see also next page) Scatter plots of concentration against age for each metabolite determined in basal ganglia (♦, n=215) and white matter (○, n=183).

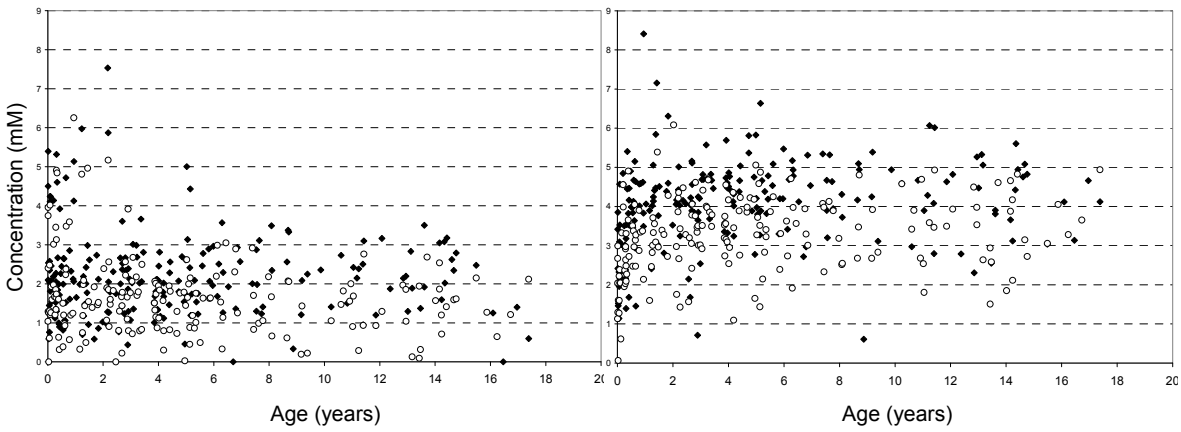

Glutamine **Glutamate**

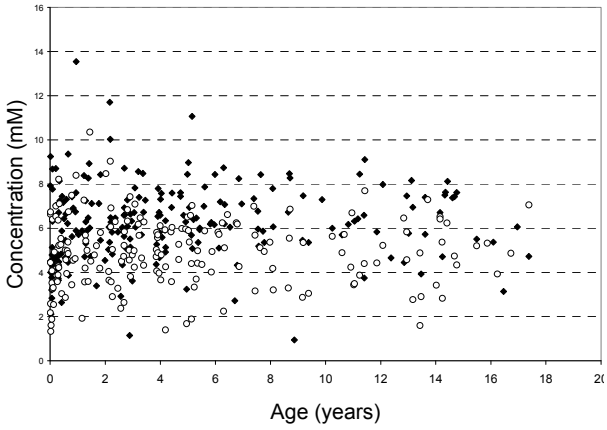

Glutamine+Glutamate

◆ **Basal ganglia**

○ **White matter**

X-axis: age (years)
Y-axis: metabolite concentration (mM)

Pearson coefficient for correlation between age and metabolite concentration

	Cr	Ins	tNAA	Gln+Glu	Gln	Glu	tCho	Tau
Basal ganglia	0.05	-0.18†	0.34†	0.09	-0.07	0.20†	-0.36†	-0.57†
White matter	0.30†	-0.07	0.62†	0.02	-0.19†	0.23†	-0.16*	-0.56†

Figure 4.14: (see also previous page) Scatter plots of concentration against age for each metabolite in basal ganglia (♦, n=215) and white matter (○, n=183). Correlation coefficients for age and metabolite concentration, *, $p<0.05$; †, $p<0.01$.

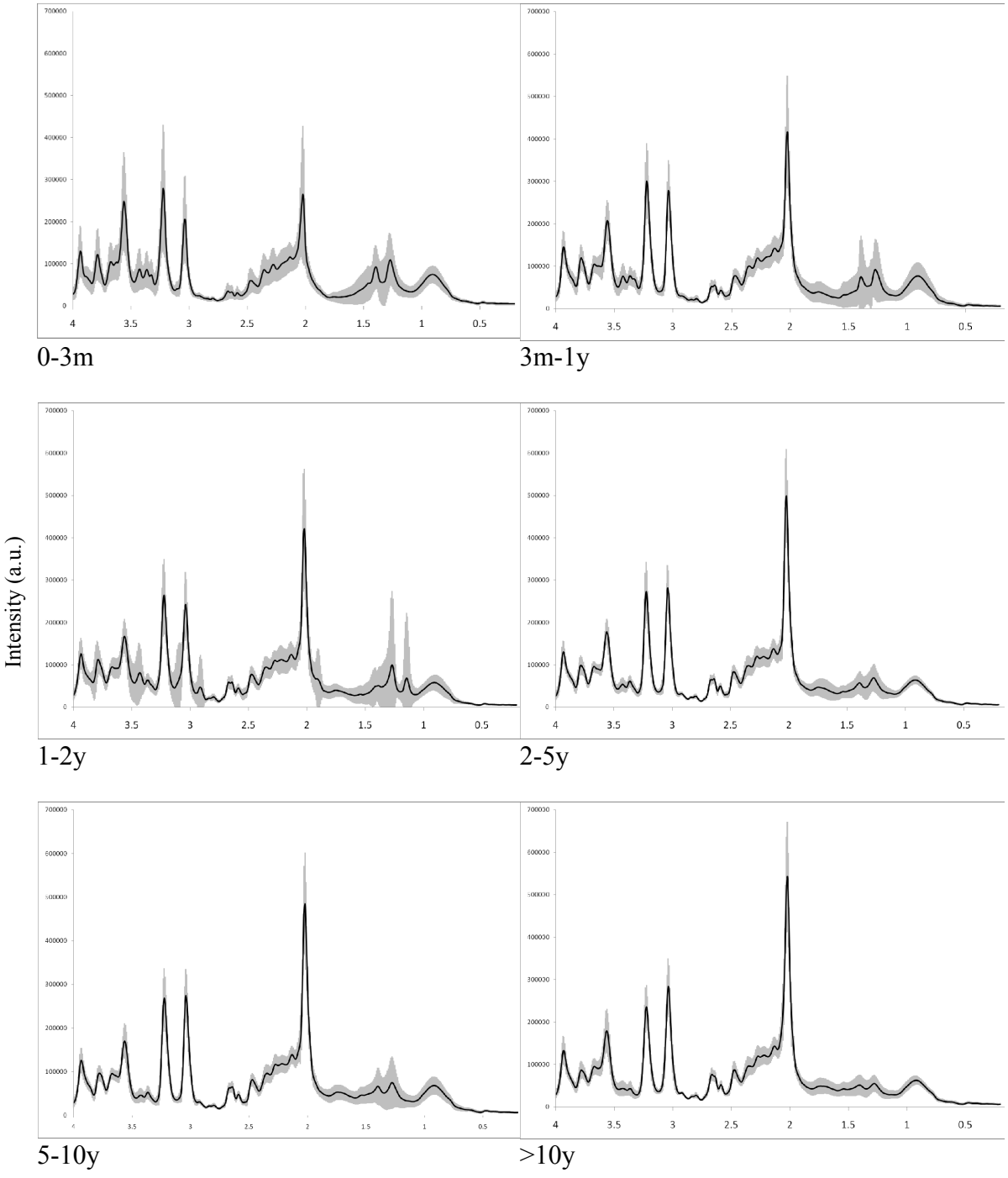

Figure 4.15: Mean spectra from white matter voxel for each age cohort. n=183. Shaded area indicates standard deviation.

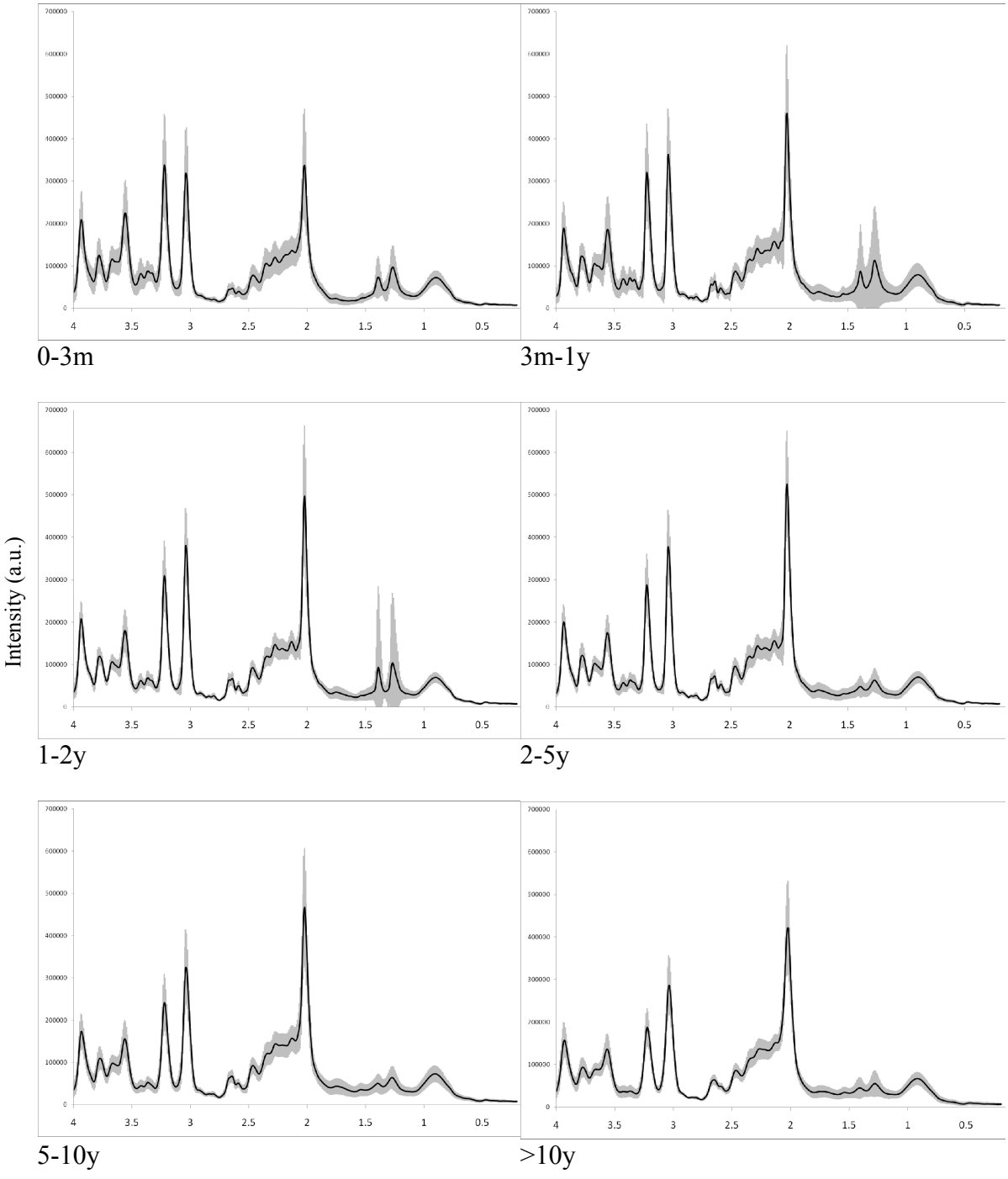

Figure 4.16: Mean spectra from basal ganglia voxel for each age cohort. n=215. Shaded area indicates standard deviation.

4.4. Metabolite statistical distributions

The typical distribution of concentrations was examined by generation of histograms for each metabolite and the skewness statistic calculated (SPSS v 17). The basal ganglia age variation dataset (n=215) was used for this analysis. It can be seen that the major metabolites detected by *in vivo* brain MRS approximate to a normal distribution, with skewness values within ±1.5 for Ins, Cr, Gln+Glu, tNAA, tCho, Gua, and Tau. The lower concentration metabolites tended to have substantial positive skews (e.g. lactate). The parametric statistical analyses applied in this thesis (including Student's t-test) assume normality of variables. The skewness values for the major metabolites here suggest that these tests can be validly applied to those metabolite variables.

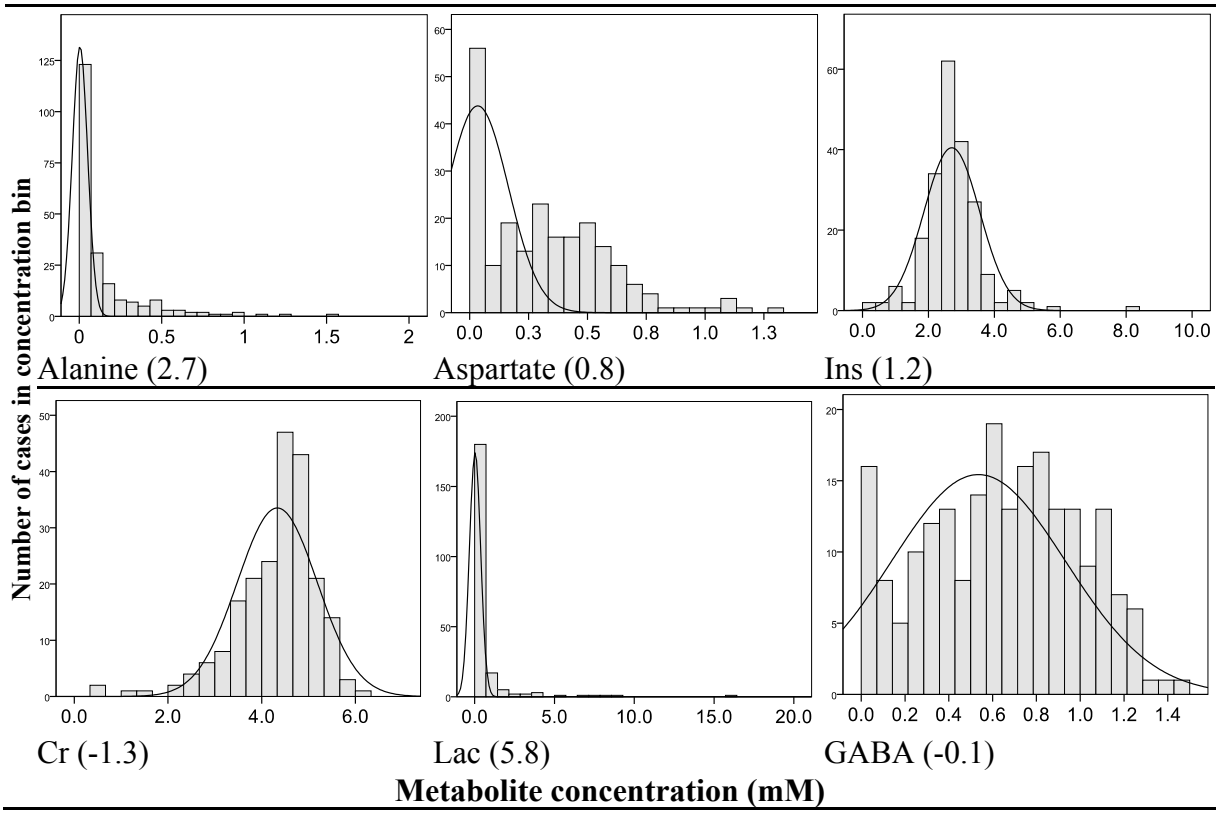

Figure 4.17: (See also next page) Histograms of metabolite concentration distribution in n=215 acquisitions from basal ganglia. Number in parentheses indicates skewness statistic.

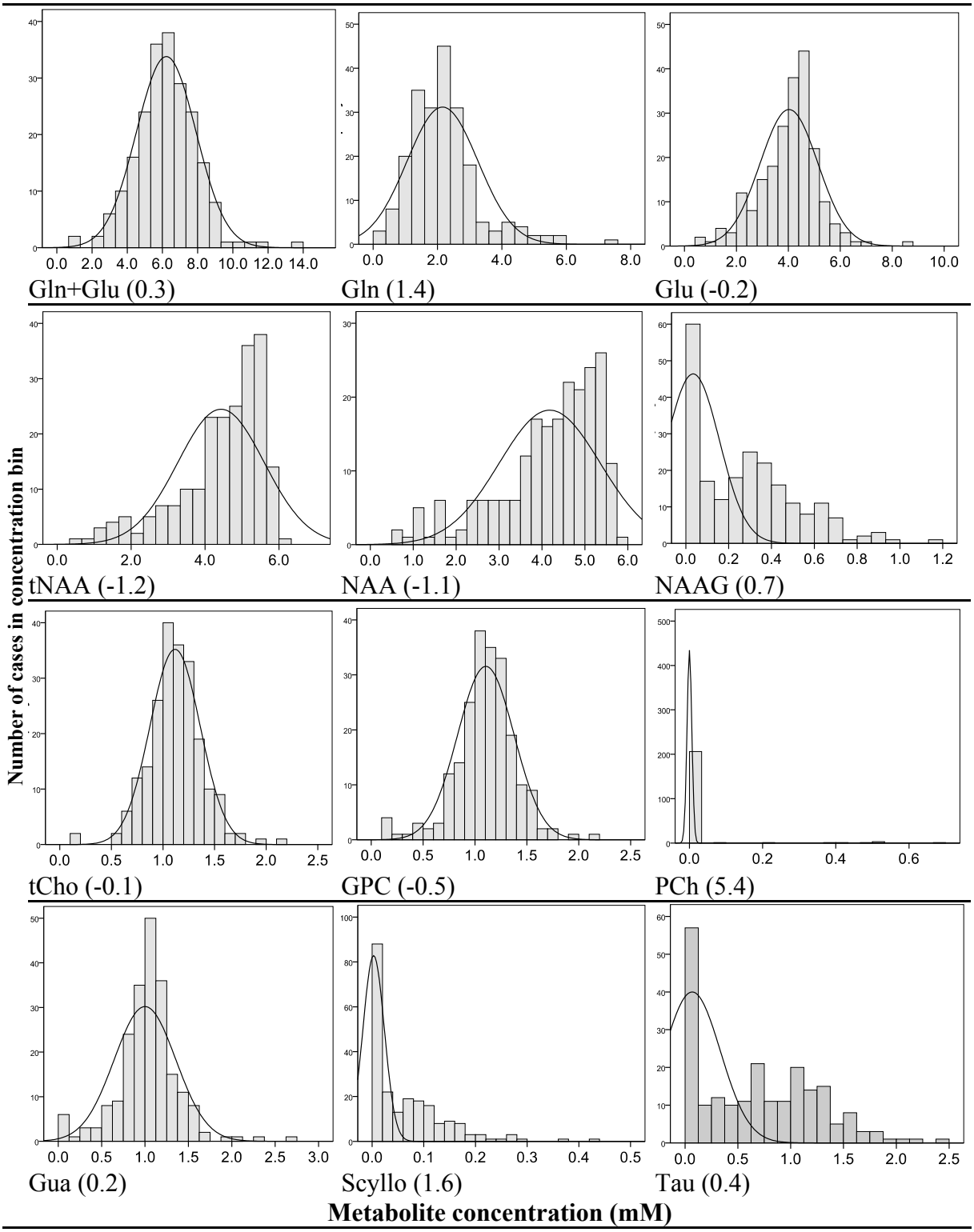

Figure 4.17: (see also previous page). Histograms of metabolite concentration distribution in n=215 acquisitions from basal ganglia. Number in parentheses indicates skewness statistic.

4.5. Comparator cohort generation

Analysis of MRS data from a single case or group of cases from a disease cohort of interest requires a normal control group to provide information about normal metabolite concentrations. Ideally this should be matched to the age profile of the cohort of interest, given the variability of metabolite concentrations with age. An initial comparator cohort was established using children over 6 months of age, as there is significantly less alteration in metabolite concentrations after this initial developmental period.

4.5.1. Cohort identification

In the absence of MRS data from a large cohort of "normal" children, interim alternative comparator cohorts were required. Indeed there is some merit in establishing normative data for the type of child that might be undergoing investigation by MRS, namely children with neurodegenerative or developmental delay-related symptoms. In order to establish a pseudo-normal control group, a sub-cohort of children was identified with normal neuroimaging, as established by assessment by consultant paediatric radiologist. All MRS studies included had passed the quality assessment analysis. Cases from children under 6 months of age were excluded at this stage, as the predominant age variation in metabolite concentrations was found in the group less than 6 months of age.

63 studies from basal ganglia in children aged over 6 months and 53 from white matter were identified. Metabolite and spectral data were extracted and mean (standard deviation) spectra and mean (standard deviation) metabolite values established (figures 4.18 and 4.19, table 4.3). To evaluate the effect of selecting cases with normal MR imaging features, comparison was made with mixed cohorts of children (over 6 months) with abnormal MR imaging (basal ganglia n=82, white matter n=68).

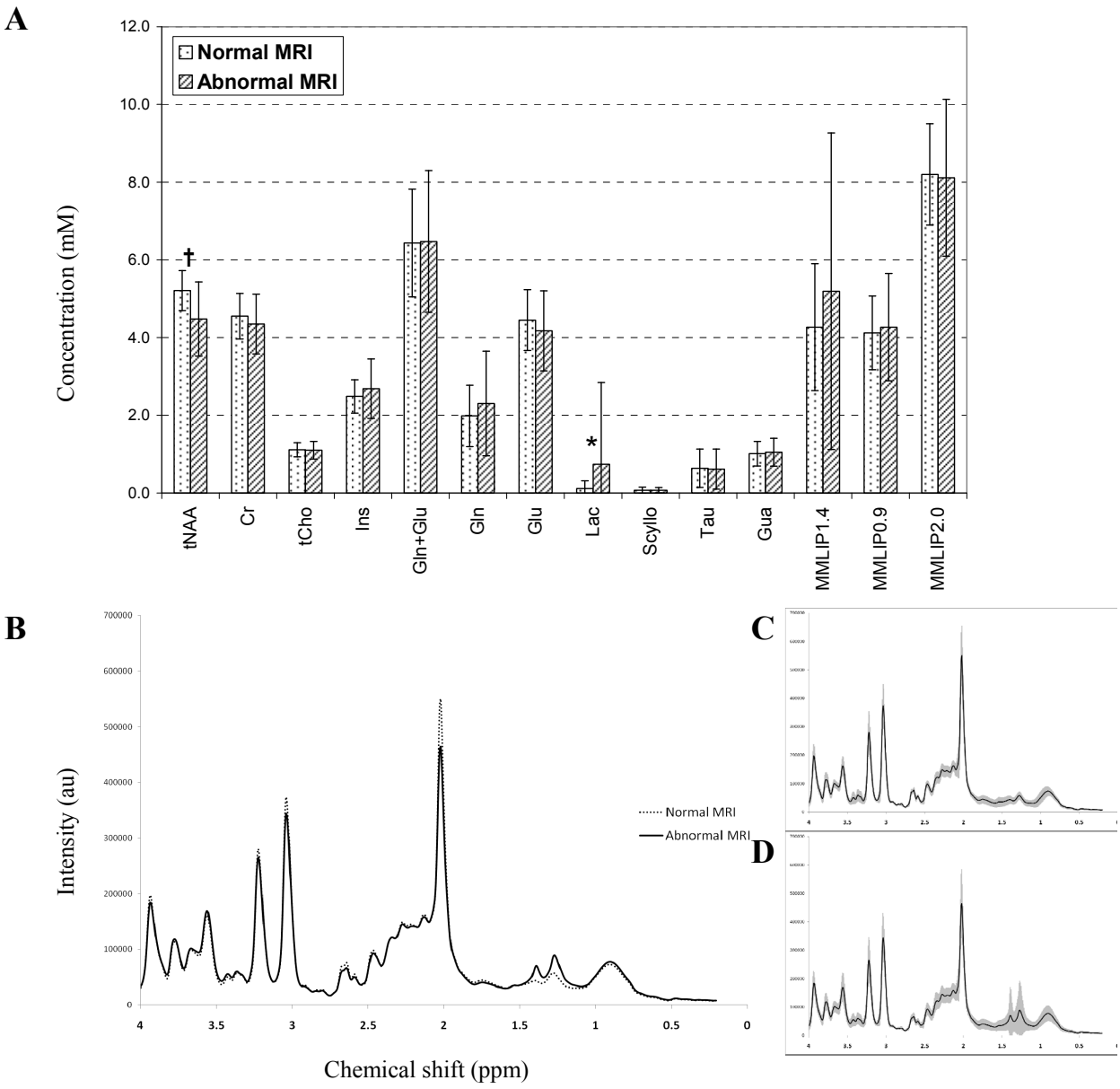

Figure 4.18: Basal ganglia data. (A) Bar chart showing mean metabolite concentrations (error bars – standard deviation) for normal and abnormal MRI cohorts. Between group unpaired t-test: * $p<0.05$, † $p<0.01$. (B) Mean spectra for normal and abnormal MRI cohorts. (C) Mean spectra (shaded area - standard deviation) of normal MRI cohort. (D) Mean spectrum (shaded area - standard deviation) of abnormal MRI cohort.

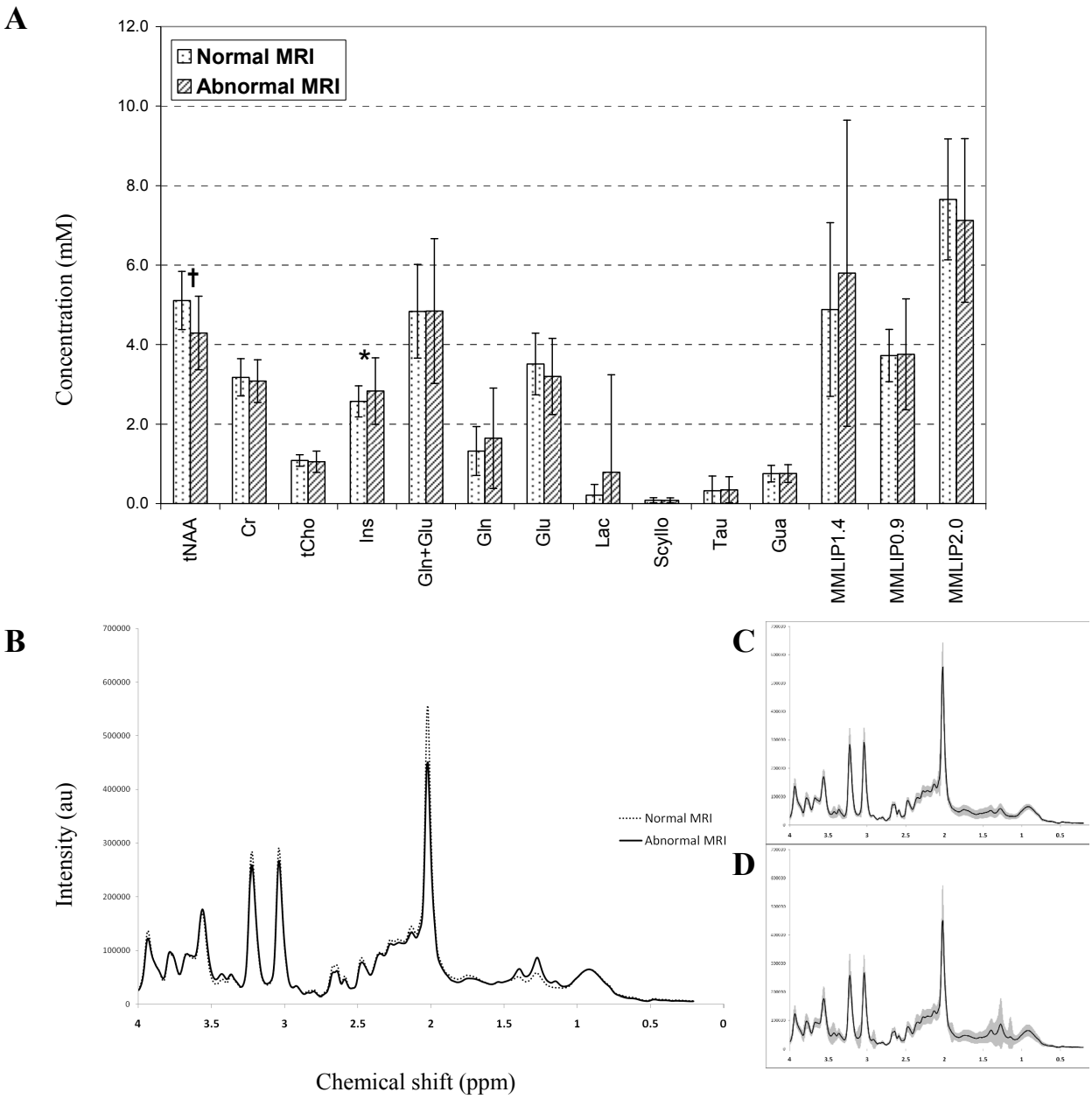

Figure 4.19: White matter data. (A) Bar chart showing mean metabolite concentrations (error bars – standard deviation) for normal and abnormal MRI cohorts (see text). Between group unpaired t-test: * $p<0.05$, † $p<0.01$. (B) Mean spectra for normal and abnormal MRI cohorts. (C) Mean spectra (shaded area - standard deviation) of normal MRI cohort. (D) Mean spectrum (shaded area - standard deviation) of abnormal MRI cohort.

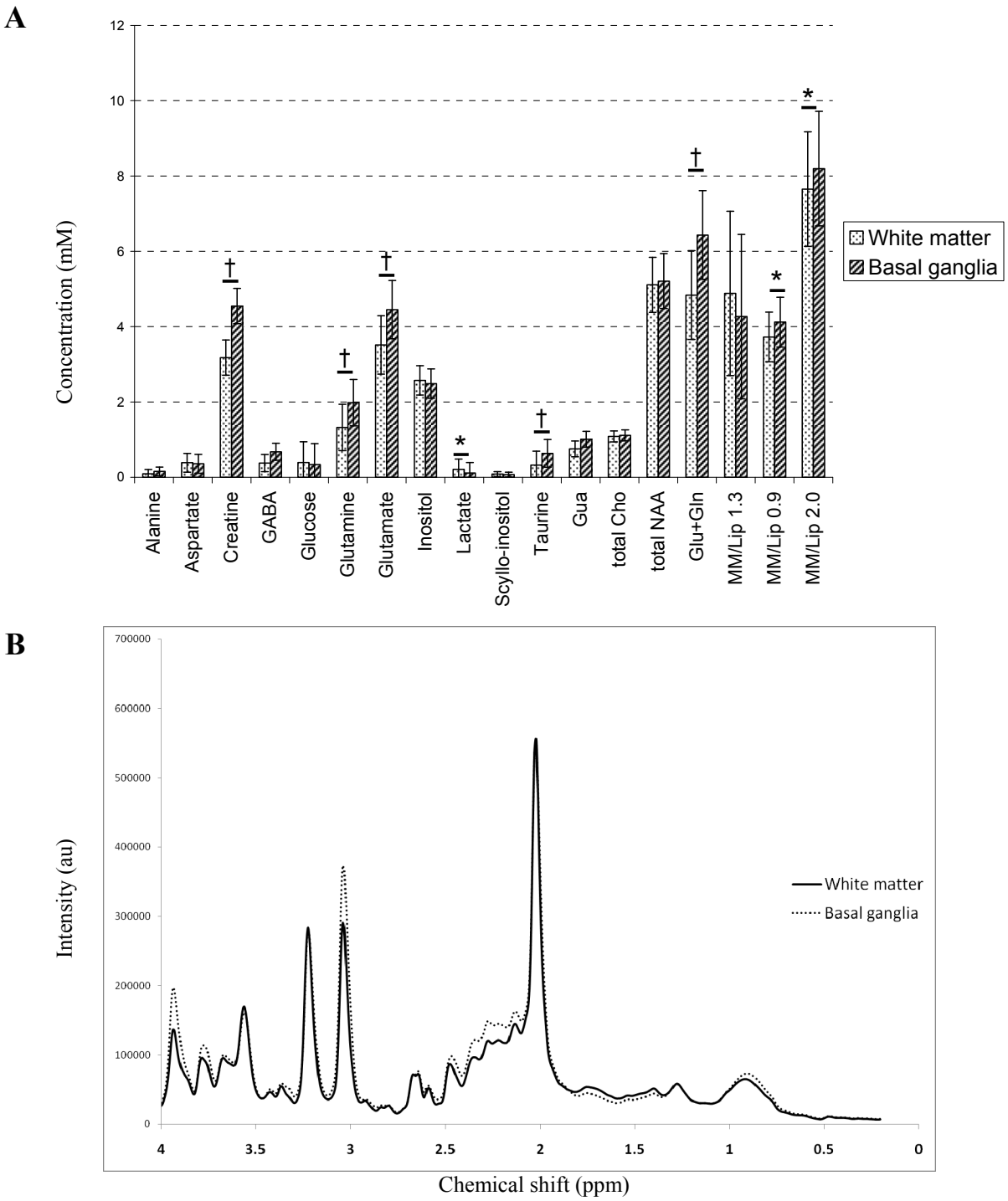

Figure 4.20: Comparison of normal MRI cohort spectra for white matter and basal ganglia. (A) Bar chart showing mean metabolite concentrations (error bars – standard deviation) for white matter and basal ganglia. Between group unpaired t-test: * $p<0.05$, † $p<0.01$. (B) Mean spectra for white matter and basal ganglia

	Basal ganglia			White matter			Normal MRI basal ganglia v white matter
	Normal MRI	Abnormal MRI	t-test p-val	Normal MRI	Abnormal MRI	t-test p-val	t-test p-val
n	63	82		53	68		
Age (y)	5.73 (4.69)	5.15 (3.58)	ns	6.23 (4.73)	5.76 (3.93)	ns	
tNAA	5.21 (0.51)	4.48 (0.95)	<0.001	5.11 (0.73)	4.29 (0.93)	<0.001	ns
Cr	4.55 (0.59)	4.35 (0.77)	ns	3.18 (0.47)	3.08 (0.54)	ns	<0.001
tCho	1.11 (0.18)	1.10 (0.23)	ns	1.08 (0.15)	1.05 (0.27)	ns	ns
Ins	2.49 (0.43)	2.68 (0.76)	ns	2.57 (0.39)	2.83 (0.84)	<0.05	ns
Gln+Glu	6.43 (1.39)	6.47 (1.82)	ns	4.84 (1.18)	4.84 (1.82)	ns	<0.001
Gln	1.98 (0.79)	2.31 (1.34)	ns	1.32 (0.62)	1.64 (1.26)	ns	<0.001
Glu	4.45 (0.78)	4.17 (1.03)	ns	3.51 (0.78)	3.20 (0.96)	ns	<0.001
Lac	0.11 (0.20)	0.74 (2.10)	<0.05	0.21 (0.28)	0.79 (2.45)	ns	<0.05
Scyllo	0.07 (0.08)	0.07 (0.07)	ns	0.09 (0.06)	0.08 (0.06)	ns	ns
Tau	0.63 (0.49)	0.61 (0.52)	ns	0.32 (0.37)	0.35 (0.33)	ns	<0.001
Gua	1.01 (0.32)	1.05 (0.36)	ns	0.75 (0.21)	0.76 (0.22)	ns	<0.001
MMLIP1.4	4.27 (1.63)	5.19 (4.07)	ns	4.88 (2.18)	5.80 (3.85)	ns	ns
MMLIP0.9	4.12 (0.95)	4.27 (1.38)	ns	3.73 (0.66)	3.75 (1.39)	ns	<0.05
MMLIP2.0	8.20 (1.30)	8.11 (2.02)	ns	7.65 (1.52)	7.12 (2.06)	ns	<0.05

Table 4.3: Mean metabolite values for basal ganglia and white matter in cohorts with normal and abnormal MR imaging. Difference between cohorts evaluated by Student's t-test.

4.5.2. Comparison of normal MRI and abnormal MRI cohort

Visual inspection of mean spectra (figures 4.18 and 4.19) revealed a lower NAA peak and elevated lactate in the abnormal MRI group for both basal ganglia and white matter. Comparison of the mean metabolite concentrations demonstrated significantly ($p<0.05$) lower tNAA and elevated lactate in basal ganglia of children with abnormal MR imaging. In white matter the tNAA was also significantly lower in the abnormal MRI group, and inositol was significantly elevated in the abnormal MRI group. There were no other statistically significant differences. Choline was consistent in all cohorts, and there were no significant differences in the lipid/macromolecular peaks in the normal and abnormal cohorts.

4.5.3. Comparison between anatomical regions

The two groups used to generate the normal MRI comparator groups for basal ganglia and white matter did not differ significantly in age. Significant differences in several metabolites were evident by visual inspection of the mean spectra (figure 4.20) and by formal analysis of the LCModel derived metabolite concentrations (table 4.3). Thus in basal ganglia there was higher creatine, taurine and guanidinoacetate. Glutamate+glutamine, glutamine and glutamate were also higher in basal ganglia. There were no significant differences in tNAA, choline or inositol between the two regions.

These regional differences correspond to previous studies that demonstrated significantly higher creatine, glutamine+glutamate and taurine in basal ganglia, and similar tNAA, choline and inositol levels in the two regions [67].

4.6. Discussion

The metabolite variations across anatomical regions seen in the current dataset are similar to those previously described, and the typical "normal" metabolite profiles generated are similar to other published normal control cohorts [67, 118]. However, the absolute concentrations for each metabolite were different to these other published normal cohorts, likely due to differences in MR scanners, acquisition parameters and post-processing techniques. This underlines the need for such factors to be accounted for when comparing data from multiple sources, and also in the future design of multicentre studies.

The standard deviation in the data on the spectra is relatively small, suggesting good reproducibility in the data collected across a large number of cases. Although the data for the

comparator cohorts is not from a strictly normal population since the majority of children had an MRI performed because of neurologic or developmental signs or symptoms, the selection of data from children with normal MRI features does provide a workable comparator cohort which has parameters consistent with those published elsewhere. Indeed, a similar approach to generating control datasets has been employed in other studies [118].

It should also be noted that although differences between the normal and abnormal MRI groups were seen, that many of the differences were relatively subtle and significantly less prominent that the alterations in the metabolite profile seen in MRS profiles from brain tumours and other lesions [76]. This emphasises the importance of using large cohorts of children and repeated sampling to validate observations of metabolite alterations, as well as the importance of removing as far as possible non-biological sources of variability within the data generated.

Chapter Five

5. The identification of non-standard brain metabolite peaks

The appearance in an MR spectrum of a metabolite peak not expected in normal brain can suggest specific metabolic disorders, as discussed in Chapter 2. Tools that estimate metabolite profiles by fitting a linear combination of known metabolite spectra rely on *a priori* assumptions of the metabolites that will be present in the spectrum, and thus unexpected metabolites will result in either distortion of the fitting of standard metabolites, or leave a large residual between the fitted and original data spectra [45]. LCModel has a standard metabolite basis set with 17 expected metabolites [44].

The MRS dataset acquired in this study was evaluated for the presence of such unfitted metabolite peaks, with the objective of identifying potential specific disease biomarkers or metabolites that give specific information about alterations in brain metabolites in known diseases.

5.1. Methods

5.1.1. Case identification

All MR spectra acquired were visually reviewed for the appearance of obvious unfitted peaks or significant baseline distortions that may suggest erroneous fitting due to the presence of an unfitted metabolite.

All MR spectra were also screened by plotting the residual signal remaining by subtraction of the LCModel fitted spectrum from the original data spectrum. Spectra with large residuals were further evaluated to determine whether the residual was due to low signal to noise ratio, appearance of technical artefact, or potentially from the presence of an unfitted peak.

5.1.2. Metabolite identification

Spectra that had potential unfitted peaks were further evaluated. Standard libraries were screened on the basis of the chemical shift of the unfitted peak, and sample experimental or predicted spectra for potential candidate metabolites examined [109].

In some cases, test solutions of candidate metabolites were prepared for one dimensional proton NMR spectroscopy using high field laboratory NMR spectrometers (see Chapter 3). MR spectra of the test solutions were also acquired using the clinical MR scanner to evaluate differences between the high field spectrometer and the clinical system.

5.2. Results

Potential unfitted metabolite peaks were identified in a small number (circa 2.3%) of children (table 5.1, figure 5.1). Several of the metabolites detected corresponded to the underlying metabolic defect in the child. Thus succinate was detected in a child subsequently found to have succinate dehydrogenase deficiency (see below); glycerol was detected in a child with glycerol kinase deficiency (see below); while glycine was detected in a child with non-ketotic hyperglycinaemia due to a novel *AMT* mutation and also in a neonate with an incompletely characterised fatty acid oxidation defect. Of these metabolites, the *in vivo* detection in brain of

glycerol has not been previously described. Elevated glycine may be a useful biomarker of malignancy in childhood brain tumours [45] and the identification in the IMD cohort benefitted from the availability of an extended LCModel basis set that included glycine parameters (see figure 5.1 E and F).

In some cases peaks were identified that appeared to be not due to artefact or low signal to noise ratio, but no specific metabolite identity was able to be assigned.

Peak Chemical shift (ppm)	Metabolite Identity	Seen at short echo time?	Seen at long echo time?	Metabolic Disease	OMIM reference
2.40	Succinate	Y	Y	Succinate dehydrogenase deficiency (*SDHB* mutation)	#252011 *185470
3.65	Glycerol	Y	N	Glycerol kinase deficiency	#307030
3.55	Glycine	N (Co-resonant with Inositol)	Y	Non-ketotic hyperglycinaemia (*AMT* mutation)	#605899
3.55	Glycine	N (Co-resonant with Inositol)	Y	Uncharacterised fatty acid oxidation defect	
2.25	?Acetone/ acetoacetate	Y	Y	Pyruvate carboxylase deficiency	#266150
1.9	?Acetate	Y	Y, inverted	Methylmalonic aciduria, Down's Syndrome	#190685 #251000
1.1, 1.2	Unidentified	Y	Y, inverted	Mitochondrial (*DGUOK* mutation)	#251880

Table 5.1: Non-standard brain metabolite peaks identified using MR spectroscopy.

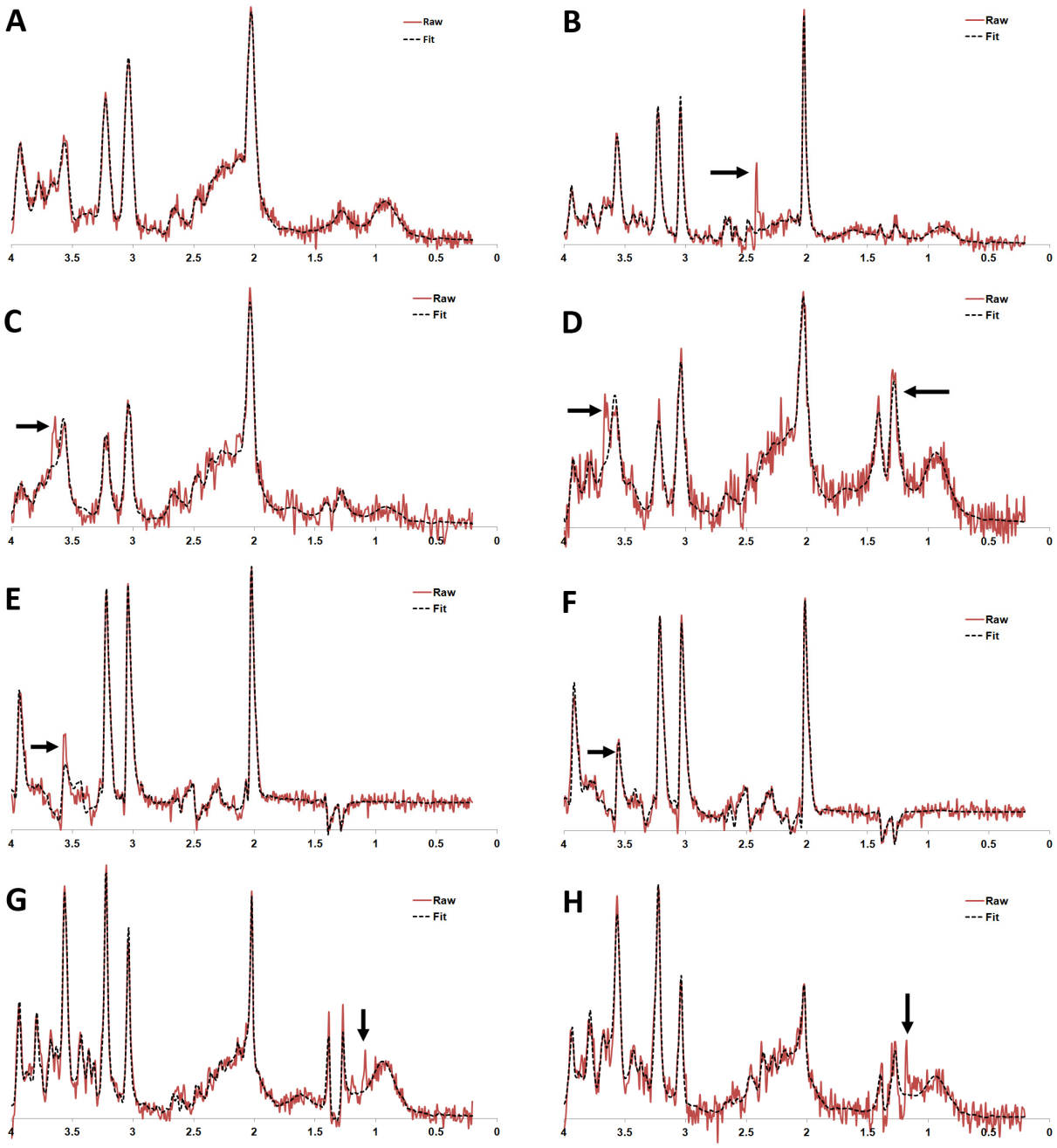

Figure 5.1: MR spectra showing peaks not accounted for by LCModel fit. (A) and (B): Short echo time (TE 30ms) spectra from (A) Basal ganglia and (B) white matter in child with succinate dehydrogenase deficiency giving rise to peak at 2.4ppm in white matter but not in basal ganglia consistent with succinate accumulation. Also note low glutamine+glutamate in white matter (B). (C) and (D): Short echo time (TE 30ms) spectra from child with glycerol kinase deficiency and pyruvate dehydrogenase deficiency giving rise to peak at ~3.6ppm seen before (C) and after bilateral basal ganglia stroke (D) when high lactate signal was seen. (E) and (F): Long echo time (TE 135ms) spectra from child with clinical Leigh-like syndrome showing prominent peak at 3.55ppm leading to over-fitting of inositol (E) but improved fitting when glycine parameters added to LCModel basis set (F). (G) and (H): Short echo time (TE 30ms) from two neonates with high lactate levels, with peaks identified of uncertain significance and identity at ~1.2ppm.

5.2.1. Succinate

5.2.1.1.Clinical Case Description

A female child was born at term to consanguineous Asian parents. Growth and developmental milestones were normal until one year of age by which time she could cruise around furniture and was babbling. Subsequently over a six week period she lost the ability to walk, and became unsteady and had repeated falls. There was no associated head injury or febrile illness. She became very hypotonic with poor head control and difficulty feeding. After the six week period of deterioration she made slow developmental progress, and by the age of four years she could stand briefly with support but was mainly wheelchair-bound. There were no further episodes of developmental regression, but by 6 years of age she remained wheelchair dependent, and had developed flexion contractures in arms and legs.

5.2.1.2.MRI and MRS

Magnetic resonance imaging acquired at the initial presentation and at four years of age (figure 5.2) revealed a leucodystrophy with extensive white matter signal changes in the deep cerebral white matter sparing U-fibres, with abnormalities also present in cerebellum and brainstem. MRS was acquired concurrently with the MRI scan at age 4 years (figure 5.2). The short echo time MR spectrum of the dystrophic white matter demonstrated the presence of a singlet peak at 2.4ppm, seen also at long echo time (not shown), not detected in the control group or in the normal appearing basal ganglia of the child. The MRS profile of the white matter also demonstrated significantly decreased glutamine and glutamate, relative preservation of N-acetylaspartate, and increased myo-inositol. The metabolite profile of the basal ganglia appeared normal with no succinate detected.

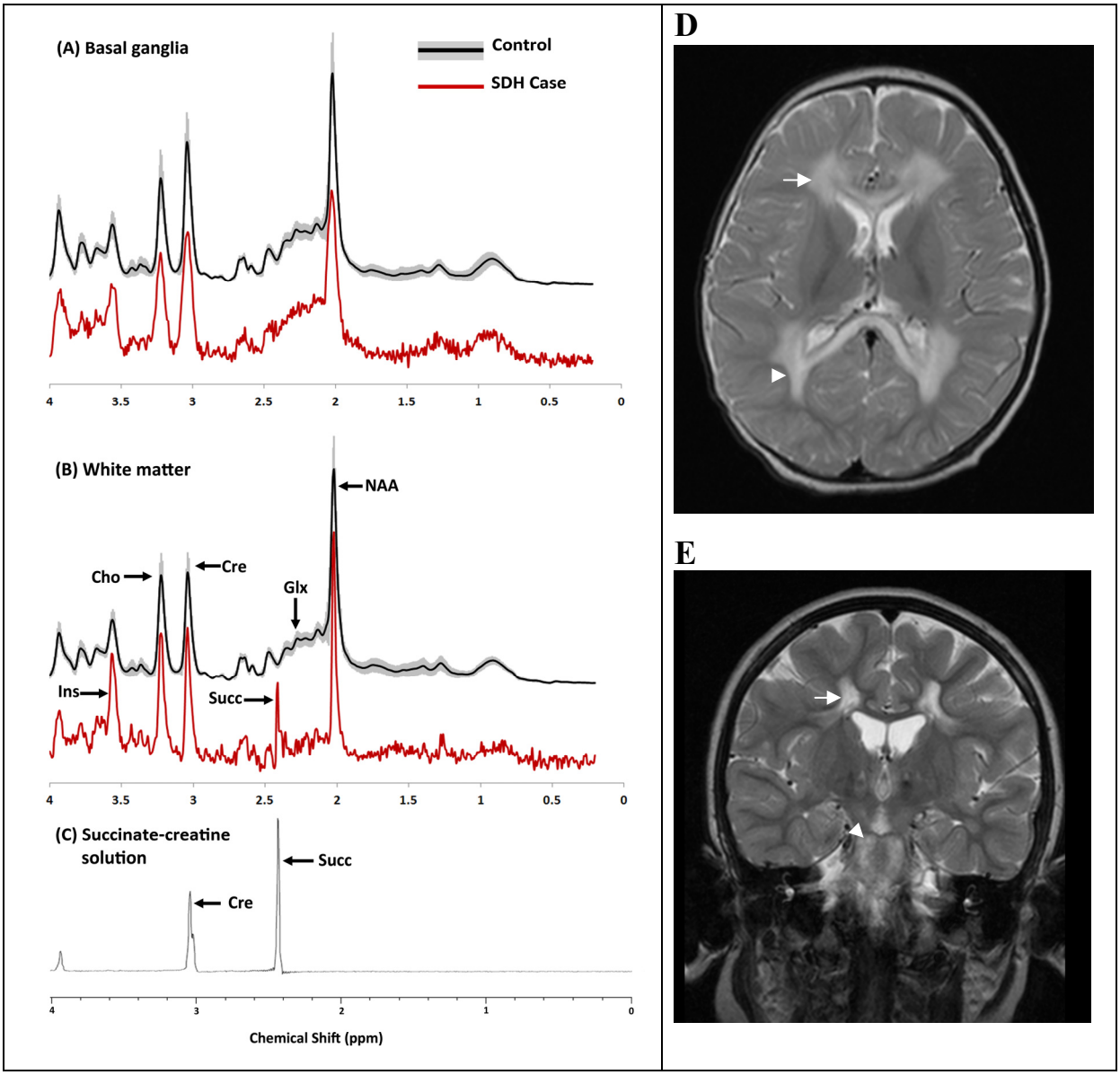

Figure 5.2: MR spectra and MR imaging from child with *SDHB* mutation. MR spectra (TE 30ms) from patient (red line) and control groups (mean, gray line; standard deviation, shaded area), from (A) basal ganglia, (B) white matter and (C) succinate-creatine solution. Major metabolite peaks: N-acetylaspartate, NAA; glutamine+glutamate, Glx; creatine, Cre; choline compounds, Cho; myo-inositol, Ins; succinate, Succ. Chemical shift (x) axis: parts per million, ppm. (D) T_2 weighted axial MR image at 1 year age demonstrating high signal intensity in white matter (arrow), sparing subcortical U-fibres (arrow head). Normal basal ganglia signal. (E) T_2 weighted coronal MR image at age 4.5 years demonstrating persistent high signal intensity in white matter with cystic degeneration, sparing subcortical U-fibres (arrow), and abnormal high signal in corticospinal tracts in pons (arrow head) and upper cervical cord.

5.2.1.3.Metabolite Peak Identification

By reference to a standard metabolite library the chemical shift of the observed peak was found to be consistent with that of succinate [109]. The molecular structure of succinate has four magnetically equivalent protons (figure 5.3) giving rise to a singlet resonance peak [36]. This was observed in the *in vivo* spectra at both short (TE 30ms) and long (TE 135ms) echo times.

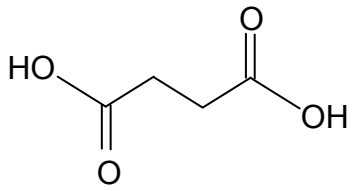

Figure 5.3: Structure of succinic acid

One dimensional proton NMR spectra of a test solution of succinic acid and creatine at various pH values were acquired as described (Chapter 3). The singlet resonance peak of succinate was observed at 2.4ppm at physiologically relevant pH; at more acidic pH the resonance moved further downfield (figure 5.4).

MR spectroscopy was also acquired from a 1L bottle of the test solution using the clinical MR scanner (pH 5.6). Identical parameters to that used for the *in vivo* MRS were used. Again, the singlet resonance peak of succinate was seen at 2.4ppm (figure 5.2C).

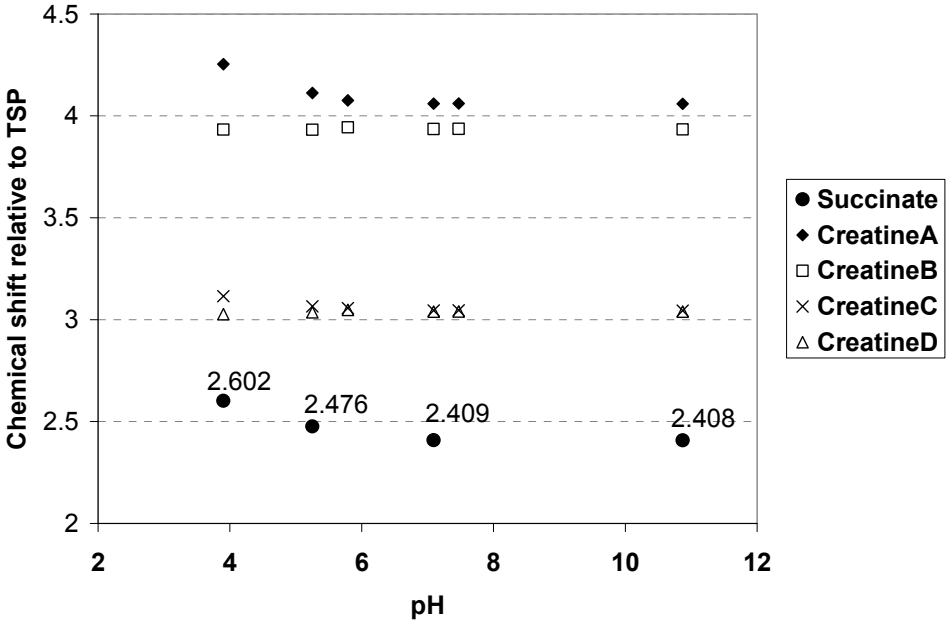

Figure 5.4: Plot of chemical shift of succinate and creatine peaks at varying pH, ascertained using 500MHz spectrometer.

5.2.1.4.Further Metabolic Investigations

An open rectus femoris muscle biopsy was obtained at 5 years of age (figure 5.5). This demonstrated decreased succinate dehydrogenase staining. Assay of mitochondrial respiratory chain complex activity demonstrated a marked decrease in Complex II (succinate dehydrogenase) activity (0.049 nmol DCPIP reduced /min (control mean 0.145). She has subsequently been found to have a novel homozygous mutation in *SDHB* (C.Alston and R.Taylor, Mitochondrial Research Group, Institute for Ageing and Health, Newcastle University, Newcastle upon Tyne, UK).

5.2.1.5.Case Discussion

The *in vivo* MRS demonstrated significant accumulation of succinate within abnormal brain regions, but not in a non-affected brain region. The identity of the succinate peak was suggested by its chemical shift consistent with published and experimental test solution data, and also consistent with the underlying enzyme defect subsequently demonstrated both

histochemically and by direct enzyme assay. The genetic basis for the disease was confirmed by identification of a novel homozygous *SDHB* mutation.

The detection *in vivo* of elevated brain succinate has been reported in three children previously with confirmed SDH enzyme deficiency [119], although not in a child with a genetically confirmed diagnosis, and represents a specific biomarker of SDH/complex II deficiency.

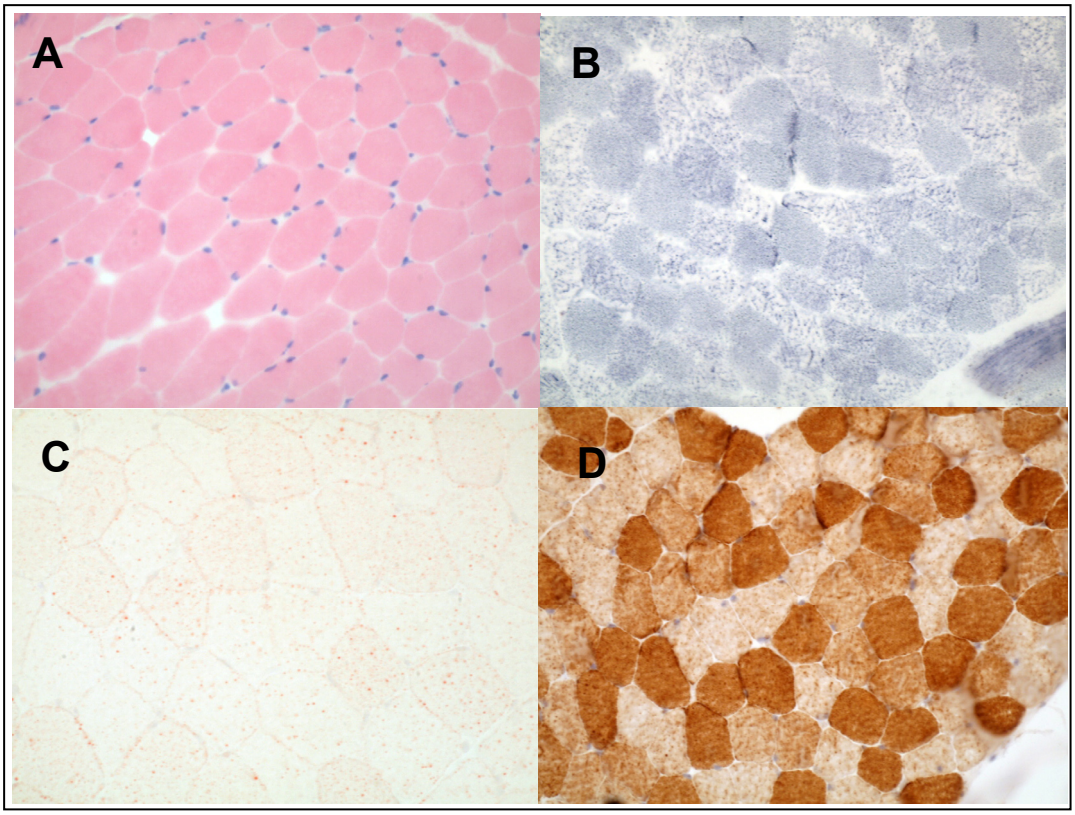

Figure 5.5: Skeletal muscle biopsy histology from child with *SDHB* mutation. (A) H&E stain: tightly packed uniformly sized muscle fibres. x40 magnification. (B) SDH stain: generalised decrease in staining. x40 magnification. (C) Oil Red O stain: very subtle increase in intrafibre lipid. x60 magnification. (D) COX stain: normal checkerboard pattern, no COX negative fibres x40 magnification (Images courtesy of Dr Marie-Anne Brundler).

5.2.2. Glycerol

5.2.2.1.Case description

A Caucasian male child was diagnosed with X-linked glycerol kinase deficiency (OMIM #307030) after the finding of pseudohypertriglyceridaemia during investigation following of an episode of hypoglycaemia. (The analytic method for quantification of blood triglycerides measures glycerol released by the action of lipase by a colorimetric method, thus hyperglycerolaemia gives a false high estimate of blood triglycerides). Blood glycerol was 1910 μmol/l (normal 61-232 μmol/l), and urinary glycerol was elevated. Fibroblast C14 glycerol incorporation studies demonstrated a marked deficiency. He was shown to be a hemizygote for the C256R gene mutation.

Following the symptomatic presentation of Leigh encephalopathy in his sibling, both children were also diagnosed with pyruvate dehydrogenase deficiency due to a defect of the E3 subunit (chromosome 7q31-q32).

5.2.2.2.MRI & MRS

MR imaging at age 15 years demonstrated tiny foci of high T_2 signal intensity in bilateral globus pallidi (figure 5.6). At 15 ½ years he suffered an extensive metabolic stroke following an influenza-like illness (figure 5.6) necessitating palliative care.

MRS was acquired with both MRI studies from the basal ganglia, demonstrating the presence of an unfitted peak just downfield of the inositol peak (figure 5.1C and D) at circa 3.65ppm. There was also substantial elevation of lactate demonstrated in the second MRS study following the stroke.

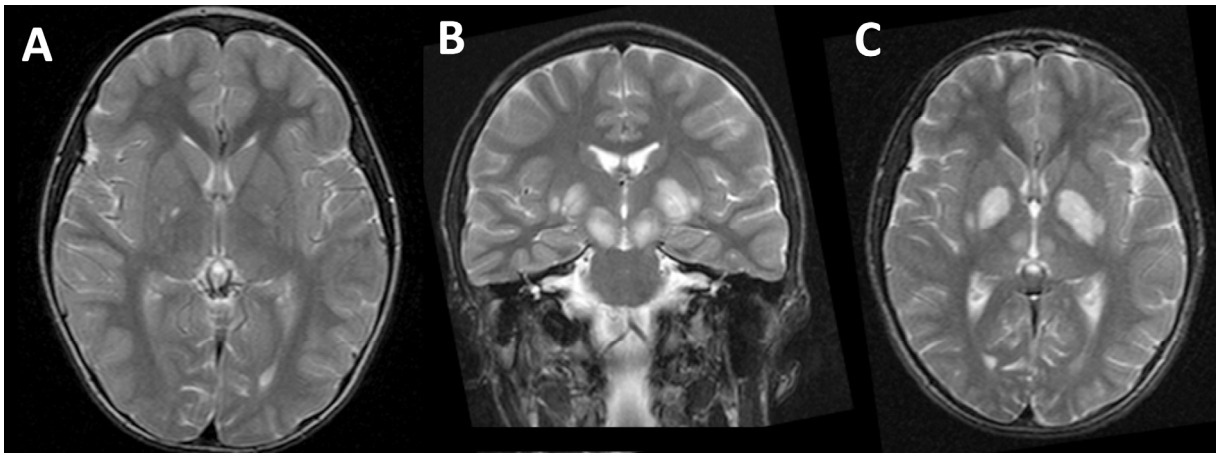

Figure 5.6: T_2-weighted images from child with glycerol kinase deficiency and pyruvate dehydrogenase deficiency. (A) Axial view at age 15 years. (B) Coronal and (C) axial views at age 15 ½ years following metabolic stroke. Note high T_2 signal in bilateral basal ganglia

5.2.2.3.Metabolite Peak Identification

By reference to a standard metabolite library the chemical shift of the observed peak was found to be consistent with that of glycerol [109]. The molecular structure of glycerol has five spins from two equivalent methylene groups and a single CH proton (figure 5.7) giving rise to resonances centred at 3.55 and 3.65ppm [36].

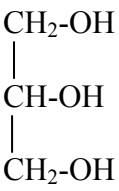

Figure 5.7: Structure of glycerol

One dimensional proton NMR spectra of the glycerol-creatine test solution was acquired as described (Chapter 3). The multiplet resonances of glycerol were seen centred at 3.55 and 3.65ppm (figure 5.8). MR spectroscopy was also acquired from a 1L bottle of the test solution using the clinical MR scanner. Identical parameters to that used for the *in vivo* MRS were used. The glycerol resonances were seen as a broad peak at around 3.6-3.62ppm (figure 5.9).

As seen in figure 5.9, automated fitting software partially accounted for the glycerol peak by fitting inositol.

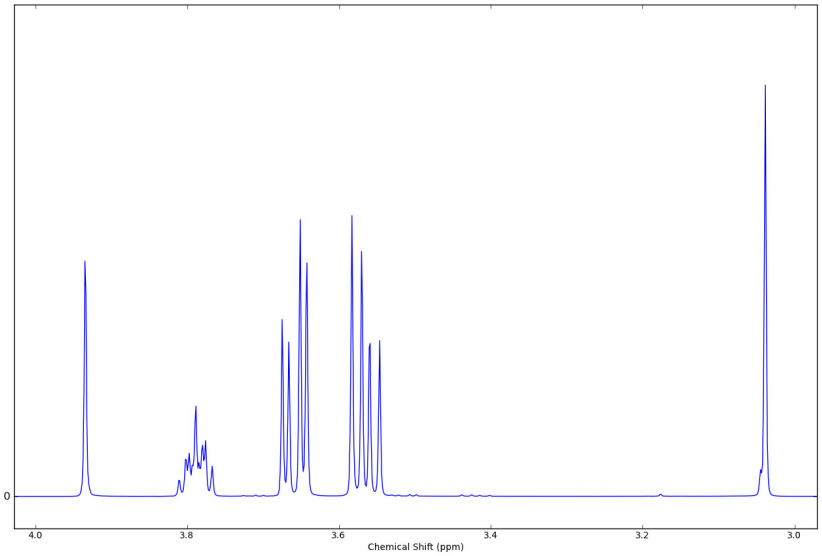

Figure 5.8: Proton NMR spectrum of glycerol and creatine test solution acquired on 500MHz spectrometer. Spectral region 3.0-4.0ppm shown only.

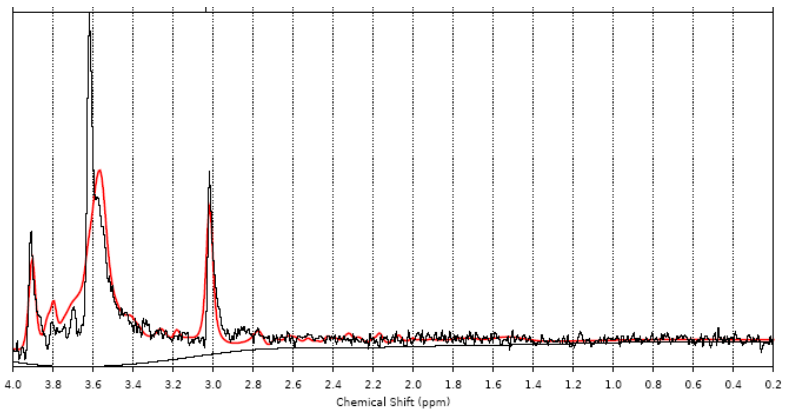

Figure 5.9: TARQUIN fitting of glycerol-creatine test solution spectroscopy acquired on 1.5T clinical MR scanner. Creatine peaks seen at 3.0 and 3.9ppm; broad peak centred at 3.6-3.62 from glycerol, partially fitted as inositol.

5.2.2.4.Case Discussion

Glycerol is not observed in MRS from normal brain, probably because it is embedded in membrane phospholipids and therefore has restricted rotational mobility, but has been

detected in *post mortem* brain homogenates [36]. The detection *in vivo* of elevated brain glycerol has not previously been reported.

Glycerol kinase deficiency usually presents with hypoglycaemic episodes in childhood but may not present until adulthood [120]. Beyond secondary effects of hypoglycaemia it is not usually associated with brain pathology. The case described here is complicated by the presence of a second disease, pyruvate dehydrogenase deficiency, which often results in a Leigh-like syndrome as encountered in this patient. Thus the clinical relevance of the elevated brain glycerol demonstrated is uncertain, although it is possible that these two energy metabolism disorders may have had synergistic pathological effects.

5.3. Discussion

Unfitted metabolite peaks were identified in only a small number of cases in the current cohort (circa 2.3%). In several children, however, the metabolites detected related directly to the underlying metabolic disorder and contributed significantly to the diagnostic process.

The putative identification of unfitted metabolite peaks described here relied on a combination of chemical shift libraries and evaluation of test solutions of potential metabolites using high field and clinical magnet spectroscopy. The certain identification of metabolite peaks may also be aided by analysis of body fluid samples from patients, as has been demonstrated for several disorders including adenylosuccinate lyase deficiency [98], while in brain tumour studies it has been possible to correlate *in vivo* spectroscopy with high resolution magic angle spinning spectroscopy of *ex vivo* tissue samples [29]. In the cases described here CSF samples were not available for NMR spectroscopy, although the children

with high glycine on brain MRS also had elevated CSF glycine on routine clinical testing. The putative assignment of metabolite identities described here is supported by the direct correlation to the underlying metabolic disorder.

In clinical practice the identification of unexpected metabolites in MR spectra would rely initially on clinical radiologists recognising their presence, and thus dissemination of information about these rare but potentially clinically very useful findings will be important. For some of the metabolites discussed here, such as glycine, post-processing steps would likely be required to distinguish the presence of the metabolite from other metabolite peaks in close proximity.

Chapter Six

6. Mucopolysaccharidosis Type II (Hunter Syndrome)

In this chapter, the use of MR spectroscopy in monitoring disease progression in Hunter Syndrome is evaluated. The initial baseline MRS data presented in this chapter have been published in the *Journal of Inherited Metabolic Disease* 2010 (see Appendix B) [121].

6.1. Introduction to lysosomal storage disorders

The lysosomal storage disorders (LSD) are caused by defects within the endosomal-lysosomal system, resulting in the abnormal accumulation of products that are normally degraded by the lysosomal system (figure 6.1). The endosomal-lysosomal system is responsible for the trafficking and recycling or degradation of internalised materials including endocytosed signalling molecules (e.g. hormones, neurotransmitters), phagocytosed bacteria or pinocytosed extracellular fluid. The lysosomes, which appear as "dense bodies" on electron microscopy, characteristically have a low acidic pH and contain enzymes that function optimally in an acidic environment [122]. Many LSD are caused by deficiency of the acidic enzymes, but defects at several other points with the endosomal-lysosomal system also result in LSD. This includes defects of protective or activator proteins within the lysosome; abnormalities of processing of lysosomal enzymes within the endoplasmic reticulum (e.g. multiple sulfatase deficiency, OMIM #272200); and failure of mannose-6-phosphate receptor

addition resulting in defective trafficking of correctly synthesised enzymes to the lysosome (e.g. I-cell disease, OMIM #252500) [123].

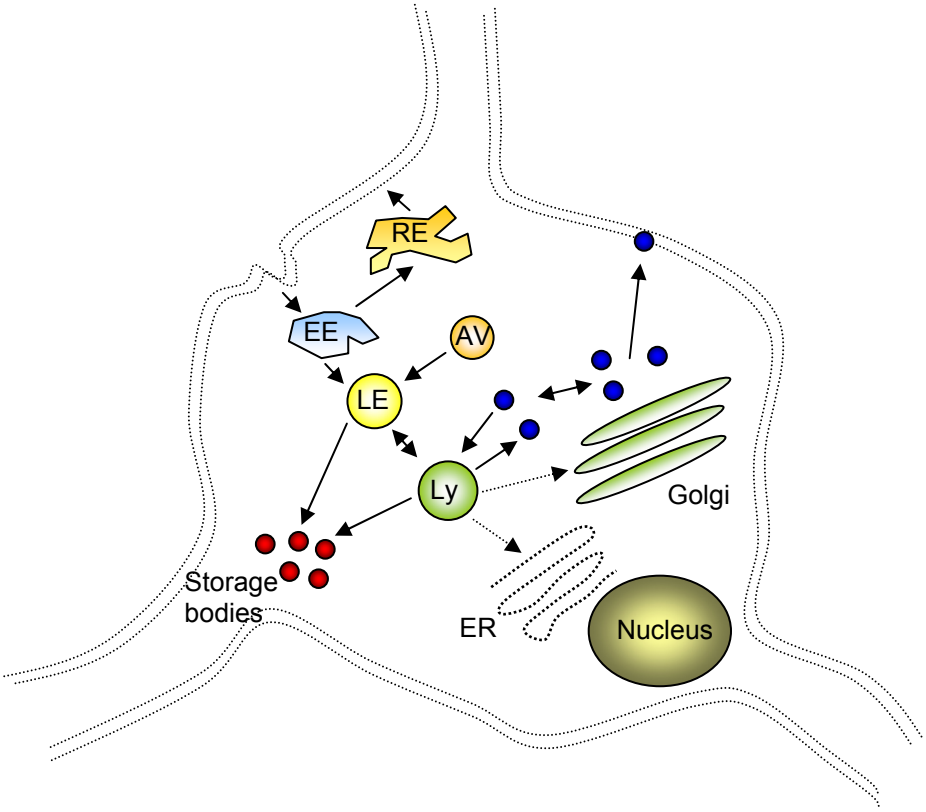

Figure 6.1: The endosomal – lysosomal system**. (**Early endosome, EE; recycling endosome, RE; late endosome, LE; lysosome, Ly; endoplasmic reticulum, ER; autophagic vesicle, AV; Adapted from [123]).

6.2. Introduction to the Mucopolysaccharidoses

The mucopolysaccharidoses (MPS) are a subset of the LSD characterised by the lysosomal accumulation of glycosaminoglycans (GAGs, also known as mucopolysaccharides), which are normal components of connective tissues and widely expressed in the CNS with a variety of functions [124]. Proposed diverse GAG functions in the CNS include roles in cell-cell interactions, axon growth and targeting, neurogenesis and dendrite maturation [124]. GAGs are polysaccharides formed of uronic acid and hexosamine residues that are degraded within

the lysosomal system, a process requiring a number of acid hydrolases including sulfatases, exoglycosidases, transferases and endoglycosidases [125]. The deficiency of these enzymes results in the specific MPS disorders [126]. The main classes of GAGs are the heparan, dermatan, chondroitin and keratan sulfates and hyaluronic acid, which accumulate depending on the specific enzyme defect in the different MPS disorders (table 6.1).

The MPS are progressive multisystem disorders, characterised by typical "coarse" facial appearances, skeletal dysplasia (dysostosis multiplex), organomegaly, cardiorespiratory compromise and neurological deterioration in several of the disorders [126].

Disease	Name	Deficient Enzyme	Stored material	Chromosome locus
MPS I	Hurler/Scheie	Iduronidase	DS, HS	4p16.3
MPS II	Hunter	Iduronate-2-sulfatase	DS, HS	Xq27-28
MPS III	Sanfilippo			
	IIIA	Heparan-N-sulfatase	HS	17q25.3
	IIIB	N-acetyl-glucosaminidase	HS	17q.21.1
	IIIC	Acetyl CoA glucosamine N-acetyl transferase	HS	?
	IIID	N-acetyl-glucosamine-6-sulfatase	HS	12q14
MPSIV	Morquio			
	IVA	N-Acetylglucosamine-6-sulfatase	KS	16q24
	IVB	β-Galactosidase	KS	3p21-pter
MPSVI	Maroteaux-Lamy	N-Acetylgalactosamine-4-sulfatase	DS	
MPSVII	Sly	β-Glucuronidase	HS,DS	
MPS IX		Hyaluronidase	HA	

Table 6.1: The mucopolysaccharidoses: enzyme defect, storage material and chromosome locus. Dermatan sulfate, DS; heparan sulfate, HS; keratan sulfate, KS; hyaluronic acid, HA. (Adapted from [126]).

6.3. Mucopolysaccharidosis type II (Hunter Syndrome)

Mucopolysaccharidosis type II (MPS II; Hunter syndrome; OMIM #309900) is an X-linked MPS caused by deficiency of the lysosomal enzyme iduronate-2-sulfatase (I2S, EC 3.1.6.13) [127]. Iduronate-2-sulfatase is encoded by the *IDS* gene located at Xq27-28. MPS II is characterised by intra-lysosomal accumulation of dermatan and heparan sulfates in most organ systems, with expected mortality if untreated in the second decade of life [128]. MPS II has an estimated prevalence of around 1 in 150,000 live births, predominantly affecting males although female cases have been reported [129].

The diagnosis of MPS II is based on the analysis of urinary GAGs, with confirmation by assay of I2S enzyme activity in leukocytes, fibroblasts or plasma (multiple sulfatase deficiency should be excluded). Molecular genetic studies may also be undertaken [129]. In excess of 300 different mutations in *IDS* have been reported [127], including gene single point mutations, whole/partial deletions and gene rearrangements. In the context of significant gene disruption resulting in complete absence of enzyme activity, the phenotype is usually severe, however there is significant phenotypic variation in the context of preserved enzyme activity [127].

6.3.1. Central Nervous System Disease in MPS II

Data from the Hunter Outcome Survey (HOS) suggest that cognitive involvement is indicative of more severe disease and a lower life expectancy [130]. This dichotomy between a “severe” and an “attenuated” phenotype was confirmed in a recent neurocognitive study of 50 male patients [131]. Around 2/3 of patients manifest the severe phenotype [132]. Patients who are likely to progress to the severe phenotype usually present at an earlier age, and during

follow-up will develop progressive signs and symptoms of CNS involvement with progressive intellectual deterioration [133]. The measured enzyme activity level does not correspond to the clinical phenotype [129, 131], and other biomarkers including urinary GAG concentrations, and the heparin cofactor-II thrombin complex do not correspond well to disease severity [129]. It has been suggested that early clinical markers of CNS involvement can be identified that could potentially identify patients who could benefit from brain targeted therapies. These clinical markers included sleep disturbance, increased activity, behaviour difficulties, seizure-like activity, chewing behaviour, and failure to achieve bowel and bladder training [134]. These clinical parameters are, however, non-specific and may not accurately predict the likely disease trajectory. Indeed, no well-validated severity scoring system has yet been produced [129] and remains an important research goal, particularly given the need to appraise the efficacy of novel brain-targeted therapies.

Central neurological involvement manifests with behavioural problems (50%), seizure disorders (39%), sensorineural hearing loss (45%), and progressive cognitive decline (32%) [130]. The cellular pathogenesis of CNS involvement in MPS II and other MPS disorders is however not well elucidated. For the LSDs in general Walkley has proposed that defective function of the endosomal-lysosomal system results in

"...a host of downstream or cascade events, which take time to accrue, [and] is the ultimate cause of cell and organ dysfunction. Importantly, this finding offers a glimmer of hope that if corrective measures could be taken to intervene early in the disease process, significant neurological dysfunction might be prevented." [124]

This cascade of events may affect intrinsic cell function, and also affect cell-cell interactions. Potential mechanisms include loss of function of the parent molecule being degraded, depletion of a product of the degradative process used in downstream synthesis, secondary disruption of the normal function of the endosomal-lysosomal system and its roles in signal transduction, and direct toxicity of the sequestered material e.g. psychosine in Krabbe disease [124]. It has also been noted that the storage material is not restricted to the primary compound acted upon by the (defective) enzyme, but that secondary storage of other compounds may also occur. Thus in the MPS disorders there is evidence for the accumulation of GM2 and GM3 gangliosides and unesterified cholesterol [135] in addition to the primary GAG. These secondarily stored compounds may then result in cascades of events common to disorders accumulating those products.

Neuropathological studies in MPS II have demonstrated brain atrophy, cortical neuronal and Purkinje cell dendritic swelling due to storage material, enlarged perivascular spaces and decreased white matter density without significant gliosis [136]. This study did not detect significant neuronal loss in the basal ganglia, thalami or other deep gray nuclei.

6.3.2. Limitations of current disease modifying therapies in MPS II

Enzyme replacement therapy (ERT) with recombinant iduronate-2-sulfatase is clinically available (idursulfase, Elaprase®; Shire Human Genetic Therapies, Inc., Cambridge, MA, USA) [128, 132, 137, 138]. This is administered by regular (weekly) intravenous infusions, and utilises the mannose-6-phosphate receptor system to target the enzyme to the lysosomal compartment (the principle of "cross-correction"). A recent Cochrane Review concluded that evidence for the efficacy of the ERT was limited, restricted to improvements in *"functional*

capacity (distance walked in six minutes and forced vital capacity), liver and spleen volumes and urine glycosaminoglycan excretion in patients with mucopolysaccharidosis type II compared with placebo" [139]. The clinical relevance of these endpoint measurements has been questioned [140].

While ERT results in improvement to systemic features idursulfase does not cross the blood brain barrier and so is not anticipated to alter the CNS pathology, nor the cognitive or behavioural manifestations of the disease [129]. That said, ERT may provide benefit to patients with the severe phenotype by improving systemic manifestations [129, 132]. A recent small case series reported that MRI features may stabilise or improve in children receiving ERT in MPS I and II, however this study did not include control data [141].

The existence of insulatory layers around the CNS provides the effective isolation required for reliable neuronal electrochemical signalling. This isolation is achieved by the blood-brain barrier formed by capillary endothelial cells, the blood-cerebrospinal fluid barrier formed by the choroid plexus epithelia, and the avascular arachnoid epithelium beneath the dura mater that effectively encloses the CNS and so isolates the extracellular fluids of the CNS from the remainder of the body [142]. The function of this multi-component barrier is achieved by physical tight junctions, transport mechanisms and metabolic mechanisms [142]. Macromolecules including proteins can not cross the barrier, and indeed many serum proteins are deleterious if they enter the CNS. Furthermore mechanisms exist, including the presence in the CSF of protease inhibitors, to deal with "micro-leaks" of proteins in to the CNS [142].

This poses a significant challenge for the delivery of large molecule therapies to the CNS in neurodegenerative diseases such as MPS II. Various brain-targeted approaches have been attempted in pre-clinical studies including the use of fusion proteins, encapsulation techniques (liposomal delivery), and nanoparticle systems that attempt to overcome the blood brain barrier by utilising its various transport mechanisms [143]. The direct application of large molecule therapies to the CNS has been attempted by intraventricular injection or via the intrathecal route. Intrathecal injection of radio-iodine labelled recombinant idursulfase to canine and nonhuman primates has been shown to result in widespread enzyme distribution throughout the CNS including specifically in the lysosomal compartment, and furthermore in a murine model of MPS II this technique resulted in a reduction in storage of glycosaminoglycans in the brain [143]. A phase I/II clinical trial is currently evaluating the safety of intrathecal idursulfase in human subjects (Shire Human Genetic Therapies, Inc., Cambridge, MA, USA; US National Institutes of Health clinical trials register (www.clinicaltrial.gov) reference NCT00920647). The primary endpoint of this trial is drug safety, but a number of CSF and other biofluid biomarkers are also being evaluated to assess the effect of the therapy.

6.3.3. MR Imaging Features and Monitoring of MPS II

Typical MR imaging findings in MPS II include progressive brain atrophy, white matter lesions which correlate to disease duration [144], dilated perivascular spaces (PVS), progressive ventriculomegaly and hydrocephalus. In a large cross-sectional and longitudinal study of 36 Italian MPS II patients (14 with the attenuated form and 22 the severe form) MRI findings that correlated with the severe phenotype included white matter abnormalities (97%), third ventricular dilatation (100%), and cranial hyperostosis (19%). White matter

abnormalities, cerebral atrophy, communicating hydrocephalus and spinal stenosis progressed over time, and the authors suggested that these may provide potential disease severity markers [145].

A study of 60 patients with MPS (types I, II, IVa and VI combined) analysed the correlation between disease duration and several quantitative MR parameters [144]. Only the normalised white matter lesion load was found to correlate, albeit weakly ($r=0.28$), with disease duration. In analysis of MPS II patients only ($n=31$), this correlation was somewhat stronger ($r=0.44$, $p=0.02$). In this study, no correlation between MRS derived metabolites and age or disease duration was identified. Furthermore, no correlation was found between urinary GAG concentrations or enzyme activity and the MR parameters.

In a prospective study of 19 male patients with MPS II, patients were subjected to standard neurocognitive assessments as well as neuroimaging [146]. Patients were classified according to the presence or absence of cognitive impairment. MRI investigations were analysed for the presence of white matter lesions (mild or severe), brain atrophy (present or absent), and hydrocephalus (as adjudged by the semi-quantitative ratio of maximum occipital horn diameter/ biparietal diameter). Single voxel spectroscopy was also performed in gray matter and white matter. Of the 19 patients studied 12 had cognitive impairment. The authors found that white matter lesion severity was greater in the cognitively impaired group ($p=0.04$), and that hydrocephalus and brain atrophy were also more common in the cognitive impairment group. Children with cognitive impairment had a significantly ($p<0.05$) higher inositol/creatine ratio in both gray and white matter compared to those without cognitive impairment, although levels were similar to the control group. There was a non-significant

trend to lower NAA/Cr in the white matter of children with cognitive impairment. The authors proposed that the higher inositol levels may indicate astrogliosis, or be an indirect marker of GAG deposition. This study relied on MRS peak area estimation using in-built scanner hardware and used metabolite ratios and not absolute quantification.

A previous study reported the use of MRS in 7 patients with MPS including 4 with MPS II. This demonstrated elevated Cho/Cr ratio in white matter lesions in MPS. Peaks in the spectrum to the left (downfield) of myo-inositol were assigned to "presumptive MPS", i.e. GAG accumulation. However this assignment is not accurate as the peaks identified in the paper are properly assigned as the secondary peaks of creatine, glucose, glutamine and inositol [147].

6.4. Aims and Objectives

Robust and objective tools to monitor neurological involvement in MPS II would enable evaluation of the effects of ERT and of novel therapies on neurological progression. Furthermore such biomarkers could provide early indication of patients likely to develop CNS manifestations and who could benefit from such novel therapies. In addition to clinical and biochemical evaluation methods, objective magnetic resonance (MR) based techniques could make a valuable contribution [144]. As discussed above, MR based scoring systems have been produced to this end [145]. However, visible MRI features correspond to significant structural damage to the brain that may not be reversible, and may not possess the required sensitivity in assessing small effects/ benefits of therapy. Functional imaging modalities including MRS could provide additional information about brain disease processes that could be used in understanding the disease pathogenesis, and in identifying biomarkers of disease

that could be combined in the assessment of the efficacy of novel brain-targeted therapies. The few previous reported MRS studies in MPS II (and MPS generally) as discussed above had several methodological limitations that may restrict the sensitivity of the technique to detect subtle early features.

We aimed therefore to evaluate the potential contribution of MR spectroscopy in describing the neuropathology in MPS II, and in providing means of monitoring disease progression alongside conventional MR imaging.

6.5. A brief introduction to Morquio Syndrome (MPS IVa)

Available MR imaging studies from a cohort of children with a different MPS disorder, MPS IVa (Morquio syndrome, OMIM #253000) were used as a comparison dataset for the quantitation of ventricular size (see methods below). MPS IVa is an autosomal recessive lysosomal storage disorder caused by deficiency of *N*-acetylgalactosamine-6-sulfatase (GALNS, EC 3.1.6.4; encoded by *GALNS* gene at 16q24.3). The classical phenotype includes skeletal dysplasia with short stature, dental abnormalities, impaired endurance and corneal clouding, with the high risk of cervical spine instability and respiratory failure as the main causes of death [148]. In contrast to other mucopolysaccharidoses the CNS has not previously been reported to be directly affected in MPS IVa and intelligence has been thought to be normal [149, 150], although a recent combined neurocognitive and neuroimaging study has provided some evidence that subtle neuroimaging and neurocognitive abnormalities may form part of the MPS IVa phenotype [151]. Any CNS abnormalities in MPS IVa are, however, subtle. Substantial numbers of serial MRI studies were available in this cohort, and thus this data was considered to be suitable to provide an initial comparison for the MPS II imaging data.

6.6. Methods

6.6.1. Patients

Patients were recruited from a single tertiary paediatric IMD unit. Clinical data were extracted from medical records including age at diagnosis, enzyme activity assay at baseline where available, and history of ERT treatment.

Formal neurocognitive assessment was not universally available. Therefore the degree of cognitive impairment was determined by consensus opinion of senior medical and nursing professionals, and binary-classified depending on age-appropriate performance in standard areas of neurodevelopment (speech-language-hearing, social-emotional functioning, fine motor and vision, gross motor), into either no-slight or moderate-severe cognitive impairment. Consensus opinion was also gathered on the clinical progression of the disease in each patient.

6.6.2. Neuroimaging analysis

All available brain MRI studies were retrospectively reviewed, including review of the qualitative radiology report by the consultant paediatric radiologist. Two quantitative parameters were derived from the axial T_2-weighted image sequences to assess firstly white matter abnormalities and secondly the degree of hydrocephalus. White matter abnormalities were scored according to the method of Manara *et al* [145] (figure 6.2) by a single operator (JED, not blinded to other data). Thus the supratentorial white matter involvement was scored as 0 (minimal/absent), 1 (mild), 2 (moderate) or 3 (severe).

The degree of ventricular enlargement was quantified using the method of Vedolin *et al* by measurement of the occipital horn: biparietal diameter ratio (maximum distance between outer borders of occipital horns / maximum biparietal distance, i.e. B/A in figure 6.3). Evan's

ratio (index) was also calculated, i.e. the maximum distance between outer borders of the frontal horns / maximum biparietal distance (C/A in figure 6.3) [152]. Comparison was made with Evan's ratio and occipital horn ratio data derived from 40 MRI examinations carried out on 14 children with MPS IVa (Morquio syndrome).

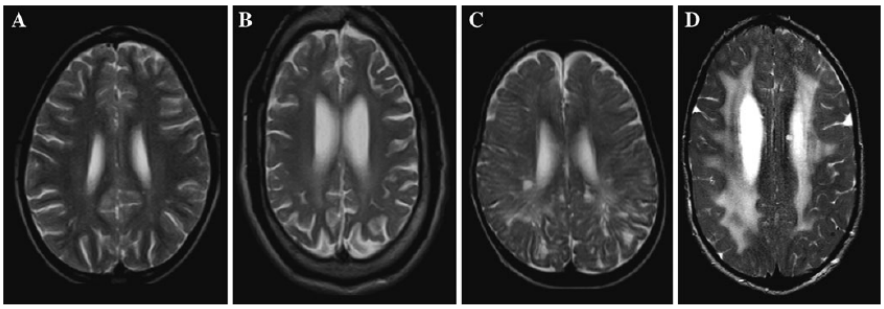

Figure 6.2 White matter abnormality scoring system for MPS II, from [145] assessed on T_2 weighted image at level of lateral ventricles. (A) minimal/absent (score 0); (B) mild (1); (C) moderate (2); (D) severe (3).

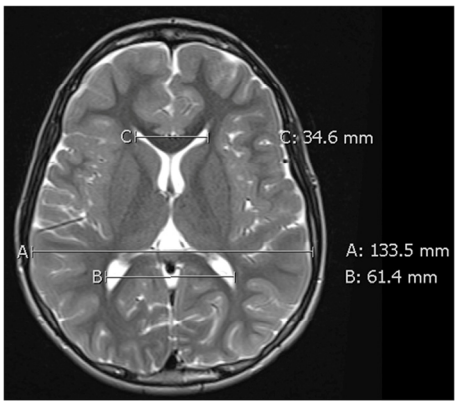

Figure 6.3: Anatomic landmarks used to derive occipital and frontal horn: biparietal diameter ratios

6.6.3. Magnetic resonance spectroscopy

MRS studies were performed concurrently with clinically indicated MRI studies at 1.5Tesla facilitated by general anaesthesia as needed according to the standard protocol, with voxels in standard positions in the white matter and basal ganglia. Metabolite data from the initial MRS from each child were compared with metabolite data from the standard comparison cohort of

children with normal appearing MRI (white matter, n=53, median (range) age 4.7(0.5-16.7) years; basal ganglia n=63, 4.1(0.5-16.7) years) by inspection of mean spectra and independent sample t-test to compare mean metabolite concentration.

Correlations between age, quantitative MR parameters and MRS metabolite values were assessed using Pearson correlation coefficient or between-group ANOVA, and the correlations also re-analysed for metabolite values corrected for the total metabolite concentration detected. For children with serial imaging and MRS data, trends in parameters were compared to the observed clinical course.

6.7. Results

6.7.1. Patient characteristics

Thirty three neuroimaging studies were available from 10 boys with MPS II. Nineteen MRS studies were available from 8 of the boys. Clinical characteristics are summarised in table 6.2. The majority had some evidence of CNS involvement (severe phenotype), although the degree of impairment was variable. One of the boys had the attenuated form of MPS II.

6.7.2. Conventional MRI Findings

All boys had evidence of multiple enlarged perivascular spaces; the degree of other MR features including white matter abnormalities, ventricular enlargement/hydrocephalus and cerebral atrophy varied between patients and also over time. Examples of typical MRI features from three of the patients at three consecutive time points are shown in figure 6.4, illustrating the variable clinical course.

6.7.3. Quantitative MRI parameters

6.7.3.1. Ventricular ratios

Baseline comparison values for Evans ratio and the occipital horn ratio were established from the MPS IVa group, demonstrating no alteration with increasing age (figure 6.5). The Evans ratio and occipital horn ratios correlated well with each other (figure 6.6, r=0.91) although the occipital horn ratio appeared to give greater separation between MPS II and MPS IVa children (figure 6.7). Figure 6.7 presents the Evans ratio and occipital horn ratio for each MRI study plotted against age of patient at time of study. Serial data from individual patients are indicated by lines joining data points.

Most of the MPS II boys have ratios above the range established by the MPS IVa cohort. One MPS II child (patient 7) with the attenuated form had normal ratio values that were stable over time. The rate of change of the ratio scores appears to correspond to the clinical course encountered by each child. Thus patients with more rapid clinical deterioration (e.g. patients 1, 5) had correspondingly rapid rises in ventricular ratio scores; those with stable clinical disease (e.g. patients 2, 6) had more stable although still progressively increasing ventricular ratios.

6.7.3.2. White matter abnormalities

The alterations in the ventricular ratios were mirrored by the white matter abnormality score (figure 6.8). Increasing ventricular ratio corresponded significantly to increasing white matter abnormality score (ANOVA: $p<0.001$).

Patient	Age at diagnosis (m)	Residual enzyme activity	Age starting ERT (y-m)	Age first MRS (y)	Cognitive impairment	MRI Features			
						WMA Score	Cerebral atrophy	Ventricular enlargement	Perivascular spaces
1	~24	2.5%	12-0	12.5	Moderate-severe	1 → 2	+++	Ex-vacuo dilatation	Multiple enlarged
2	21	n/a	7-2	7.6	Moderate-severe	2 → 2	++	Ex-vacuo dilatation	Multiple enlarged
3	48	0%	7-0	7.6	Moderate-severe	2 → 2	+	Slight	Multiple enlarged
4	24	n/a	7-0	6.4	Moderate-severe	1 → 3	++	Ex-vacuo dilatation	Multiple enlarged
5	12	n/a	3-10	4.0	Moderate-severe	1 → 3	+	Slight-moderate	Multiple enlarged
6	24	0%	2-2	2.1	Normal-slight	1 → 2	+	Normal	Multiple enlarged
7	~48	n/a	12-0	12.1	Normal-slight	0 → 0	-	Normal	Multiple enlarged
8	35	n/a	4-0	-	Moderate-severe	1	-	Normal	Multiple enlarged
9	38	n/a	3-2	-	Normal-slight	1	++	Moderate	Multiple enlarged
10	42	n/a	3-6	8.6	Normal-slight	2	+	Moderate	Multiple enlarged

Table 6.2: Summary of clinical characteristics of MPS II patients. ERT, enzyme replacement therapy; m, months; y, years; MRS, magnetic resonance spectroscopy; WMA, white matter abnormality score (see text for details; 1 → 2 indicates progression of score during study).

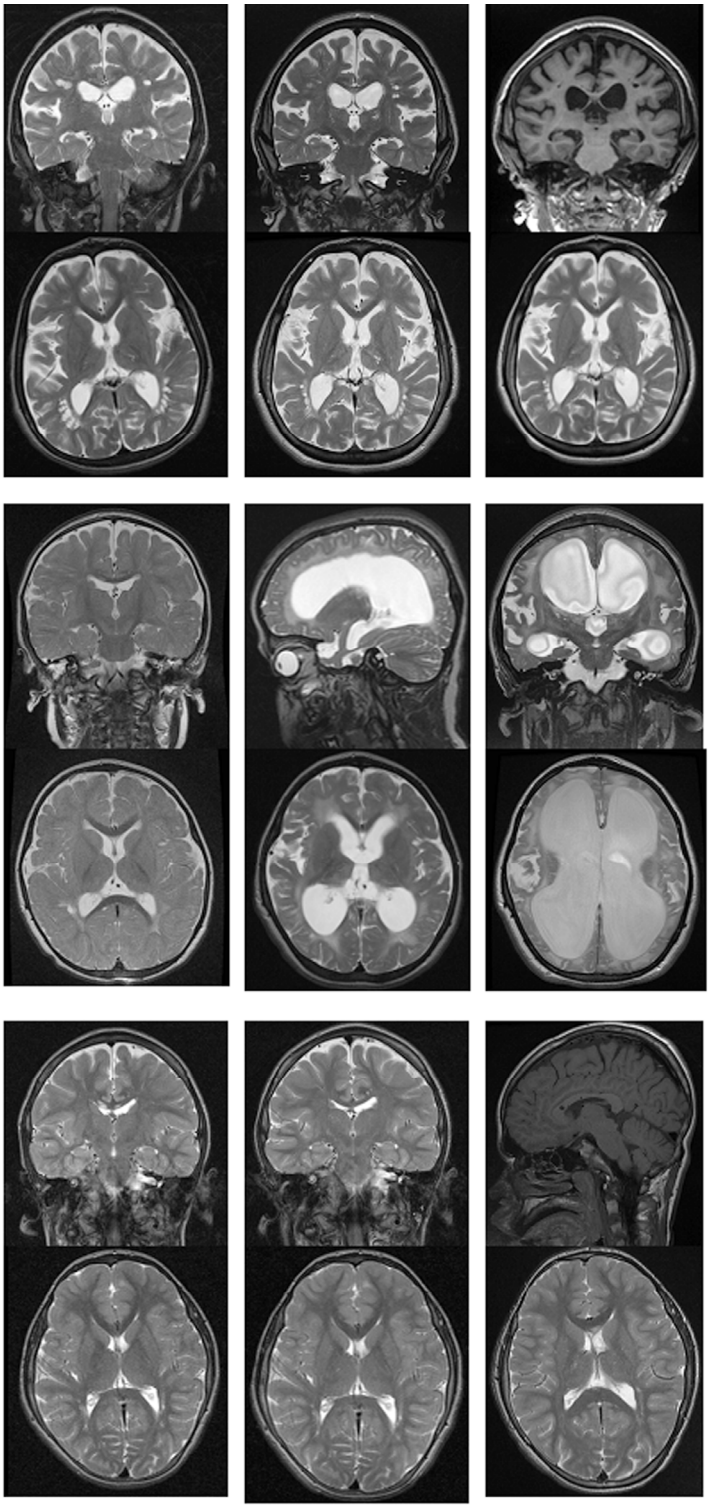

Figure 6.4: T_2 weighted images of three MPS II patients. (Coronal (or sagittal if coronal not available) and axial slices). Top panel patient 2: moderate cerebral atrophy, ventricular enlargement and mild white matter abnormalities stable over sequential imaging. Middle panel patient 5: progressive ventricular dilatation and development of severe white matter abnormalities with less evidence of atrophy. Bottom panel patient 7: attenuated phenotype. No/absent white matter changes, no ventriculomegaly, no atrophy, and stable over time.

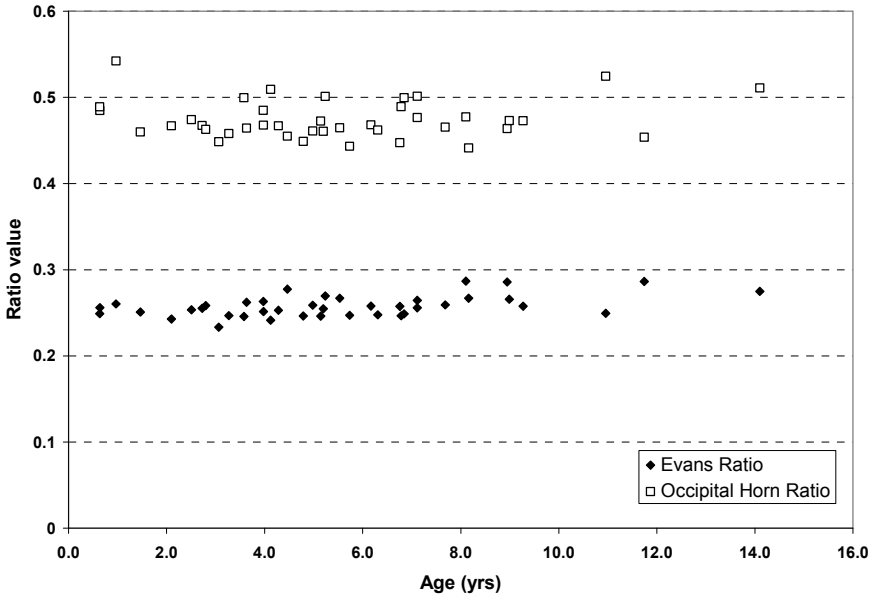

Figure 6.5: Evans ratio and occipital horn ratio plotted against age for the MPS IVa (Morquio) cohort

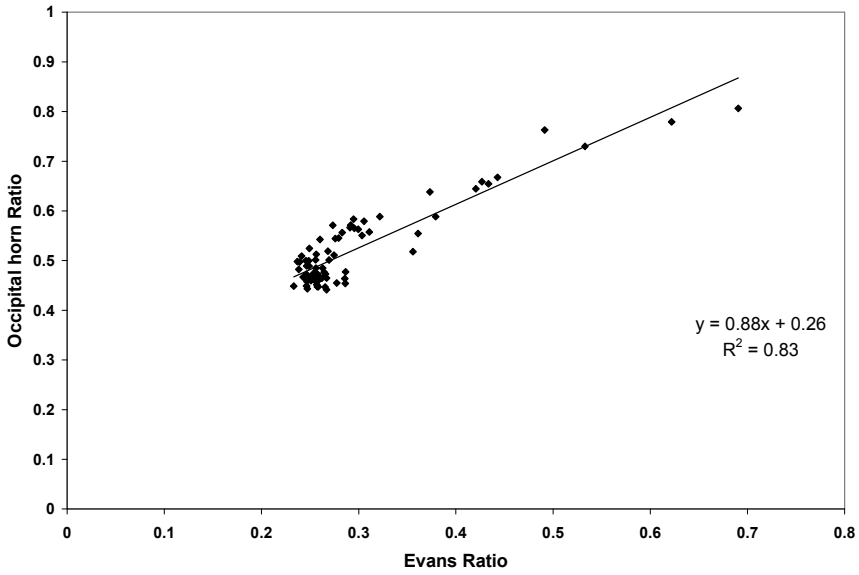

Figure 6.6: Correlation between frontal horn (Evans) ratio and occipital horn ratio across MPS II and MPS IVa patients.

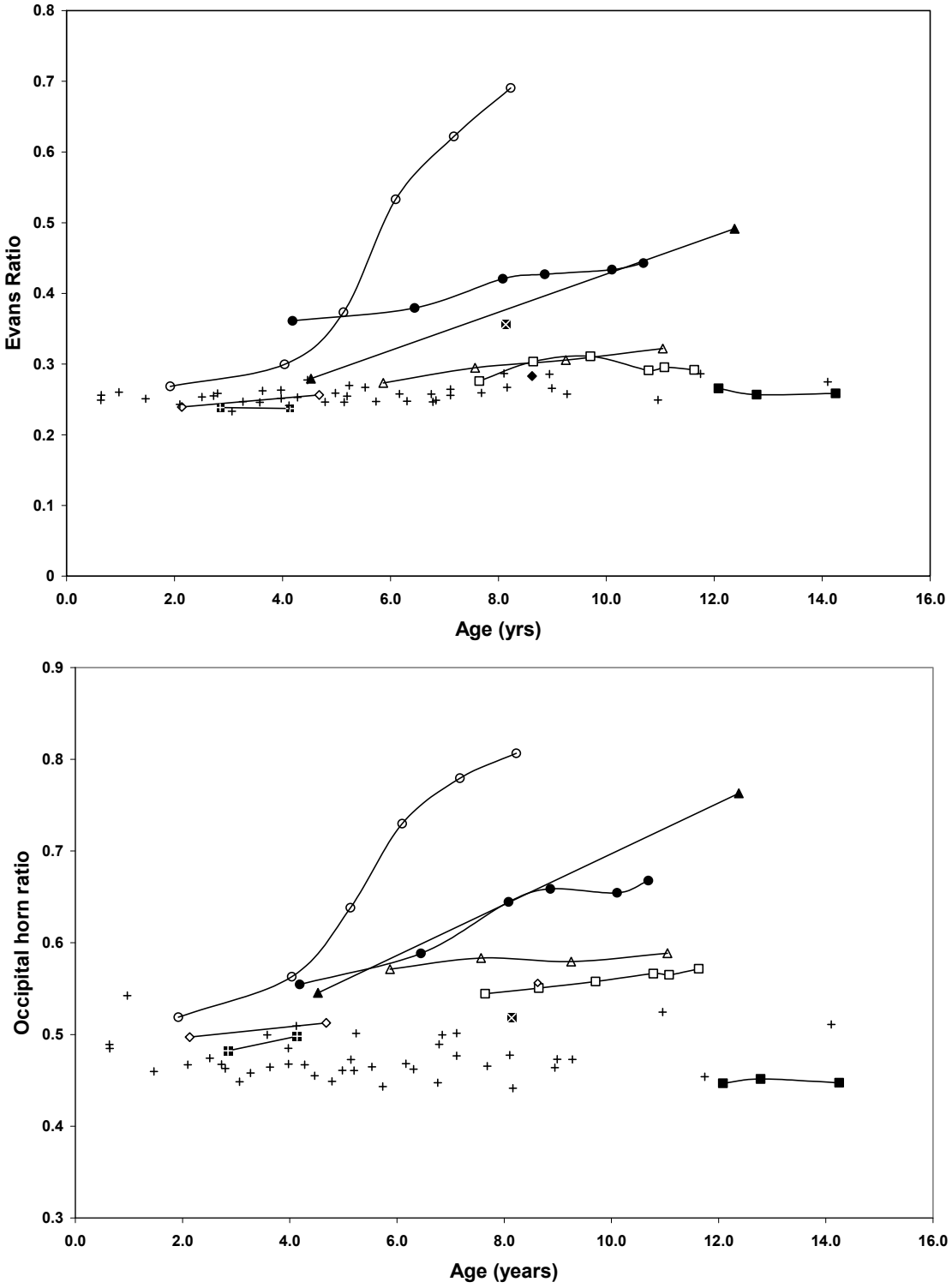

Figure 6.7: Plots of Evans ratio (upper panel) and occipital horn ratio (lower panel) against age. + indicates data from MPS IVa (Morquio) comparison set. Lines connecting points indicate data from individual children obtained at sequential time points. (Patient 1- ▲, 2-□, 3-△, 4-●, 5-○, 6-◇, 8-⊞, 9-⊠, 10-⋄, MPS IVa - +).

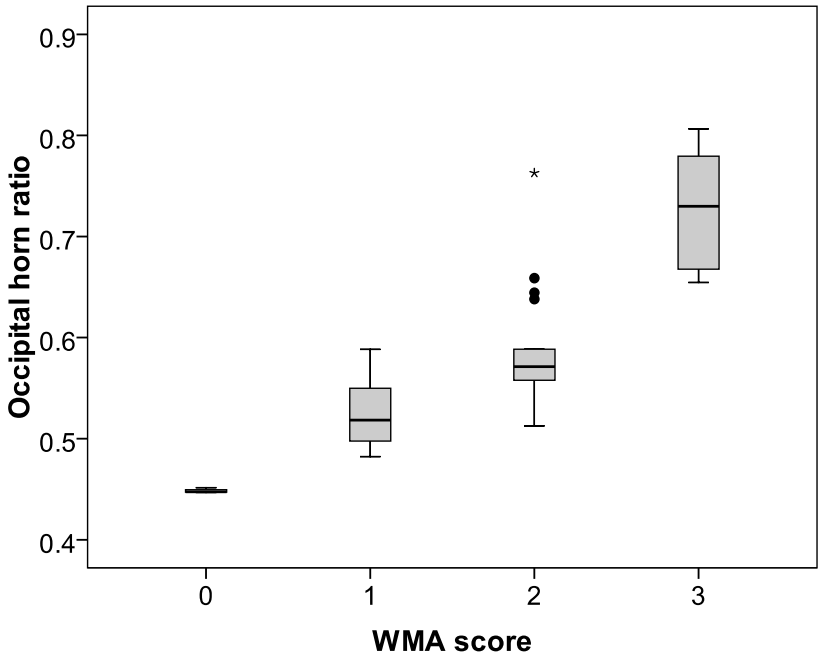

Figure 6.8: Boxplot of occipital horn ratio according to white matter abnormality score in MPS II cohort. (ANOVA p=0.000 between groups).

6.7.4. MR Spectroscopy data

Metabolite values from the initial MRS study for each child in the MPS II cohort were compared to the standard normal MRI comparator groups (figures 6.9 and 6.10 and table 6.3). In white matter MPS II patients had significantly decreased tNAA, creatine, glutamine+glutamate and choline and significantly elevated macromolecular/lipid signal at 1.3ppm compared to the standard normal MRI comparator group. These metabolite changes were not seen in basal ganglia, where the only significant difference was in glutamine which was higher in the MPS II group although total glutamine+glutamate was not significantly elevated.

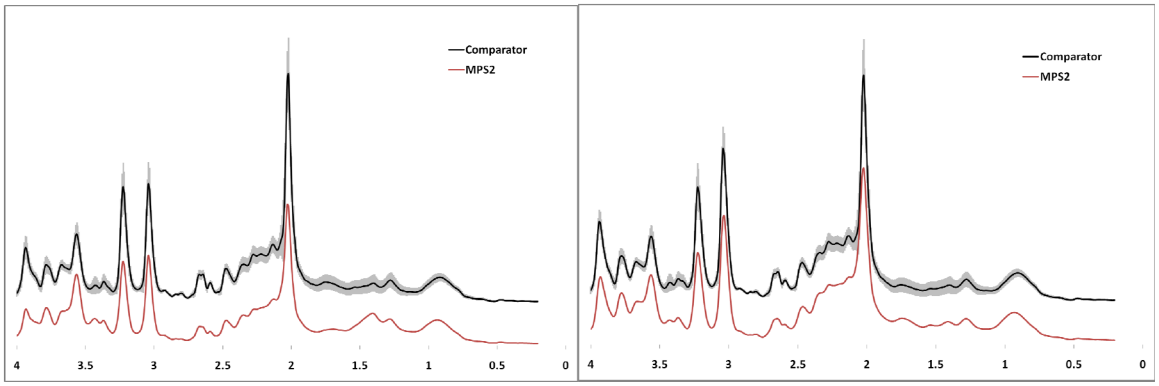

Figure 6.9: Mean MR spectra for MPS II (red line) and comparator group (black line, shaded area indicates standard deviation) for white matter (left) and basal ganglia (right).

	Basal ganglia		White matter	
	MPS2	Comparator	MPS2	Comparator
n	8	63	8	53
Median (range) age (yrs)	7.9	4.1 (0.5-16.7)	8.6	4.7 (0.5-16.7)
Cr	4.22 (0.63)	4.55 (0.59)	2.47 (0.53) †	3.18 (0.47)
Gln	3.01 (1.27)†	1.98 (0.79)	1.35 (0.60)	1.32 (0.62)
Glu	4.56 (1.34)	4.45 (0.78)	2.26 (1.00) †	3.51 (0.78)
Ins	2.77 (0.65)	2.49 (0.43)	2.77 (0.59)	2.57 (0.39)
Lac	0.19 (0.49)	0.11 (0.20)	0.27 (0.33)	0.21 (0.28)
Scyllo	0.14 (0.09)*	0.07 (0.08)	0.12 (0.05)	0.09 (0.06)
Tau	0.32 (0.65)	0.63 (0.49)	0.21 (0.22)	0.32 (0.37)
Gua	1.14 (0.20)	1.01 (0.32)	0.70 (0.21)	0.75 (0.21)
tCho	1.01 (0.18)	1.11 (0.18)	0.81 (0.17) †	1.08 (0.15)
tNAA	4.82 (0.87)	5.21 (0.51)	3.34 (1.24) †	5.11 (0.73)
Gln+Glu	7.57 (2.55)	6.43 (1.39)	3.60 (1.32) †	4.84 (1.18)
MMLip1.4	5.21 (2.31)	4.27 (1.63)	7.27 (2.35) †	4.88 (2.18)
MMLipd0.9	3.80 (1.09)	4.12 (0.95)	3.64 (0.56)	3.73 (0.66)
MMLip2.0	7.97 (2.53)	8.20 (1.30)	6.83 (1.40)	7.65 (1.52)

Table 6.3: Mean MR spectroscopy derived brain metabolite values for MPS II and comparator cohorts for basal ganglia and white matter. Student's t-test between MPS II and comparator cohorts, † $p<0.01$, * $p<0.05$.

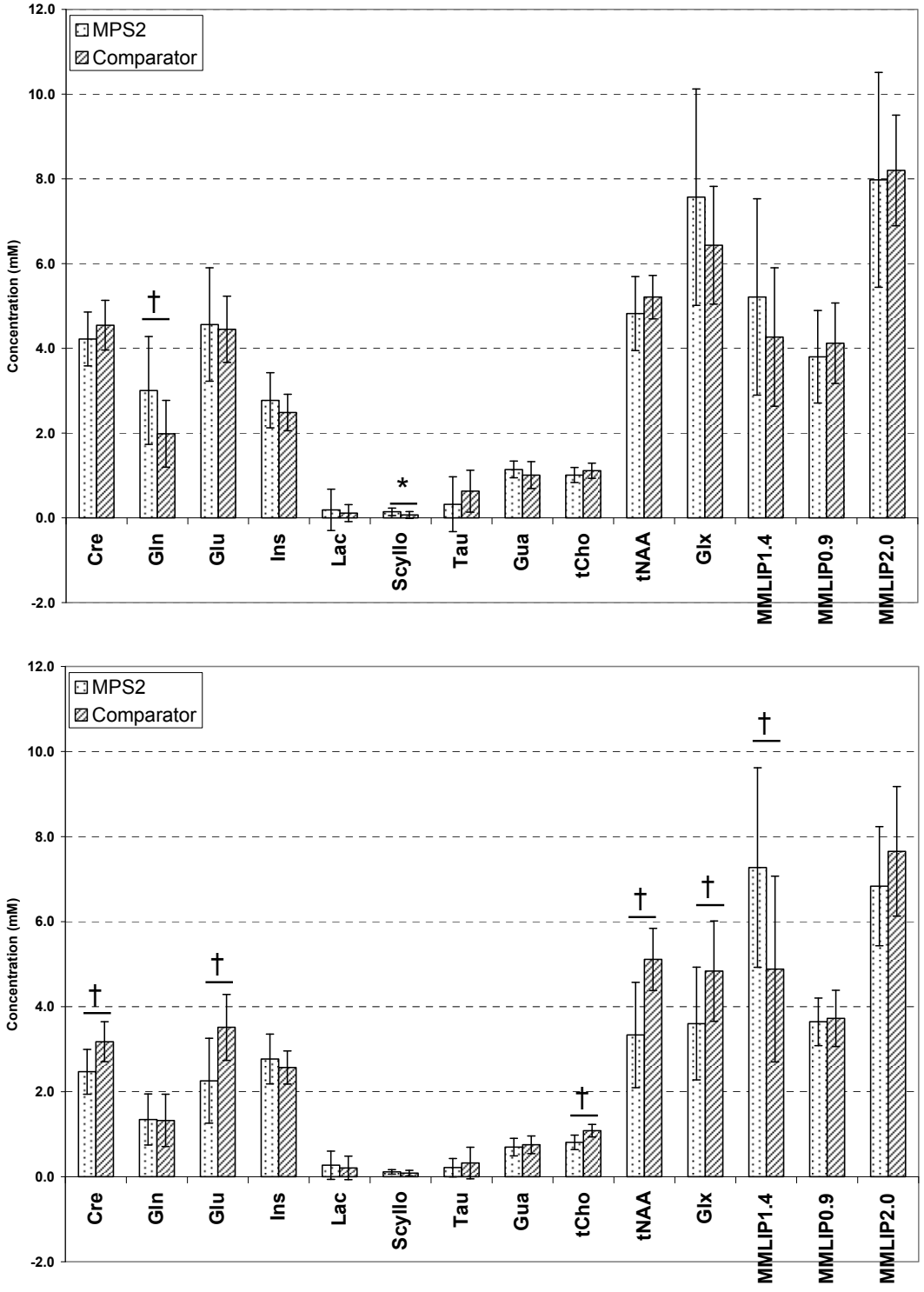

Figure 6.10: Bar charts of mean metabolite concentrations for MPS II and comparator cohort from basal ganglia (upper panel) and white matter (lower panel). Student's t-test between MPS II and comparator cohorts, † $p<0.01$, * $p<0.05$.

6.7.5. Correlation of MRS, age and quantitative MRI parameters

Correlations between the MRS-determined metabolite concentrations, age and the quantitative MRI parameters were analysed (figures 6.11 and table 6.4). No significant correlation was found between white matter metabolites and age, whereas in basal ganglia there was a significant ($p<0.01$) negative correlation between creatine ($r=-0.61$), inositol (-0.67) and choline (-0.79) and age (table 6.4).

All metabolites had a negative correlation with both of the ventricular ratio scores, reaching statistical significance for white matter creatine, tNAA and glutamine+glutamate and for basal ganglia tNAA and glutamine+glutamate. The strongest correlation was between white matter tNAA and occipital horn ratio ($r=-0.79$).

The data above have shown that the white matter abnormality score correlated with the ventricular ratio. The white matter tNAA also varies significantly with the white matter abnormality score (ANOVA $p=0.001$; figure 6.13).

All of the metabolites showed a trend to decrease with increasing ventricular index, with several reaching significance. To evaluate whether this simply reflected a loss of metabolites within the voxel due to generalised cell loss, individual metabolites were normalised to the total metabolite concentration detected and the correlation between the corrected metabolite values and the ventricular index re-appraised (figure 6.12, table 6.5).

Corrected white matter tNAA and white matter glutamine+glutamate were significantly negatively correlated to ventricular index, while white matter inositol was significantly positively correlated to ventricular index. In basal ganglia only glutamine+glutamate showed

significant (negative) correlation with ventricular index. The negative correlation between white matter creatine and ventricular index and between basal ganglia tNAA was not seen in the analysis of the corrected metabolite data.

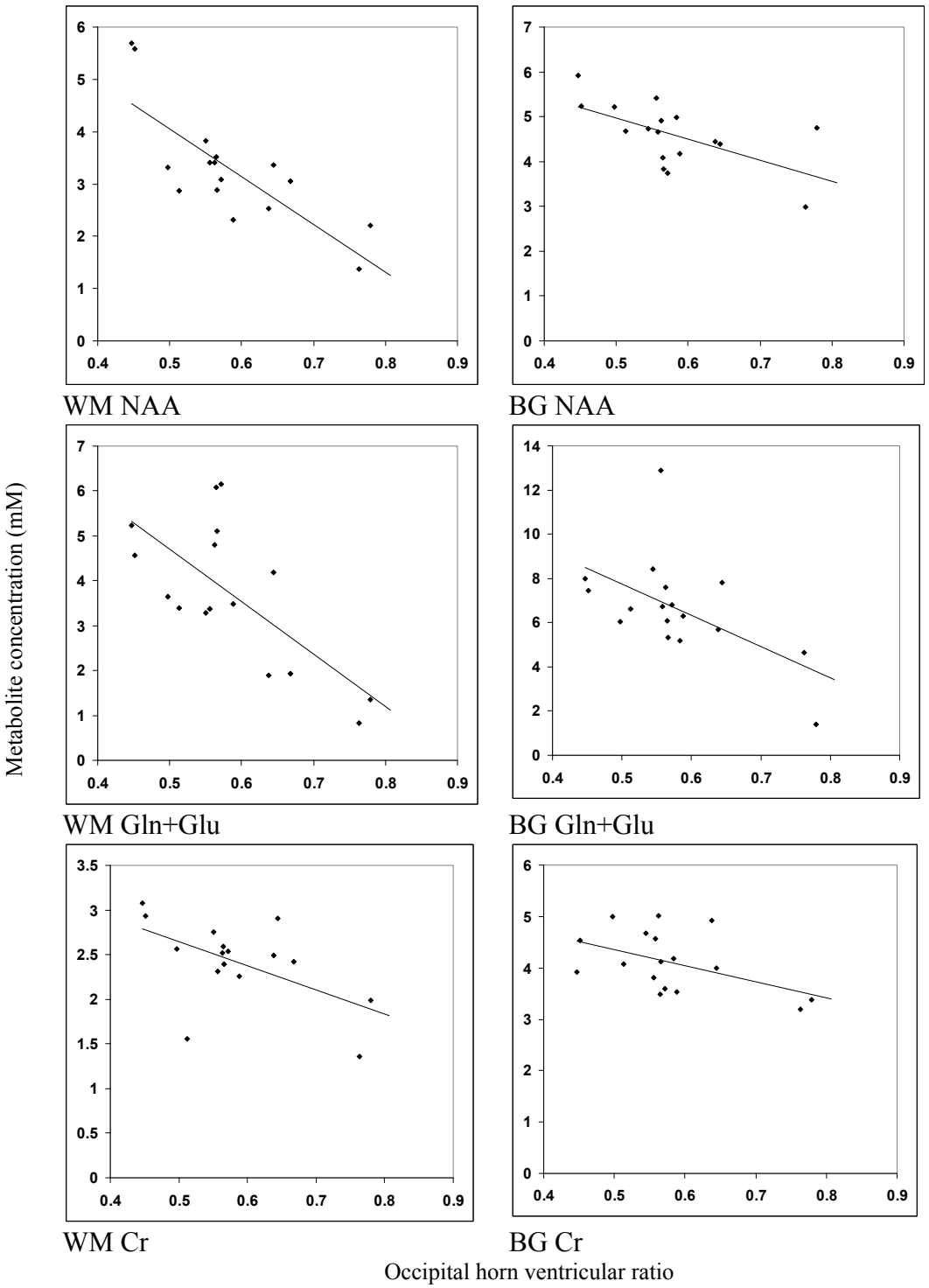

Figure 6.11: (see over for caption)

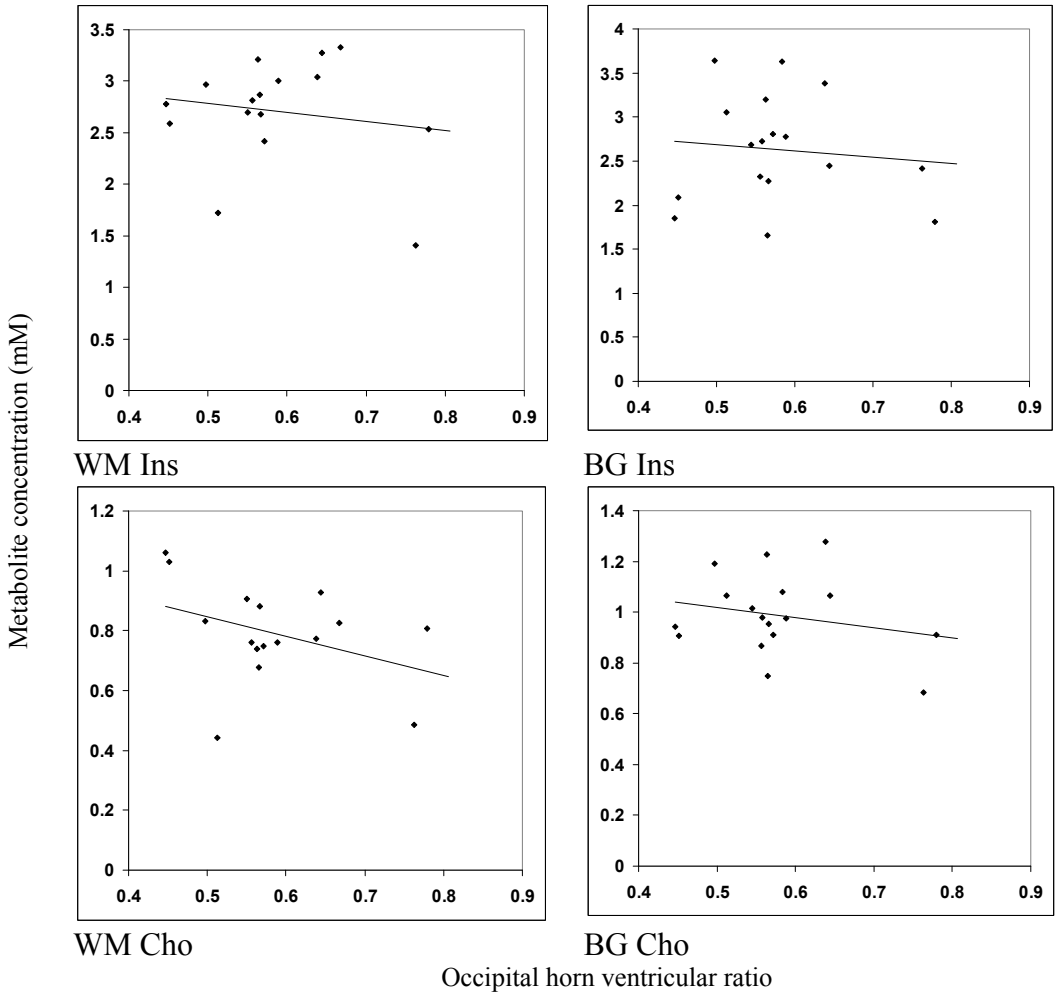

Figure 6.11: (See also previous page). Plots of correlation between metabolites (absolute value) and occipital horn ventricular ratio for white matter (WM) and basal ganglia (BG).

	White matter					Basal ganglia				
	Cr	Ins	Cho	tNAA	Gln+Glu	Cr	Ins	Cho	tNAA	Gln+Glu
Age at MRI	0.12	-0.19	0.23	0.22	0.20	-0.61†	-0.67†	-0.79†	-0.31	0.05
Evans Ratio	-0.40	-0.11	-0.15	-0.56*	-0.70†	-0.48	-0.31	-0.25	-0.38	-0.60*
Occipital horn Ratio	-0.55*	-0.16	-0.38	-0.79†	-0.69†	-0.48	-0.11	-0.24	-0.60*	-0.56*

Table 6.4: Pearson correlation coefficients for correlation between brain metabolites, age, Evans ratio and occipital horn ratio in MPS II cohort. Significance, † $p<0.01$, * $p<0.05$

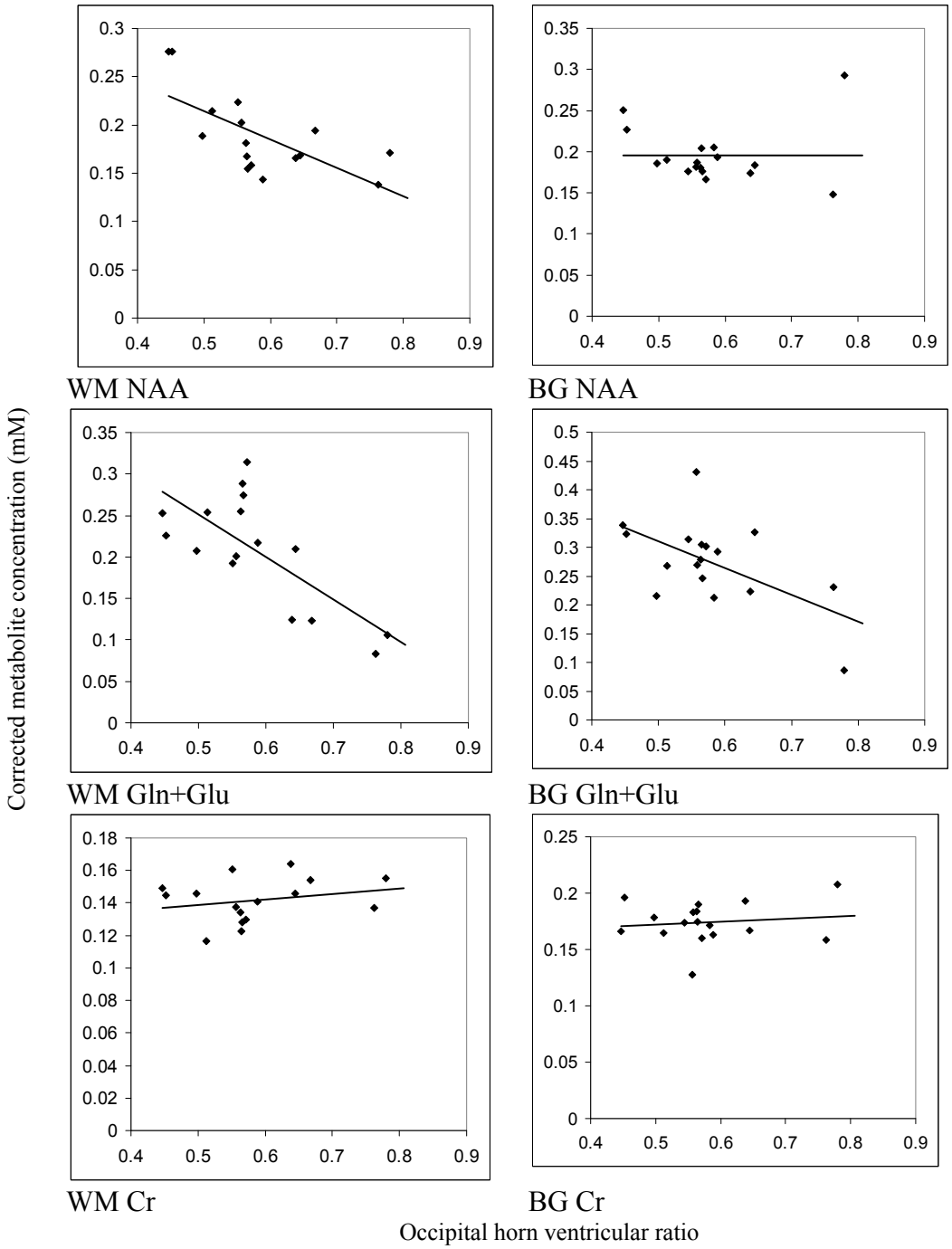

Figure 6.12: (see over for caption)

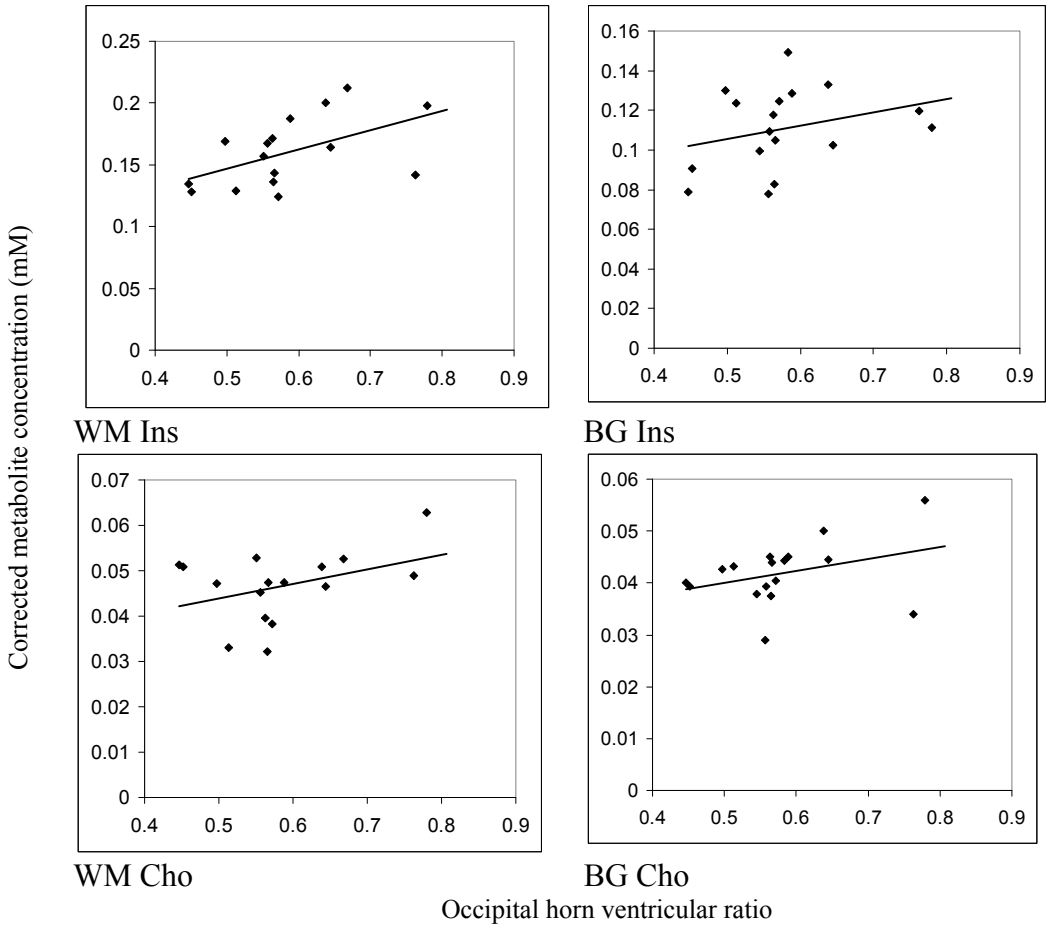

Figure 6.12: (See also previous page) Plots of correlation between metabolites (corrected for total metabolite concentration) and occipital horn ventricular ratio for white matter (WM) and basal ganglia (BG).

	White matter					Basal ganglia				
	Cr	Ins	Cho	tNAA	Gln+Glu	Cr	Ins	Cho	tNAA	Gln+Glu
Age at MRI	-0.09	-0.36	0.11	0.10	0.09	-0.17	-0.45	-0.40	0.07	0.33
Occipital horn ratio	0.24	0.52*	0.39	-0.68†	-0.72†	0.13	0.29	0.34	0.01	-0.57*

Table 6.5: Pearson correlation coefficients for correlation between brain metabolites corrected for total metabolite concentration, age and occipital horn ratio in MPS II cohort. Significance, † $p<0.01$, * $p<0.05$

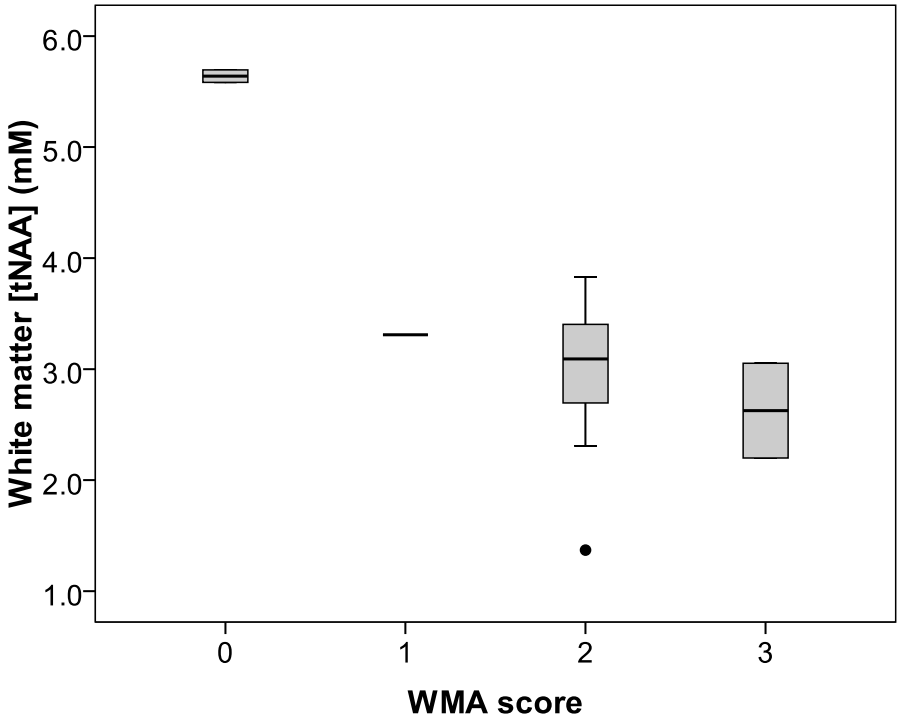

Figure 6.13: Boxplot of tNAA concentrations in each white matter abnormality score (WMA) category in MPS II cohort.

6.7.6. Serial trends in imaging and MRS data

Serial trends in metabolite concentrations were analysed across the cohort and on a case-by-case basis. As shown above, several of the metabolites varied significantly with age in the basal ganglia. A strong correlation was found between white matter tNAA and occipital horn ratio, seen in both uncorrected data and data corrected for total metabolite concentration. White matter tNAA was also significantly different in the MPS II cohort from the normal MRI comparator group.

On this basis, case-by-case trends in white matter tNAA were analysed (figure 6.14, which also shows the normal age variation in tNAA from the normal MRI comparison datasets). All MPS II cases apart from patient 7 (attenuated phenotype) had white matter tNAA levels that were below the range of normal values. The lowest tNAA levels corresponded to the most severely affected boys (e.g. case 1). In all children where serial MRS data was available the tNAA fell with time, with progressive decreases seen in children with ongoing clinical deterioration (e.g. case 5).

The trends seen in case-by-case analysis of tNAA corresponded to the trends in occipital horn ratio (figure 6.15), e.g. for case 5 the ventricular ratio increased as tNAA decreased in white matter; for case 2 the ventricular ratios remained relatively stable, although in this child there appeared to be a progressive fall in the tNAA in both white matter and basal ganglia suggesting ongoing disease progression.

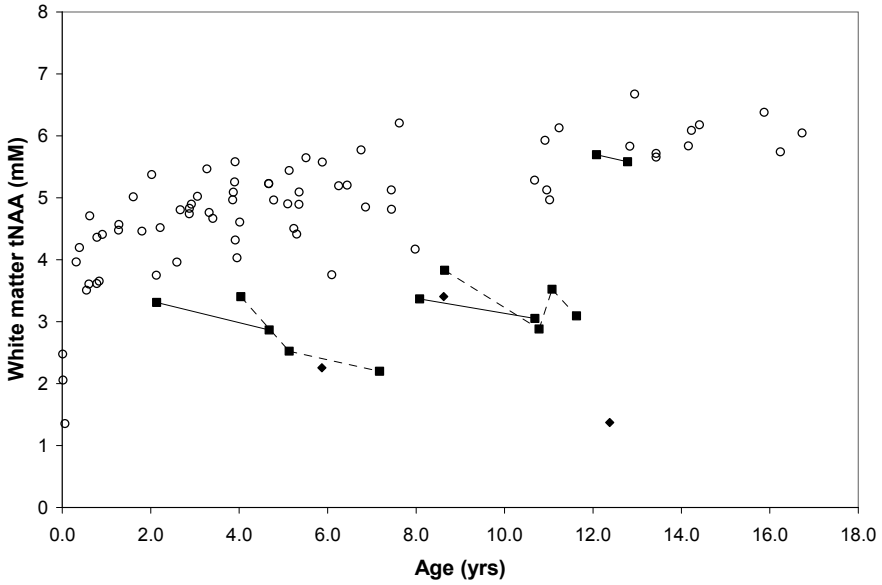

Figure 6.14: Plot of white matter tNAA concentration against age for normal MRI comparator group (open circles) and MPS II patients with serial determinations (squares) and single time point only (diamonds)

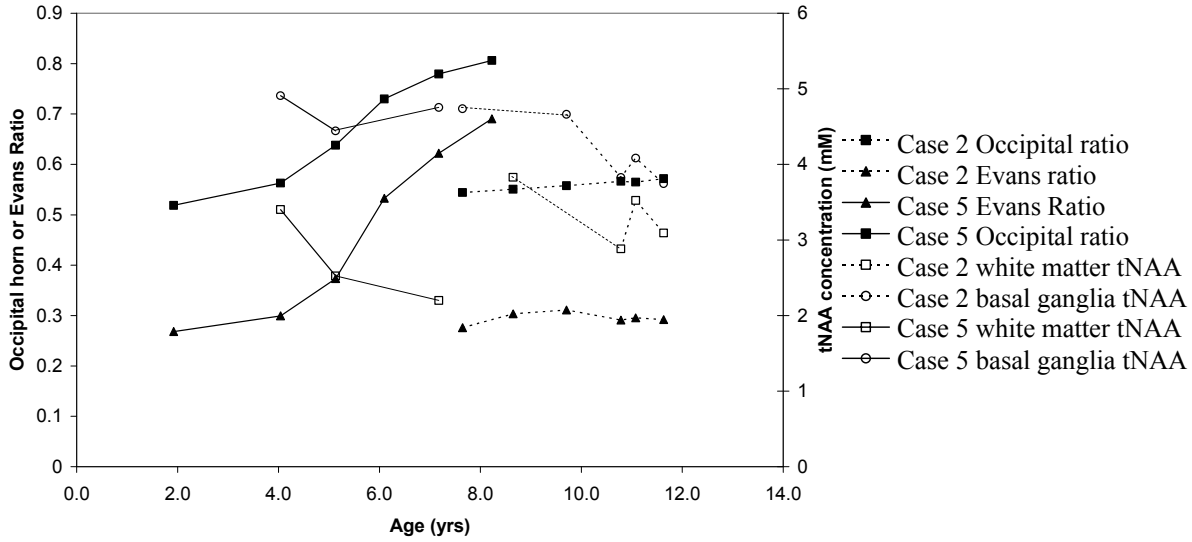

Figure 6.15: Age related trends in occipital horn (filled squares) and Evans (filled triangles) ratios and white matter tNAA (open squares) and basal ganglia tNAA (open circles) for two MPS II patients with serial data.

6.8. Discussion

Involvement of the CNS in MPS II is indicative of the "severe" phenotype; in the present study the majority of subjects had some degree of CNS disease evidenced by clinical characteristics and supported by MR imaging features. Only one of the boys studied (patient 7) fell within the classical "attenuated" phenotype, with relatively normal neurology and cognitive function maintained to the middle of the second decade. That said, considerable variation in the degree of cognitive and neurological disease was evident in the cohort, supporting the concept of a disease continuum rather than two distinct phenotypic groupings often reported in the literature.

All of the subjects studied were receiving ERT, and the MRS data presented (apart from one examination) were obtained in boys while on ERT. Some MR imaging data was available ante-dating the commencement of ERT. The clinical and imaging features described here are, therefore, a description of the amended natural history of the disease in the "ERT era" [128]. The fact that the same range and progression of imaging abnormalities are seen here as reported in the older (pre-ERT) literature supports the view that systemic ERT has little impact on CNS involvement in MPS II. Many of the subjects described here, however, did not start ERT until several years of life when ERT first became clinically available, and it can be argued that they may have already accrued several years of neuronal damage before the start of treatment.

The MRI features seen in this cohort are consistent with previous descriptions of brain involvement in MPS II, in particular progressive ventricular enlargement/ hydrocephalus, brain atrophy, white matter abnormalities and enlarged perivascular spaces (PVS) [144-146].

Enlarged PVS were seen in all children irrespective of neurocognitive status, as previously reported. The quantitative assessment of ventricular size and assessment of white matter abnormality scores found that these two features correlated with each other, suggesting that they are common features of the brain pathological insult rather than independent processes. Furthermore, progressive alterations in both measures of brain disease were seen in all children, with more rapid elevations in ventricular size corresponding to children with more aggressive clinical deterioration. This finding is in agreement with a previous study of MRI features in MPS II that found that white matter abnormalities, ventricular enlargement and spinal stenosis (not assessed in the current work) are potential disease severity markers [145]. It should be noted that the quantitative MR parameters assessed in this work were derived by a single observer (JED) not blinded to diagnosis, MRS data or clinical information; for future prospective analyses multiple observers blinded to clinical characteristics should undertake confirmation of these preliminary findings.

Previous studies using semi-quantitative MRS have demonstrated an elevated inositol/creatine ratio and a non-statistically significant trend to decreased NAA/creatine ratio in cognitively impaired children with MPS II [144, 146]. The present data confirm and extend these MRS findings in the cohort of children with MPS II using a large comparator cohort with normal MR imaging. In general, metabolite alterations were more pronounced in the white matter than the basal ganglia.

In this study tNAA was decreased in both white matter and to a lesser degree in basal ganglia, reflecting the predominantly white matter changes seen on MRI and neuropathological studies. However the decreased tNAA in basal ganglia implies that the deep gray matter

structures are not spared entirely, as reported in severely affected patients [153]. NAA originates in neuronal cells [50], and decreased concentrations have been correlated with disease progression and loss of neuronal viability in many lysosomal storage disorders [8, 9]. The observation of higher tNAA in children with mild cognitive impairment compared to those with moderate-severe impairment, and the progressive alterations with time mirroring clinical progression suggest that tNAA may be a useful disease biomarker.

Elevated inositol, a phosphoinositide precursor located in glial cells, may imply glial proliferation or gliosis. Inositol was higher (non-significant trend) in MPS II in white matter and basal ganglia compared to the normal MRI comparator group; the ratio of inositol to creatine was increased in both regions compared to the comparator group in line with the previous MRS studies reported. This underlines the problem of using creatine as a supposed static denominator, since it can be seen that creatine does in fact alter in pathological states. That said, the relative preservation or modest increase in inositol compared to loss of creatine and tNAA suggests that there may be a mild expansion of the glial compartment, in agreement with neuropathological reports in MPS that found minor gliosis [136]. Further evidence for this is given by the positive correlation between the total metabolite-corrected white matter inositol and ventricular index, suggesting that there is relatively more inositol present with increasing brain degeneration as documented by ventricular index.

White matter also showed decreased levels of glutamine+glutamate, predominantly due to a decrease in glutamate, reflecting loss of active neuronal cells, while glutamine which is predominantly synthesised in glial cells was relatively spared (see Chapter 7 for discussion of validity of interpretation of glutamate and glutamine separately). Elevated lipids were

detected in white matter but not basal ganglia and this may reflect the neuropathological process in white matter. Increased lipids are seen in a range of brain pathologies including malignancies and acute inflammatory disorders and are associated with cell stress, apoptosis and necrosis [154].

In the analysis of the correlation between brain metabolites and the quantitative MRI parameters, all metabolites were seen to have a negative correlation with the ventricular index, reaching statistical significance for white matter tNAA, glutamine+glutamate and creatine, and for basal ganglia tNAA and glutamine+glutamate. This suggests that there may be general loss of metabolite signal due to either increased water (CSF) within the voxel or loss of tissue (cell number). Gross contamination of voxels with CSF was excluded by visual appraisal of voxel contents, but to assess whether the metabolite alterations seen were simply a reflection of tissue loss, such that there was less cell mass within the MRS voxel giving rise to the metabolite signal, metabolites were corrected using the total metabolite concentration as denominator.

This revealed some interesting findings: corrected white matter tNAA and glutamine+glutamate again showed a significant negative correlation with ventricular index, and corrected white matter inositol was significantly positively correlated with ventricular index. These data suggest that as the brain disease worsens (evidenced by increasing ventricular index) there is progressive neuronal loss (decrease in tNAA and Gln+Glu) but relative increase in the glial compartment as evidenced by the rising inositol levels. Within the basal ganglia, corrected tNAA did not correlate with the ventricular index ($r=0.1$) suggesting preservation of the basal ganglia neuronal cells. However, there was a negative

correlation between basal ganglia glutamine+glutamate and ventricular index, suggesting that these amino acids are depleted.

The trends in metabolite alterations were detected on analysis of the total cohort. Analysis of the data on a per-case basis found that the changes in both the quantitative MRI parameters and also the white matter tNAA corresponded to the clinical course of the disease in each patient, such that the tNAA was higher and ventricular index lower with better neurocognitive status, and that rates of progressive changes corresponded to alterations in the clinical status. In the absence, however, of formal neurocognitive assessment it is difficult to convincingly demonstrate this link, and neurocognitive assessment should be a part of future prospective studies.

6.9. Conclusions & Future Perspectives

The MRS data presented here throws light on the neurochemical correlates of conventional imaging features, and seem to be consistent with current understanding of the disease neuropathology of MPS II. Furthermore, alterations in the neurochemical profile do correspond to the alterations in quantitative MR parameters, suggesting that a composite model combining multiple parameters from conventional and functional imaging could provide a means of monitoring disease progression, as has been proposed for another LSD, late infantile neuronal ceroid lipofuscinosis [100]. That said, incorporation of MRS data into a multi-parameter imaging scoring system must be shown to provide added benefit over and above the conventional imaging parameters. While both the conventional parameters and metabolite data seem to track the clinical progression well, loss of brain mass (i.e. ventriculomegaly) and the development of white matter abnormalities are relatively late steps in the pathological cascade. MRS has the potential to detect earlier alterations, prior to the

appearance of MRI-visible changes. As has been noted, the boys studied here already have established brain disease. In all cases with brain involvement, the tNAA was below the normal comparator range even in the earliest available MRS studies, at a time when the ventricular index scores were (near) normal, suggesting that neurochemical alterations may predate the neuroimaging alterations. It would be interesting to have further prospective multimodal imaging data acquired in boys from a young age without evidence of clinical CNS involvement to evaluate this hypothesis further.

In addition to conventional MRI and MR spectroscopy, other functional modalities may also provide further information that could be incorporated in to a multi-parameter model, such as diffusion weighted or diffusion tensor imaging that give information about tissue microstructural alterations. These modalities warrant further investigation, particularly for their ability to detect early microstructural alterations prior to changes visible on conventional MRI. A direct method of non-invasive quantification of tissue GAG content would provide another means of monitoring disease progression. GAGs are not readily visible using the standard one dimensional proton MRS technique presented here, and a previous paper that reported GAG detection was methodologically flawed as discussed above [147]. Alternative imaging methods are available with the potential to measure GAGs, specifically the chemical exchange-dependent saturation transfer (CEST) method which is based on the transfer of spin saturations from protons to the bulk water pool [155], achieving significant enhancement of the signal detected. This method has been used to image tissue pH and liver glycogen [156], and a similar technique has been applied to brain experiments [157].

Chapter Seven

7. Propionic Acidaemia

In this chapter data are presented illustrating the use of MR imaging and MR spectroscopy in the evaluation of the brain pathology of a specific disorder of branch chain amino acid metabolism, propionic acidaemia. In particular, the techniques are employed to investigate the pathogenesis and pathophysiology of strokes affecting children with this disorder. The MR spectroscopy data has been reported in *Orphanet Journal of Rare Diseases* 2011 and is the first report of the use of MRS in this disorder during acute metabolic decompensation (see Appendix B)[158].

7.1. Introduction to Propionic Acidaemia

The organic acidaemias are disorders resulting from abnormalities within the branch chain amino acid (BCAA) catabolic pathways (figure 7.1) [159]. Propionic acidaemia (PA, OMIM #606054) is an autosomal recessive disorder resulting from deficiency of the biotin-dependent mitochondrial enzyme propionyl CoA carboxylase (PCC, EC 6.4.1.3) [160, 161].

PCC is composed of six α and six β subunits; the α subunit is encoded by *PCCA* (chromosome 13q32) while the β subunit is encoded by *PCCB* (3q13.3-q22) [162]. Over 100 mutations in *PCCA* and *PCCB* have been reported [162, 163]. *PCCB* mutations are more frequent, the commonest being c.1218_1231del14ins12 reported in 32% of alleles in a Caucasian population [161]. PCC normally converts propionyl-CoA to methylmalonyl-CoA,

which is subsequently metabolised to succinyl-CoA which enters the Krebs cycle (figures 7.1 and 7.2) [164]. Propionyl-CoA is formed from the catabolism of the branch chain amino acids, cholesterol side chains and odd-chain length fatty acids and is also generated by gastrointestinal bacterial activity [165]. In the absence of functional PCC, propionyl-CoA is alternatively metabolised resulting in accumulation of propionate, 3-hydroxy-propionate, 2-methylcitrate (from condensation with oxaloacetate) and propionylglycine. Common biochemical derangements in PA include ketoacidosis, hyperglycinaemia and hyperammonaemia [166].

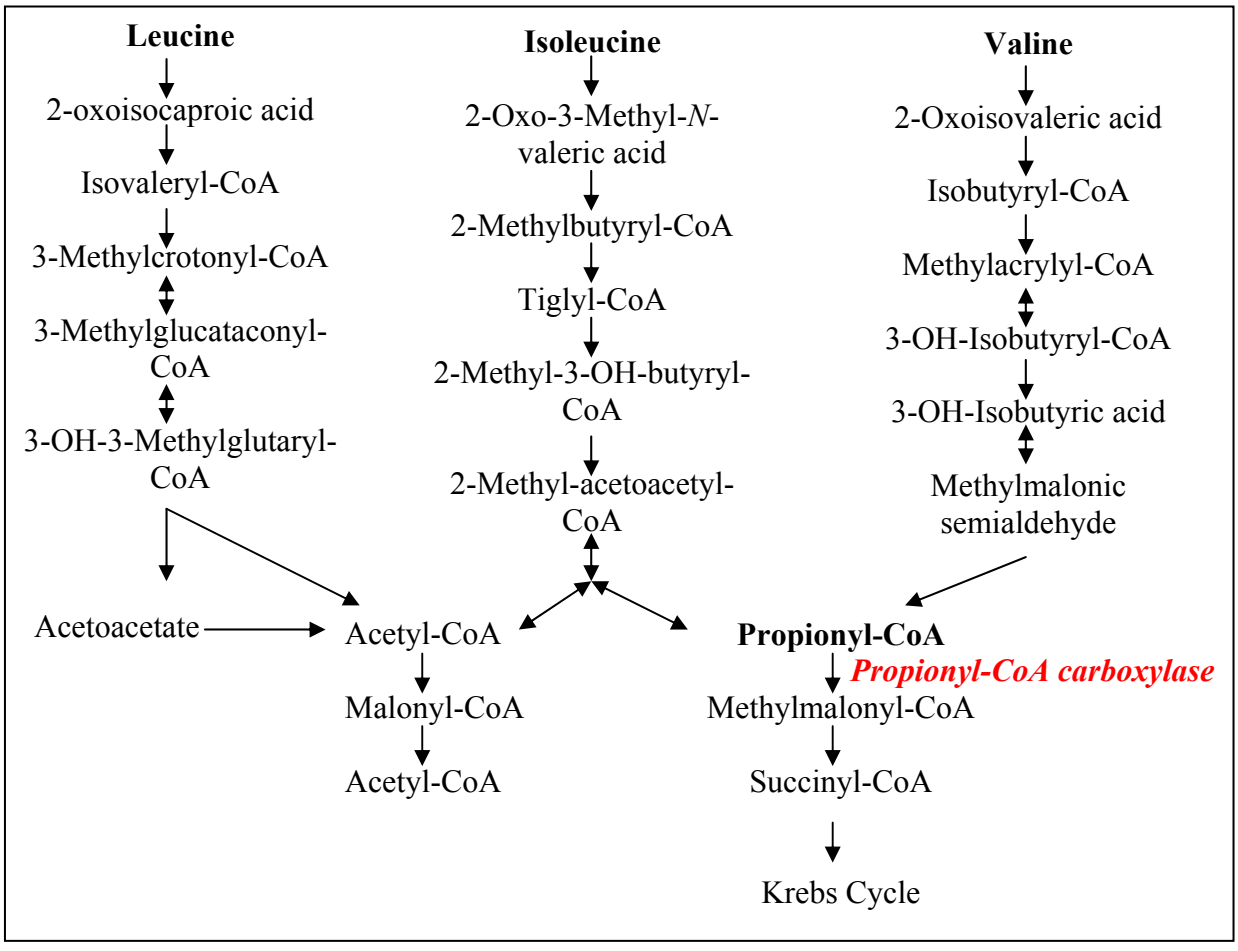

Figure 7.1: Branch chain amino acid catabolic pathways. (Adapted from [167]).

The commonest and most severe form of PA presents in the neonatal period with acute metabolic acidosis, hyperammonaemia and progressive encephalopathy requiring urgent intensive medical support [164]. Newborn screening can identify PA by elevated propionylglycine, but in countries including the UK where this expanded screening panel is not employed patients still present clinically [168]. The ability of newborn screening to provide benefit in terms of reduced morbidity has however been questioned [169].

PA is associated with numerous multi-system complications in addition to the acute metabolic decompensation. Outside the CNS these include dilated cardiomyopathy, cardiac arrhythmias (including prolonged QT syndrome and sudden death), pancreatitis, and pancytopaenia in particular neutropaenia [161].

The mainstays of treatment are: dietary protein restriction with attention to ensuring adequate nutrition is provided, sometimes necessitating nasogastric or gastrostomy feeding; carnitine supplementation; use of pro-motility agents and bactericidal therapy to reduce gastro-intestinal bacterial load and consequent propionate production; and aggressive management of acute metabolic derangements and other associated pathologies including pancreatitis [170]. Some centres utilise alternative pathway drugs including sodium benzoate to minimise the consequences of hyperammonaemia although the evidence for their use is not strong [170]. Orthotopic liver transplantation may prevent neurocognitive decline but its role remains controversial [171, 172], and current consensus guidelines recommend it may be considered where individuals suffer recurrent episodes of hyperammonaemia or acidosis [170].

7.2. Neurologic involvement in propionic acidaemia

The neurological manifestations of PA include both acute events (e.g. acute coma and metabolic stroke-like episodes) and chronic long-term complications. Despite optimal management, later neurologic sequelae are a major cause of morbidity, and include hypotonia, neurodevelopmental delay, seizure disorders and myoclonus, episodic acute encephalopathy, and movement disorders due to a propensity to basal ganglia infarction [10, 19] which can be responsive to L-DOPA therapy [173]. Additionally optic nerve atrophy, cerebral atrophy and extra-pyramidal syndromes have been reported [161]. Developmental delay and intellectual impairment are very common in PA, even where metabolic control is well maintained [174]. The degree of cognitive impairment is related to the age of disease onset, such that children with early-onset PA have lower IQ scores than those presenting with a presumably milder disease at an older age [175]. However, other neurological features including acute basal ganglia injury and movement disorders may affect children presenting with either early or late onset disease [175].

The natural history of neuroimaging features in PA has not been systematically studied. Common MRI features reported in small case series include generalised brain atrophy [176] and delayed myelination [19]. Cerebellar haemorrhage has been reported at presentation in neonates, but may be an incidental finding [19]**.** Imaging features corresponding to acute basal ganglia injuries include increased T_2 signal and alterations in diffusion parameters, with later evidence of atrophy of these structures. A combined MRI and positron emission tomography (PET) study demonstrated progressive alterations in the basal ganglia: initial imaging and uptake were normal, but subsequent examinations found increased basal ganglia T_2 signal and

increased ^{18}fluro-2-deoxyglucose (^{18}FDG) uptake [177]. At a later time point the basal ganglia were found to be atrophied with decreased ^{18}FDG uptake implying a "burned out" end stage.

The deep gray matter structures are vulnerable particularly during metabolic decompensation [175, 178, 179] but may also be affected during apparent metabolic stability [19]. Acute basal ganglia injury may be the initial presentation of late onset disease in previously asymptomatic children [10, 180, 181]. Acute changes in the basal ganglia can be seen at an earlier age, for example in a 6 month old child presenting with infantile spasms [182]. In this case, the child received vigabatrin therapy for the infantile spasms that the authors suggested protected the basal ganglia from irreversible excitotoxic damage.

The basal ganglia are gray matter nuclei sited near the base of each cerebral hemisphere, comprised of the striatum (caudate, putamen and ventral striatum), globus pallidus, substantia nigra and subthalamic nucleus [183]. They facilitate action selection in the control of movement, and damage to the pathways results in movement disorders such as in Parkinson's disease [184]. The striatum receives excitatory inputs from the cortex and thalamus; dopaminergic projections flow from the striatum to the globus pallidus and substantia nigra; finally outputs from the basal ganglia arising from the globus pallidus then connect to the thalamus and other nuclei resulting in the modulation of cortical movement signalling [184].

Post mortem neuropathological studies in children with PA have demonstrated a range of abnormalities. A 9 year old child was found to have acute haemorrhagic lesions in the basal ganglia with evidence of vascular proliferation and swollen endothelial cells suggestive of compromise of the blood brain barrier [185]. A 3 year old child was reported to have vascular

and parenchymal mineralisation and spongy change with foci of acute neuronal injury [185]. An infant who succumbed to severe disease in the first two weeks of age had spongiform changes in the white matter and basal ganglia [186]. Interesting findings were demonstrated in one child with neonatal onset disease who died of respiratory complications at 4 years of age [187]. The child was found to have a normal brainstem and cerebellum, but there was significant vacuolization in the frontal and occipital cortices, with prominent changes and loss of neurons in the hippocampus. The basal ganglia (caudate, putamen and globus pallidi) also showed vacuolization.

7.3. Pathophysiological mechanisms of neurologic complications

The pathophysiology of the neurological complications of PA is incompletely understood, with different mechanisms at work during acute metabolic decompensation and the chronic "insidious" phase [19]. In particular, it is not known why the basal ganglia appear to be so vulnerable to infarction in PA. During acute presentations systemic metabolic alterations may have deleterious effects on the CNS, including hypoglycaemia, keto-lactic acidosis and hyperammonaemia which may all cause neuronal injury. Cerebral oedema is common, resulting in hypoperfusion of the CNS and subsequent ischaemic/hypoxic insults.

7.3.1. Hyperammonaemia

High blood ammonia concentrations (hyperammonaemia) is an important contributor to neuropathological processes in PA [188]. Hyperammonaemia is known to be deleterious in urea cycle disorders and acute liver failure [189]. In these disorders several mechanisms are postulated to mediate the deleterious effects of ammonia, including: direct neurotoxicity; cell and brain oedema secondary to the conversion of ammonia to glutamine by astrocytes; glutamate mediated excitotoxicity; effects on vasculature (vasogenic oedema) and or altered

water and potassium homeostasis [189]. Similar mechanisms may play a role in PA. Hyperammonaemia in PA arises by different mechanisms, and may be secondary to inhibition of the urea cycle enzyme carbamoyl-phosphate synthase-1 due to decreased availability of its activator *N*-acetylglutamate, which is caused by competitive inhibition of *N*-acetylglutamate synthase by propionyl CoA [190]. In contrast to urea cycle disorders, hyperammonaemia in PA may be associated with low glutamine levels [188].

7.3.2. Toxic metabolite accumulation

A number of metabolites accumulate in PA, which may have neurotoxic effects. For example, intra-striatal injection of propionate causes seizures in rats. These effects are ameliorated by the non-competitive *N*-methyl-D-aspartate (NMDA) receptor antagonist MK801 suggesting that the NMDA receptor may play an important role in the disease pathogenesis [191]. Propionate is metabolised oxidatively by glial cells but not neurons, suggesting that glia may be more vulnerable to toxicity in PA [192].

Glycine may have excitatory effects via the NMDA receptor, which may be important given the high glycine concentrations found in CSF and blood in PA [178]. Furthermore, locally synthesised dicarboxylic acids and tricarboxylic acids may be trapped within the central nervous system exacerbating their pathological effects [193].

7.3.3. Compromised energy metabolism

Several components of normal energy metabolism may be compromised in PA, which would have the greatest impact on tissues with the highest energy requirements such as the basal ganglia. Several key enzymes including the pyruvate dehydrogenase complex, complex III of

the electron transfer chain, and the α-ketoglutarate dehydrogenase complex are all inhibited by propionyl-CoA, and *in vitro* analysis of energy pathways in muscle biopsies of patients with PA supports the finding of compromised energy metabolism [194]. There is also evidence for a role of oxidative stress, thus for example ascorbic acid affords protection to rats injected with propionate [19].

7.3.4. Compromised Krebs Cycle Anaplerosis Theory

Dysfunction of the Krebs cycle may also result from depletion of its intermediary metabolites due to compromised "anaplerosis". Anaplerosis *is "the re-filling of the catalytic intermediates of the [Krebs] cycle that carry acetyl-CoA as it is oxidized"* [195]. Cataplerosis is the opposite balancing mechanism of removal of excess Krebs cycle intermediates. The Krebs cycle converts the carbon atoms of acetyl-CoA to carbon dioxide, with the production of reducing equivalents NADH and $FADH_2$ (reduced flavin adenine dinucleotide) that then enter the electron transport chain resulting in ATP generation. The Krebs cycle finally regenerates the acetyl group acceptor oxaloacetate (figure 7.2) [196].

It has been estimated that 1-2% of the total pool of Krebs cycle intermediates is depleted via cataplerosis per minute [195]; this loss of metabolites must be corrected by anaplerotic mechanisms to ensure the cycle can continue to function. In addition to maintaining appropriate pools of the Krebs cycle intermediates, these pathways also play roles in gluconeogenesis from amino acids, lactate and pyruvate, the regulation of neurotransmitter synthesis in brain, and insulin secretion in pancreatic β-cells [195].

There are several important anaplerotic reactions (figure 7.2), notably the supply of oxaloacetate from pyruvate by pyruvate carboxylase, the supply of α-ketoglutarate from glutamate and glutamine, and the supply of succinyl CoA via the metabolism by PCC of propionyl-CoA derived from intestinal propionate, odd chain fatty acids, propionylcarnitine and branch chain amino acids. This third anaplerotic route has been successfully manipulated in the treatment of pyruvate carboxylase deficiency by supply of the propionyl-CoA precursor triheptanoin [197].

Krebs cycle anaplerosis is compromised in PA for several reasons. Firstly, propionyl CoA cannot be metabolised and therefore the third anaplerotic supply route cannot function. Secondly, oxaloacetate is depleted by condensation with propionyl-CoA to form methylcitrate. Thirdly, propionate may also inhibit pyruvate conversion to oxaloacetate. There is evidence that there is subsequent citrate depletion, and the functional lack of α-ketoglutarate shifts the equilibrium of reactions catalysed by glutamate dehydrogenase resulting in the production of ammonia and consumption of glutamate [188]. It is proposed that supply of anaplerotic substrates could improve Krebs cycle function in several conditions, and a clinical trial of dietary supplements in PA with glutamine or α-ketoglutarate is in progress (US National Institutes of Health clinical trials register (www.clinicaltrial.gov) reference NCT00645879).

Extensive alterations in the plasma amino acid profile are detected in PA, many of which may be secondary to the depletion of α-ketoglutarate [166, 198]. Depleted amino acids include glutamine, histidine, threonine, the branch chain amino acids leucine, isoleucine and valine, phenylalanine and arginine. Concentrations of glycine, lysine, alanine and aspartate are

increased [198]. Hyperglycinaemia is caused by inhibition of the hepatic glycine cleavage system, although this is not the case within the brain [199]. Alanine is elevated secondary to lactic acidosis caused by propionyl CoA inhibition of pyruvate dehydrogenase.

Amino acids within the CSF are also deranged, with particular elevations of alanine and glycine reported at times of metabolic decompensation [179]. Glutamine in CSF was elevated in the presence of low plasma glutamine and hyperammonaemia in an acutely ill neonate [200]; in a 10 year old child during an acute encephalopathic episode CSF glutamine was elevated and plasma glutamine decreased following hyperammonaemia. However other reports have demonstrated low/normal CSF glutamine in metabolic stability associated with normal ammonia concentrations [201].

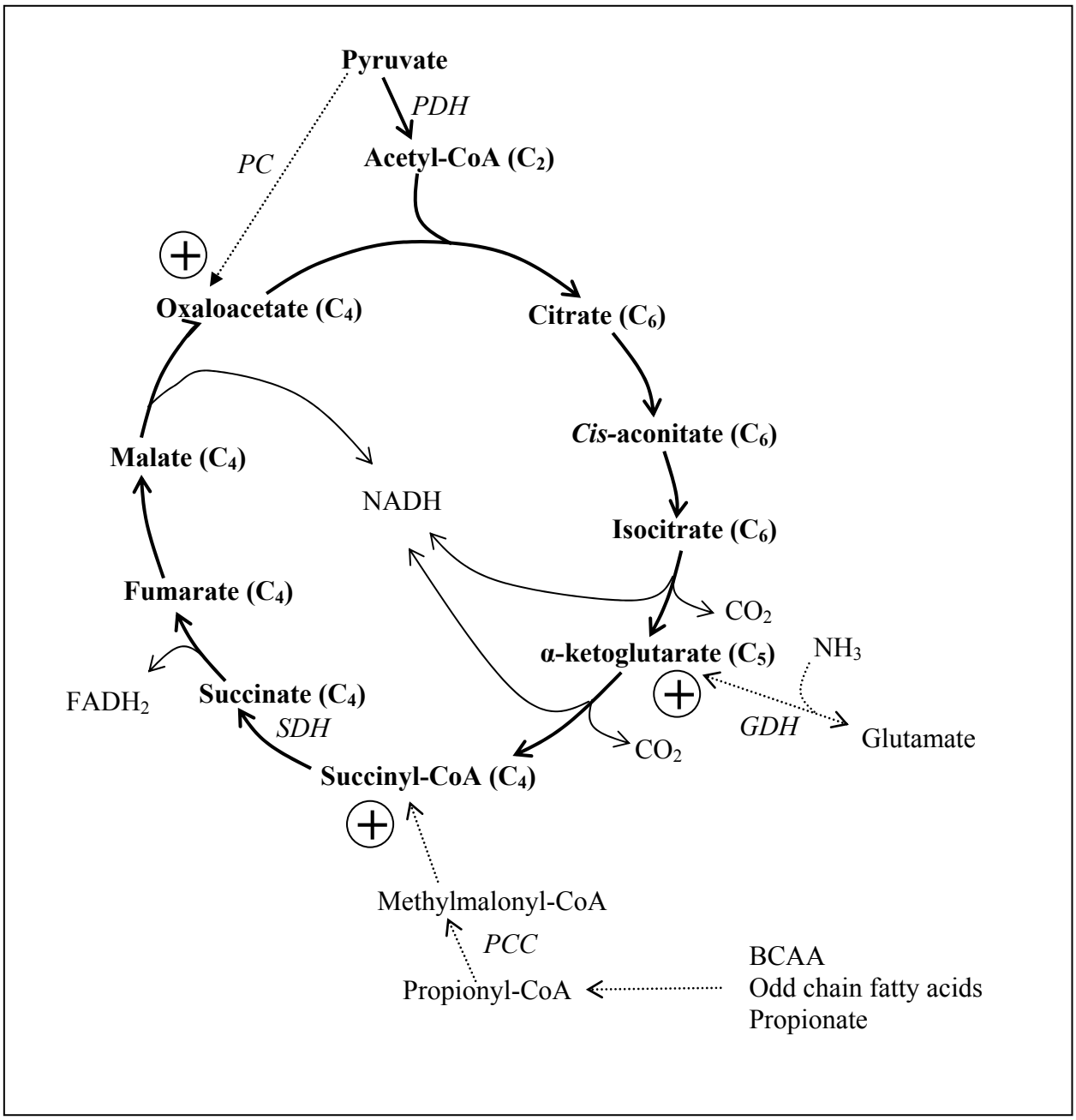

Figure 7.2: Anaplerosis of the Krebs cycle. Main points of anaplerosis indicated by (+). PC, pyruvate carboxylase; PDH, pyruvate dehydrogenase; GDH, glutamate dehydrogenase; SDH, succinate dehydrogenase. NADH, $FADH_2$ (Adapted from [196]).

7.4. *In vivo* brain MRS in propionic acidaemia

The many suggested pathogenic mechanisms discussed above could result in alterations in brain tissue metabolism which would be amenable to study using non-invasive MRS. Two previous small studies have been reported in the context of PA, all reporting findings in patients who were "well" i.e. metabolically stable at the time of MRS.

Chemelli *et al* reported brain MRS data from four patients with PA using long echo time single voxel or chemical shift imaging with semi-quantitative peak area estimation [202]. Two children had mild brain atrophy, and these patients had decreased NAA/Cho ratio in periventricular white matter, while NAA/Cho was normal in the two children with normal MR imaging. None of the patients had basal ganglia abnormalities on MRI, and MRS did not sample the basal ganglia. All four children had elevated levels of lactate detected, not seen in control patients. This suggests that brain tissue metabolism may be compromised even when systemic metabolism is well controlled; organic acids within the CSF are known to be elevated even in stable patients [193, 203].

Bergman *et al* investigated three children with PA and compared them to eight controls [201]. This study employed a single voxel short echo time acquisition technique (STEAM) at 1.5T, sampling over the basal ganglia and using peak area estimation to quantify NAA, choline and inositol, and glutamine+glutamate/creatine ratio. All patients had normal ammonia at the time of MRI, and all had mild ventricular enlargement. One of the three had T_1 and T_2 signal abnormalities in the caudate and putamen. In general, NAA and myo-inositol were decreased, and one child had elevated choline. The glutamine+glutamate/creatine ratio was elevated compared to controls. The authors suggest a mechanism whereby hyperammonaemia results

in elevated glutamine, with a secondary compensatory decrease in inositol to regulate osmotic pressures. However, since ammonia levels were normal alternative mechanisms may exist within the brain.

7.5. Aims & Objectives

This section of the current work aimed to explore the various pathogenesis hypotheses described above, specifically by analysis of the differential alterations in brain metabolite profiles seen during metabolic stability and during acute metabolic decompensation in PA patients.

7.6. Methods

7.6.1. Patients

Patients were recruited from a single tertiary paediatric IMD unit. Clinical data were extracted from medical records including age at diagnosis, mode of presentation, therapeutic modalities and history of subsequent acute neurological events. Available blood quantitative amino acid and ammonia determinations were also collated from the medical record. MR imaging and MR spectroscopy were performed either electively or in the context of acute metabolic decompensation requiring intensive care support.

7.6.2. Conventional MRI: qualitative and quantitative analysis

All available brain MRI studies were retrospectively reviewed, including review of the qualitative radiology reports by the consultant paediatric radiologist with particular attention paid to appearances of the basal ganglia.

Signal abnormalities within the basal ganglia were further assessed by a semi-quantitative analysis of the T_2 signal and apparent diffusion coefficient (ADC; see Appendix A for discussion of this DWI parameter). An axial slice at the level of the inferior border of the corpus callosum was identified and axial T_2 weighted and axial ADC maps were co-registered. Regions of interest (ROI) defining the head of caudate, putamen, globus pallidus and posterior-medial thalamus were manually delineated (single observer, JED) on T_2 images and ADC maps and the average signal from each ROI recorded. The ratio of signal from each basal ganglion ROI to the signal from the medial thalamus was calculated to allow inter-scan comparison. Measurements were made using the clinical picture archiving and communication system (PACS, Agfa Impax 6.4.0.4841, Apache Software Foundation, Agfa Healthcare, Belgium) by a single observer (JED) (figure 7.3). Comparison of data from PA patients was made with data from 47 MRI studies from patients without PA who had normal MR imaging as adjudged from the qualitative radiologist report.

Figure 7.3: Manual identification of basal ganglia structures in axial T_2 weight image (left) at level of inferior border of corpus callosum (right).

7.6.3. MR Spectroscopy

MRS studies were performed concurrently with clinically indicated MRI scans at 1.5 Tesla facilitated by general anaesthesia as needed. It was possible to acquire MRS for some patients during episodes of acute metabolic decompensation/ encephalopathy, when patients required intensive care support. Comparison was made with MRS metabolite data from the standard cohort of children with normal appearing MRI and similar age profile (white matter, n=53, median (range) age 4.7(0.5-16.7) years; basal ganglia n=63, 4.1(0.5-16.7) years). Comparison was also made between MRS data acquired in stable PA patients with data acquired from acutely unwell children to evaluate alterations in brain metabolite profile in these settings.

7.6.4. Urine NMR Spectroscopy

Mid stream random urine samples were collected from PA patients attending outpatient clinic. Samples were processed, stored and analysed as described in Chapter 3.

7.7. Results

7.7.1. Patient characteristics

Nine children (two female) with propionic acidaemia were studied (median age at first MRS, 36 months (range 4-190 months) (see table 7.1). All were diagnosed in the neonatal period, four requiring neonatal haemofiltration due to severe hyperammonaemia and metabolic acidosis. Two children had received elective orthotopic liver transplantation during early childhood. The remaining seven children all received regular oral carnitine and sodium benzoate, and three received sodium phenylbutyrate, in addition to dietary protein control under management of a specialist dietetic team.

Four children had one or more severe acute episodes with encephalopathy beyond the neonatal period requiring intensive care support ("severe acute episode" hereafter). During these episodes all children required ventilatory support and three required continuous veno-venous haemofiltration (CVVH), and only one episode was associated with significant persistent hyperammonaemia. During these episodes three children received intravenous sodium benzoate and two received sodium phenylbutyrate, while two received N-Carbamylglutamate to treat hyperammonaemia with good effect.

	Neonatal CVVH?	Liver Transplant (age, years)	Other diagnoses	Age at MRI (years)	Status at time of MRI	Metabolic Drugs & Dietary Restrictions		Acute encephalopathic episodes: complications	MRI findings	
						Maintenance	Acute		Basal ganglia	Other features
1	Yes			1.3	Stable	LC, SB, PR			Normal	
2	Yes		Hypo-thyroidism	1	Enceph.	SP, SB, LC, T, M, PR	SP, SB, NC	Sepsis & hyper-ammonaemia,	Acutely swelling caudate, dentate	
				1.2	Stable	SB, LC, T, PR			Resolving swelling	Delayed myelination, enlarged ventricles
				3	Enceph.	SB, LC, T, PR		Cardiomyopathy, pneumonia	Acute swelling caudate, putamen, dentate	Delayed myelination, enlarged ventricles, hippocampal atrophy
3	No		Epilepsy	6.2	Enceph.	SB, LC, PR	SB, LC		Atrophic, high T2. Haemorrhage	Global loss of cerebral volume
				9.5	Enceph.	SB, LC, PR	SB LC	Rhabdomyolysis	Cystic encephalomalacia	Enlarged ventricles / cerebral volume loss
4	Yes		Hypo-thyroidism	1.2	Stable	SB, SP, LC, PR			Normal	Mild volume loss
				4	Stable	SB, SP, LC, PR			Normal	Mild volume loss, thin corpus callosum
				6	Enceph.	SB, SP, LC, PR	SP, SB, LC	Pneumonia	Acute swelling caudate + putamen	Cerebral volume loss, small hippocampi
5	Yes			0.6	Stable	SB, LC, PR			Normal	Mild ventricular dilation
				3.1	Stable				Normal	Disturbed myelination
6	No			3	Stable	SB, SP, LC, PR			Normal	Hippocampal sclerosis
7	No	Yes (1.3)		15	Stable	Anti-rejection			Normal	
8	No	Yes (2.5)	Myoclonic epilepsy	6.5	Stable	Anti-rejection LC			Normal	Mild ventricular enlargement
				13	Stable	Anti-rejection LC			Normal	Mild ventricular enlargement. Unilateral mesial temporal sclerosis
9	No			0.3	Stable*	LC, PR			Normal	Normal
				1.5	Enceph	LC, PR	NC (x2)	Varicella	Acute high T2 signal globus pallidi.	Increased ventricular size & white matter T2.

*required ventilation for RSV bronchiolitis but not encephalopathic.

Table 7.1: Summary of clinical characteristics of propionic acidaemia cohort and MR imaging findings. MRS, magnetic resonance spectroscopy; CVVH, Continuous veno-venous haemofiltration; LC, L-carnitine; SP, Sodium Phenylbutyrate; SB, Sodium Benzoate; M, metronidazole; T, thyroxine; NC, N-Carbamylglutamate; PR, dietary protein restriction; Enceph., denotes acute encephalopathic episode.

7.7.2. Magnetic Resonance Imaging

The basal ganglia appeared qualitatively normal in all children (n=7) prior to any severe acute episode beyond the neonatal period (figure 7.4), and also the quantification of T_2 and ADC signal in the basal ganglia was also normal in this group (figure 7.5). MRI scans obtained during severe acute episodes demonstrated abnormal signal in the basal ganglia variably including the caudate heads, putamen and globus pallidi and in some cases there was also evidence of acute changes in the dentate nuclei and cerebral cortex. Affected areas had elevated T_2 signal, while alterations in the ADC demonstrated both increased and decreased values, reflecting the heterogeneity of the insult. One child demonstrated evidence of previous basal ganglia infarction relating to a previous acute encephalopathic episode, with cystic degeneration of caudate, putamen and globus pallidus.

Interestingly the hippocampi appeared atrophic in seven cases; however, formal quantitative volumetric analysis of hippocampal structures was not possible as 3D volume series had not been routinely included in the MRI protocol. Cerebral volume loss was most marked in children with preceding severe acute episodes. The two children who had liver transplantation had normal appearing basal ganglia, cortex and white matter on MRI undertaken more than 10 years post-transplant, with one showing probable temporal mesial sclerosis.

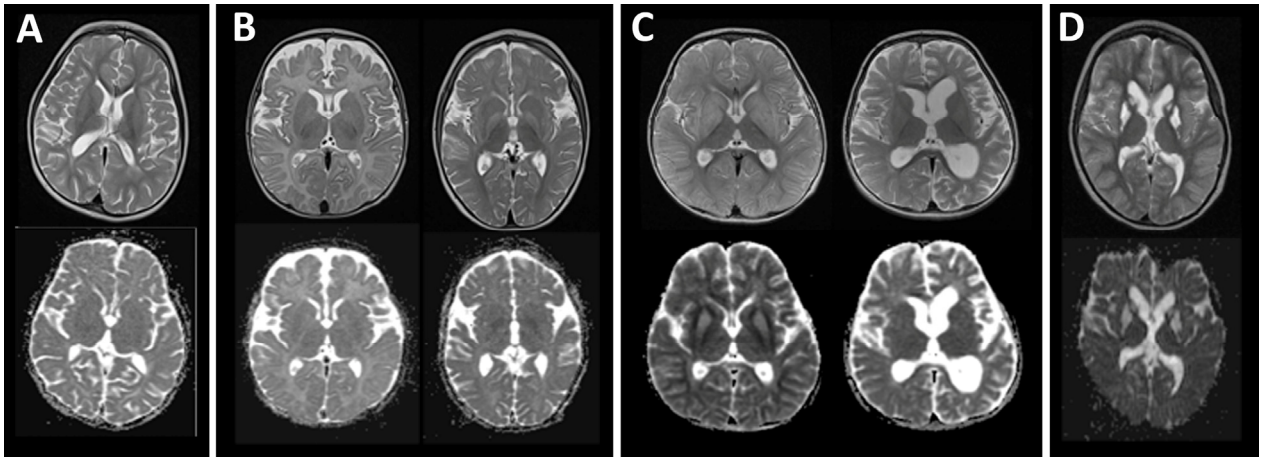

Figure 7.4: MR images of propionic acidaemia patients. Upper row: T_2 weighted axial images. Lower row: ADC maps. (A) Patient 5 aged 3.1years. Normal basal ganglia. (B) Patient 9 with (left) normal basal ganglia aged 0.3months and (right) hyperintense T_2 signal in globus pallidus with restricted diffusion on ADC map aged 1.5 years. (C) Patient 2 with (left) acutely swollen hyper intense basal ganglia with mixed pattern of restricted and increased diffusion on ADC map aged 1 year and (right) resolution of swelling and abnormal diffusion aged 1.2 years. (D) Patient 3 aged 9.5 years, hyperintense and atrophic basal ganglia (cystic encephalomalacia) with increased ADC.

Caudate

T_2

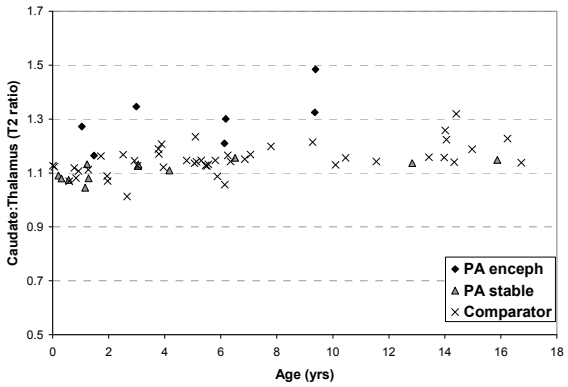

ADC

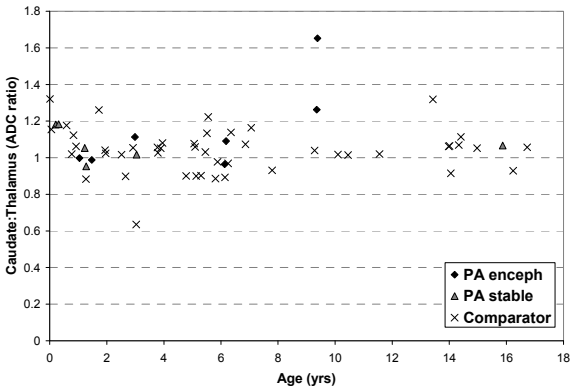

Putamen

T_2

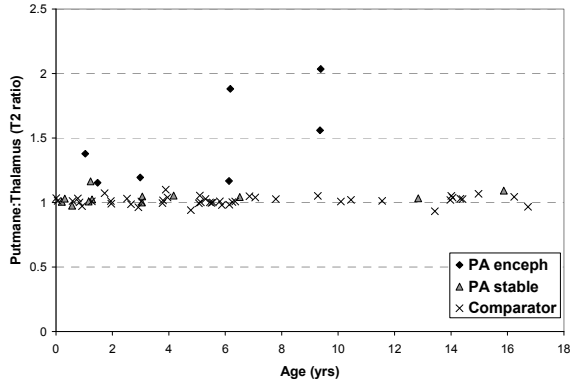

ADC

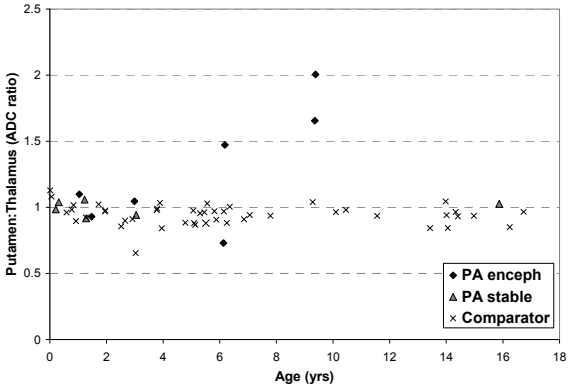

Globus pallidus

T_2

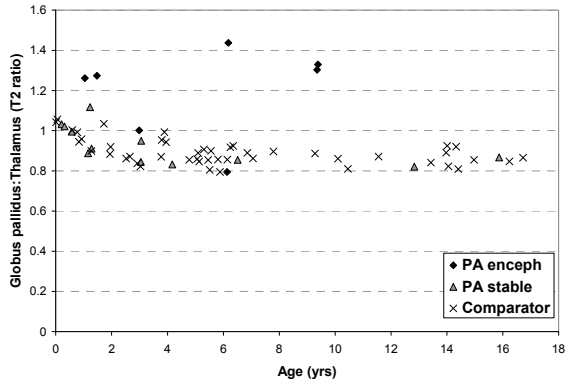

ADC

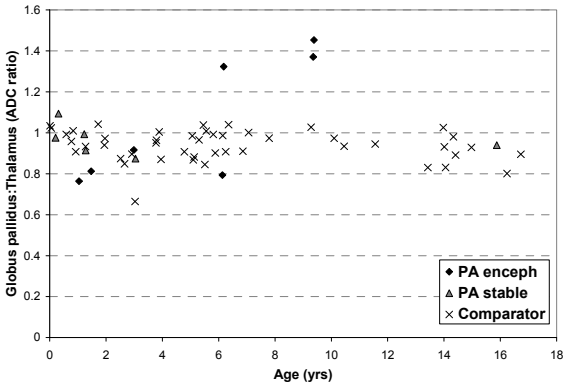

Figure 7.5: Quantitative analysis of basal ganglia T_2 and ADC signal in propionic acidaemia patients and normal MRI control group. Values plotted as ratio to signal from medial thalamus.

7.7.3. Magnetic Resonance Spectroscopy

Six studies from four children were acquired during severe acute episodes requiring intensive care support. Seven studies from six children were acquired with elective outpatient MRI studies undertaken during metabolic stability and before any severe acute episode had occurred. Analysis of mean spectra (figure 7.7) and mean metabolite concentrations (figure 7.6 and table 7.2) demonstrated metabolite alterations in basal ganglia and parieto-occipital white matter, in particular during severe acute episodes.

MRS studies undertaken during metabolic stability before any severe acute episodes beyond the neonatal period demonstrated decreased Gln+Glu in basal ganglia compared to the normal MRI comparator group but a trend to increase in white matter. Glutamine alone was significantly decreased in basal ganglia during metabolic stability. Mean lactate was not elevated, although two cases had reliably detected lactate in basal ganglia. There was no significant decrease in the total N-acetylaspartate and N-acetylaspartylglutamate (tNAA) in this group.

MRS studies acquired during severe acute episodes demonstrated significantly decreased tNAA, Gln+Glu and creatine, and significantly elevated lactate, in the basal ganglia compared to both the normal MRI comparator group and to the metabolically stable propionic acidaemia cohort. In white matter lactate was significantly elevated but other metabolites were not significantly altered. (Data shown are for all severe acute episodes; analysis of first severe acute episode only demonstrated similar findings). There were no significant differences between groups in brain *myo*-inositol.

Separate analysis of brain metabolites from the two children post-liver transplant demonstrated normal basal ganglia tNAA and slightly decreased Gln+Glu. tNAA was elevated in white matter and total choline decreased.

7.7.3.1.Detection of brain glycine and propionate precursors

MR spectra acquired at long echo time (TE 135ms) were reviewed visually for the presence of the singlet peak of glycine at c. 3.54ppm. This peak co-resonates with myo-inositol, but at longer echo times the myo-inositol peaks have usually decayed due to the short T_2 and so the glycine peak may be detected (see also Chapter 5). In two cases (during metabolic stability), possible small glycine peaks were identified, with putative glycine concentrations of c. 0.7mmol/L. In the remainder, visible glycine peaks were not identified. The spectral region 3.4-4.0 was noted to often have lower signal/noise ratio than up-field regions making the identification of small glycine peaks difficult.

Spectra were also visually reviewed for the presence of other unfitted peaks that could represent propionic acid or associated propionate metabolites, but no such peaks were identified.

Basal ganglia metabolites (mM, mean (standard deviation))

	Propionic Acidaemia			Normal MRI comparator group
	Metabolic stability (7 studies from 6 patients)	Acute encephalopathy (6 studies from 4 patients)	Post-liver transplant (2 studies from 2 patients)	(63 studies)
Median age (years, (range))	3.1 (0.6-15.9)	4.6 (1.0-9.4)	14.4 (12.9-15.9)	4.1 (0.5-16.7)
N-Acetylaspartate	5.06 (0.49)	4.07 (0.35)†#	5.35 (0.28)	5.21 (0.51)
Creatine	4.56 (0.43)	4.02 (0.25)† $	4.42 (0.14)	4.55 (0.59)
Glutamine	1.39 (0.39) *	0.99 (0.90)*	1.27 (0.25)	1.98 (0.79)
Glutamate	4.34 (0.27)	3.37 (0.49)†#	4.30 (0.39)	4.45 (0.78)
Glutamine+Glutamate	5.73 (0.57) *	4.36 (0.80)†#	5.57 (0.28)	6.43 (1.39)
myo-Inositol	2.62 (0.26)	2.88 (0.71)	2.39 (0.0)	2.49 (0.43)
Lactate	0.31 (0.34)	0.80 (0.53)†	0.00 (0.32)	0.11 (0.20)
Choline	1.08 (0.18)	1.22 (0.21)	0.90 (0.63)	1.11 (0.18)

White matter metabolites (mM, mean (standard deviation))

	Propionic Acidaemia			Normal MRI comparator group
	Metabolic stability (7 studies from 6 patients)	Acute encephalopathy (5 studies from 4 patients)	Post-liver transplant (2 studies from 2 patients)	(53 studies)
Median age (years, (range))	3.1 (0.3-15.9)	6.13 (1.5 -9.4)	14.4 (12.9-15.9)	4.7 (0.5-16.7)
N-Acetylaspartate	4.91 (0.90)	4.41 (0.58) *	6.11 (0.39)	5.11 (0.73)
Creatine	3.48 (0.26) *	3.47 (0.28)	3.70 (0.00)	3.18 (0.47)
Glutamine	1.76 (0.79)	1.30 (1.22)	1.62 (0.49)	1.32 (0.62)
Glutamate	3.45 (0.78)	2.58 (0.70) †$	4.27 (0.31)	3.51 (0.78)
Glutamine+Glutamate	5.21 (0.73)	3.88 (1.72)	5.89 (0.80)	4.84 (1.18)
myo-Inositol	2.76 (0.38)	2.86 (0.60)	2.79 (0.02)	2.57 (0.39)
Lactate	0.58 (0.51)*	0.69 (0.73)*	0.32 (0.45)	0.21 (0.28)
Choline	0.99 (0.29)	1.20 (0.26)	0.83 (0.09)	1.08 (0.15)

Table 7.2: Mean MRS derived brain metabolite concentrations in propionic acidaemia and normal MRI comparator group. Mann Whitney U test (2 tailed exact significance) for difference in metabolite concentrations between stable and encephalopathic propionic acidaemia cohort, $ $p<0.05$, # $p<0.01$.

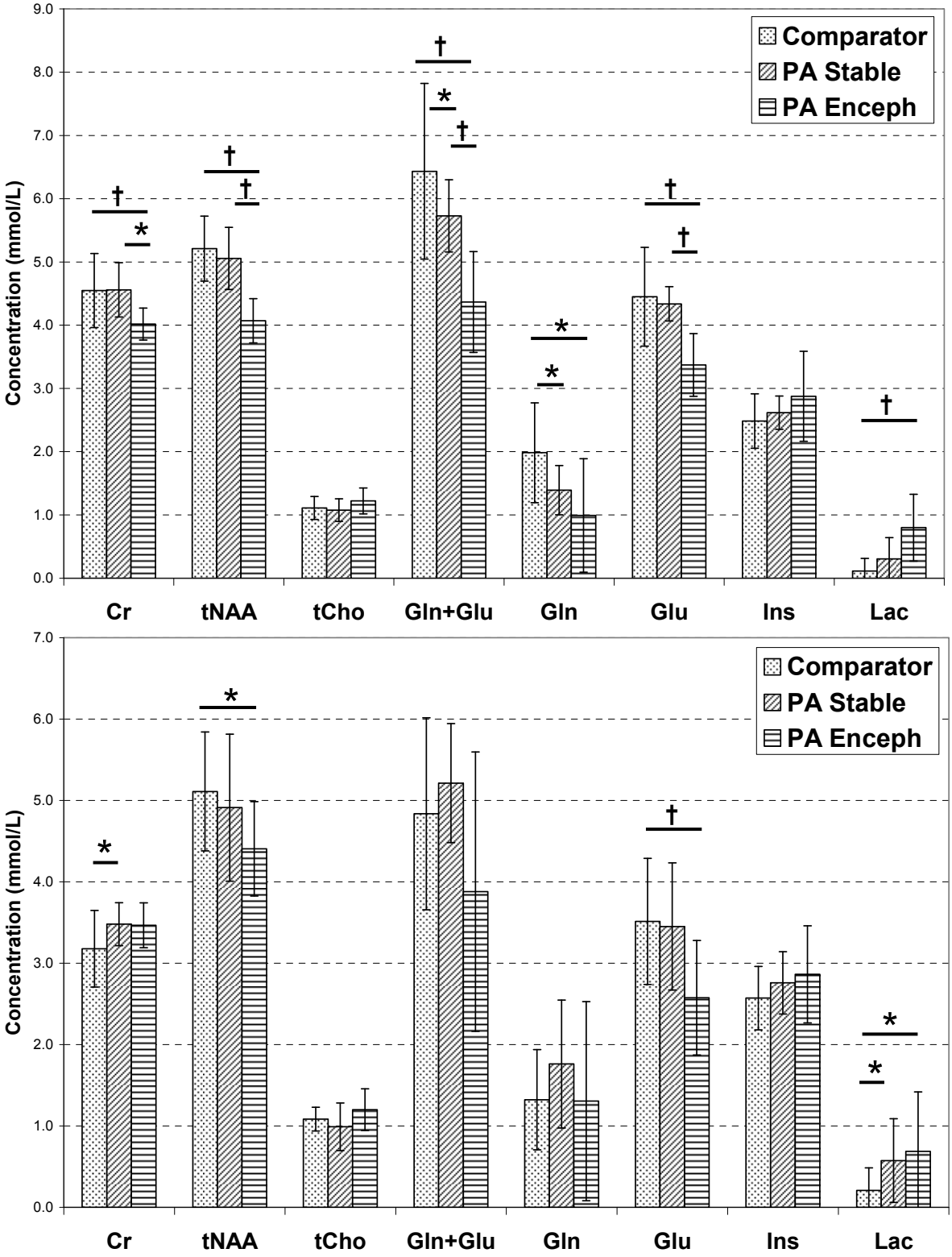

Figure 7.6: Bar charts of mean metabolite concentrations for basal ganglia (upper panel) and white matter (lower panel) for stable and encephalopathic propionic acidaemia patients and comparator group. Error bars indicate standard deviation. † $p<0.01$, * $p<0.05$.

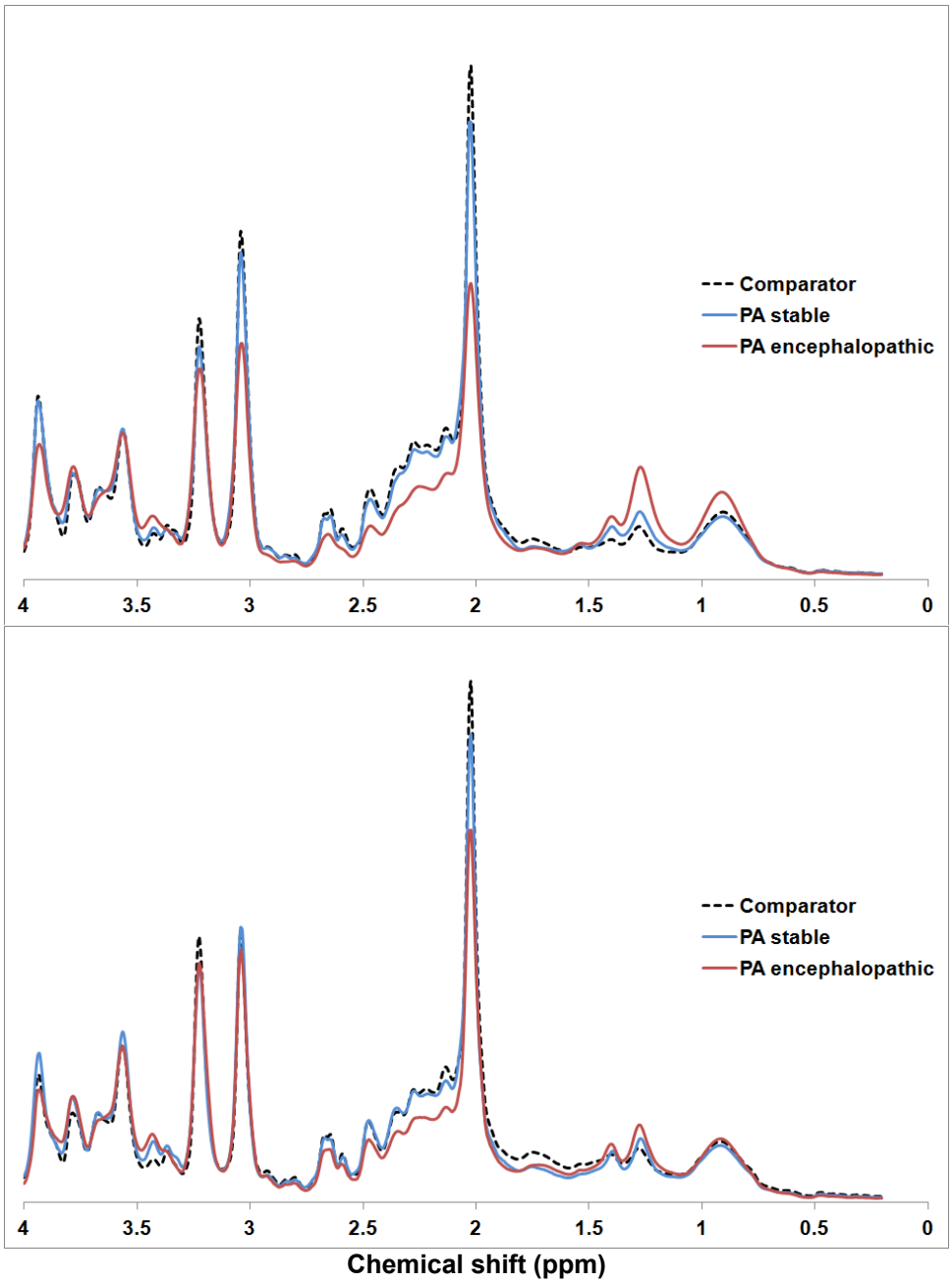

Figure 7.7: Mean MR spectra from propionic acidaemia cohort during metabolic stability (blue) and acute encephalopathy (red) and comparator cohort (black dash) from basal ganglia (upper panel) and white matter (lower panel). ppm, parts per million.

7.7.4. Quantitative amino acids

105 plasma quantitative amino acid analyses from the PA cohort were available. 88 of these had a concurrent (<24hours) ammonia estimation available. Correlation with ammonia concentration was calculated for each amino acid (Pearson correlation coefficient, r, see table 7.3). Significant correlations between amino acids were also evaluated (table 7.4).

Compared to standard control quantitative amino acid concentrations, amino acids elevated in PA patients included alanine, glycine and lysine; glutamine was often low as were the branch chain amino acids (see table 7.3 and figure 7.8). The only significant correlations with ammonia were between lysine (r=0.45) and tyrosine (r=0.42). Glutamine+glutamate (r=0.04) and glutamine alone (r=0.08) did not display a correlation with ammonia (figure 7.9).

Glutamine displayed moderate degree of correlation with each of the urea cycle-related amino acids (figure 7.10 and table 7.4).

	Mean (standard deviation)	Control values Median (2.5th-97.5th centile)	Ammonia Pearson correlation (r)
Alanine	423 (171)	300 (112-592)	-0.199
Arginine	55 (24)	51 (14-102)	-0.065
Aspartate	15 (7)		-0.124
Citrulline	17 (10)		0.074
Cysteine	15 (13)		0.028
Glutamine	388 (176)	539 (326-800)	0.080
Glutamate	95 (53)	88 (31-219)	-0.154
Gln+Glu	483 (172)		0.036
Glycine	580 (304)	246 (120-436)	-0.019
Histidine	71 (25)	74 (43-111)	-0.151
Isoleucine	29 (15)	50 (20-91)	0.031
Leucine	70 (35)	97 (44-169)	0.046
Lysine	186 (70)	130 (66-242)	0.447†
Methionine	20 (8)	20 (10-41)	-0.065
Ornithine	43 (23)	59 (24-154)	-0.052
Phenylalanine	48 (16)	48 (30-76)	-0.127
Proline	200 (70)	154 (66-330)	-0.104
Serine	145 (56)	127 (69-206)	-0.142
Taurine	71 (31)	70 (26-169)	-0.178
Threonine	141 (102)	104 (43-218)	-0.120
Tyrosine	53 (23)	51 (29-92)	0.419†
Valine	90 (39)	178 (79-313)	0.207

Table 7.3: Plasma quantitative amino acid concentrations (μmol/L) in propionic acidaemia patients and correlation of amino acids with concurrent ammonia estimate. Control values: plasma amino acid reference intervals calculated from 271 subjects from 8 different laboratories, courtesy Mrs MA Preece. † $p<0.0001$ for correlation.

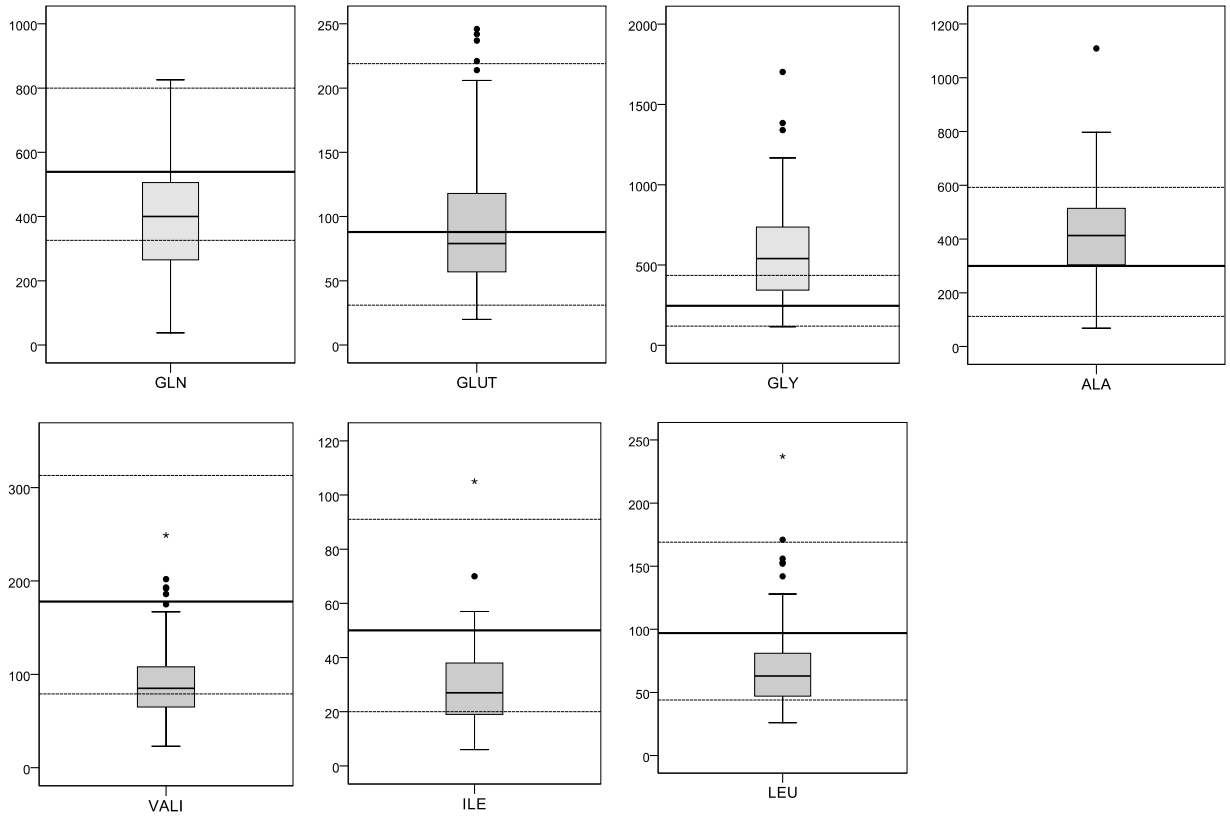

Figure 7.8: Box plots of plasma amino acid concentrations for propionic acidaemia cohort. Solid line (median) and dotted lines (2.5th and 97.5th centile) from normal control data. GLN, glutamine; GLUT, glutamate; GLY, glycine; ALA, alanine; VALI, valine; ILE, isoleucine; LEU, leucine.

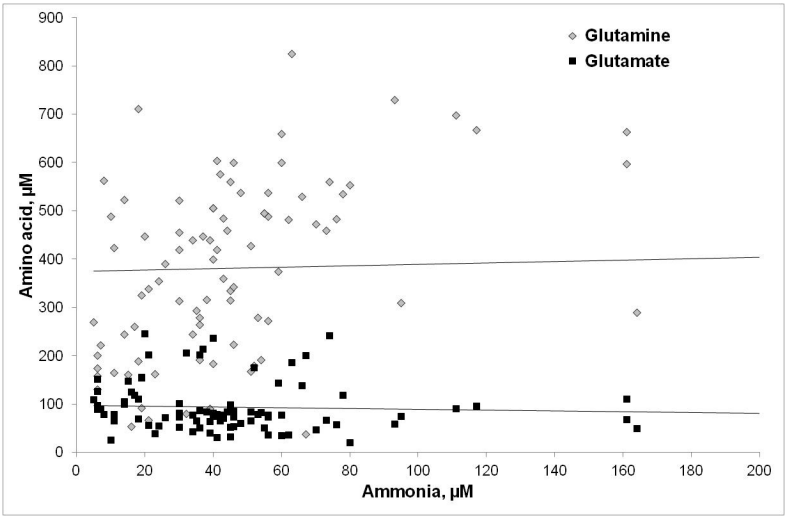

Figure 7.9: Plot of plasma glutamine and glutamate against concurrent ammonia level in propionic acidaemia patients. Lines: linear regression fits.

	ARG	ASP	CIT	CYST	GLN	GLUT	GLY	HIS	ILE	LEU	LYSI	MET	ORN	PHE	PROL	SER	TAU	THR	TYR	VALI	Gln+Glu
ALA	**0.472**	**0.361**	**0.491**	0.175	**0.302**	**0.258**	0.126	0.185	**0.332**	0.135	**0.266**	**0.373**	**0.194**	-0.128	**0.680**	**0.580**	**0.309**	**0.227**	**0.268**	0.170	0.387
ARG		**0.319**	**0.549**	0.004	**0.320**	**0.226**	0.181	**0.211**	**0.367**	**0.297**	**0.448**	**0.338**	**0.268**	0.023	**0.432**	**0.365**	0.082	-0.024	**0.332**	**0.255**	0.396
ASP			**0.260**	0.088	0.105	**0.356**	-0.016	**0.285**	**0.232**	0.004	0.115	**0.405**	**0.279**	0.010	**0.220**	**0.611**	**0.217**	**0.389**	0.131	0.175	0.216
CIT				0.135	**0.460**	0.009	**0.302**	0.054	**0.308**	0.151	**0.324**	**0.199**	**0.317**	-0.184	**0.475**	**0.387**	0.102	-0.029	**0.402**	**0.245**	0.473
CYST						-0.133	0.051	-0.066	0.082	0.049	0.010	**0.233**	-0.036	0.073	**0.269**	0.055	0.061	0.109	-0.028	**0.212**	0.063
GLN						**-0.224**	**0.418**	0.041	0.181	**0.334**	**0.431**	0.005	**0.228**	-0.063	**0.422**	**0.228**	0.016	-0.140	**0.450**	0.128	0.955
GLUT							**-0.393**	0.165	**0.337**	0.135	0.021	0.114	0.086	-0.051	**0.241**	0.109	0.114	**0.230**	-0.052	**0.247**	0.077
GLY								**-0.271**	-0.035	0.132	**0.257**	0.026	0.022	-0.021	0.098	0.119	-0.041	**-0.419**	**0.232**	-0.117	0.308
HIS									0.033	0.049	0.156	0.164	0.150	0.192	**0.304**	**0.285**	0.082	**0.209**	**0.204**	**0.227**	0.093
ILE										**0.544**	0.081	**0.570**	**0.209**	0.068	**0.388**	**0.216**	0.014	**0.306**	0.103	**0.709**	0.288
LEU											**0.364**	0.128	**0.239**	**0.480**	**0.338**	-0.103	-0.180	-0.159	**0.304**	**0.565**	0.383
LYSI												0.052	0.192	0.109	**0.333**	0.153	-0.003	-0.095	**0.674**	**0.202**	0.447
MET													0.156	0.163	**0.269**	**0.503**	0.025	**0.591**	0.119	**0.412**	0.040
ORN														0.100	0.171	**0.281**	-0.014	**0.223**	**0.208**	0.138	0.392
PHE															0.129	-0.071	**-0.262**	-0.045	**0.282**	**0.297**	-0.080
PROL																**0.299**	0.030	0.113	**0.328**	**0.388**	0.506
SER																	**0.326**	**0.468**	**0.301**	0.012	0.267
TAU																		0.148	-0.119	**-0.292**	0.051
THR																			-0.170	0.164	-0.073
TYR																				**0.210**	0.444
VAL																					0.206

Table 7.4: Pearson correlation coefficient, r, calculated for associations between amino acids in propionic acidaemia patients (n=105 samples). **Bold**: significant $p<0.05$. Red, $r>0.5$

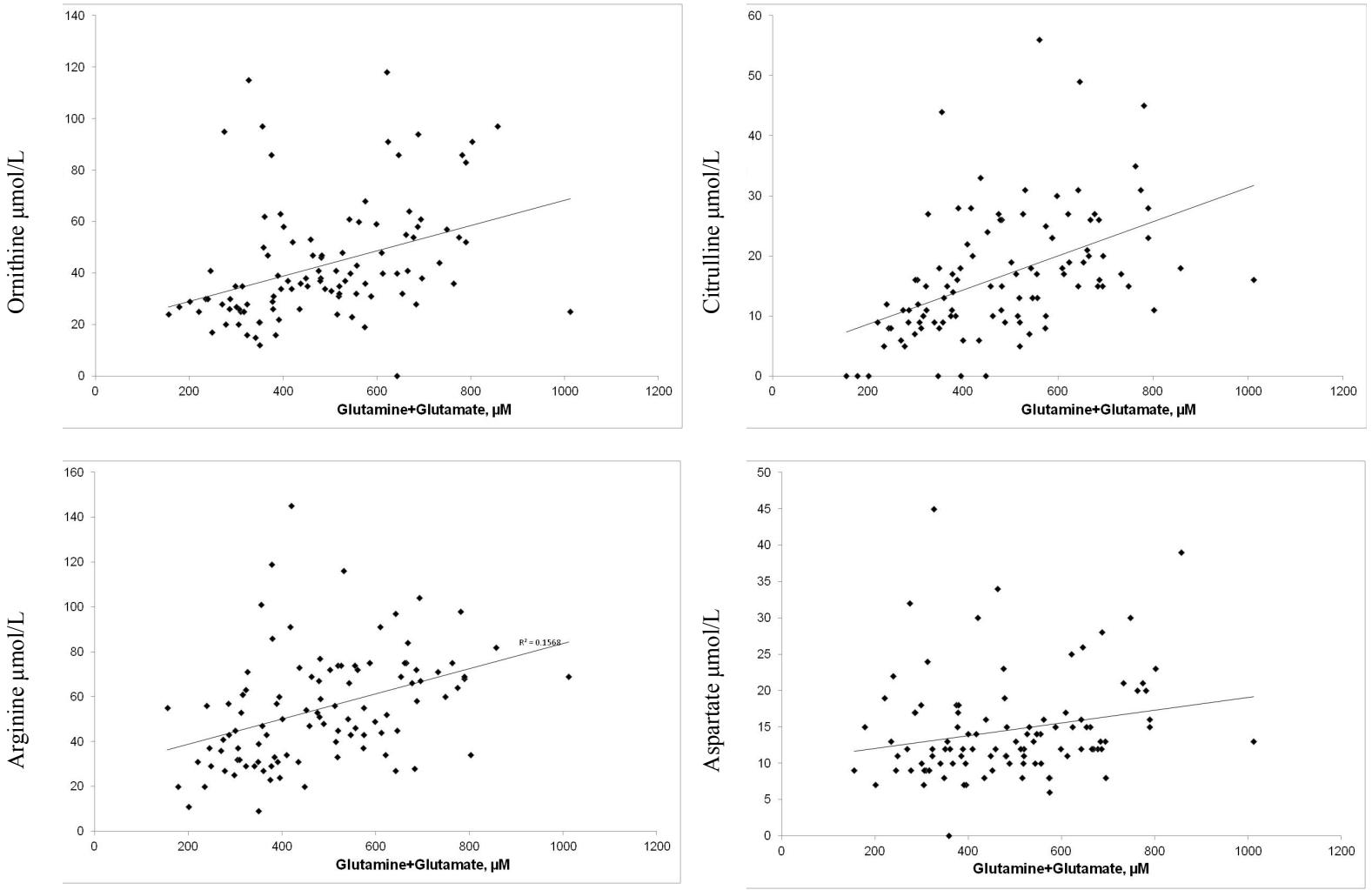

Figure 7.10: Scatter plots of plasma glutamine+glutamate versus urea cycle amino acids in propionic acidaemia cohort. Line – linear regression line. Ornithine (upper left), citrulline (upper right), arginine (bottom left) and aspartate (bottom right)

7.7.5. Urine NMR Results

Seven random urine samples from six patients with PA were available, including one sample from a child who had previously had a liver transplant for PA. Samples were compared to data from healthy controls (n=8). Urine samples from all PA patients demonstrated the presence of several metabolites substantially elevated compared to, or not detected, in controls. In particular glycine, propionylcarnitine and betaine were elevated in PA patients compared to controls (see figures 7.11 and 7.12). Tiglylglycine was also observed, and peaks consistent with propionylglycine. Methylcitrate was not convincingly observed.

Principal component analysis of spectra generated separate clusters of control and PA patients, although two sub-groups within the PA patients were identified (figure 7.12). Review of the loading plots of the first and second principal components found similar profiles with elevated peaks of glycine, propionylcarnitine and betaine identifying the PA patients, although the relative ratios between these main discriminators differed such that in PC1 dominant peaks were betaine > glycine > propionylglycine, while in PC2 propionylcarnitine > glycine > betaine, corresponding to the patterns seen in the spectra from those children.

A urine sample from a PA patient who had previously received liver transplantation had notably lower glycine than the other PA patients, although this was still at a higher concentration than seen in the control samples. Furthermore elevated betaine, carnitine and propionylcarnitine were observed in the urine of this child indicating that liver transplantation had not completely normalised systemic propionate metabolism.

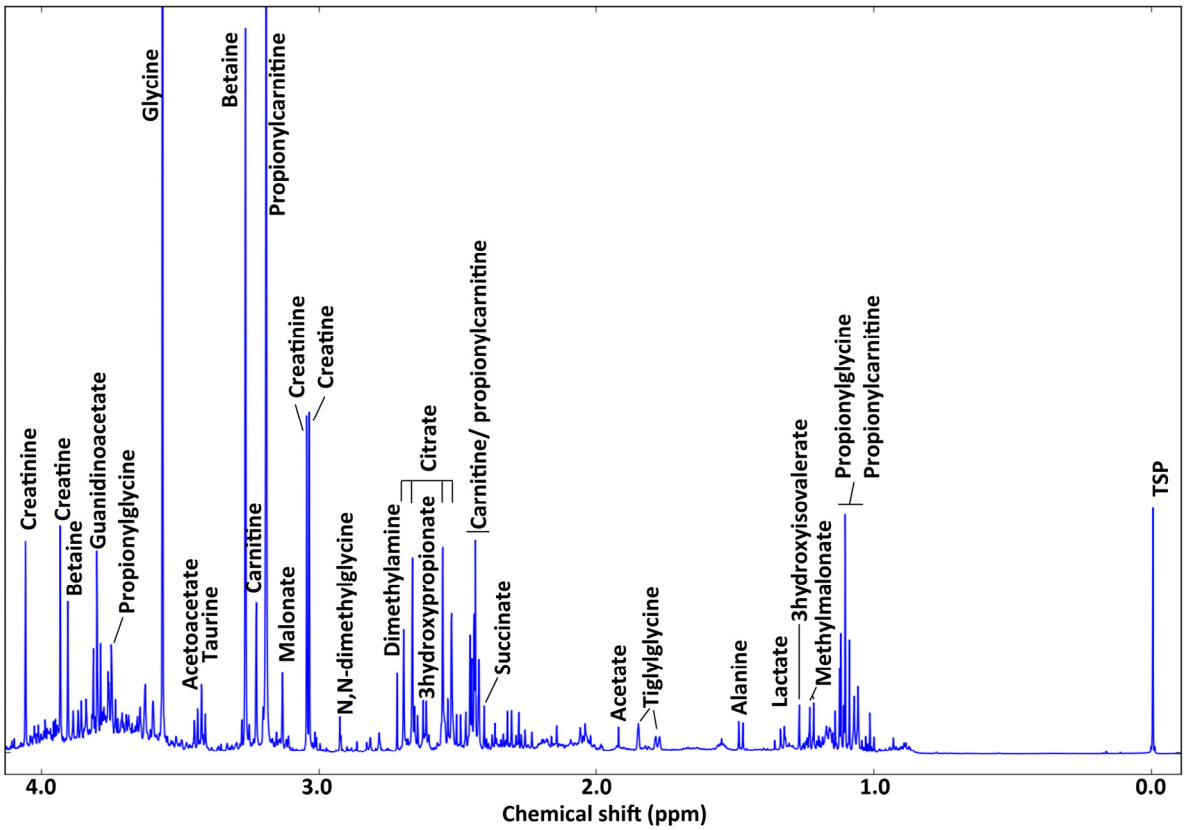

Figure 7.11: Example one dimensional proton NMR spectrum of urine from propionic acidaemia patient.

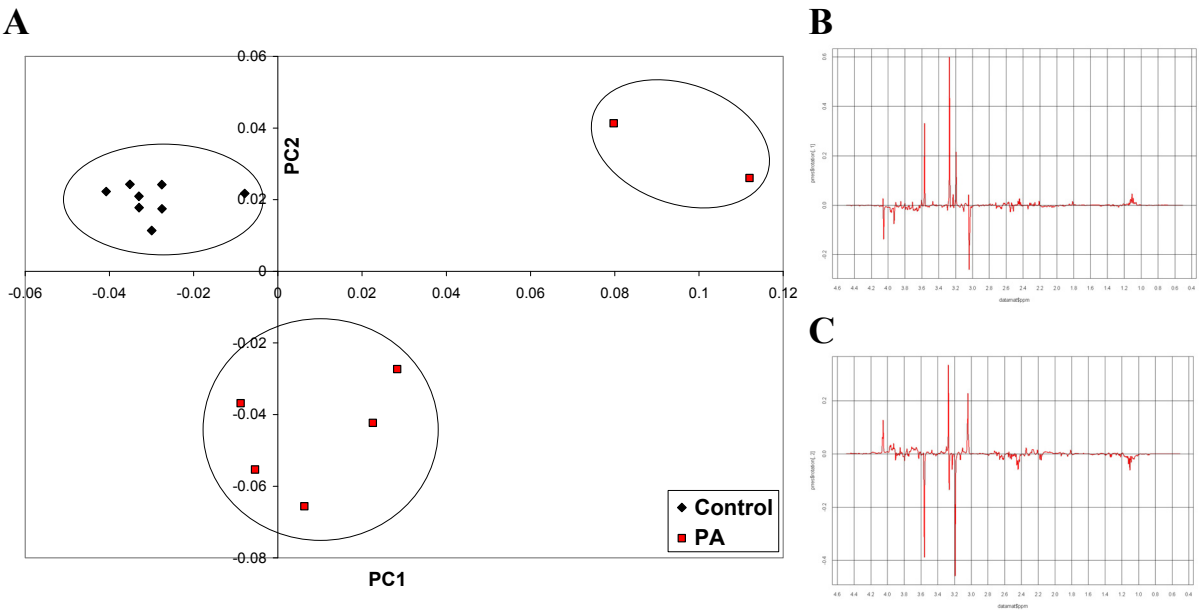

Figure 7.12: Principal component analysis of one dimensional proton NMR spectra of urine from propionic acidaemia and control patients. (A) Scores plot (PC1 and PC2) and loadings plots for (B) PC1 and (C) PC2. Diamonds, control patients; squares, PA patients.

7.8. Discussion

The data presented represent the largest series of children with the severe neonatal form of propionic acidaemia to be investigated with brain MRS, and is to the author's knowledge the first to study children during severe acute encephalopathic episodes. The selective vulnerability of the basal ganglia in PA is well established, and this data has provided further insight in to processes occurring within the basal ganglia.

7.8.1. Clinical and Biochemical Features

The clinical and biochemical features of the cohort are consistent with those previously reported for children with the severe neonatal onset form of PA. In particular the plasma quantitative amino acid profiles and urinary metabolite profiles (as determined by NMR spectroscopy) show alterations consistent with the diagnosis.

7.8.2. Quantitative amino acid analysis

The plasma quantitative amino acid profiles seen in the PA cohort here are consistent with some of the key observations made elsewhere [166]. Thus concentrations of alanine and glycine are elevated in the PA group, while glutamine and the branch chain amino acids were found to be frequently lower than standard reference ranges. Analysis of the cohort dataset did not confirm previous findings of the correlation between plasma amino acids and ammonia concentrations [188], and in particular the current data were not consistent with an inverse relationship between glutamine and ammonia. The only significant correlations with ammonia were for lysine and tyrosine, both of which increased with increasing ammonia.

Similarly, it has been reported that glutamine+glutamate levels were strongly correlated with the urea cycle amino acids ornithine and arginine but not citrulline or aspartate. In the current

dataset, glutamine+glutamate had moderate correlations with each of ornithine, arginine, citrulline and aspartate (r=0.392, 0.396, 0.473 and 0.216 respectively).

7.8.3. Urine NMR metabolite profiling

The data presented from the one dimensional proton NMR examination of random urines demonstrated in all PA children, including one post-liver transplantation, the excretion of elevated glycine, betaine, tiglylglycine, propionylglycine and 3-hydroxypropionate, as described previously [204]. In addition, high levels of propionylcarnitine and carnitine were observed, consistent with the now routine use of carnitine supplementation in PA [205]. The high concentration of betaine observed in the urine of PA patients is also of interest; the reasons for its excretion and possible effects are not well documented [206]. The urinary profile provides insight in to the highest concentration metabolites accumulating in PA, but these may not be present in the CNS in the same concentrations.

7.8.4. MR imaging findings

The MRI findings in this cohort are consistent with those previously reported in PA, with many of the children displaying cerebral volume loss, ventricular enlargement and/or disturbed myelination. The observation of hippocampal abnormalities has not previously been reported in PA and warrants further investigation. In particular, formal analysis of hippocampal volumetric alterations using 3D T_1 volume acquisitions would help substantiate this qualitative observation, and if confirmed would provide an interest neuroanatomical correlate for some of the reported memory and learning difficulties encountered in PA patients.

Basal ganglia abnormalities were observed in four children in the cohort, but only at the time of, or following, acute severe encephalopathic episodes occurring outside of the neonatal period. Indeed, the basal ganglia appeared normal on conventional MRI in all children who had not had a severe acute encephalopathic episode beyond the neonatal period. The quantitative analysis of T_2 and ADC signal in the basal ganglia also confirmed that prior to acute severe episodes the signal from the basal ganglia was within the normal range.

Given that all of the patients presented acutely ill during the neonatal period, it therefore appears that the basal ganglia are uniquely protected at this early stage in development, as has been similarly reported in glutaric aciduria [11]. One possible explanation could be the differential expression of receptor types that mediate later neurotoxicity. For example it is known that the expression of different constituent subunits of the NMDA receptor alters during the neonatal and post-neonatal period [207] and thus if NMDA-mediated excitotoxicity is part of the pathogenesis of the basal ganglia insult this might only occur at a later developmental stage when the NMDA receptor is fully expressed.

The abnormal basal ganglia MR imaging features observed in the children with basal ganglia damage demonstrated variable involvement of the different basal ganglia structures, but including caudate, putamen and globus pallidus. MR imaging in the acute phase often demonstrated swelling of these structures with associated restricted ADC patterns consistent with cytotoxic oedema. In follow up imaging, basal ganglia features either partially resolved or progressed to atrophy and cystic degeneration.

7.8.5. MR Spectroscopic findings

Evaluation of *in vivo* brain metabolite alterations presented here during metabolic stability and acute encephalopathy could help evaluate the various hypotheses explaining the brain pathology seen, notably the vulnerability of the basal ganglia. Some of the metabolite alterations described are a reflection or result of the insult that has occurred, and are not causative of the insult. For example decreased tNAA is seen in many pathologies, and is thought to reflect loss of viable neurons [50] including following acute ischemic stroke [208].

Other metabolite alterations shed light on disease-specific mechanisms. Elevated lactate suggests a switch to anaerobic respiration, and may secondarily reflect local ischaemia, but the finding of elevated brain lactate in two children during metabolic stability suggests that brain tissue metabolism is not normal even when metabolism is well controlled. This may, for example, suggest sub-critical tissue ischaemia, or mitochondrial dysfunction pre-existing in the vulnerable brain regions.

The alterations seen in glutamine and glutamate in basal ganglia are of particular note. Gln+Glu was significantly decreased in basal ganglia during severe acute episodes, with a smaller decrease noted in basal ganglia in studies acquired during metabolic stability. In white matter there was a non-significant trend to decreased Gln+Glu during encephalopathy.

Although the spectral signals from glutamine and glutamate overlap, there is increasing evidence that they can be differentiated in the analysis of cohorts even at 1.5Tesla using software such as LCModel. Such evidence includes Montecarlo simulations of normal brain spectra fitted with LCModel [209], comparisons of experimental and simulated basis sets

[210], and the finding of a significant correlation between *in vivo* and *in vitro* results for both glutamate and glutamine detected in brain tumours [29, 211].

Bearing this caveat in mind, the separate alterations in glutamine and glutamate seen in the MRS studies are of interest. It appears that glutamine in the basal ganglia is depleted even during metabolic stability, and remains low when acute basal ganglia events occur. In contrast, glutamate was normal during metabolic stability, and fell significantly in both basal ganglia and white matter in the acute encephalopathy acquisitions. The decreased glutamine detected by brain MRS is consistent with the plasma glutamine reduction previously reported in PA [166], also seen in plasma glutamine levels in the current cohort.

There are several possible explanations for the low glutamine and glutamate levels seen. Firstly, this may simply reflect neuronal loss as suggested by the lower NAA levels. However, the ratio of Gln+Glu/tNAA was lower in the propionic acidaemia cohort than in cohorts of children with other defined inherited metabolic disorders including a cohort with confirmed respiratory chain disorders, while the Gln+Glu/NAA ratio was elevated in a cohort with the urea cycle disorder argininosuccinic aciduria. This suggests that the alterations seen in Gln+Glu here were not simply a reflection of neuronal loss represented by lower tNAA.

Secondly, the administration of the alternative pathway drugs (phenylbutyrate and benzoate) used to control hyperammonaemia depletes plasma glutamine and glycine and may contribute to the decreased brain Gln+Glu seen. Thirdly, furthermore, children were often haemofiltered during severe acute episodes which may further deplete glutamine due to its high sieving

coefficient [212]. However CVVH was instigated after the MRI/MRS in 80% of cases suggesting that glutamine levels were already low before CVVH was commenced.

Fourthly, the finding of decreased Gln+Glu in basal ganglia during metabolic stability and subsequent acute decreases seen during encephalopathy, supports the hypothesis that glutamine and glutamate are consumed to replenish a depleted Krebs cycle [188], and that this decrease is a marker of compromised aerobic cellular respiration within brain tissue. As discussed above, anaplerosis could be compromised in PA at several steps. The low brain Gln+Glu levels seen here could suggest that glutamine and glutamine are being consumed to support a deplete Krebs cycle, or alternatively if they are being depleted by another route, that the potential for anaplerosis from glutamate conversion to α-ketoglutarate is limited. It remains to be determined whether the decreased Gln+Glu is directly detrimental or simply a secondary marker of compromised metabolic status. Interestingly the decrease in Gln+Glu was greater in the basal ganglia than in white matter, correlating with the more vulnerable brain region.

These findings are in disagreement with the one previous MRS study of basal ganglia metabolism using MRS. This study reported elevated basal ganglia Gln+Glu in three metabolically stable propionic acidaemia patients who had normal plasma ammonia and near-normal glutamine and glutamate in plasma and cerebrospinal fluid, leading the authors to suggest that differential mechanisms regulated brain parenchymal metabolism [201]. That study relied on peak area estimation, manual baseline fitting and metabolite ratio to creatine, whereas the current study provides more robust quantification. However several factors may explain a real biological difference in the results seen. Patients in the previous study reported

in 1996 were not receiving sodium phenylbutyrate therapy, whereas the majority of patients in the current study were on this glutamine-depleting therapy at the time of MRS. Furthermore, the patients reported in the earlier study were not reported to be receiving carnitine therapy, and so it is plausible that the discrepant results in basal ganglia Gln+Glu are due to alterations in the metabolic status of the two cohorts of patients secondary to medication and therapy factors. Elevated Gln+Glu in the urea cycle disorders is thought to reflect conversion of ammonia to glutamine, and since hyperammonaemia is encountered in PA this has been proposed as one possible cause of the neuropathology. However, as with the previous study described, significant and persistent hyperammonaemia was not seen in this cohort.

The previous reports of elevated CSF glutamine in some PA patients also appear to be at odds with the findings reported here. However, both patients previously reported to have elevated CSF glutamine and low plasma glutamine had evidence of significant hyperammonaemia either concurrently or within a day of the CSF sampling [179, 200]. It is possible that in these patients hyperammonaemia stimulated compensatory generation of glutamine within the brain, subsequently excreted in to the CSF. Importantly, these patients in whom MRS of the basal ganglia was performed had normal CSF glutamine levels.

Unfortunately CSF samples of amino acid analysis were not routinely collected in the patients reported here. It would be interesting prospectively to directly compare plasma, CSF and brain glutamine and glutamate levels in association with determination of ammonia and other propionate metabolites. In particular, differences between brain tissue and CSF metabolites could shed light on protective/excretory mechanisms within the CNS.

The accumulation of other neurotoxic metabolites may contribute to the pathology, particularly via NMDA receptor mediation. The current MRS technique did not detect substantial elevations in brain glycine, particularly this was not seen in any of the acute encephalopathy studies, and in two cases where possible glycine peaks were seen the concentration was substantially lower than seen in a child with non-ketotic hyperglycinaemia (see Chapter 5). The urine NMR studies did demonstrate high glycine excretion in to the urine (up to around 10mmol/L); it would be interesting to quantitate CSF glycine levels to investigate further whether there is evidence of persistent glycine elevations in the CNS. Furthermore no "unfitted" peaks were identified that could be consistent with other PA-related toxic metabolites. It is probable, however, that any such toxic metabolites would be present at concentrations below the threshold for detection with MRS, so this negative finding does not exclude the neurotoxin hypothesis.

Basal ganglia strokes are not limited to PA, but seen in other organic acidurias including glutaric aciduria type I and in methylmalonic aciduria, where the "neonatal period protection effect" is also seen. It is possible that common mechanisms operate in these different disorders, either accumulation of toxic metabolites common to all three conditions, or common secondary effects. MRS studies in these disorders have demonstrated low NAA levels in basal ganglia, with the detection of lactate in some instances, but none of the studies evaluated alterations in glutamine and glutamate [213-216]. One study evaluated the effects of carnitine therapy in methylmalonic aciduria on the basal ganglia MRS profile, finding normalisation of NAA and lactate levels [217]. Evaluation of brain energy metabolites using phosphorous spectroscopy has also been attempted in glutaric aciduria type I, although no significant results were reported [218].

7.8.6. Effects of Liver Transplantation

The two children who had liver transplant have had no severe acute encephalopathic episodes beyond the neonatal period, and have normal appearing basal ganglia on MRI. MRS demonstrated normal/high tNAA reflecting the absence of major neuronal loss and correlating with their good neurocognitive status, and no reliably detected lactate. The small numbers preclude statistical significance, but Gln+Glu was slightly increased in white matter but decreased in basal ganglia compared to the comparator group. These results support the hypothesis that liver transplantation provides systemic metabolic stability by providing a hepatic pool of functional propionyl CoA carboxylase, thus preventing further acute metabolic decompensations which are associated with the risk of brain infarction. The observation of persistent PA-related abnormalities in the urine NMR analysis of the child post-liver transplantation highlights the fact that liver transplantation does not correct the "total body" metabolic defect in PA.

7.9. Limitations & future investigations

The data presented here have yielded some interesting initial observations. There are, however, a number of technical and sample-size related limitations to the work that would need to be addressed to confirm or refute the hypotheses made.

From a technical perspective, more robust differentiation of the metabolites of interest, notably glutamine and glutamate, is required. At 1.5T the resonances of glutamine and glutamate overlap significantly. At higher field strengths with narrower line-widths and better spectral resolution these metabolites can be differentiated with a greater degree of certainty. The use of the single voxel technique has targeted the investigation to two distinct brain

regions, but even so at 1.5T the spatial resolution is limited to 2cm x 2cm x 2cm cubes, representing a substantial volume of brain. Across this volume there could be significant regional differences in the metabolite profile, and the data presented here give an average effect for the volume. Thus alterations in glutamate, for example, are a bulk effect on the total metabolite concentration and do not provide information about the neuronal/synaptic/glial compartmentalisation of metabolite concentrations.

The second major limitation to the current work relates to the sample size, both in terms of numbers of patients (albeit the world's largest cohort of neonatal onset PA) and in terms of the number of time points sampled for each patient. The metabolite alterations reported for metabolic stability and encephalopathy represent the mean effects in the cohort. It would be desirable to be able to describe and evaluate metabolite alterations in single subjects before, during and after encephalopathic episodes. As has already been noted, only two of the patients had liver transplantation, and further data is required to help evaluate the proposed neuro-protective effect of this therapy.

That said, there is a need for brain protective strategies during acute metabolic decompensations, with potential methods including brain cooling, optimising energy provision, and anaplerotic therapies. MRS could provide a tool to monitor the effect of dietary supplements aimed at increasing glutamine levels, specifically monitoring metabolite levels within the target-organ of interest, namely the brain.

While direct observation *in vivo* of brain metabolite profiles in patients with PA has yielded some useful and interesting data, there is limited capacity for experimental manipulations in

human subjects. An animal model of disease would provide a useful platform for further investigations, allowing the use of both non-invasive techniques such as MRS and direct tissue evaluation. A PCCA -/- knockout mouse has been generated, with rapid mortality in the early neonatal period The phenotype can be rescued by postnatal liver specific expression of PCC using a transgene technique [219], and also by gene therapy approaches using an AAV8 vector [220, 221] with survival up to and beyond 6 months of age. No neuropathological studies have yet been reported in these animal model systems, but could provide an important means of exploring the hypotheses discussed here if the brain insults seen in human patients can be recapitulated in the animal model.

7.10. Conclusions

The data presented demonstrate that quantitative MRS is able to offer insight in to *in vivo* brain metabolic derangements, and can feasibly be employed in children with acute encephalopathy. In propionic acidaemia the use of MRS in conjunction with MRI has confirmed the basal ganglia as a particularly vulnerable target and has demonstrated novel insights in to alterations in neurotransmitter metabolites. Evaluation of patients in long-term follow up after liver transplantation demonstrates the potential for good neurological outcome and near-normal brain metabolism. MRS provides a tool to directly evaluate the tissue-level effects of novel treatment strategies including anaplerotic therapies.

Chapter Eight

8. Argininosuccinic Aciduria

In this chapter data are presented illustrating the investigation of the urea cycle disorder argininosuccinic aciduria, which has unique neurological characteristics. Novel MR imaging features are reported and the MR spectroscopy method is used to evaluate specific hypotheses pertaining to the neurological features of this disorder.

8.1. The Urea cycle and disorders of the urea cycle

The disposal of excess nitrogen in mammals is achieved by the hepatic urea cycle (figure 8.1). The six enzymes that constitute the cycle convert ammonia synthesised from the amino acid nitrogen pool to urea, which is subsequently excreted in the urine [222]. The cycle operates across both mitochondrial and cytosolic compartments, but the total complement of enzymes is only fully expressed in liver cells; outside the liver argininosuccinate synthase (ASS, EC 6.3.4.5) and argininosuccinate lyase (ASL, E.C. 4.3.2.1) are ubiquitously expressed and form the citrulline-nitric oxide (NO) cycle which recycles citrulline generated by nitric oxide synthase (NOS, EC 1.14.13.39) during NO production back to arginine (figure 8.2) [223].

Deficiencies of all of the urea cycle enzymes have been described, and result in malfunction of the cycle, specifically with accumulation of toxic ammonia and disordered amino acid metabolism [222]. The clinical presentation of the urea cycle defects (UCD) is heterogeneous, with severe forms presenting in the early neonatal period with significant hyperammonaemia

resulting in lethargy, poor feeding and progressing to seizures, neurological depression and death if untreated. Proximal defects (carbamoyl phosphate synthase 1 (CPS, EC 6.3.4.16, OMIM #237300) and ornithine transcarbamoylase (OTC, EC 2.1.3.3, OMIM #311250) deficiency) in particular tend to present with an early fulminant neonatal phenotype [224]. Partial or distal cycle defects can present with a milder phenotype at a later stage either during infancy, or even present in adulthood with episodic neuro/psychiatric symptoms [222], but are still associated with significant neurological damage [224].

A large cross-sectional multi-centre study of 183 UCD patients in the USA reported substantial rates of intellectual disabilities (39%), learning disabilities (35%) and psychiatric disorders including mood disorders (8%), while up to 15% had seizure disorders [225]. Furthermore, around 50% had objectively abnormal neurological examination. There were, however, substantial differences in the rates of these abnormalities between the different types of UCD. In particular, patients with argininosuccinic aciduria (ASA) had significantly higher rates of intellectual disabilities (70%, $p<0.05$), and also had higher rates of seizure disorders (32%, $p<0.05$) and abnormal neurological examination findings such as abnormal deep tendon reflexes (30%) or altered tone (50%).

Acute hyperammonaemia is responsible for many of the neurological features of the UCD, with the survival and neurological outcome related to the ammonia levels (peak and duration) during the initial presentation [224, 226]. Ammonia enters the CNS by diffusion through the blood-brain barrier, where it is converted to glutamine by astrocytic glutamine synthase [224]. The accumulation of glutamine exerts an osmotic pressure resulting in astrocytic-mediated cerebral oedema, responsible for much of the neuro-pathology. Other mechanisms, however,

are also important components of the neurological disease in UCD, including energy deficiency due to secondary enzyme inhibition, alterations in neurotransmitters and their receptors, and secondary effects of chronic "mild" hyperammonaemia.

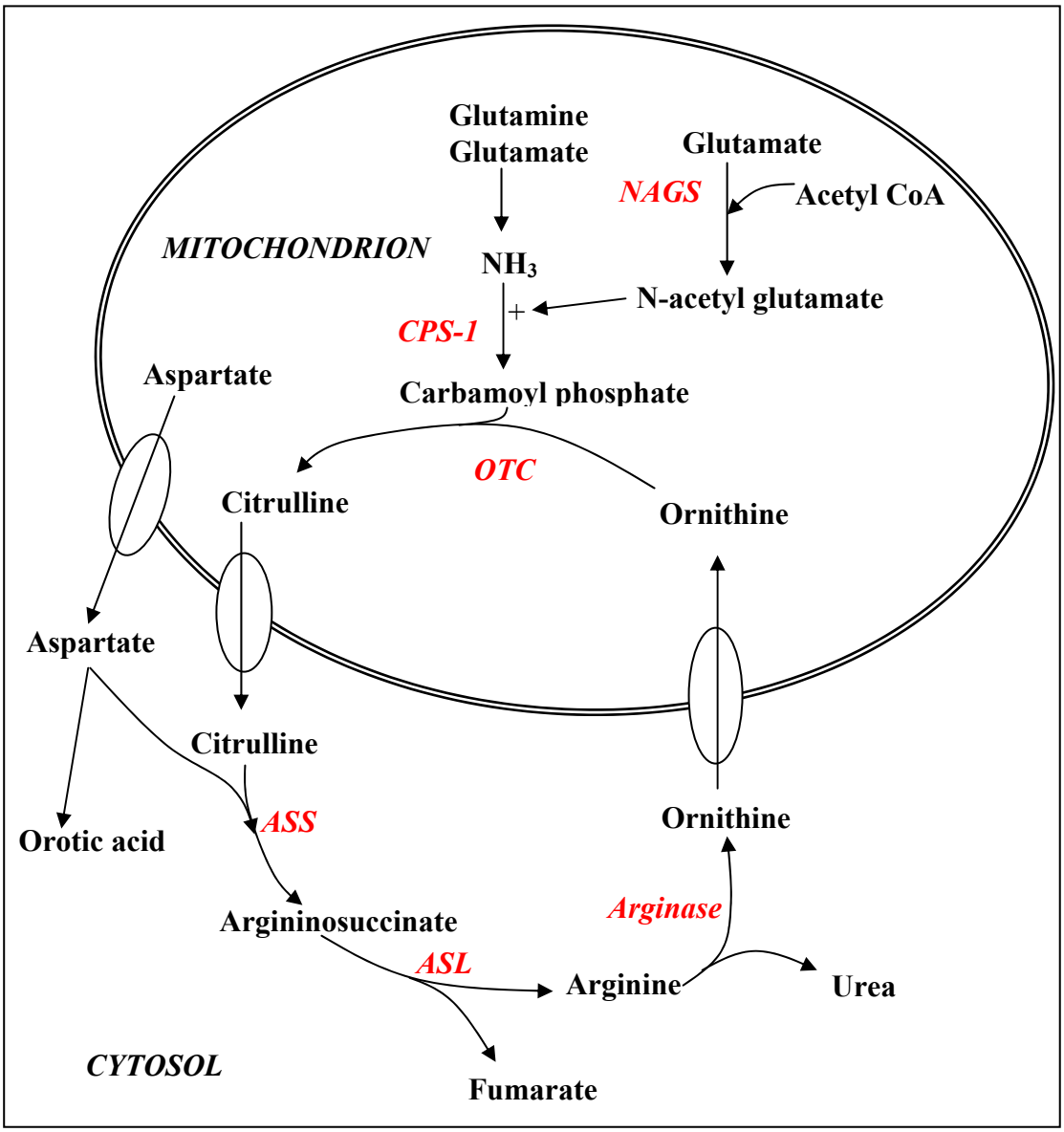

Figure 8.1: Outline of the urea cycle. CPS1, carbamoyl phosphate synthase 1; OTC, ornithine transcarbamoylase; ASS, argininosuccinate synthetase; ASL, argininosuccinate lyase. NAGS, N-Acetylglutamate synthase.

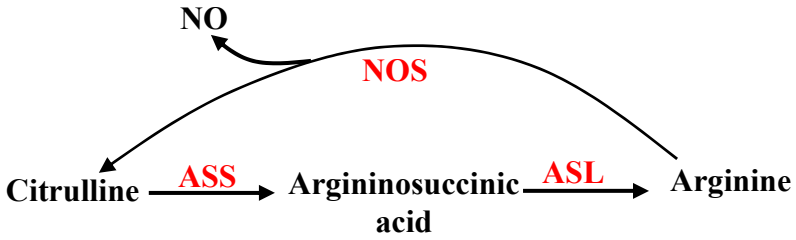

Figure 8.2: Citrulline-Nitric Oxide cycle. Abbreviations as figure 8.1.

8.2. Argininosuccinic aciduria

Argininosuccinic aciduria (ASA, OMIM #207900) is an autosomal recessive urea cycle disorder (UCD) caused by inherited mutation in the *ASL* gene (7cen-q11.2) resulting in deficiency of argininosuccinate lyase (ASL, E.C. 4.3.2.1). ASL catalyses the cleavage of argininosuccinate to fumarate and arginine in the hepatic urea cycle, and as noted already is also widely expressed in cells outside of the liver, forming part of the citrulline-NO cycle.

Two forms of ASA are clinically distinguished depending on severity and age of onset. The early neonatal onset severe form is similar to the other UCDs presenting in the neonatal period, with associated hyperammonaemia in the first days of life, while the late onset form presents with either episodic hyperammonaemia, or neurocognitive deficits [227, 228]. However, as described above, significant developmental delay, epilepsy and other neurological features occur in ASA even when metabolic control is generally good, and in the absence of significant hyperammonaemic encephalopathic episodes [229]. Anecdotal evidence suggests that seizure disorders and intellectual impairment are a particular problem in ASA patients despite good ammonia control. These clinical features suggest that disease-specific mechanisms have a role in the neurological damage sustained in ASA.

ASA is also associated with high rates of liver disease, including hepatomegaly, liver enzyme derangements and liver fibrosis, and as with the neurological disease this may occur despite

the absence of persistent or severe hyperammonaemia [228, 230]. Trichorrhexis nodosa (brittle hair) is another common feature in untreated patients with ASA, resulting from the deficiency of arginine that constitutes some 10% of the normal hair shaft [228]. Systemic hypertension has also been described in ASA [231, 232], potentially due to decreased nitric oxide synthesis.

Typical biochemical findings in ASA are the presence of hyperammonaemia with elevated argininosuccinic acid in plasma and urine, with elevated citrulline, alanine, glutamine and glycine, and arginine deficiency. Orotic aciduria may be detected due to impaired ornithine recycling [228]. Deficiency of ASL activity is assayed in erythrocytes or skin fibroblasts by indirect (radio-labelled citrulline incorporation) or direct (arginine or fumarate synthesis) assays [233]. These assays do not however correlate with the disease severity, and in a model of bacterially expressed enzymes similarly there was not a good enzyme activity-phenotype correlation [233].

Neuroimaging features in ASA are not well documented. In a large 27 year follow up study of 23 patients identified by newborn screening classified with the mild phenotype, cognitive function was generally good, although four patients had electroencephalogram (EEG) abnormalities in the absence of seizures, but no MR imaging was reported [234]. Similarly in a study of 13 patients (12 with mild phenotype) again identified by newborn screening, CNS dysfunction was evident as four had learning difficulties, six had EEG abnormalities and three had clinical seizure disorders [235]. None had MRI studies reported. Of note a separate cohort of late onset (mild phenotype) patients diagnosed symptomatically rather than by screening had significantly worse mental retardation, seizures and ataxia.

In other UCDs imaging features include significant cerebral oedema resembling hypoxic-ischaemic damage during severe hyperammonaemia [236], visible with both computed tomography (CT) and MRI scanning. MRI delineates specific regions of the cortex and gray matter with specific vulnerabilities, including insular cortex, perirolandic cortex and globus pallidi, and notably not sparing the subcortical U fibres [237].

8.3. Neuro-pathogenesis theories

Patients with ASA have, therefore, a unique neurological phenotype amongst the UCD, which is not fully explained by hyperammonaemia alone. A number of hypotheses regarding the pathogenesis of the neurological features in ASA have been proposed in addition to the common effects of hyperammonaemia.

8.3.1. Argininosuccinic acid toxicity

Argininosuccinic acid is excreted at high concentrations in the urine of patients with ASA and is also present at relatively high concentrations in plasma and substantially higher levels in CSF [235]. Although it is the abundant metabolite present in ASA, direct toxicity from argininosuccinic acid has not been convincingly demonstrated. One potential mechanism is via formation of guanidinosuccinic acid from the combination of argininosuccinic acid and free radicals; guanidinosuccinate can mimic NO and also activate NMDA receptors [238]. Similarly argininosuccinate has been suggested to cause hepatotoxicity but direct evidence is scarce.

8.3.2. Effects of arginine deficiency

ASL is the key enzyme for arginine synthesis. In the liver most arginine synthesised is consumed in the urea cycle, but net arginine synthesis is achieved by the kidney which expresses high levels of ASL and specifically takes up citrulline for this purpose. In ASA

arginine is therefore an essential amino acid that must be supplied from the diet. Arginine is a precursor for many metabolic pathways (figure 8.3), which could be affected if arginine is deficient, exemplified by the clinical occurrence of trichorrhexis nodosa due to deficient arginine for hair shaft synthesis.

In utero it is likely that sufficient arginine will be supplied by trans-placental active transport, since the placenta expresses specific transporters for amino acids including arginine [239]. Following diagnosis with ASA patients are quickly supplemented with high doses of arginine and may have supra-normal plasma levels. Prior to diagnosis it is possible that arginine deficiency may contribute to the clinical phenotype, particularly in relation to creatine synthesis.

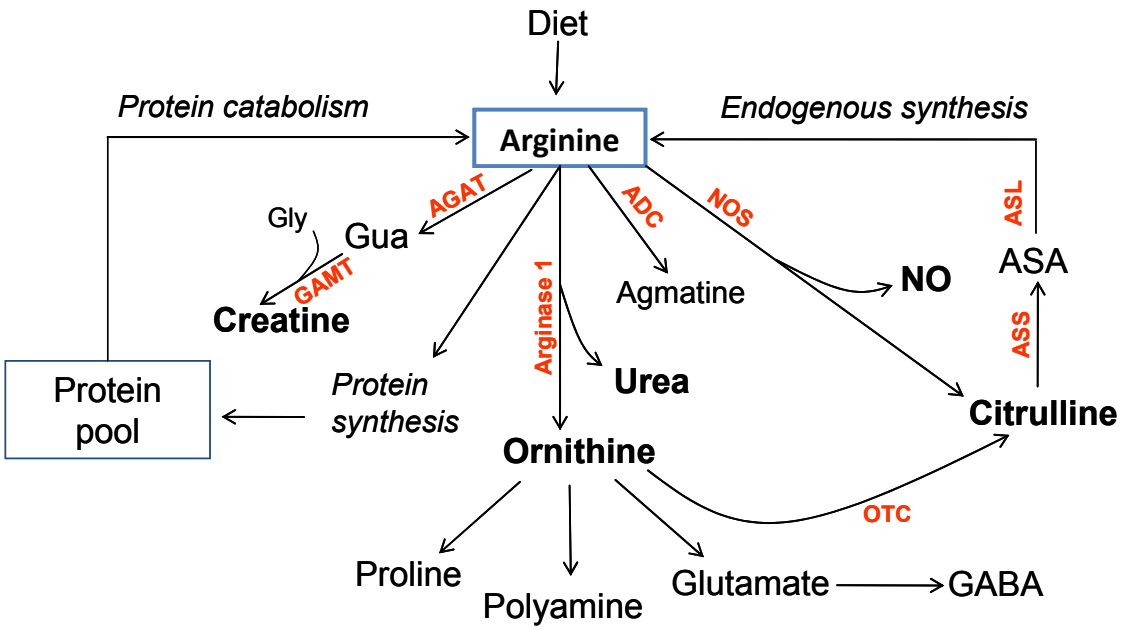

Figure 8.3: Key metabolic pathways supplied by arginine. ASA, argininosuccinic acid; NO, nitric oxide; NOS, nitric oxide synthase; Gua, guanidinoacetate; Gly, glycine; ADC, arginine decarboxylase; AGAT arginine:glycine amidinotransferase; GAMT, guanidinoacetate methyltransferase; OTC, ornithine transcarbamoylase. (Adapted from [228]).

8.3.3. Creatine deficiency

Creatine is formed from arginine by two enzymes, arginine:glycine amidinotransferase (AGAT) and guanidinoacetate methyltransferase (GAMT). Creatine plays a central role in energy metabolism providing a means for high energy phosphate shuttling [240] (see Chapter 2). Although available from dietary sources, *de novo* synthesis is also important since the turnover of the substantial creatine pool to renally excreted creatinine is rapid (1.7% per day) [241]. AGAT activity is greatest in kidney, while GAMT activity is highest in liver suggesting a "renal-hepatic axis" for creatine synthesis. Creatine is transported into tissues (particularly muscle) by the specific transporter SLC6A8 [64, 240].

Within the brain AGAT, GAMT and SLC6A8 are all expressed but in different cell populations. The blood brain barrier has restricted permeability to creatine, and so the CNS must synthesise much of its creatine requirements endogenously [64]. The specific creatine deficiency syndromes due to absence of AGAT, GAMT or SLC6A8 are all associated with severe neurodevelopmental delay, and in GAMT seizures are particular problem [64, 242].

Secondary creatine deficiency is reported in the UCD, with decreased plasma and urine guanidinoacetate and creatine [243]. MRS was used to document brain creatine deficiency in a patient with late onset ASA prior to treatment, with improved brain creatine levels after arginine supplementation [244]. This patient also had low plasma concentrations of creatine and guanidinoacetate that corrected with treatment.

In addition to arginine deficiency causing a secondary creatine deficiency, ammonia is known to produce creatine deficiency, potentially via the inhibition of AGAT and by altering the expression of AGAT, GAMT and SLC6A8 genes [245].

8.3.4. Guanidinoacetate toxicity

It has also been proposed that the propensity to epilepsy in ASA may be due in part to excessive brain levels of guanidinoacetate, due to excessive supplementation with arginine. In GAMT deficiency where there are very high levels of guanidinoacetate seizures are a particular problem, possibly due to toxic effects of the accumulated guanidinoacetate [246]. The detection of possibly raised brain guanidinoacetate levels in two patients with ASA support this hypothesis, although urinary guanidinoacetate was high in only one of the patients [247, 248]. If excessive guanidinoacetate in ASA is iatrogenic, i.e. due to arginine supplementation, it could not explain neuropathological features occurring prior to the onset of therapy.

8.3.5. Nitric Oxide Synthase Dysfunction

Recent evidence suggests that the role ASL plays in the nitric oxide system results in many of the specific pathological features of ASA. NO has many diverse functions, including control of vasodilatation, as well as in platelet function, neurotransmission and is important in normal and pathological conditions within the CNS [223, 228, 249-252]. If NOS function is disrupted or uncoupled, free radical generation increases with subsequent pathological effects [253].

The “arginine paradox” describes the phenomenon whereby exogenous arginine can increase NO production despite high and saturating levels of arginine within cells, suggesting that

arginine supply at the specific sites of NO synthesis are rate limiting. Thus there may be "intracellular compartmentalisation" of arginine [228].

In some elegant experimental work with a conditional *Asl* hypomorphic mouse, Erez *et al* demonstrated evidence for pathological features that recapitulate many of the phenotypic features of patients with ASA, including similar biochemical derangement, multiorgan dysfunction, and systemic hypertension [223]. They showed that the mice had a global NO deficiency, and that fibroblasts from patients also had deficiency of NOS-dependent NO production. Furthermore they demonstrated that patients with ASA have decreased NO generation from extracellular arginine. It is likely that NO dysfunction contributes to many of the features of ASA, but as yet this has not been applied to the CNS pathology, and no neuropathological features in the mouse model have yet been reported.

8.3.6. Previous MRS studies in ASA

Many of the hypotheses relating to brain disease in ASA could be explored using MRS, since many of the relevant metabolites are readily identified. No large systematic study of brain metabolite profiles in ASA patients has been undertaken using MRS. However several case studies have been reported. As mentioned previously, creatine deficiency was demonstrated in an adult with late onset disease that corrected with treatment [244]. This patient also had low guanidinoacetate levels in brain that increased with treatment. Other cases reported had normal choline, creatine, inositol, glutamate/glutamine, and *N*-acetylaspartate levels but potentially high levels of guanidinoacetate, using a long echo time chemical shift imaging technique [247, 248]. A 24 year old male who received a liver transplant for recurrent metabolic decompensations in ASA was studied and found to have elevated basal ganglia

glutamine+glutamate prior to transplant, which decreased following transplantation. In this patient creatine was high in basal ganglia before and after transplant, while guanidinoacetate increased following transplant. This paper reported metabolite ratio data, and did not present the original spectra, and so firm conclusions are difficult to draw given the potential alterations in creatine making ratio data hard to interpret [254].

8.4. Aims & Objectives

This section of the study aimed to explore the various hypotheses relating to causes of brain disease in ASA by applying the MRI/MRS technique. Specific objectives were to generate a detailed phenotypic description of the cohort clinically and biochemically, and to test the following hypotheses: (a) Brain guanidinoacetate is elevated in ASA patients and may contribute to generation of epilepsy; (b) Brain creatine is deficient in ASA patients; (c) Brain glutamine+glutamate is elevated in ASA patients

8.5. Methods

8.5.1. Patient characteristics

Patients were recruited from a single tertiary paediatric IMD unit. Clinical data were extracted from medical records including age at diagnosis, mode of presentation, therapeutic modalities and history of subsequent neurological events. Available blood quantitative amino acid and ammonia determinations were also collated from the medical record.

8.5.2. Conventional MRI: qualitative analysis

MR imaging and MR spectroscopy were performed electively in conjunction with clinically indicated studies. All available brain MRI studies were retrospectively reviewed, including review of the qualitative radiology reports by the consultant paediatric radiologist.

8.5.3. MR Spectroscopy

MRS studies were performed concurrently with clinically indicated MRI scans at 1.5 Tesla facilitated by general anaesthesia as needed. Comparison was made with MRS metabolite data from the standard cohort of children with normal appearing MRI (white matter, n=53, median (range) age 4.7(0.5-16.7) years; basal ganglia n=63, 4.1(0.5-16.7) years). Comparison was also made between MRS data acquired from mild and severe phenotype ASA patients.

8.5.4. CSF NMR Spectroscopy

A CSF sample from one ASA patient was available for analysis. This was submitted to 1D 1H NMR spectroscopy as described (Chapter 3).

8.6. Results

8.6.1. Patients

Eleven patients (4 female) with biochemically confirmed ASA were included (table 8.1). Patients were classified as severe phenotype if they presented with neonatal hyperammonaemia, or were prospectively diagnosed as a later sibling of another child with severe ASA phenotype. Patients were classified as partial/mild phenotype if they presented beyond the neonatal period (late presentation) or were prospectively diagnosed as a later sibling of another child with partial/mild ASA. Five severe ASA and 6 partial/mild ASA patients were thus identified. Three children were diagnosed by sibling screening.

ASA enzyme activity assay (citrulline incorporation assay) was available in three patients directly (table 8.1). In most cases the residual activity corresponded to the phenotypic classification, such that very low residual activity (<1%) was associated with the severe phenotype, and higher residuals usually but not exclusively associated with partial/mild phenotype.

All patients were treated with protein restricted diet and oral arginine supplementation. Six received sodium benzoate and one phenylbutyrate alternative pathway medications.

8.6.2. Seizure disorders

Seizure disorders were present in 2/6 patients with the mild phenotype and 5/5 patients with the severe phenotype. A range of different anticonvulsant medications were used.

		Presenting mode	Age diagnosis (yrs)	Enzyme defect	Class	Neonatal high NH3	Later high NH3	Diet	Drugs	ALT raise	Hepato-megaly	Liver USS	Seizure disorder	Neurocog outcome	Motor function
1	F	Sib screen	5.5	nd	Partial	N	N	PR	Arg	N	N	-	N	Moderate LD	Ambulant
2	M	Dev delay	4	nd	Partial	N	N	PR	Arg, Risp	N	N	-	N	Severe LD & behavioural	Ambulant
3	M	Neonatal	0	28.7%	Severe	++	+	PR	Arg, SB AC	Y	Y	Abnl	Y	Global delay	Ambulant
4	F	Dev delay	2	nd	Partial	N	N	PR	Arg, AC	N	N	-	Y	Mild LD	Ambulant
5	M	Dev delay/ enceph	0.3	0.45%	Severe	(++)	++	PR	Arg, SB	Y	Y	Abnl	Y	Significant delay	Motor delay
6	F	Dev delay	1.5	20%	Partial	N	N	PR	Arg, AC	N	N	-	Y	Severe LD	Severe scoliosis
7	M	Sib screen	0	nd, sib 0.78%	Severe	+	++	PR	Arg, SB	Y	Y	Abnl	Y	Mainstream school but delayed	Ambulant
8	F	Dev delay	6	nd	Partial	N	N	PR	Arg	N	N	-	N	Mild LD, independent adult	Ambulant
9	M	Sib screen	0	nd, sib 20%	Partial	N	N	PR	Arg, SB until 4yrs	N	N	Norm	N	Mild Delay, statemented	Ambulant
10	M	Sib screen	Prenatal	nd, sib 0.78%	Severe	N	++	PR	Arg, SB, PB	Y	Y	Abnl	Y	Significant delay	Ambulant
11	M	Neonatal	0	nd	Severe	+++	+	PR	Arg, SB	Y	Y	Abnl	Y	Severe learning and language difficulties	Ambulant; Dystonia

Table 8.1: Summary of clinical characteristics of argininosuccinic aciduria patients. Enzyme defect by citrulline incorporation assay, reported as percentage residual compared to parallel control values. nd, not done. Sib, value derived in sibling of case. N, no/not present. Y, yes/present. Abnl, abnormal. Norm, normal. PR, protein restriction. Arg, arginine; SB, sodium benzoate; PB, phenylbutyrate; risp, risperidone; AC, anti convulsants; LD, learning difficulties. Shaded rows indicate mild/partial phenotype patients.

8.6.3. Cognitive and motor impairments

Formal neurocognitive assessments were not available. However, all patients had reported learning difficulties, developmental delay and behavioural difficulties to varying degrees. There did not appear to be a close correlation with phenotypic class, with some patients in the mild/partial cohort having significant cognitive impairment. The only child in the severe cohort with mild impairment had been diagnosed and treated prospectively from birth (sibling screening).

Most patients were ambulant. One had a dystonic movement disorder correlating to abnormal basal ganglia on MRI.

8.6.4. Hepatic Phenotype

All patients in the severe phenotype cohort had evidence of liver disease, evidenced by the presence of hepatomegaly (5/5), ultrasound abnormalities (5/5) and elevated ALT (5/5). The elevated ALT was seen from the earliest ages (figure 8.4). By contrast, none of the mild phenotype cohort had hepatomegaly and ALT was normal in this cohort.

Serum creatinine values were also examined (figure 8.4). Patients with partial/mild phenotype had higher blood creatinine levels than patients with the severe phenotype, though these values were not corrected for body or muscle mass or degree of dietary protein restriction.

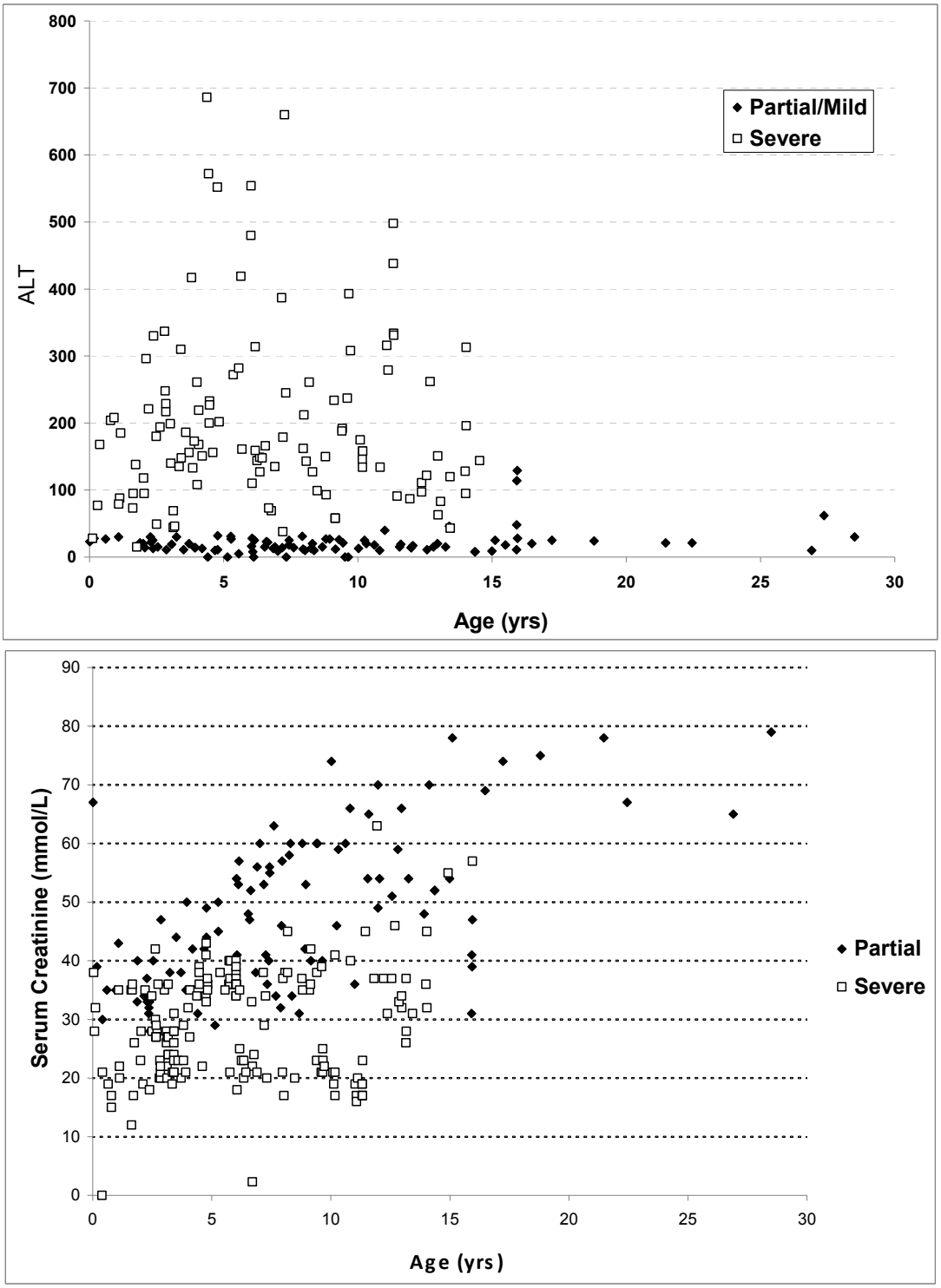

Figure 8.4: Serum alanine aminotransferase (ALT) (upper panel) and serum creatinine (lower panel) values plotted against age for partial and severe argininosuccinic aciduria cohorts.

8.6.5. Plasma amino acid profiles

172 plasma quantitative amino acid determinations were available from the clinical records of the 11 patients (figure 8.5 and table 8.2). Arginine was substantially elevated compared to normal values, while the branch chain amino acids (leucine, isoleucine, valine) were often lower than normal values. Citrulline levels were also substantially elevated (although formal normal values were not available).

Severe cohort patients had significantly higher arginine, citrulline, glutamine and glutamate, and significantly lower branch chain amino acids compared to the partial/mild cohort.

Applying a principal component analysis (unsupervised method) to the quantitative amino acid profiles clearly differentiated two groups corresponding to the mild and severe cohorts (figure 8.6), confirming that there is a substantial biochemical phenotypic basis for these two cohorts.

One CSF sample was available for further analysis by NMR spectroscopy (figure 8.7). Qualitative interpretation of metabolites present identified many of the normal CSF metabolites expected, and spectral peaks consistent with argininosuccinic acid were also identified confirming previous reports of high levels of argininosuccinic acid in CSF. Quantification of metabolites was not undertaken.

	Normal Values Median (2.5th-97.5th centile)	Argininosuccinic aciduria patients: Mean (standard deviation), μmol/L All cases	Severe cohort	Partial cohort	Severe v partial t-test p-value
Alanine	300 (112-592)	325.6 (106.9)	318.5 (93.4)	336.0 (123.7)	0.227
Arginine	51 (14-102)	160.6 (121.5)	179.7 (137.0)	132.8 (88.1)	0.004
Aspartate		13.1 (6.8)	13.8 (7.1)	12.1 (6.2)	0.060
Citrulline		213.1 (147.7)	296.8 (132.2)	92.5 (58.6)	0.000
Cysteine		20.4 (17.8)	21.6 (16.2)	18.6 (12.3)	0.147
Glutamine	539 (326-800)	569.0 (157.1)	602.7 (176.3)	520.0 (107.5)	0.000
Glutamate	88 (31-219)	91.1 (51.0)	109.9 (52.0)	63.9 (34.8)	0.000
Gln+Glu		660.1 (180.0)	712.5 (200.6)	583.9 (107.1)	0.000
Glycine	246 (120-436)	269.4 (94.1)	239.6 (78.1)	312.5 (98.8)	0.000
Histidine	74 (43-111)	80.8 (15.3)	85.4 (15.6)	74.1 (11.9)	0.000
Isoleucine	50 (20-91)	37.9 (20.5)	30.9 (19.3)	48.2 (17.9)	0.000
Leucine	97 (44-169)	62.5 (34.2)	51.3 (31.1)	82.4 (30.5)	0.000
Lysine	130 (66-242)	116.2 (47.7)	117.3 (50.1)	114.8 (44.2)	0.700
Methionine	20 (10-41)	26.3 (10.4)	30.5 (10.7)	20.2 (6.3)	0.000
Ornithine	59 (24-154)	91.6 (58.6)	95.1 (64.8)	86.5 (48.0)	0.279
Phenylalanine	48 (30-76)	49.0 (16.5)	44.4 (15.4)	55.5 (16.0)	0.000
Proline	154 (66-330)	186.4 (58.5)	187.1 (56.0)	185.4 (62.3)	0.831
Serine	127 (69-206)	113.9 (37.0)	104.2 (30.8)	127.9 (41.0)	0.000
Taurine	70 (26-169)	53.5 (30.7)	54.1 (36.7)	52.7 (19.0)	0.745
Threonine	104 (43-218)	71.8 (34.0)	64.3 (32.9)	82.7 (32.9)	0.000
Tyrosine	51 (29-92)	49.6 (19.3)	46.9 (18.9)	53.5 (19.1)	0.010
Valine	178 (79-313)	130.3 (52.2)	111.8 (49.7)	157.1 (43.6)	0.000

Table 8.2: Plasma amino acid concentrations in argininosuccinic aciduria cohorts. Control normal values: plasma amino acid reference intervals calculated from 271 subjects from 8 different laboratories, courtesy Mrs MA Preece.

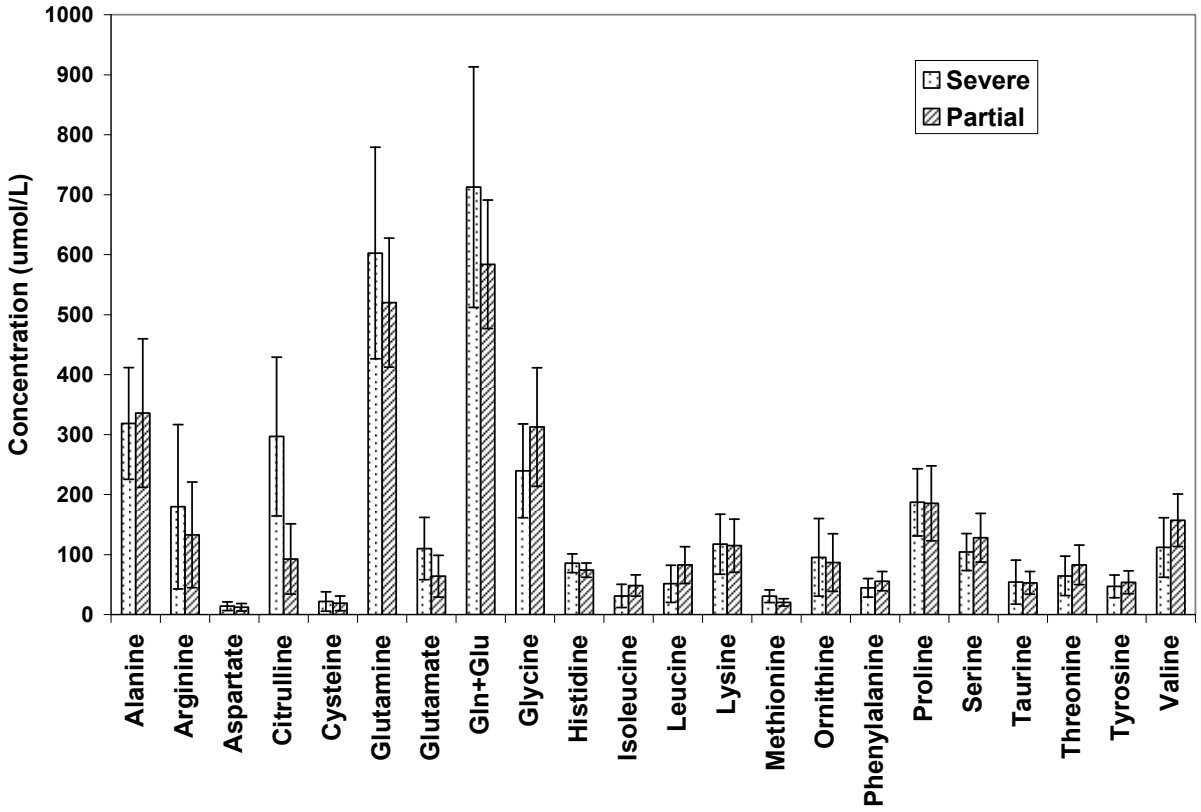

Figure 8.5: Bar chart of mean plasma amino acid concentrations in severe and partial argininosuccinic aciduria cohorts. Error bars: standard deviation. (See table 8.2 for t-test significances).

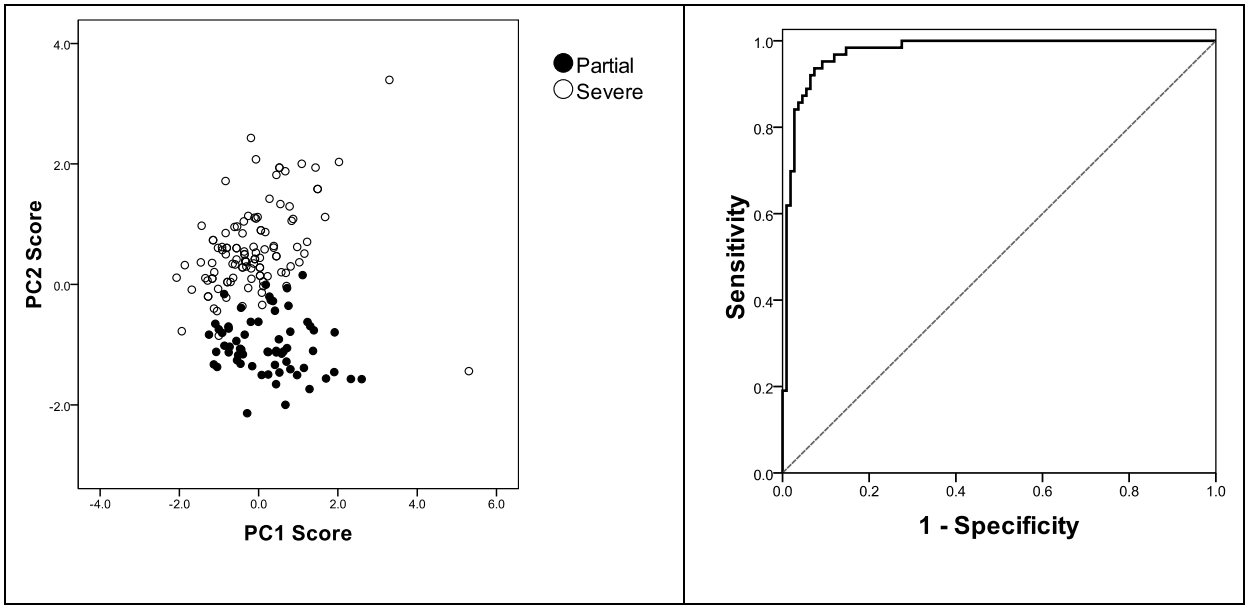

Figure 8.6: Principal component analysis scores plot (left) of plasma amino acids profile in argininosuccinic aciduria cohorts and (right) receiver-operator characteristic (ROC) curve for second principal component. Filled circles, results from partial ASA cohort; open circles, results from severe ASA cohort. Area under the curve 0.975; p=0.000.

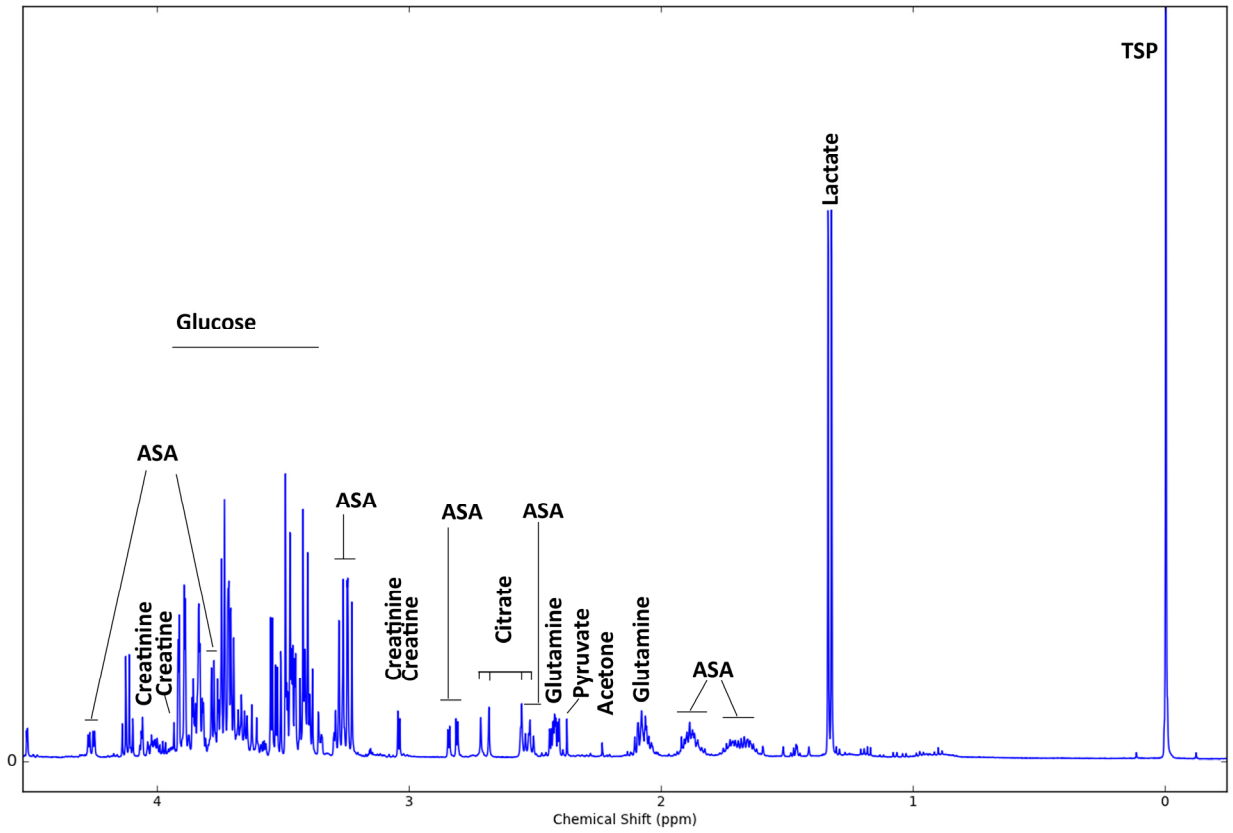

Figure 8.7: One dimensional proton NMR spectrum of cerebrospinal fluid from argininosuccinic aciduria patient 3. Prominent peaks identified. ASA, argininosuccinic acid.

8.6.6. Conventional MR Imaging

MRI examinations were available for 10 patients (table 8.3 and figure 8.8). The majority had generally normal MR imaging. All had normal myelination, and all bar one had normal basal ganglia. Two (siblings) had small areas of gray matter heterotopia (gray matter in periventricular location). Two had small subcortical or cortical infarcts, while another two had peritrigonal white matter abnormalities that may represent small infarcts or dysmyelination. One patient (11) had marked volume loss and ventricular dilatation as well as abnormalities within the caudate nuclei and putamina consistent with his dystonic movement disorder.

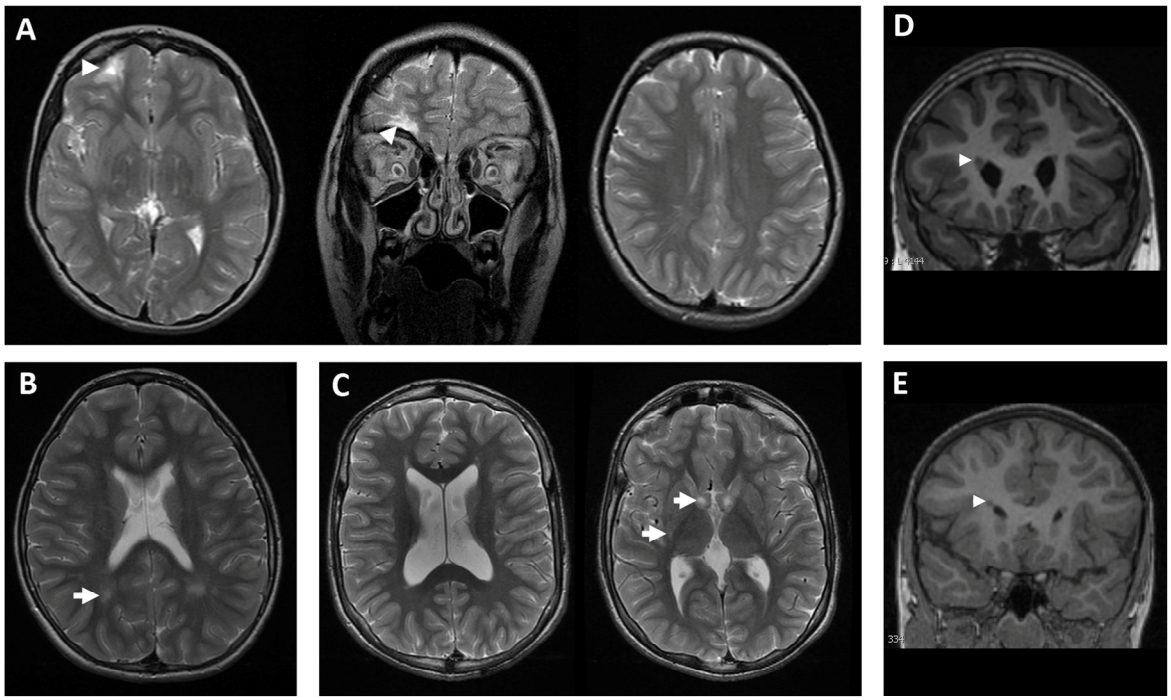

Figure 8.8: T_2 weighted (A-C) and T_1 weighted (D-E) MR images from argininosuccinic aciduria patients. (A) Axial, coronal and sagittal plane views from patient 1 demonstrating small right inferior frontal lobe infarct (arrow heads) but otherwise normal brain. (B) Axial view patient 3 showing peritrigonal white matter abnormalities (arrow). (C) Axial views patient 11 showing (left) ex-vacuo dilatation of ventricles and (right) high T_2 signal in bilateral caudate heads and posterior putamina (arrows). (D) and (E) Coronal views patients 7 and 10 showing periventricular gray matter heterotopia (arrowheads).

	Class	White matter	Myelination	Basal ganglia	Other
1	Partial	Normal	Normal	Normal	Small right inferior frontal lobe infarct
2	Partial	Normal	Normal	Normal	Small subcortical white infarct matter medial right frontal pole
3	Severe	Small foci of abnormal signal in peritrigonal white matter, ? infarcts	Normal	Normal	
4	Partial	Normal	Normal	Normal	Normal
5	Severe	Normal	Normal	Normal	Normal
6	Partial	Normal	Normal	Normal	Brain/ head generally small
7	Severe	Normal	Normal	Normal	Small areas of nodular heterotopia adjacent to frontal horns
8	Partial	No imaging available			
9	Partial	Normal	Normal	Normal	Normal
10	Severe	Foci of abnormal T2 signal in peritrigonal white matter. Abnormal foci in subcortical white matter	Normal	Normal	Small gray matter heterotopia adjacent to ventricles
11	Severe	Perirolanidc gliosis; volume loss, ex-vacuo dilatation of ventricles	Normal	Abnormal T2 signal caudate head and posterior putamen	

Table 8.3: MR imaging features in argininosuccinic aciduria patient cohort.
Shaded rows indicate mild/partial phenotype patients.

8.6.7. MR Spectroscopy

Eight MRS studies (from 7 patients) acquired from basal ganglia were available. Five were from patients in the mild cohort and 3 from the severe cohort. Four MRS studies (one mild and three from severe cohort) were available from white matter.

8.6.7.1.Basal ganglia results

ASA patients had significantly lower tNAA than the comparator group; this was most marked in the severe cohort (ANOVA $p<0.05$, figures 8.9, 8.10 and 8.11, table 8.4). Creatine was also lower in ASA patients compared to controls, with lowest levels in the severe cohort (ANOVA ns). Glutamine+glutamate was non-significantly elevated in ASA patients with contributions from both glutamine and glutamate elevations.

To account for the effect of bulk neuronal loss on glutamine and glutamate levels, ratio to NAA and Cr were calculated. Examination of metabolite ratios (figure 8.10) found that there was no difference between ASA and controls in the Cr/NAA ratio. Glutamine+glutamate/NAA and glutamine+glutamate/Cr ratios were also significantly higher in ASA patients. For each of these alterations, the highest ratios were in the severe ASA cohort, and lowest in the comparator group (ANOVA $p<0.05$ for Gln+Glu/NAA).

No elevations in guanidinoacetate were detected in the basal ganglia in any group.

Inositol was decreased in the basal ganglia in the severe ASA cohort.

8.6.7.2.White matter results

Data were examined for the four studies together, with no differentiation between severe (n=3) and mild (n=1) cases (figures 8.9 and 8.12, table 8.4). In white matter, Cr was significantly lower in ASA patients, but Cr/NAA was not significantly lower. There was no increase in the mean glutamine+glutamate in the ASA cohort. The standard deviation for white matter glutamine was very large due to one case having very high levels of glutamine identified (figure 8.13). On initial inspection the spectrum from this case appeared to have an increased guanidinoacetate peak at 3.8ppm, however on further analysis it was evident that much of this peak was due to the high glutamine level that also has a peak at ~3.8ppm.

Inositol was significantly lower in ASA patients in the white matter. There was also a slightly increased level of guanidinoacetate in ASA patients.

Basal ganglia metabolites (mM, mean (standard deviation))				
	Argininosuccinic aciduria			**Normal MRI comparator group**
	All patients (n=8)	Partial/ mild cohort (n=5)	Severe cohort (n=3)	(63 studies)
Median age (years, (range))	9.9 (1.2-14.3)			4.1 (0.5-16.7)
N-Acetylaspartate	4.61 (0.89) †	4.82 (1.02)	4.27 (0.65)	5.21 (0.51) $
Creatine	4.07 (0.76) *	4.16 (0.85)	3.92 (0.73)	4.55 (0.59)
Glutamine	2.36 (0.92)	2.22 (0.82)	2.59 (1.21)	1.98 (0.79)
Glutamate	4.63 (0.83)	4.89 (0.71)	4.19 (0.98)	4.45 (0.78)
Glutamine+Glutamate	6.98 (1.39)	7.10 (1.07)	6.78 (1.27)	6.43 (1.39)
myo-Inositol	2.31 (0.72)	2.54 (0.59)	1.93 (0.85)	2.49 (0.43)
Choline	0.94 (0.22) *	1.00 (0.27)	0.85 (0.09)	1.11 (0.18) $
Guanidinoacetate	0.99 (0.39)	1.09 (0.33)	0.81 (0.48)	1.01 (0.32)

White matter metabolites (mM, mean (standard deviation))		
	Argininosuccinic aciduria	**Normal MRI comparator group**
	All patients (n=4, 3 severe and 1 partial)	(53 studies)
Median age (years, (range))	12.3 (1.2-14.2)	4.7 (0.5-16.7)
N-Acetylaspartate	4.48 (0.37)	5.11 (0.73)
Creatine	2.45 (0.20) †	3.18 (0.47)
Glutamine	1.79 (2.54)	1.32 (0.62)
Glutamate	2.82 (0.27)	3.51 (0.78)
Glutamine+Glutamate	4.61 (2.32)	4.84 (1.18)
myo-Inositol	1.65 (0.81) †	2.57 (0.39)
Choline	0.88 (0.09) *	1.08 (0.15)
Guanidinoacetate	1.05 (0.41) *	0.75 (0.21)

Table 8.4: Mean MRS derived brain metabolite concentrations in argininosuccinic aciduria cohort and normal MRI comparator group. Student's t-test all ASA patients vs control, * $p<0.05$; † $p<0.01$. ANOVA between severe, partial and control groups, $ $p<0.05$

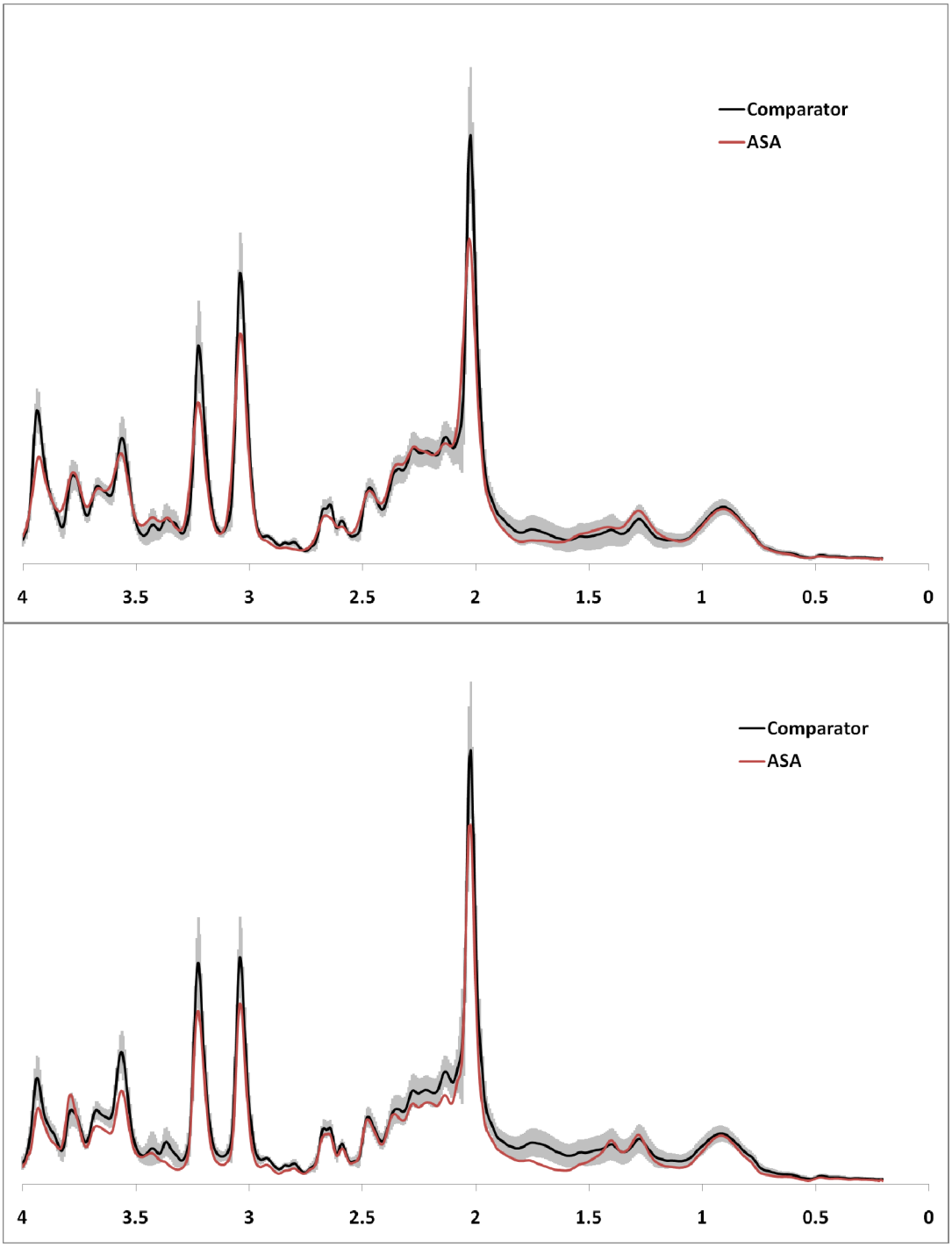

Figure 8.9: Mean MR spectra for argininosuccinic aciduria cohort (red line) and standard normal MRI comparator cohort (black line, shaded area indicates standard deviation). Top panel: basal ganglia. Bottom panel: white matter.

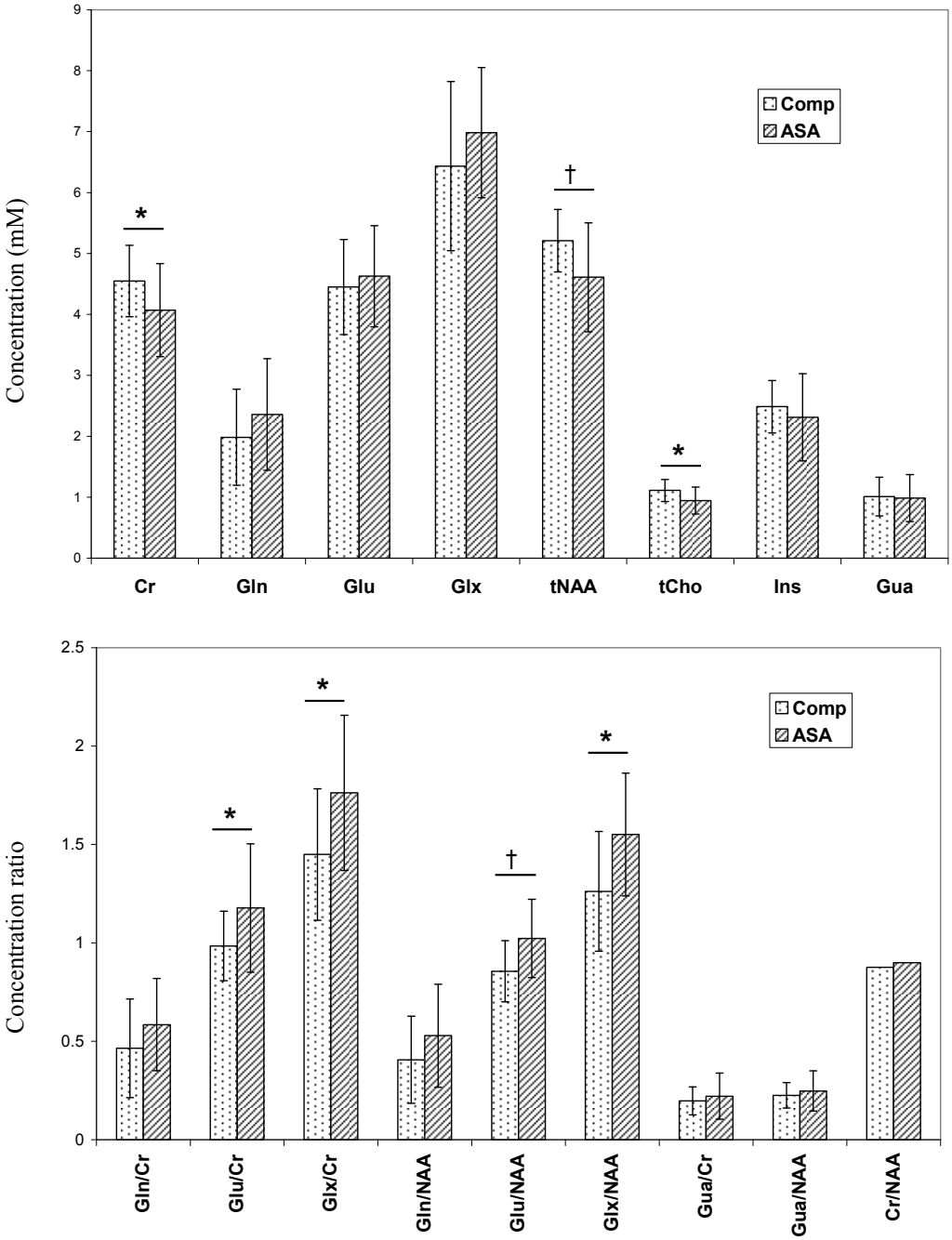

Figure 8.10: Bar charts of mean MRS derived metabolite concentrations in comparator and argininosuccinic aciduria cohorts in basal ganglia. Upper panel: absolute metabolite values. Lower panel: metabolite ratios for glutamine, glutamate and guanidinoacetate. Student t-test, * $p<0.05$, † $p<0.01$. Error bars indicate standard deviation.

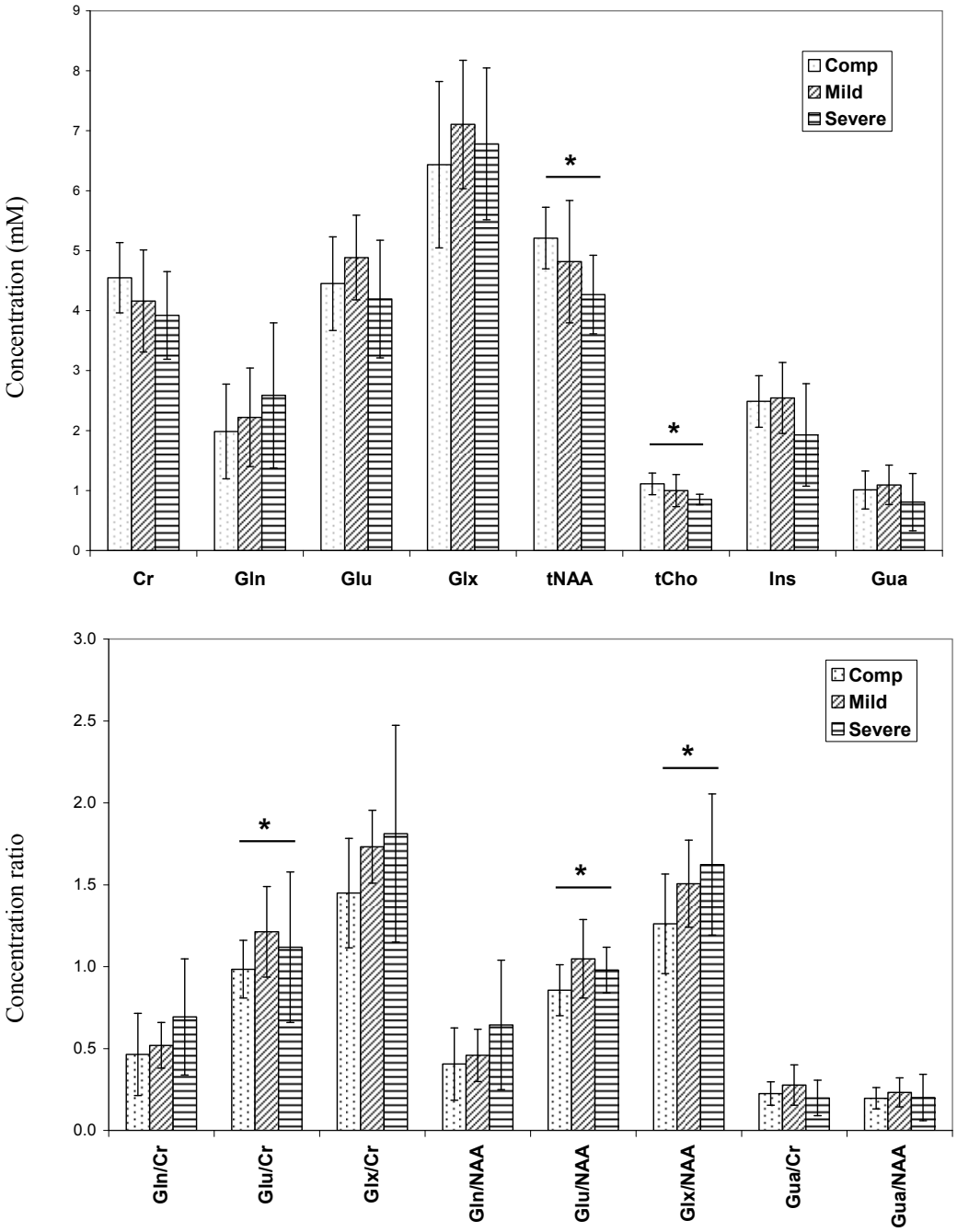

Figure 8.11: Bar charts of mean MRS derived metabolite concentrations in comparator, mild and severe argininosuccinic aciduria cohorts in basal ganglia Upper panel: absolute metabolite values. Lower panel: metabolite ratios for glutamine, glutamate and guanidinoacetate. ANOVA between groups, * $p<0.05$, † $p<0.01$. Error bars indicate standard deviation.

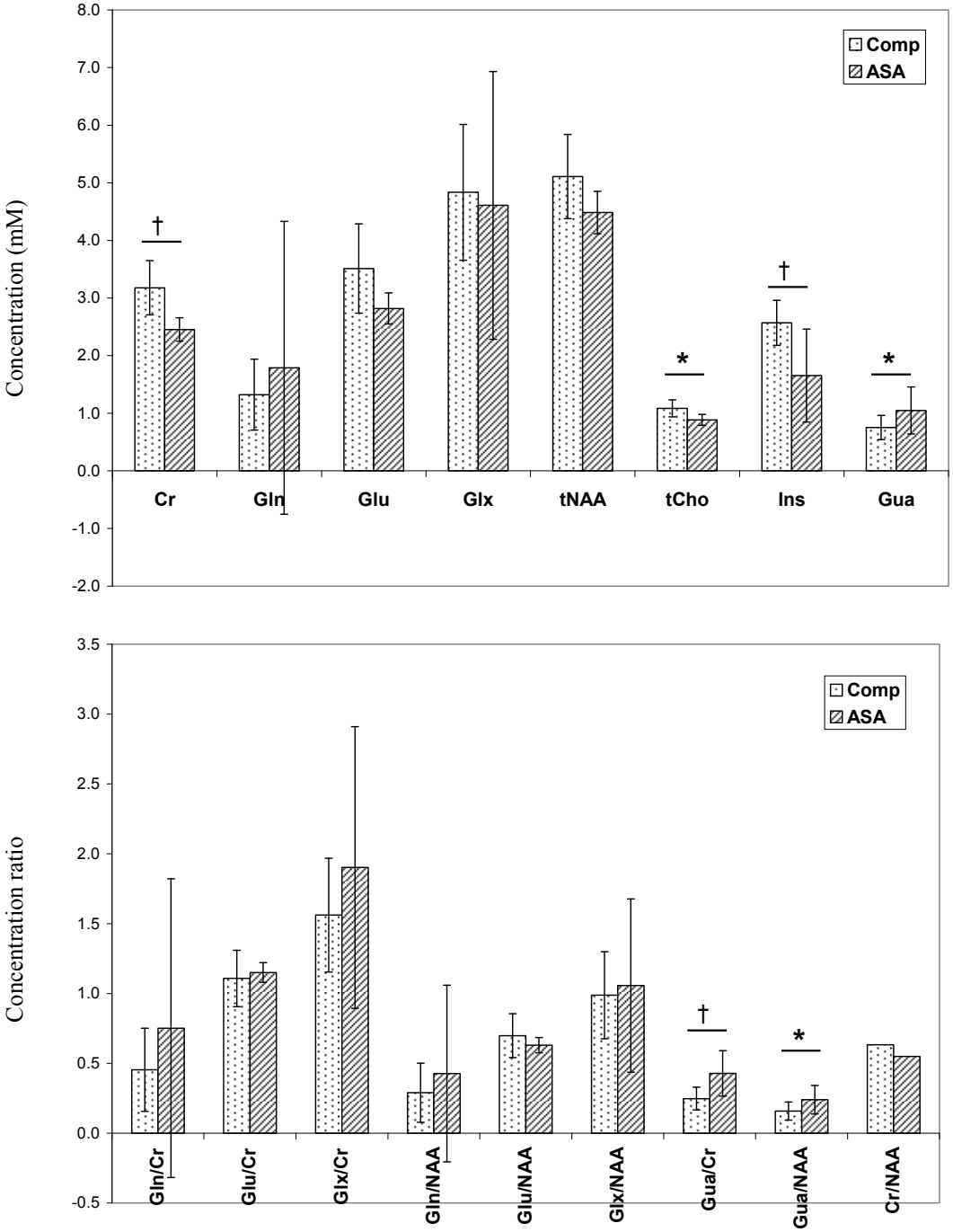

Figure 8.12: Bar charts of mean metabolite concentrations in comparator and argininosuccinic aciduria cohorts in white matter. Upper panel: absolute metabolite values. Lower panel: metabolite ratios for glutamine, glutamate and guanidinoacetate. Student t-test, * $p<0.05$, † $p<0.01$. Error bars indicate standard deviation.

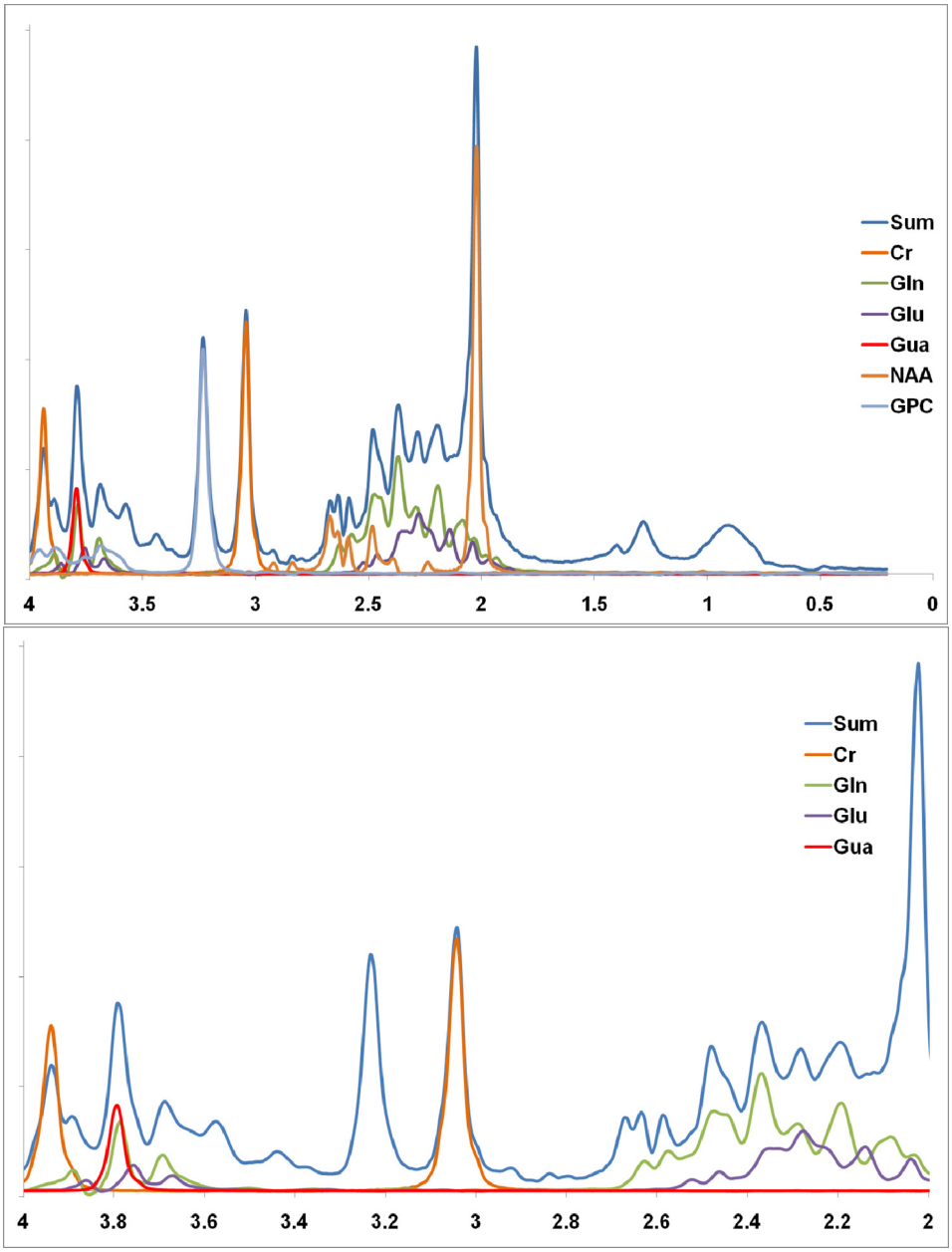

Figure 8.13: MRS spectrum from white matter from argininosuccinic aciduria patient 7 showing LCModel fitted line (sum) and individual metabolite components. Components shown for creatine (Cr), glutamine (Gln), glutamate (Glu), guanidinoacetate (Gua), N-acetylaspartate (NAA) and glycerophosphocholine (GPC). Upper panel: 0-4ppm. Lower panel: 2-4ppm only. Note guanidinoacetate and glutamine peaks overlap significantly at 3.8ppm.

8.7. Discussion

The data presented here includes the first substantial systematic report of neuroimaging and MRS data in a cohort of patients with ASA. The two phenotypic categories classically described in ASA were evident, and some interesting observations about differences and similarities between these groups have been made.

The mild/partial phenotype cohort is classified by later presentation while the severe phenotype cohort present in the early neonatal period usually with significant hyperammonaemia. The hepatic phenotype showed a striking segregation between these two cohorts, with the entire mild cohort having normal ALT levels, and no hepatomegaly, while the entire severe cohort (including one diagnosed prospectively by sibling screening) had elevated ALT, hepatomegaly and abnormalities detectable by liver ultrasound scanning. Furthermore the elevated ALT was evident from a young age.

The amino acid profile also effectively distinguishes the two cohorts, demonstrated by the unsupervised principal component analysis (PC2 generating a receiver operator characteristic (ROC) curve (i.e. plot of 1-specificity versus sensitivity) with area under the curve of 98%). Many amino acids were significantly different between the two groups, with the severe cohort having significantly higher arginine, citrulline, glutamine and glutamate and significantly lower branch chain amino acids and glycine. This may be in part due to differences in therapy: use of alternative pathway therapies (particularly sodium benzoate that conjugates glycine) can explain the lower glycine in the severe cohort, while these medications are also implicated in causing low branch chain amino acid levels [255]. Higher doses of arginine therapy in the severe cohort may be an explanation for the higher arginine levels in that group.

Tighter protein restriction may also have an effect on the differential amino acid profiles. The amino acid differences between the two cohorts may, however, also reflect a real biological difference in the metabolic disorder between the two groups. Thus the severe cohort had higher levels of glutamine, glutamate and citrulline.

The two cohorts are less distinct in terms of the neurocognitive effects and seizure disorders. Seizure disorders were more prevalent in the severe cohort (5/5) but were still present in patients (2/6) in the mild phenotype cohort. Similarly, the presence of cognitive impairment, learning difficulties and behavioural problems crossed over both groups. One child (number 7) was educated in main stream school but still had delayed development despite prospective diagnosis and therapy following sibling screening. Formal cognitive assessment and scoring was not available in this cohort, but the use of such scoring could provide an objective assessment and evaluation of any differences between the two cohorts.

One possible explanation for why both groups seem to have significant neurocognitive deficits could relate to the timing of disease diagnosis. Patients within the severe cohort often have marked hyperammonaemia at presentation with presumably a significant detrimental effect, but these patients present earlier and are then treated from an earlier age. Patients in the mild cohort are usually diagnosed later, and so although the biochemical derangements or other pathological processes are presumably "milder" they will have been ongoing over an extended period of time, potentially accruing pathological effects during this lag time. The case of the adult reported to have creatine deficiency at time of diagnosis illustrates this point [244]. The early reports that mild phenotype patients identified by newborn screening (rather

than symptomatically) have better neurocognitive outcome also supports this “lag time” hypothesis [235].

The MR imaging features described here provide the first systematic study of ASA patient neuroimaging. In contrast to other UCD and IMD, the MRI features seen are generally very mild. Two patients had small cortical/subcortical infarcts, and another two had peritrigonal white matter abnormalities that could be consistent with ischaemic damage. Patient 11 had bilateral high signal change in the caudate and putamina, a similar pattern to that seen in some mitochondrial disorders. Thus there appears to be a propensity to possible vascular insults (infarcts), which could be related to dysfunction of normal intracranial vasoregulation. This is of interest given the likely central role of cellular-level NO deficiency in ASA [223, 228]. It would be interesting to further evaluate this in the context of the murine model of disease that has been generated. Alterations in the normal vascular functional response of the CNS in ASA could also be further validated by other functional imaging modalities such as fMRI that relies on normal vasoregulatory alterations, or perfusion MR imaging.

Two patients who are siblings had periventricular gray matter heterotopia, i.e. accumulation of neurons adjacent to the ventricles that have failed to migrate correctly to the cerebral cortex. Children with heterotopia have a high rate of epilepsy [256]. There is usually a genetic basis for such heterotopias with chromosomes X, 20 and 5 often implicated, and so it is likely that in these siblings this is an incidental occurrence. However, heterotopias have been reported in other metabolic disorders including Zellweger and neonatal adrenoleukodystrophy [256].

Nitric oxide has an important function in normal neuronal migration, demonstrated in both animal models [257] and human cell lines [258]. It is possible, therefore, that NO system dysfunction in ASA could interfere with normal patterns of neuronal migration. Although only two of the patients here had evident heterotopia, it is possible that other patients in the cohort have small lesions not detected by the conventional MRI. High resolution volumetric MRI or other functional modalities may be able to detect higher rates of neuronal migration defects in these patients, which could provide an anatomical substrate for the high rates of seizure disorders and cognitive impairments in ASA patients, and warrants further investigation.

8.7.1. MR spectroscopy findings

In parallel with the relatively normal MR imaging findings, the MRS profiles in ASA in this cohort were also relatively normal. That said, some statistically significant differences with the standard comparator groups were found, and also graduated differences from control to mild-cohort to severe-cohort. The slight decrease in tNAA seen in both brain regions studied is not specific to ASA but does imply there is some neuronal loss or loss of neuronal viability despite the relatively normal MRI appearances.

8.7.1.1.Creatine deficiency

Creatine levels were significantly decreased in both white matter and basal ganglia, however the creatine peaks were clearly present and substantially higher than the (absent) levels detected in the formal creatine deficiency syndromes. Thus the clinical significance of the creatine "deficiency" is uncertain. Furthermore, the creatine/NAA ratio was normal in both brain regions, which could imply that the lower absolute creatine levels seen were a reflection of the loss of neurons and not a specific metabolic alteration or deficiency *per se* at the

neuronal level. Thus there is not good evidence in this cohort for creatine deficiency in the brain. The previous report of creatine deficiency in ASA demonstrated this in a late-onset adult patient prior to treatment, with brain creatine levels normalising with oral arginine therapy [244]. This observation in conjunction with the relatively normal creatine levels seen in the current cohort who were all receiving arginine supplements at the time of MRS examination would suggest that the current treatment regimen with arginine supplementation is effective in treating any significant brain creatine deficiency.

It remains possible that creatine deficiency existing prior to treatment during the diagnostic "lag time" could have a detrimental effect. In the creatine deficiency syndromes creatine supplementation effectively raises brain creatine as ascertained by MRS, but does not completely ameliorate the clinical phenotype implying there may be irreversible damage sustained prior to treatment [259]. The same could be true in ASA, and could be one factor in explaining the potentially better outcome for children identified by newborn screening and treated prospectively, thereby avoiding sustained arginine and secondary creatine deficiencies. It would not be justifiable to stop arginine therapy in diagnosed patients to assess brain creatine deficiency, but potentially this could be screened for at diagnosis for example in patients identified by a newborn screening programme.

8.7.1.2.Guanidinoacetate toxicity

It has been suggested that elevated guanidinoacetate concentrations, potentially due to arginine supplementation, could be responsible for the high rates of seizures seen in ASA patients [247, 248]. The data in this study do not provide strong evidence in favour of elevated guanidinoacetate in the brain of the ASA cohort.

In the data from the basal ganglia, there was no difference in the guanidinoacetate concentration between controls and patients, and indeed there was trend to lower guanidinoacetate (non-significant) in the severe ASA cohort who had higher rates of seizure disorders. By contrast, in the smaller dataset from the white matter region, a small but significant elevation in guanidinoacetate was detected. Of note the white matter data was predominantly from severe ASA patients, but only two had seizure disorders.

In the physiological pH range, the expected spectral peak of guanidinoacetate is a singlet at 3.8ppm. Glutamine also has peaks at this chemical shift, and *in vivo* these (and other metabolites) contribute to the peak seen at circa 3.8ppm (see figure 8.13). Since glutamine also has other peaks between 2.4-2.5ppm it is theoretically possible to calculate the relative contributions of glutamine and guanidinoacetate to the peak seen at 3.8ppm. However, there remains some uncertainty as to the accuracy of the metabolite linear combination fitting to this peak. Of note in the current dataset the highest guanidinoacetate concentrations were associated with the highest glutamine concentrations, suggesting that the contribution of glutamine to the *in vivo* 3.8ppm peak may have been underestimated and that of guanidinoacetate overestimated.

Given that the proposed mechanism for generating elevated guanidinoacetate is excess arginine supplementation, it might be expected that any elevation would be seen in all brain areas analysed since AGAT and GAMT are expressed throughout the brain. The absence of elevated guanidinoacetate in the basal ganglia data therefore does not support this hypothesis. Furthermore guanidinoacetate should not be elevated prior to treatment with arginine, and so

cannot explain the development of seizures occurring prior to diagnosis in the late onset/ mild phenotype.

It should also be noted that in the report of two ASA patients with elevated brain guanidinoacetate that guanidinoacetate levels in controls were reported as "none detected" [248], whereas in the present data the comparator group did have apparently detectable levels. In GAMT deficiency, the guanidinoacetate detected was substantially higher in gray matter compared to white matter [246] in contrast to the pattern observed in the ASA patients here. For these various reasons, therefore, the data presented do not confirm the suggestion that guanidinoacetate toxicity plays a role in generating epilepsy in ASA. Analysis of a larger cohort with higher field MRI scanners may help elucidate this hypothesis further.

8.7.1.3.Elevated brain glutamine and glutamate

In the UCD generally hyperammonaemia is thought to result in elevated brain glutamine synthesis, since astrocytic glutamine synthase activity is a key protective mechanism against ammonia-induced neurotoxicity. In the acute phase, rapid increases in brain glutamine results in intracellular osmotic pressure causing cellular swelling and consequently brain oedema.

On analysis of absolute metabolite concentrations across the cohorts, there was no significant elevation of glutamine+glutamate detected in ASA patients in either white matter or basal ganglia, though there was a trend to increased concentration in basal ganglia in ASA. Importantly all children were clinically well at the time of MRS, and so ammonia levels would not be substantially elevated at the time of study.

It has been noted already that there was a significant decrease in tNAA in ASA patients. This may suggest there is a reduction in neuronal cell number or density present within the volume of interest, and so ratios of glutamine and glutamate to NAA and to creatine were calculated to provide an approximate correction for any change in neuronal density or number. In basal ganglia there was significantly increased glutamine+glutamate/creatine and glutamine+glutamate/NAA, with contributions to this from both glutamine and glutamate separately. In the smaller white matter dataset results did not reach significance, but there was a trend to elevated glutamine+glutamate/creatine.

One child had notably high glutamine levels observed by MRS, convincingly distinguished from glutamate (figure 8.13). This child also had the highest mean glutamine levels on plasma quantitative amino acids (mean 659 μmol/l). Interestingly, in this child the myo-inositol level was significantly decreased, a pattern reflected in the low mean inositol in the white matter ASA group. There was also a non-significant trend to lower inositol in the severe ASA cohort in basal ganglia. Inositol functions as an organic osmolyte, being actively transported in or out of cells (particularly glia) to counteract chronic alterations in osmotic pressure. Thus it is conceivable in these children that inositol is depleted in cells in response to chronically elevated glutamine, suggesting ongoing osmotic stress in the CNS that may contribute to the neuropathology.

Alterations in glutamine and glutamate are proposed to be due to hyperammonaemia, and so would not be specific to ASA but generally applicable to all the UCD. It is important to note that elevated levels relative to cell density (NAA) were observed in the ASA patients despite their relatively good ammonia control.

8.8. Conclusions

The MRS data presented here can answer some of the hypotheses presented to explain the CNS pathology in ASA. Firstly, brain creatine deficiency is not a significant issue in arginine treated ASA patients, but could potentially contribute to the neuropathology prior to diagnosis and the instigation of treatment particularly in late-onset/mild phenotype patients. Secondly, brain guanidinoacetate levels were not convincingly found to be elevated in the ASA patients, and levels did not correlate well with the occurrence of seizure disorders. Thirdly, brain glutamine+glutamate levels were found to be relatively elevated in at least some of the ASA patients, a feature common to other UCDs.

The MRI data highlighted the relatively normal imaging features, but did identify several patients with possible infarcts due to vascular events that raise the possibility of vascular dysregulation. The alterations and deficiencies in NO function in ASA could contribute to this, and may provide a mechanism specific to ASA to explain the neuropathological features. If ASA patients suffer the same ammonia/glutamine-induced osmotic stress and changes as other UCD patients, as evidenced by the MRS findings, it is possible that ineffective NO/vascular-mediated mechanisms as described by Erez *et al* [223] create an ASA-specific defect in how the CNS responds to this generic UCD insult. Furthermore, the possibility of NO dysfunction in ASA interfering with normal neuronal migration is suggested by the finding of significant gray matter heterotopia in two of the patients. These hypotheses require further investigation and as noted above, other functional imaging modalities could provide *in vivo* methods for evaluating vascular regulatory function and subtle evidence of neuronal migrational defects. Further investigation using murine models of ASA could also focus on the neuropathogenesis aspects of NO dysfunction.

Chapter Nine

9. Final Discussion

The work described in this thesis employed *in vivo* magnetic resonance imaging and spectroscopy techniques with the aims of firstly identifying potential biomarkers of disease that could be used in disease diagnosis and in monitoring disease progression or response to novel therapies, and secondly, to investigate the pathogenesis of neurologic damage in specific inherited metabolic disorders. The study aimed in particular to develop and use quantitative *in vivo* brain metabolite profiling by MR spectroscopy in the investigation of the inherited metabolic disorders, as an adjunct to standard neuroimaging and biochemical analyses. This thesis has set out the results of work undertaken towards meeting these aims, which are briefly summarised here (see table 9.1). Limitations of the techniques employed are discussed, and future research directions explored.

9.1. Technique Development and Assessment

Prior to applying the techniques to evaluate disease specific hypotheses, methods for the acquisition, processing and analysis of *in vivo* MRS data had to be implemented and evaluated. In particular it was important to assess the validity and quality of the data being generated, specifically the reliability and reproducibility of the metabolite quantification.

Non-standard metabolite peak detection (Chapter 5)	Succinate, glycerol, glycine detected in brain of children demonstrated to have specific defects in metabolic pathways of these metabolites.
Hunter Syndrome (Chapter 6)	NAA decreased in patients, with trends mapping to alteration in clinical neurocognitive status. MRS profile has potential to monitor and detect early changes in brain.
Propionic Acidaemia (Chapter 7)	Patients have relatively decreased glutamine and glutamate in areas of brain vulnerable to stroke, and evidence of impaired brain energy metabolism.
Argininosuccinic Aciduria (Chapter 8)	Neither creatine deficiency nor guanidinoacetate toxicity confirmed as major factors in predilection to epilepsy. Relatively increased glutamine and decreased inositol supportive of ammonia-induced osmotic stress. Novel neuroimaging features consistent with NO dysfunction described in ASA patients.

Table 9.1: Summary of key results from application of MRS technique to disease cohorts.

A standard acquisition protocol was implemented to facilitate the collection of *in vivo* MRS data, benefitting from pioneering work undertaken in the study of childhood brain tumours. The use of a standard protocol with pre-determined sampling sites (voxel positions) meant that metabolite data from different patient cohorts was comparable since the acquisition and anatomical parameters were standard, removing non-biological sources of data variability. The standard protocol demonstrated the feasibility of implementing such a study in a routine clinical paediatric setting with large datasets generated, with over 300 MRS examinations included in the period of the study. Although the standard MRS examination sampled only the basal ganglia and parietal white matter thus restricting the analysis to these regions, these regions are commonly involved in metabolic diseases and allowed for the generation of specific comparator cohorts.

In addition to a standard acquisition process, the use of a standard post-processing method employing a well-validated software tool (LCModel^{TM}) enabled automatic user-independent post-processing to be undertaken, again removing a potential source of non-biological variation. The detailed data quality assessment described found that good quality data was obtained after processing in around 95% of cases. Furthermore this process provided a feedback loop aiming to correct specific data acquisition problems and thereby prospectively improving the quality of data collected.

A particular focus was placed on the analysis of the effects of different post-processing steps and the implications of acquiring data from two different MR scanner systems. This analysis found systematic differences in the metabolite estimations from the two scanner systems. Specific algorithms were developed to allow integration of data from the two systems. This experience in a single centre study highlighted the importance of considering such factors in the design of larger multicentre studies where potentially multiple scanner systems would be employed. Furthermore such considerations must play a part in the design of any multicentre study employing local data collection and analysis hardware, be it imaging or biochemical bio-fluid analysis.

9.2. Background data and standard comparator cohorts

Having established the reliability of the acquisition and processing protocols, the next requirement was the analysis of regional and age-related metabolite variation and the generation of a standard comparator cohort. These were required to enable the interpretation of brain metabolite data derived from specific disease cohorts and individual cases. The regional and age variation of the metabolite data described was found to be consistent with

previous studies in the literature, and furthermore the standard comparator cohort metabolite profile was comparable with other published normal control datasets. Indeed, the approach of using patients with normal MR imaging features as a comparator group was found to be employed in numerous other studies, and given the difficulties in obtaining a truly normal control group from the wider paediatric population, was found to be a workable and effective method. The large numbers of children included meant that the effect of metabolite "outliers" was reduced, such that narrow standard deviation values were seen for the cohort mean spectra and metabolite ranges.

9.3. Identification of Diagnostic Disease Biomarkers

Non-standard brain metabolites were detected in only a small percentage of children (~2.3%). When present, however, such metabolites may provide an important diagnostic handle. During the period of this study this approach contributed to the diagnostic process for several children. If such an approach were to have wider clinical relevance it would be important both that MRS was acquired routinely as part of the clinical assessment of patients with undiagnosed neurodegenerative disorders, and that methods for the identification and recognition of such peaks were established.

9.4. Development of disease and therapy monitoring biomarkers

The methods developed were applied to a cohort of children with Hunter Syndrome, a disease for which novel brain-targeted therapies are in development. One of the clinical challenges is in determining the efficacy of such therapies, and a multimodal MR approach was taken to evaluate the potential contribution of brain metabolite profiling to this process. Alterations in brain metabolite profiles were studied in serial assessments in a cohort of patients and found

to reflect alterations in the clinical status of the patients. The brain metabolite profile alterations also mirrored the changes in some quantitative MR imaging parameters. It was also suggested that brain metabolite alterations may provide an earlier marker of disease progression than structural MR changes, although this requires further prospective evaluation in cohorts of children with less advanced disease than the group studied here.

A robust disease biomarker requires exquisite sensitivity and reproducibility if it is to accurately detect early signs of disease, and as such the inherent variability and limited sensitivity in the MRS technique may be a limiting factor. The clinical relevance of using endpoints such as alterations in MR imaging or spectroscopic parameters must also be addressed, since in the design of the clinical trials of novel therapies it is desirable to have meaningful clinical endpoints. That said, objective methods of evaluating the effect of therapies on the brain can play an important role in such research.

9.5. Investigating disease pathogenesis

Towards meeting the second aim of the study, namely to investigate the pathogenesis of neurologic damage in specific IMDs, the techniques developed were applied to cohorts of children with two different disorders, propionic acidaemia and the urea cycle disorder argininosuccinic aciduria. In both instances the cohorts represent the largest groups of patients systematically studied using a neuroimaging and MR spectroscopy approach.

9.5.1. Propionic acidaemia

Children with this disorder of branch chain amino acid catabolism face a wide range of complications, but have a particularly poor neurological outcome with a specific propensity to developing strokes affecting the basal ganglia. Data were collected from this group of patients

both electively while the children were well, and also from a group who were acutely unwell requiring intensive care support. By this means it was possible to generate and compare brain metabolite profiles from 'stable' and 'unstable' metabolic situations, providing some preliminary findings that support current hypotheses relating to glutamine depletion and Krebs cycle impairment in this disorder. The observations made require further substantiation, but importantly the study demonstrated the feasibility of employing such methods in the acute setting, with the potential to monitor the effects of brain protective strategies.

9.5.2. Argininosuccinic aciduria

The methodology was then applied to the study of argininosuccinic aciduria, which has CNS features unique amongst the urea cycle disorders including significant cognitive impairment and high rates of epilepsy that suggest disease-specific mechanisms. The study provided the first systematic neuroimaging analysis in a cohort of patients with this disease, identifying several features that warrant further investigation and that may support the nitric oxide dysfunction hypothesis. Several other specific hypotheses to explain the CNS features were investigated using the MRS methods. The presence of creatine deficiency in appropriately arginine-supplemented patients was not found, and furthermore the role of guanidinoacetate toxicity was not supported from the data.

9.6. Limitations

With some notable exceptions, previous reports of the use of MR spectroscopy in the inherited metabolic disorders have been limited to single case qualitative descriptions or small case series. This study has implemented a robust and reproducible quantitative methodology, deriving some important results in several different disease cohorts. As such this work

represents a substantial advance in this field of research. That said several remaining limitations warrant discussion including technical and patient sampling limitations.

The MRS method is limited by the inherent insensitivity of the NMR technique and the difficulty of detecting low metabolite concentrations against the predominant water background signal. MRS is restricted to the detection of brain metabolites present at or around 0.5mmol/l, and therefore biologically significant alterations in lower concentration metabolites will not be detected. The work described here has benefitted from a focus on several diseases where alterations have occurred within the standard metabolites detected: i.e. the technique is best employed to address questions it is capable of answering.

A second limitation is the spatial resolution of the method. The standard single voxel approach used here samples a volume of $8cm^3$, a volume containing presumably millions of neurons and glial cells. The metabolite signal is therefore an average across the volume, and is not capable of detecting alterations in the distribution of metabolites across cell types or small anatomical structures. This again must be borne in mind in the interpretation of the metabolite data. Comment has already been made to the limited spatial coverage of the single voxel technique, sampling only one or two selected brain regions.

Thirdly the question of data reproducibility needs to be addressed, particularly as the alterations in metabolites in these disorders have been shown to be often subtle, and also as discussed above that the detection of early disease alterations requires greater sensitivity.

Fourthly, at low-field strength (1.5T) there is significant overlap of many of the metabolite peaks. This is particularly a problem for metabolites that are represented by multiplets rather than singlet peaks, notably glutamine and glutamate. The current methods may be able to provide some differentiation but further improvements in metabolite detection and differentiation will be possible with the use of higher field strength scanners, and also the application of spectral editing methodologies.

Beyond the technical limitations the study was also subject to "patient sampling limitations". By this is meant that the patient cohorts available for study are often small due to the limited incidence and prevalence of rare diseases. Furthermore the number of sampling time points is restricted. While functional imaging is considered non-invasive it is not necessarily feasible to obtain multiple acquisitions at differing time points within the natural history of the disease in a single patient, with the result that the data obtained even within one disease cohort is likely to reflect different stages of the disease. Additionally there is very limited scope for experimental manipulation in human subjects, particularly in the paediatric population.

Despite these limitations the work in this thesis has demonstrated that *in vivo* MR spectroscopy can generate valuable information, and has been successfully obtained in many children with different IMDs. The value of the information can be maximised by the use of a systematic quantitative approach to data acquisition and analysis as implemented here. The use of a large comparator cohort has also provided a strong baseline for comparison of individual cases and cohorts of patients with specific disorders; the use of a large comparator group was found to be particularly valuable when dealing with the small numbers of cases encountered in the rare diseases.

9.7. Future Perspectives

The current study has made progress towards meeting the initial aims and has also generated several further hypotheses. The study has, however, highlighted several limitations that will be addressed in future work.

Some of the technical limitations will be improved upon with the use of higher field MR systems that are becoming more widely available, including in clinical paediatric settings such as the recently opened NIHR-funded 3T MRI Research Centre at the Birmingham Children's Hospital. The use of such systems will go some way to improving the limitations of sensitivity and metabolite separation. Thus, for example, the initial findings reported in this thesis pertaining to the distinction of glutamine from glutamate in disorders such as propionic acidaemia and urea cycle disorders will be validated and tested in prospective MRS studies at higher field strength. Specific spectral editing routines will also be useful in detection of specific metabolites of interest, e.g. as mentioned previously for the detection of GABA.

Higher field scanners will also allow improvements in spatial resolution, since smaller voxel size regions of interest can be employed with a reasonable acquisition time. This will allow more specific anatomical regions of interest to be investigated, for example potentially studying different nuclei within the basal ganglia. Even with high field scanners, however, the single voxel approach still samples volumes in the order of cubic centimetres.

Spatial coverage with MRS can be enhanced substantially by the use of magnetic resonance spectroscopic imaging (MRSI, or chemical shift imaging (CSI)) techniques, allowing evaluation of metabolite profiles across larger regions of the tissue being examined. These

methods do present additional challenges in terms of data processing, reproducibility and inter-voxel cross-contamination, but in some circumstances may be a useful way of studying spatial metabolite variation. (An example of a CSI study is given in Appendix C). This will be of particular value in studying disorders where there is likely to be regional variation in metabolite profiles, and in studying differences between normal appearing and abnormal appearing brain regions.

Other functional imaging modalities have been alluded to in this thesis, notably those based on diffusion weighted imaging, which can provide information about tissue micro-structural changes. The combination of different modes of functional imaging data could be synergistic, allowing for example investigation of metabolite profile alterations in regions with altered tissue microstructural properties (as identified by DWI or DTI). Such an approach may be of value in identifying biomarkers of disease progression. The work described in Chapter Six relating to Hunter Syndrome provided an initial approach to combining quantitative structural imaging parameters with metabolite profile data, and work on-going will evaluate the potential to incorporate DTI parameters within such a model, particularly focussing on the detection of early changes that would not be identified with conventional MRI.

The second major challenge faced in the investigation of rare diseases such as the IMDs is the "patient sampling limitation", caused by the inherently small sample size available for study and the heterogeneous sampling time point in the disease course. As with other rare diseases such as the paediatric brain tumours, this necessitates multi-centre studies in order to acquire sufficient data to obtain statistically significant results. Future studies, particularly where functional imaging forms part of an interventional/therapeutic trial, will require the

acquisition of data from multiple centres. The work in this thesis highlights the importance in this context of prospectively considering the impact of acquiring data from multiple sources, and taking into account inter-scanner variability.

Key clinical problems remain unresolved, notably the issue of the large cohort of children with undiagnosed neurodegenerative disorders. This study has found that the majority of these children do not have novel metabolite peaks within their brain metabolite profile. It is possible that the use of higher field scanners will enable detection of lower concentration non-standard metabolites. An alternative approach is to apply pattern recognition methods to the standard metabolites present to classify and diagnose disorders. Multivariate analysis methods such as principal component analysis have been applied in this thesis to *in vitro* metabolite data including plasma amino acids, and urinary NMR spectral profiles. Similar methods can also be applied to the metabolite profiles derived from *in vivo* MRS, as demonstrated previously in the classification of paediatric brain tumours [260]. A multivariate approach to identifying children with mitochondrial diseases is also being explored (see Appendix D where preliminary results are presented), and the incorporation of multiple metabolite parameters may improve the diagnostic power of MRS. A similar pattern recognition approach has been demonstrated by others in the study of the leukodystrophies (inherited white matter disorders) using well defined cohorts of children with confirmed diseases [118], and that model is now being applied to the current cohort of children with undiagnosed white matter disorders.

Finally, as already noted there is a limited scope for experimental manipulation in paediatric subjects, and this combined with the issues of patient sampling limitations highlights the importance of the development of disease model systems. Importantly, the research methods

of *in vivo* metabolite profiling developed and described in this thesis can be used in the evaluation of such systems, both cell-based and animal disease models. As such the functional imaging techniques are truly translational and will continue to play an important role. Several potential hypotheses suggested in the study of propionic acidaemia and the urea cycle disorders could be further evaluated and tested in appropriate model systems; furthermore these could be adapted to provide means of screening potential novel therapies.

This thesis aimed to contribute to improved clinical outcomes for children affected by neurodegeneration in the context of inherited metabolic disorders, and the work described here provides evidence of progress made towards this end.

Appendix A

Comments on Diffusion Weighted Imaging

A brief description of diffusion weighted imaging of the brain is given here, including the underlying principles of the technique, discussion of the pathophysiological correlates of alterations in diffusion parameters, and specific examples of its use in the IMDs.

A1. Paediatric Diffusion Weighted Imaging of Brain

Diffusion weighted imaging sequences are routinely available in paediatric clinical practice [261], with a short acquisition time (typically around 1-2mins [262]) meaning they can be feasibly appended to other imaging sequences. Conventional MR imaging is based on the detection of hydrogen nuclei predominantly from water molecules, and at the simplest level contrast is seen due to the variation in water concentration (proton density) in different tissues, e.g. between gray and white matter.

A2. Principles of DWI

Diffusion weighted imaging determines how easily water is able to diffuse by Brownian motion in different tissues, and alterations in the apparent diffusion are seen in different pathologies. “Diffusivity” is a property of water, depending on temperature. Alterations in “diffusion” seen in DWI are due to other tissue and cellular factors that affect how easily water can diffuse, and is referred to as the apparent diffusion coefficient. Diffusion increases when water is able to diffuse more readily, while diffusion decreases (is restricted) when water is less able to diffuse. DWI takes account of the magnitude of diffusion. Diffusion that can occur equally in all directions in space is isotropic, while diffusion that can occur more

easily in one direction or other (e.g. along an axon) is anisotropic. Diffusion tensor imaging (DTI) takes account of this directionality of diffusion.

The DWI sequence uses diffusion-sensitising gradients added to a basic spin-echo sequence. An initial 90^{o} pulse results in proton spin coherence, i.e. all proton spins are in phase with each other. A first magnetic gradient de-phases the spins, while a second magnetic gradient after the 180^{o} inversion pulse re-phases the spins, providing spatial encoding. In the situation that no water molecules have moved with respect to the gradient direction (i.e. no diffusion at all), all the proton spins will be re-phased and high signal will be returned. When water molecules have moved (diffused) during the acquisition, they will sit at a different place with respect to the gradient and will be incompletely re-phased by the second gradient, resulting in loss of signal. Thus in DWI, lower signal reflects more diffusion.

Typically two sequences are obtained, the first b zero image without additional gradients, and the second (high b) with the diffusion-sensitising gradient. The data from these two sequences are combined to give the Apparent Diffusion Coefficient (ADC) by

Equation (A1) $$S=S_0e^{-2bADC}$$

where S is high b signal, S_0 is the b zero signal.

Two series of images are generated. On the DWI image, areas of high (bright) signal are due to reduced (restricted) diffusion (and hence less dephasing). Areas with reduced signal (dark) represent increased diffusion, thus CSF in ventricles appear dark. Conversely on an ADC

map, bright areas indicate increased diffusion values, while dark areas indicate restricted (decreased) diffusion.

DWI sequences are heavily T_2-weighted and sensitive to increased T_2 signal. The phenomenon of T_2 shine through describes a high T_2 signal lesion that will appear bright on T_2-weighted images and also bright on DWI. Increased DWI suggests decreased diffusion, but if the lesion also appears bright on ADC then diffusion is actually increased, and the brightness on DWI is caused by T_2-shine through and not decreased diffusion.

The diffusion of water molecules is unrestricted in a glass of water, but in brain water is compartmentalised and comes across barriers to diffusion. Typically intracellular water is less able to diffuse than extracellular water. Furthermore water is more able to diffuse along axons and brain tracts than perpendicular to the axon and the tracts, thus white matter has a typical "direction" to diffusion. Because axons and tracts in the brain do not all lie in the same direction, diffusion in different brain regions is not the same in all directions. DWI sequences typically therefore acquire signal using at least 3 gradients in different directions. An average DW image is then generated. This counteracts the effect of diffusion anisotropy, providing a measure of the magnitude of diffusion in that region but ignoring the directionality of the diffusion. Diffusion tensor imaging takes account of this diffusion directionality to yield further information.

A3. Diffusion Pathophysiological Correlate

In general it is accepted that intracellular water is less able to diffuse freely than extracellular water, therefore in situations of increased intracellular water diffusivity will decrease, whereas increased extracellular water will lead to a rise in the apparent diffusion [263].

Restricted diffusion is seen following an acute ischaemic insult; hypoxia-ischaemia results in energy failure and acute failure of the Na-K ATPase, resulting in acute cellular oedema, with increased intracellular water and decreased extracellular volume due to cell swelling. Diffusion is thus decreased (restricted). In the early stages after an acute ischaemic episode diffusion is restricted in affected areas, and there is robust evidence from adult ischaemic stroke that DWI will delineate affected areas in stroke earlier than conventional MRI. Decreased diffusion can also be seen in a range of other disorders, including hypercellular tumours, in areas containing viscous fluid such as pyogenic abscess, and also in Canavan disease. The "prognosis" of restricted diffusion is not straightforward, as diffusion abnormalities may normalise without tissue loss.

Increased diffusion is thought to occur when there is increased extracellular water i.e. vasogenic or interstitial oedema, which may be an acute or chronic process (e.g. development of cystic encephalomalacia). Acute episodes may be associated with loss of blood brain barrier integrity causing vasogenic oedema, or acute hydrocephalus causing interstitial oedema.

A4. Reports of DWI in Inherited Metabolic Disorders

DWI has been employed in the evaluation of foetal ischaemic infarction, acute hypoxia-ischaemia-reperfusion injury in infants/children, arterial stroke, sinovenous thrombosis, vasculitis, tumours and infections [263]. Within the inherited metabolic disorders a wide range of diffusion alterations are reported, some disorders associated with increased diffusion (ALD, Alexander, Wilson), others with restricted (MLD, Canavan) or mixed picture (PKU, MSUD, Leigh) depending on disease stage [263]. With regard to disorders considered further within this dissertation, no reports were found in the literature of diffusion imaging data for Hunter Syndrome, with one report of diffusion changes in the wider mucopolysaccharidosis group [264]. Several case descriptions of propionic acidaemia reported diffusion changes in cortex and basal ganglia in acute episodes of metabolic derangements [10, 179], and DWI and DTI have been reported in methylmalonic acidaemia [265-269]. Mitochondrial disorders have also been explored using these modalities [262, 270-301].

Appendix B

Published articles arising from the current study.

Facsimile copies of the following published articles arising from the work undertaken during the current period of study are included in the following pages.

Davison JE, Hendriksz CJ, Sun Y, Davies NP, Gissen P, Peet AC: **Quantitative in vivo brain magnetic resonance spectroscopic monitoring of neurological involvement in mucopolysaccharidosis type II (Hunter Syndrome).** *J Inherit Metab Dis* 2010, **33:**819.

Davison JE, Davies NP, Wilson M, Sun Y, Chakrapani A, McKiernan PJ, Walter JH, Gissen P, Peet AC: **MR spectroscopy-based brain metabolite profiling in propionic acidaemia: metabolic changes in the basal ganglia during acute decompensation and effect of liver transplantation.** *Orphanet J Rare Dis* 2011, **6:**19.

Davison JE, Davies NP, English MW, Philip S, Macpherson LK, Gissen P, Peet AC: **Magnetic resonance spectroscopy in the diagnostic evaluation of brainstem lesions in alexander disease.** *J Child Neurol* 2011, **26:**356-360.

Davison JE, Kearney S, Horton J, Foster K, Peet AC, Hendriksz CJ: **Intellectual and neurological functioning in Morquio syndrome (MPS IVa).** *J Inherit Metab Dis* 2012, **In press**.

J Inherit Metab Dis
DOI 10.1007/s10545-010-9197-0

RESEARCH REPORT

Quantitative in vivo brain magnetic resonance spectroscopic monitoring of neurological involvement in mucopolysaccharidosis type II (Hunter Syndrome)

James E. Davison · Christian J. Hendriksz · Yu Sun · Nigel P. Davies · Paul Gissen · Andrew C. Peet

Received: 30 June 2010 / Revised: 11 August 2010 / Accepted: 24 August 2010

Abstract Neurological involvement in X-linked mucopolysaccharidosis type II (Hunter syndrome) is indicative of more severe disease, but is not attenuated by current enzyme replacement therapy which does not significantly penetrate the blood–brain barrier. Magnetic resonance spectroscopy is an objective method of determining brain metabolites and has the potential to identify disease biomarkers with utility in evaluating current and novel therapies. MRS studies from seven patients with MPSII all receiving enzyme replacement therapy were compared with a large cohort of children with various neurocognitive disorders with normal MR imaging. All studies were completed on 1.5Tesla clinical MR scanners. Brain metabolite concentrations were determined from basal ganglia and parieto-occipital white matter using LCModel quantification. Serial trends in brain metabolites were analysed. Examination of mean spectra and quantitative metabolite concentrations demonstrated significantly decreased white matter N-acetylaspartate (a neuronal marker), total choline and glutamate, and elevated myo-inositol (glial marker) in MPSII patients. Analysis of serial determinations of white matter N-acetylaspartate demonstrated no change in two patients with stable MR imaging features but decreasing N-acetylaspartate in two patients more severely affected or deteriorating. These data demonstrate the utility of MRS to monitor serial alterations in brain metabolites including N-acetylaspartate which could be used as biomarkers of progressive neurological disease in MPSII. Integrated as an adjunct to MRI, such an approach could aid the evaluation of the efficacy of current ERT and also novel CNS-targeted therapies in MPSII.

Abbreviations

MPSII	Mucopolysaccharidosis Type II
CNS	Central nervous system
ERT	Enzyme replacement therapy
MRS	Magnetic resonance spectroscopy
tNAA	Total N-acetylaspartate
Ins	Myo-inositol
GABA	Gamma-amino-butyric acid
MRI	Magnetic resonance imaging

Communicated by: Ed Wraith

Competing interest: None declared.

J. E. Davison · C. J. Hendriksz · P. Gissen
Clinical Inherited Metabolic Disorders,
Birmingham Children's Hospital NHS Foundation Trust,
Birmingham, UK

J. E. Davison · P. Gissen
Clinical & Experimental Medicine, College of Medical & Dental Sciences, University of Birmingham,
Birmingham, UK

Y. Sun · N. P. Davies · A. C. Peet
Cancer Sciences, College of Medical & Dental Sciences,
University of Birmingham,
Birmingham, UK

Y. Sun · N. P. Davies · A. C. Peet
Birmingham Children's Hospital NHS Foundation Trust,
Birmingham, UK

J. E. Davison (✉)
Institute of Child Health,
Birmingham Children's Hospital NHS Foundation Trust,
Birmingham B4 6NH, UK
e-mail: j.e.davison@bham.ac.uk

Published online: 01 October 2010

ORPHANET JOURNAL OF RARE DISEASES

RESEARCH Open Access

MR spectroscopy-based brain metabolite profiling in propionic acidaemia: metabolic changes in the basal ganglia during acute decompensation and effect of liver transplantation

James E Davison[1,2*], Nigel P Davies[1], Martin Wilson[2], Yu Sun[2], Anupam Chakrapani[1], Patrick J McKiernan[1], John H Walter[3], P Gissen[1,2†] and Andrew C Peet[1,2†]

Abstract

Background: Propionic acidaemia (PA) results from deficiency of Propionyl CoA carboxylase, the commonest form presenting in the neonatal period. Despite best current management, PA is associated with severe neurological sequelae, in particular movement disorders resulting from basal ganglia infarction, although the pathogenesis remains poorly understood. The role of liver transplantation remains controversial but may confer some neuro-protection. The present study utilises quantitative magnetic resonance spectroscopy (MRS) to investigate brain metabolite alterations in propionic acidaemia during metabolic stability and acute encephalopathic episodes.

Methods: Quantitative MRS was used to evaluate brain metabolites in eight children with neonatal onset propionic acidaemia, with six elective studies acquired during metabolic stability and five studies during acute encephalopathic episodes. MRS studies were acquired concurrently with clinically indicated MR imaging studies at 1.5 Tesla. LCModel software was used to provide metabolite quantification. Comparison was made with a dataset of MRS metabolite concentrations from a cohort of children with normal appearing MR imaging.

Results: MRI findings confirm the vulnerability of basal ganglia to infarction during acute encephalopathy. We identified statistically significant decreases in basal ganglia glutamate+glutamine and N-Acetylaspartate, and increase in lactate, during encephalopathic episodes. In white matter lactate was significantly elevated but other metabolites not significantly altered. Metabolite data from two children who had received liver transplantation were not significantly different from the comparator group.

Conclusions: The metabolite alterations seen in propionic acidaemia in the basal ganglia during acute encephalopathy reflect loss of viable neurons, and a switch to anaerobic respiration. The decrease in glutamine + glutamate supports the hypothesis that they are consumed to replenish a compromised Krebs cycle and that this is a marker of compromised aerobic respiration within brain tissue. Thus there is a need for improved brain protective strategies during acute metabolic decompensations. MRS provides a non-invasive tool for which could be employed to evaluate novel treatments aimed at restoring basal ganglia homeostasis. The results from the liver transplantation sub-group supports the hypothesis that liver transplantation provides systemic metabolic stability by providing a hepatic pool of functional propionyl CoA carboxylase, thus preventing further acute decompensations which are associated with the risk of brain infarction.

* Correspondence: j.e.davison@bham.ac.uk
† Contributed equally
[1]Birmingham Children's Hospital NHS Foundation Trust, Birmingham UK
Full list of author information is available at the end of the article

Background

Propionic acidaemia (PA, OMIM #606054) results from deficiency of the biotin-dependent mitochondrial enzyme propionyl CoA carboxylase. The commonest and most severe form of PA presents in the neonatal period with acute metabolic acidosis, hyperammonaemia and progressive encephalopathy. Despite optimal management, later neurologic sequelae are a major cause of morbidity, and include neurodevelopmental delay, episodic acute encephalopathy, and movement disorders due to a propensity to basal ganglia infarction [1]. The mainstays of current treatment are dietary protein restriction, carnitine supplementation, and aggressive management of acute metabolic derangements. Some centres utilise alternative pathway drugs including sodium benzoate to minimise the consequences of hyperammonaemia. Orthotopic liver transplantation may prevent neurocognitive decline [2] but its role remains controversial.

The pathogenesis of the neurological insult remains poorly understood. Neurological damage may occur secondary to hyperammonaemia; alternatively inhibition of the mitochondrial Krebs cycle and electron transfer chain by accumulating metabolites may lead to a "bioenergetic stroke" [3]. Based on alterations in plasma amino acids associated with hyperammonaemia it has been hypothesised that the use of dietary supplements including glutamine that can replenish the Krebs cycle (anaplerotic therapy) may support aerobic cellular energy metabolism and hence improve clinical outcome [4]. Conflicting changes in cerebrospinal fluid glutamine concentrations have been reported in PA [5,6].

Magnetic resonance spectroscopy (MRS) is a non-invasive technique capable of probing *in vivo* changes in regional metabolites within the brain, and could be specifically employed to monitor directly alterations in brain energy metabolites including glutamine, glutamate and lactate. Previous MRS reports have demonstrated elevated glutamine+glutamate (Glx) in the basal ganglia of metabolically stable PA patients [6], while lactate has been detected in periventricular white matter [7].

The present study utilises quantitative MRS to investigate brain metabolite alterations both during metabolic stability and acute encephalopathic episodes, confirming the basal ganglia as a particular target and demonstrating novel insights in to alterations in neurotransmitter metabolites in particular glutamine and glutamate.

Methods

Patients

Eight children (two female) with propionic acidaemia were studied (median age (range) at first MRS, 36 (7-190) months) (see table 1). Research Ethics Committee approval and informed consent were obtained. All were diagnosed in the neonatal period, four requiring neonatal haemofiltration due to severe hyperammonaemia and metabolic acidosis. Two children had received elective orthotopic liver transplantation during early childhood. The remaining six children all received regular oral carnitine and sodium benzoate, and three received sodium phenylbutyrate, in addition to dietary protein control under management of a specialist dietetic team.

Three children had one or more severe acute episodes with encephalopathy beyond the neonatal period requiring intensive care support ("severe acute episode" hereafter). During these episodes all children required ventilatory support and continuous veno-venous haemofiltration (CVVH), and only one episode was associated with significant persistent hyperammonaemia. During these episodes three children received intravenous sodium benzoate and two received sodium phenylbutyrate.

Magnetic Resonance Spectroscopy

MRS studies were performed concurrently with clinically indicated MRI scans at 1.5 Tesla (Siemens Symphony Magnetom, NUM4 or GE Signa Excite & HDx) facilitated by general anaesthesia as needed. Five studies from three children were acquired during severe acute episodes requiring intensive care support. Six studies from six children were acquired with elective outpatient MRI studies undertaken during metabolic stability and before any severe acute episode had occurred.

MRS was acquired using point resolved spectroscopy (PRESS) technique (echo time 30 ms and 135 ms, repetition time 1500 ms, 128 repetitions) with 2 cm-sided voxels located in the left basal ganglia and right parieto-occipital white matter. Voxels were placed in standard positions guided by T1 and T2 weighted image sequences in coronal, sagittal and axial planes. Spectra were quality-assessed to ensure appropriate voxel localisation, shimming and water suppression. Raw data were processed using LCModel [8] to generate quantitative metabolite concentrations scaled to the water signal.

Comparison was made with MRS metabolite data from a cohort of children with normal appearing MRI and similar age profile who had undergone MRI/MRS for investigation of various suspected neurodegenerative and neurocognitive conditions (white matter, n = 53, median (range) age 4.7(0.5-16.7) years; basal ganglia n = 63, 4.1(0.5-16.7) years).

Statistical Analysis

Mean spectra were generated for each cohort for basal ganglia and white matter from LCModel fitted spectra after baseline subtraction. Spectra were compared by qualitative visual inspection.

Table 1 Clinical features of propionic acidaemia cohort and MR Imaging findings

	Neonatal CVVH?	Liver Transplant (age, years)	Other diagnoses	Age at MRS (years)	Status at time of MRS	Metabolic Drugs & Dietary Restrictions		Acute encephalopathic episodes: complications	MRI findings	
						Maintenance	Acute		Basal ganglia	Other features
1	Yes			1.5	Stable	LC, SB, PR			Normal	
2	Yes		Hypo-throidism	1	Enceph.	SP, SB, LC, T, M, PR	SP, SB, NC	Sepsis & hyper-ammonaemia,	Acutely swelling caudate, dentate	
				1.2	Stable	SB, LC, T, PR			Resolving swelling	Delayed myelination, enlarged ventricles
				3	Enceph.	SB, LC, T, PR		Cardiomyopathy, pneumonia	Acute swelling caudate, putamen, dentate	Delayed myelination, enlarged ventricles, hippocampal atrophy
3	No		Epilepsy	9.5	Enceph.	SB, LC, PR	SB LC	Rhabdomyolysis	Cystic encephalomalacia	Enlarged ventricles/cerebral volume loss
4	Yes		Hypo-thyroidism	4	Stable	SB, SP, LC, PR			Normal	
				6	Enceph.	SB, SP, LC, PR	SP, SB, LC	Pneumonia	Acute swelling caudate + putamen	Cerebral volume loss, small hippocampi
5	Yes			0.6	Stable	SB, LC, PR			Normal	Mild ventricular dilation
6	No			3	Stable	SB, SP, LC, PR			Normal	Hippocampal sclerosis
7	No	Yes (1.3)		15	Stable	Anti-rejection			Normal	
8	No	Yes (2.5)	Myoclonic epilepsy	13	Stable	Anti-rejection LC			Normal	Mild ventricular enlargement. Unilateral mesial temporal sclerosis

MRS, magnetic resonance spectroscopy; CVVH, Continuous veno-venous haemofiltration; LC, L-carnitine; SP, Sodium Phenylbutyrate; SB, Sodium Benzoate; M, metronidazole; T, thyroxine; NC, N-Carbamylglutamate; PR, dietary protein restriction; Enceph., denotes acute encephalopathic episode

Metabolite concentrations for each region were compared between groups by Mann Whitney nonparametric U test (SPSS Statistics 17.0), with the p-value determined by the exact 2-tailed significance, with significance level set at $p < 0.05$.

Results

Magnetic Resonance Imaging

The basal ganglia appeared normal in all children (n = 6) prior to any severe acute episode beyond the neonatal period. MRI obtained during severe acute episodes demonstrated abnormal signal in the basal ganglia variably including the caudate heads, putamen and globus pallidi and in some cases there was also evidence of acute changes in the dentate nuclei and cerebral cortex. One child demonstrated evidence of previous basal ganglia infarction relating to a previous acute encephalopathic episode, with cystic degeneration of caudate, putamen and globus pallidus. Interestingly the hippocampi appeared atrophic in seven cases. Cerebral volume loss was most marked in children with preceding severe acute episodes. The two children who had liver transplantation had normal appearing basal ganglia, cortex and white matter on MRI undertaken more than 10 years post-transplant, with one showing probable temporal mesial sclerosis.

Magnetic Resonance Spectroscopy

Analysis of mean spectra (figure 1) and mean metabolite concentrations (table 2) demonstrate metabolite alterations in basal ganglia and parieto-occipital white matter, in particular during severe acute episodes.

MRS studies undertaken during metabolic stability before any severe acute episodes beyond the neonatal period demonstrated decreased Glx in basal ganglia compared to the normal MRI comparator group but a trend to increase in white matter. Glutamine alone was significantly decreased in basal ganglia during metabolic stability. Mean lactate was not elevated, although two cases had reliably detected lactate in basal ganglia. There was no significant decrease in the total N-acetylaspartate and N-acetylaspartylglutamate (tNAA) in this group.

MRS studies acquired during severe acute episodes demonstrated significantly decreased tNAA, Glx and creatine, and significantly elevated lactate, in the basal ganglia compared to both the normal MRI comparator group and to the metabolically stable propionic acidaemia cohort. In white matter lactate was significantly elevated but other metabolites were not significantly altered. (Data shown are for all severe acute episodes; analysis of first severe acute episode only demonstrated similar findings). There were no significant differences between groups in brain *myo*-inositol, and no propionic acid was detected in the propionic acidaemia cohort.

Separate analysis of brain metabolites from the two children post-liver transplant demonstrated normal basal ganglia tNAA and slightly decreased Glx. tNAA was elevated in white matter and total choline decreased.

Discussion

The data presented represent the largest series of children with the severe neonatal form of propionic acidaemia to be investigated with MRS, and is to our

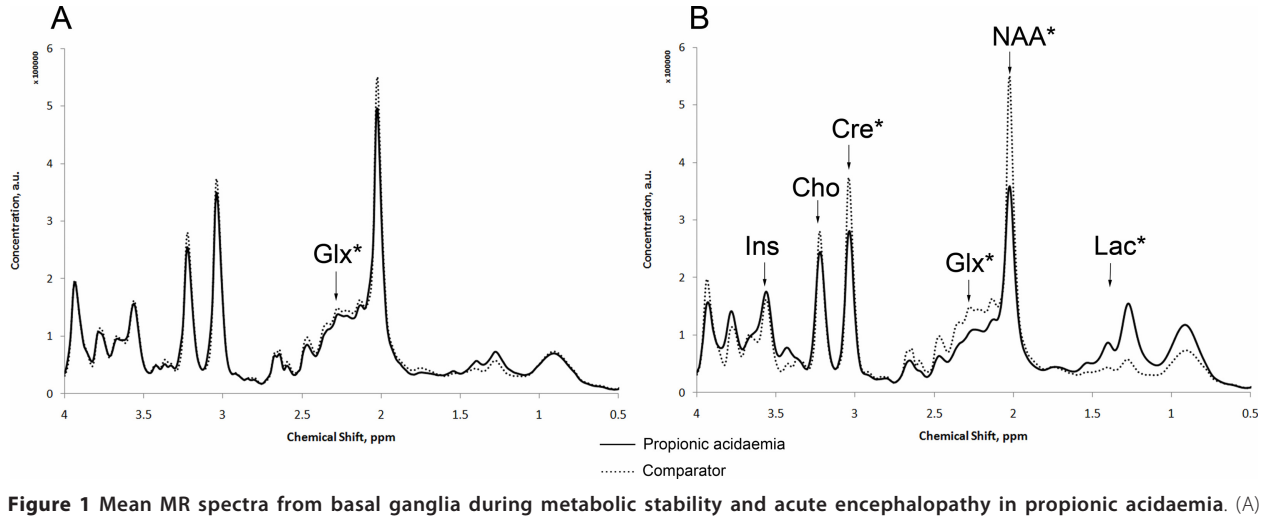

Figure 1 Mean MR spectra from basal ganglia during metabolic stability and acute encephalopathy in propionic acidaemia. (A) Metabolically stable and (B) acutely encephalopathic propionic acidaemia patients compared to normal imaging comparator cohort. ppm, parts per million; a.u., arbitrary units. Major metabolite peaks identified (labelled arrows), significant differences indicated by *. Glx, glutamine + glutamate; Ins, myo-inositol; Cre, Creatine; NAA, N-acetylaspartate; Lac, lactic acid.

Table 2 Metabolite concentrations in basal ganglia and parieto-occipital white matter

Basal ganglia metabolites (mM, mean (standard deviation))				
	Propionic Acidaemia			**Normal MRI comparator group**
	Metabolic stability (6 studies from 6 patients)	Acute encephalopathy (5 studies from 3 patients)	Post-liver transplant (2 studies from 2 patients)	(63 studies)
Median age (years, (range))	3.6 (0.6-15.9)	6.13 (1.0-9.4)	14.4 (12.9-15.9)	4.1 (0.5-16.7)
N-Acetylaspartate	5.03 (0.53)	3.89 (0.20)†#	5.35 (0.28)	5.21 (0.51)
Creatine	4.57 (0.47)	3.71 (0.58)† $	4.42 (0.14)	4.55 (0.59)
Glutamine	1.29 (0.30) *	1.00 (1.00)*	1.27 (0.25)	1.98 (0.79)
Glutamate	4.28 (0.25)	3.07 (0.60)†#	4.30 (0.39)	4.45 (0.78)
Glutamine +Glutamate	5.57 (0.41) *	4.07 (1.19)† $	5.57 (0.28)	6.43 (1.39)
myo-Inositol	2.58 (0.26)	2.79 (0.90)	2.39 (0.0)	2.49 (0.43)
Lactate	0.21 (0.25)	0.93 (0.34)†#	0.00 (0.32)	0.11 (0.20)
Choline	1.10 (0.18)	1.16 (0.29)	0.90 (0.63)	1.11 (0.18)
White matter metabolites (mM, mean (standard deviation))				
	Propionic Acidaemia			**Normal MRI comparator group**
	Metabolic stability (5 studies from 5 patients)	Acute encephalopathy (4 studies from 3 patients)	Post-liver transplant (2 studies from 2 patients)	(53 studies)
Median age (years, (range))	3.1 (0.6-15.9)	7.74 (3.0 -9.4)	14.4 (12.9-15.9)	4.7 (0.5-16.7)
N-Acetylaspartate	5.28 (0.80)	4.50 (0.47)	6.11 (0.39)	5.11 (0.73)
Creatine	3.55 (0.19) *	3.33 (0.53)	3.70 (0.00)	3.18 (0.47)
Glutamine	1.43 (0.54)	1.34 (1.30)	1.62 (0.49)	1.32 (0.62)
Glutamate	3.83 (0.45)	2.65 (0.44)*$	4.27 (0.31)	3.51 (0.78)
Glutamine +Glutamate	5.26 (0.89)	3.98 (1.54)	5.89 (0.80)	4.84 (1.18)
myo-Inositol	2.73 (0.31)	2.57 (0.39)	2.79 (0.02)	2.57 (0.39)
Lactate	0.40 (0.30)	0.81 (0.74)*	0.32 (0.45)	0.21 (0.28)
Choline	0.93 (0.15)*	1.12 (0.37)	0.83 (0.09)	1.08 (0.15)

Comparison between propionic acidaemia cohorts and normal MRI comparator group.

Mann Whitney U test (2 tailed exact significance) for difference in metabolite concentrations between Normal MRI Comparator group and propionic acidaemia cohorts,*$p < 0.05$, † $p < 0.01$. Mann Whitney U test (2 tailed exact significance) for difference in metabolite concentrations between stable and encephalopathic propionic acidaemia cohort, $ $p < 0.05$, # $p < 0.01$

knowledge the first to study children during severe acute encephalopathic episodes. The selective vulnerability of the basal ganglia in PA is well established, and our data provide further insight in to processes occurring within the basal ganglia. MRI results found that basal ganglia appeared normal in children who had not had a severe acute encephalopathic episode beyond the neonatal period, as similarly reported in glutaric aciduria [9], but were acutely damaged during episodes of acute illness. Similarly brain metabolite alterations were more marked during severe acute episodes.

Decreased tNAA is seen in many pathologies, and is thought to reflect loss of viable neurons [10] including following acute ischemic stroke [11]. Elevated lactate suggests a switch to anaerobic respiration, reflecting local ischaemia or mitochondrial dysfunction. As previously reported, elevated lactate was seen in two of the cases during metabolic stability, suggesting that brain tissue metabolism is not normal even when metabolism is well controlled.

The alterations seen in glutamine and glutamate in basal ganglia are of particular note. Glx was significantly decreased during severe acute episodes, with a smaller (non-significant) decrease noted in basal ganglia in studies acquired during metabolic stability. The ratio of Glx/tNAA was lower in the propionic acidaemia cohort than in cohorts of children with other defined inherited metabolic disorders including a cohort with confirmed respiratory chain disorders, while the Glx/NAA ratio was elevated in a cohort with the urea cycle disorder argininosuccinic aciduria (JED, unpublished data). This suggests that the alterations seen in Glx here were not simply a reflection of neuronal loss represented by lower tNAA.

Although the spectral signals from glutamine and glutamate overlap, there is increasing evidence that they can be differentiated in the analysis of cohorts even at 1.5Tesla using software such as LCModel. Such evidence includes Montecarlo simulations of normal brain spectra fitted with LCModel [12], comparisons of experimental and simulated basis sets [13], and the finding of a significant correlation between in vivo and in vitro results for both glutamate and glutamine detected in brain tumours [14,15].

A previous MRS study reported elevated basal ganglia Glx in three metabolically stable propionic acidaemia patients who had normal ammonia and near-normal glutamine and glutamate in plasma and cerebrospinal fluid leading the authors to suggest differential mechanisms regulating brain parenchymal metabolism [6]. However this study relied on peak area estimation and ratio to creatine, whereas the current study provides more robust quantification. Moreover the reduced glutamine detected by brain MRS is consistent with the plasma glutamine reduction previously reported in PA [16], also seen in plasma glutamine levels in our cohort (data not shown).

The administration of the alternative pathway drugs used to control hyperammonaemia depletes plasma glutamine and glycine and may contribute to the decreased brain Glx seen. Furthermore, all children were haemofiltered during severe acute episodes which may further deplete glutamine due to its high sieving coefficient [17]. However CVVH was instigated after the MRI/MRS in 80% of cases suggesting that glutamine levels were already low before CVVH was commenced.

The acute decrease seen in Glx supports the hypothesis that they are consumed to replenish a depleted Krebs cycle [4], and that this decrease is a marker of compromised aerobic cellular respiration within brain tissue. It remains to be determined whether the decreased Glx is directly detrimental or simply a secondary marker of compromised metabolic status. Interestingly the decrease in Glx was greater in the basal ganglia than in white matter, correlating with the more vulnerable brain region.

There is a need for brain protective strategies during acute metabolic decompensations, with potential methods including brain cooling, adequate energy provision, and anaplerotic therapies. MRS could provide a tool to monitor the effect of dietary supplements aimed at increasing glutamine levels, specifically monitoring metabolite levels within the target-organ of interest, namely the brain.

The two children who had liver transplant have had no severe acute encephalopathic episodes beyond the neonatal period, and have normal appearing basal ganglia on MRI. MRS demonstrated normal/high tNAA reflecting the absence of major neuronal loss and correlating with their good neurocognitive status, and no reliably detected lactate. The small numbers preclude statistical significance, but Glx was slightly increased in white matter but decreased in basal ganglia compared to the comparator group. These results support the hypothesis that liver transplantation provides systemic metabolic stability by providing a hepatic pool of functional propionyl CoA carboxylase, thus preventing further acute metabolic decompensations which are associated with the risk of brain infarction.

The data presented here have yielded some interesting observations, however further prospective data collection and analysis could overcome some of the specific limitations of the present work. In particular, use of higher field strength MRI scanners (3Tesla and above) would provide more robust differentiation of the metabolites of interest, notably glutamine and glutamate. Serial data collection in specific patients could also confirm the alterations in brain metabolites seen before, during and after metabolic decompensations. Finally analysis of a larger cohort of post-liver transplant patients as well as longer follow up with serial studies will provide stronger evidence for the therapeutic value of liver transplantation in PA.

Conclusions

We have demonstrated that quantitative MRS is able to offer insight in to *in vivo* brain metabolic derangements, and can feasibly be employed in children with acute encephalopathy. In propionic acidaemia the use of MRS in conjunction with MRI has confirmed the basal ganglia as a particularly vulnerable target and has demonstrated novel insights in to alterations in neurotransmitter metabolites. Evaluation of patients in long-term follow up after liver transplantation demonstrates the potential for good neurological outcome and near-normal brain metabolism. MRS provides a tool to directly evaluate the tissue-level effects of novel treatment strategies including anaplerotic therapies.

Acknowledgements

The authors are grateful to the radiologists who reported the MRI scans in particular Dr LKR MacPherson and Dr K Foster, and to the radiographic staff for assistance with data collection.

JED funded by Research Fellowships from Birmingham Children's Hospital Research Foundation and from Sparks: The Children's Medical Research Charity.

A.C.P. group funded in part by Cancer Research UK, EPSRC, MRC, NIHR Cancer Imaging Programme Grant.

N.P.D. funded by CSO/NIHR Healthcare Scientist Fellowship

P.G. is a GSK Clinician Scientist Fellow

Author details

[1]Birmingham Children's Hospital NHS Foundation Trust, Birmingham UK. [2]University of Birmingham, Edgbaston UK. [3]Willink Biochemical Genetics Unit, Manchester UK.

Authors' contributions

JED carried out data analysis and collated clinical data and drafted the manuscript.
NPD, MW, YS assisted with data processing including software development.
AC, PJM and JHW provided clinical management for subjects, assisted with patient recruitment and critically appraised the manuscript.
PG and ACP conceived of the study and participated in its design.
All authors read and approved the final manuscript.

Competing interests

The authors declare that they have no competing interests.

Received: 8 December 2010 Accepted: 9 May 2011
Published: 9 May 2011

References

1. Johnson JA, Le KL, Palacios E: **Propionic acidemia: case report and review of neurologic sequelae.** *Pediatr Neurol* 2009, **40**:317-320.
2. Barshes NR, Vanatta JM, Patel AJ, Carter BA, O'Mahony CA, Karpen SJ, Goss JA: **Evaluation and management of patients with propionic acidemia undergoing liver transplantation: a comprehensive review.** *Pediatr Transplant* 2006, **10**:773-781.
3. Schwab MA, Sauer SW, Okun JG, Nijtmans LG, Rodenburg RJ, van den Heuvel LP, Drose S, Brandt U, Hoffmann GF, Ter Laak H, *et al*: **Secondary mitochondrial dysfunction in propionic aciduria: a pathogenic role for endogenous mitochondrial toxins.** *Biochem J* 2006, **398**:107-112.
4. Filipowicz HR, Ernst SL, Ashurst CL, Pasquali M, Longo N: **Metabolic changes associated with hyperammonemia in patients with propionic acidemia.** *Molecular Genetics and Metabolism* 2006, **88**:123-130.
5. Ierardi-Curto L, Kaplan P, Saitta S, Mazur A, Berry GT: **The glutamine paradox in a neonate with propionic acidaemia and severe hyperammonaemia.** *J Inherit Metab Dis* 2000, **23**:85-86.
6. Bergman AJ, Van der Knaap MS, Smeitink JA, Duran M, Dorland L, Valk J, Poll-The BT: **Magnetic resonance imaging and spectroscopy of the brain in propionic acidemia: clinical and biochemical considerations.** *Pediatr Res* 1996, **40**:404-409.
7. Chemelli AP, Schocke M, Sperl W, Trieb T, Aichner F, Felber S: **Magnetic resonance spectroscopy (MRS) in five patients with treated propionic acidemia.** *J Magn Reson Imaging* 2000, **11**:596-600.
8. Provencher SW: **Estimation of metabolite concentrations from localized in vivo proton NMR spectra.** *Magn Reson Med* 1993, **30**:672-679.
9. Sauer SW: **Biochemistry and bioenergetics of glutaryl-CoA dehydrogenase deficiency.** *J Inherit Metab Dis* 2007, **30**:673-680.
10. Griffin JL, Bollard M, Nicholson JK, Bhakoo K, Griffin JL, Bollard M, Nicholson JK, Bhakoo K: **Spectral profiles of cultured neuronal and glial cells derived from HRMAS (1)H NMR spectroscopy.** *NMR in Biomedicine* 2002, **15**:375-384.
11. van der Zijden JP, van Eijsden P, de Graaf RA, Dijkhuizen RM, van der Zijden JP, van Eijsden P, de Graaf RA, Dijkhuizen RM: **1H/13C MR spectroscopic imaging of regionally specific metabolic alterations after experimental stroke.** *Brain* 2008, **131**:2209-2219.
12. Wilson M, Reynolds G, Kauppinen RA, Arvanitis TN, Peet AC: **A constrained least-squares approach to the automated quantitation of in vivo (1)H magnetic resonance spectroscopy data.** *Magn Reson Med* 2011, **65**:1-12.
13. Wilson M, Davies NP, Sun Y, Natarajan K, Arvanitis TN, Kauppinen RA, Peet AC: **A comparison between simulated and experimental basis sets for assessing short-TE in vivo (1)H MRS data at 1.5 T.** *NMR Biomed* 2010, **23**:1117-1126.
14. Davies NP, Wilson M, Harris LM, Natarajan K, Lateef S, Macpherson L, Sgouros S, Grundy RG, Arvanitis TN, Peet AC: **Identification and characterisation of childhood cerebellar tumours by in vivo proton MRS.** *NMR Biomed* 2008, **21**:908-918.
15. Wilson M, Davies NP, Grundy RG, Peet AC: **A quantitative comparison of metabolite signals as detected by in vivo MRS with ex vivo 1H HR-MAS for childhood brain tumours.** *NMR Biomed* 2009, **22**:213-219.
16. Scholl-Burgi S, Sass JO, Heinz-Erian P, Amann E, Haberlandt E, Albrecht U, Ertl C, Sigl SB, Lagler F, Rostasy K, Karall D: **Changes in plasma amino acid concentrations with increasing age in patients with propionic acidemia.** *Amino Acids* 2009.
17. Maxvold NJ, Smoyer WE, Custer JR, Bunchman TE: **Amino acid loss and nitrogen balance in critically ill children with acute renal failure: a prospective comparison between classic hemofiltration and hemofiltration with dialysis.** *Crit Care Med* 2000, **28**:1161-1165.

doi:10.1186/1750-1172-6-19
Cite this article as: Davison *et al.*: MR spectroscopy-based brain metabolite profiling in propionic acidaemia: metabolic changes in the basal ganglia during acute decompensation and effect of liver transplantation. *Orphanet Journal of Rare Diseases* 2011 **6**:19.

Journal of Child Neurology
000(00) 1-5

DOI: 10.1177/0883073810381279
http://jcn.sagepub.com
SAGE

Magnetic Resonance Spectroscopy in the Diagnostic Evaluation of Brainstem Lesions in Alexander Disease

James E. Davison, MRCPCH[1,2], Nigel P. Davies, PhD[1,3], Martin W. English, MD[1], Sunny Philip, MD[1], Lesley K.R. MacPherson, FRCR[1], Paul Gissen, PhD[1,2], and Andrew C. Peet, PhD[1,4]

Abstract

Alexander disease is a progressive neurodegenerative disease, which can present with brainstem lesions with imaging characteristics similar to multifocal low-grade glioma, thus presenting a diagnostic dilemma. The authors report a 6-year-old child presenting with multifocal brainstem lesions subsequently diagnosed to have Alexander disease. In vivo magnetic resonance spectroscopy generated a metabolite profile of the lesion allowing differentiation from low-grade glioma. Magnetic resonance spectroscopy is a powerful tool in the assessment of brainstem lesions and is a useful adjunct to conventional magnetic resonance imaging in the assessment and diagnosis of atypical brain lesions.

Keywords

brain tumors, radiology, gliomas, brainstem, Alexander disease, magnetic resonance spectroscopy

Received June 18, 2010. Received revised July 14, 2010. Accepted for publication July 14, 2010.

J Inherit Metab Dis
DOI 10.1007/s10545-011-9430-5

[Not available in the digital version of this thesis]

ORIGINAL ARTICLE

Intellectual and neurological functioning in Morquio syndrome (MPS IVa)

J. E. Davison · S. Kearney · J. Horton · K. Foster · A. C. Peet · C. J. Hendriksz

Received: 11 July 2011 / Revised: 18 November 2011 / Accepted: 22 November 2011

Abstract Mucopolysaccharidosis type IVa (MPS IVa, Morquio syndrome OMIM #253000) is a lysosomal storage disease caused by deficiency in N-acetylgalactosamine-6-sulfatase (GALNS, EC 3.1.6.4; encoded by *GALNS* gene at 16q24.3). Unlike other MPS disorders involving excessive heparan and dermatan sulfate, Morquio syndrome has not been associated with neurological involvement nor with intellectual impairment as this disorder of keratan sulfate has been described as a purely visceral and skeletal disorder. Neurocognitive assessment was undertaken of MPS IVa patients with age appropriate intellectual tests as well as a Child Behaviour Checklist as part of clinical follow up. Available neuroimaging studies (MRI and MR spectroscopy) were reviewed. Whilst more than half of the overall IQ scores fell in the average range, scores for 3/8 children fell below average. A number of behavioural problems were highlighted, including anxiety/depression, attention and somatic complaints. Subtle neuroimaging abnormalities were demonstrated in over half of the children. These findings present a challenge to existing assumptions about the nature of Morquio A syndrome. A hypothesis regarding the potential role of calcium signalling is explored.

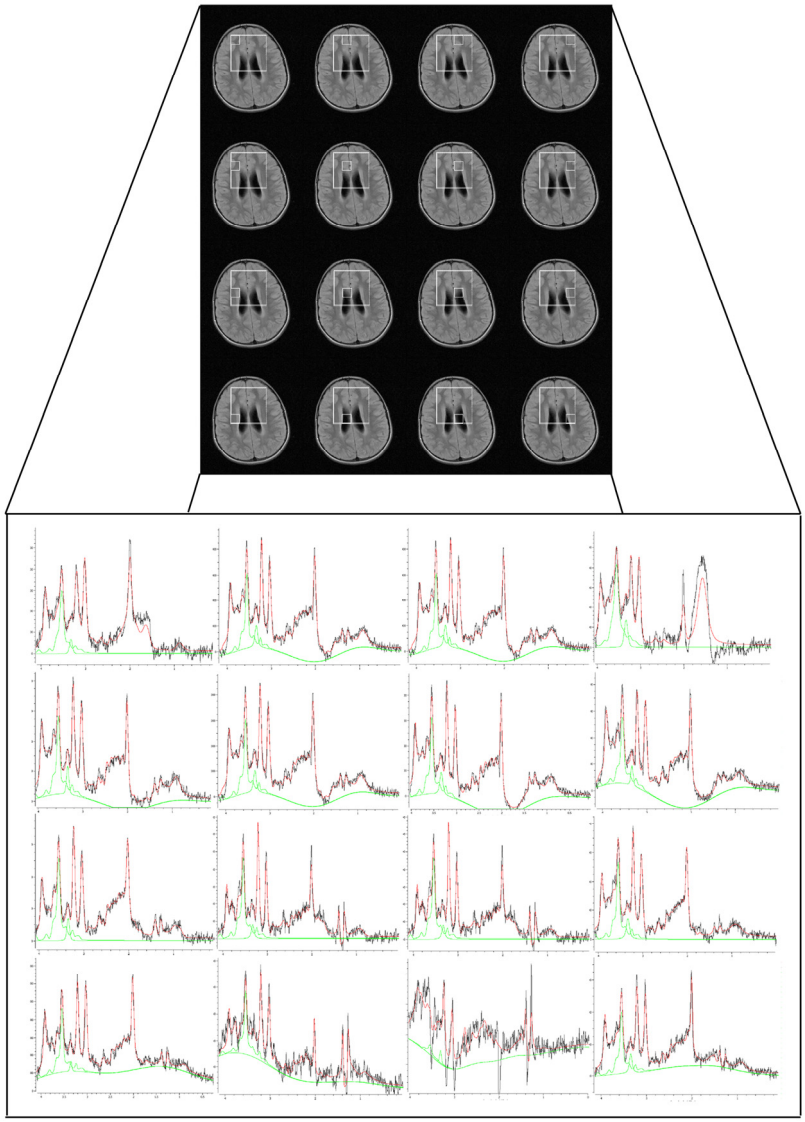

Figure C.1: Magnetic resonance spectroscopic imaging of frontal white matter in child with Alexander disease. Note high inositol and visible scyllo inositol peaks. High lactate detected from voxels overlying ventricles.

Appendix D

Towards Multivariate Analysis of Brain Metabolite Profiles

D1. Introduction

One of the common clinical indications for performing MR spectroscopy in children is in the investigation of possible mitochondrial disease, since it is thought that elevated brain lactate may be a useful marker of mitochondrial disease. As documented in this thesis (section 4.3.7.1) the sensitivity of lactate as a stand alone test is, however, low with only 27-30% of mitochondrial disease cases identified in the current cohort. One possible approach to improving the diagnostic power of MRS is to incorporate information from the other metabolites detected in a multivariate analysis. In this Appendix, initial preliminary work towards developing a multivariate analysis tool for identifying mitochondrial disease cases is described.

D2. Methods

MRS derived brain metabolite profiles from 15 studies acquired using the standard protocol from children with confirmed mitochondrial disease were compared to profiles from 186 other children with either other known IMD or unknown diagnosis. All studies included passed the quality assessment, and all had short echo time (TE 30ms) MRS data available from both basal ganglia and white matter voxels.

Differences in individual metabolites between the mitochondrial and comparison cohorts were analysed first on a univariate basis using Student's t-test and by calculation of the area under the curve (AUC) of the receiver operator characteristic (ROC) curves. A multivariate model

was then constructed using SPSS Statistics (v17.0). This first employed an unsupervised principal component analysis (PCA) to reduce the dimensionality of the metabolite dataset, incorporating metabolite concentrations from both basal ganglia and white matter voxels including lactate, creatine, tNAA, tCho, glutamine+glutamate, inositol and the composite lipid/macromolecular signals at 0.9, 1.3 and 2.0ppm. A supervised linear discriminant analysis (LDA) was then employed to construct a binary diagnostic model, taking the first 14 principal components from the PCA as its input (since the smallest group size was n=15, and to avoid "over-fitting" n-1 variables can be put in to a linear discriminant analysis). The LDA is supervised in that information about which category each case falls into is entered as the model is constructed.

An automated cross-validation of the multivariate model was then performed whereby each case was classified by the functions derived from all cases other than that case. Model loadings plots were generated by the matrix multiplication of the PCA and LDA coefficients. The linear discriminant score for each case was used to construct a ROC curve for the test. Significance of difference between the ROC curve for lactate and for the multivariate model was tested using a non-parametric test for the difference of AUC that accounts for the correlation of the ROC curves [303].

D3. Results

D3.1 Univariate analysis

Mean basal ganglia tNAA and white matter lactate were the only metabolites significantly different between the mitochondrial and comparison cohorts evaluated by Student's t-test. Assessed by ROC curve AUC, only lactate in basal ganglia or white matter generated an AUC

significantly different from 0.5. (AUC of 0.5 indicates a test is equivalent to "flipping a coin" in determining case classification).

D3.2 Multivariate model analysis

The multivariate model generated correctly classified 80.1% of all cases (76.6% in cross-validation); the ROC curve AUC of the multivariate LDA score was 0.84, significantly higher ($p<0.05$) than either basal ganglia or white matter lactate alone.

36 false positive classifications were made, of which 20 had a known diagnosis of another IMD, 4 were being evaluated as potential mitochondrial diseases, and 16 had an unknown/unclassified diagnosis. Four false negative classifications were made.

Loadings plots for the model showed that the greatest contributions to mitochondrial class were from high basal ganglia lactate and macromolecular-lipid signal (2.0ppm), and low inositol and macromolecular-lipid signal (1.4ppm) in both basal ganglia and white matter.

Metabolite concentration (mean (SD), mmol/l).										
	Basal ganglia					White matter				
			t-test	ROC				t-test	ROC	
	Mito.	Comp.	p^1	AUC	p^2	Mito.	Comp.	p^1	AUC	p^2
n	15	186				15	186			
Age (yr)	4.40 (4.64)	5.42 (4.50)	ns			4.40 (4.64)	5.42 (4.50)	ns		
Cr	4.17 (0.89)	4.50 (0.71)	ns	0.62	ns	2.98 (0.64)	3.08 (0.54)	ns	0.55	ns
tNAA	4.26 (1.17)	4.81 (0.81)	<0.05	0.65	ns	4.13 (1.39)	4.42 (1.12)	ns	0.54	ns
tCho	1.11 (0.29)	1.12 (0.23)	ns	0.53	ns	1.06 (0.29)	1.04 (0.21)	ns	0.53	ns
Gln+Glu	5.87 (1.68)	6.26 (1.63)	ns	0.57	ns	4.17 (1.61)	4.86 (1.54)	ns	0.61	ns
Ins	2.60 (0.77)	2.75 (0.83)	ns	0.55	ns	2.59 (0.66)	2.85 (0.84)	ns	0.58	ns
Lac	0.42 (0.57)	0.24 (0.48)	ns	0.65	<0.05	0.68 (0.67)	0.33 (0.46)	<0.01	0.69	<0.05

Table D1: Mean metabolite concentrations in mitochondrial (Mito.) and mixed comparison (Comp.) cohorts. ROC, receiver operator characteristic curve; AUC, area under the curve. p^1, t-test for difference between mitochondrial and comparison cohorts. p^2 significance of difference of AUC from 0.5.

		Predicted Group Membership	
		Comp	Mito
Original group membership	Comp	150	36
	Mito	4	11
Cross-validation	Comp	148	38
	Mito	9	6

Table D2: Multivariate model classification outcome

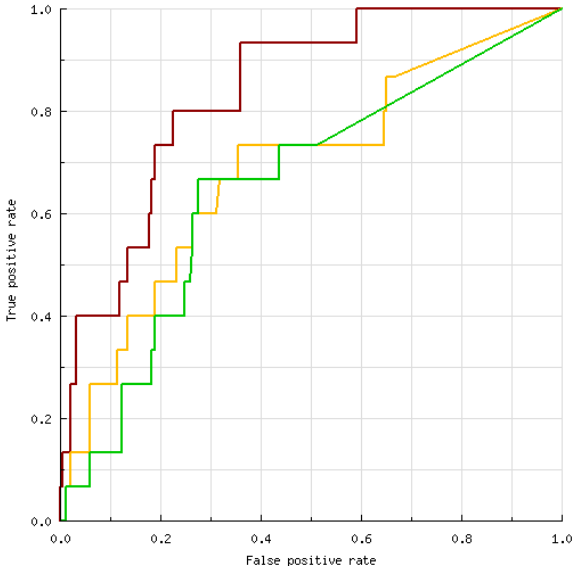

Figure D1: ROC Curves for basal ganglia lactate (green), white matter lactate (yellow) and multivariate model score (red) for identification of mitochondrial disease cases.

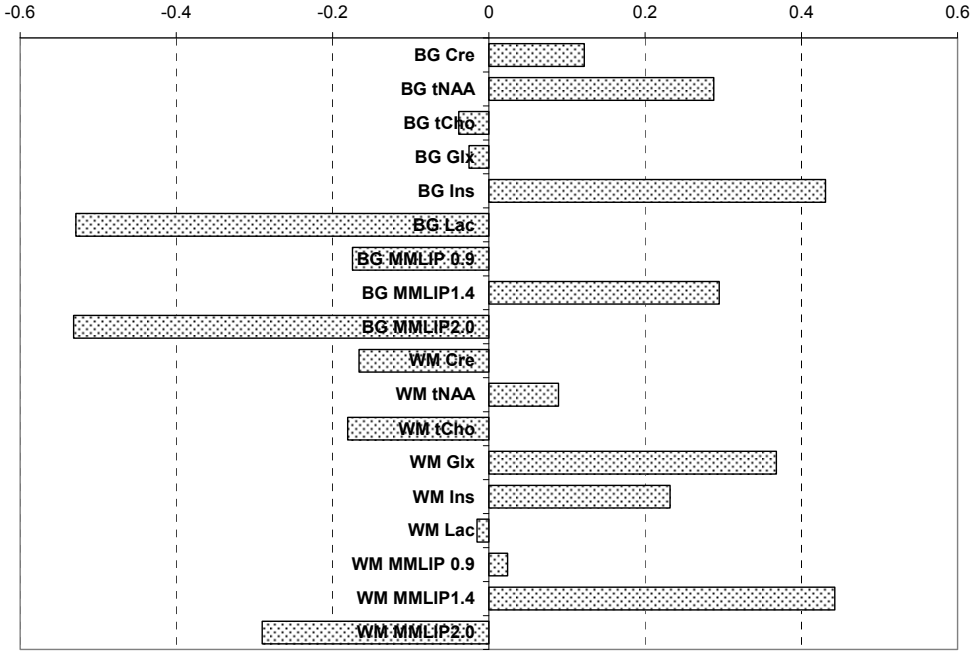

Figure D2: Loadings plot for multivariate model. Negative values indicate metabolites contributing to mitochondrial class. BG, basal ganglia; WM, white matter.

D4. Discussion

A multivariate model constructed incorporating multiple metabolite variables from two brain regions performs significantly better than lactate alone in distinguishing a cohort of mitochondrial cases from a mixed cohort of other children with known and unknown diagnoses. Assessment of apparent false positive classifications may identify patients with other IMD with brain metabolite profiles similar to the mitochondrial diseases, and potentially others with as yet undiagnosed mitochondrial disease. However, the model has a significant false negative rate (cases missed) suggesting that MRS may not be able to identify all cases. The loadings plots may provide useful information about typical brain metabolite changes occurring in the mitochondrial diseases.

This concept requires further prospective validation, and in particular the potential of over-fitting needs to be further evaluated to determine whether the model is genuinely able to identify mitochondrial disease cases.

References

1. Walters AV: **Developmental delay - causes and investigation.** *Advances in clinical neuroscience & rehabilitation* 2010, **10:**32-34.
2. Cleary MA, Green A: **Developmental delay: when to suspect and how to investigate for an inborn error of metabolism.** *Arch Dis Child* 2005, **90:**1128-1132.
3. Clarke JTR: *A clinical guide to inherited metabolic diseases.* 3rd edn. Cambridge: Cambridge University Press; 2006.
4. Rodwell VW, Kennelly PJ: **Enzymes: Mechanism of Action.** In *Harper's Illustrated Biochemistry.* 26th edition. Edited by Murray RK, Granner DK, Mayes PA, Rodwell VW. New York: Lange Medical Books/McGraw-Hill; 2003
5. Lyon G, Kolodny EH, Pastores GM: *Neurology of hereditary metabolic diseases of children.* 3rd edn: McGraw-Hill; 2006.
6. Sanderson S, Green A, Preece MA, Burton H: **The incidence of inherited metabolic disorders in the West Midlands, UK.** *Arch Dis Child* 2006, **91:**896-899.
7. Burton H, Moorthie S: *Expanded newborn screening: a review of the evidence.* Cambridge: PHG Foundation; 2010.
8. Saudubray JM, Desguerre I, Sedel F, Charpentier C: **A clinical approach to inherited metabolic diseases.** In *Inborn metabolic diseases - diagnosis and treatment.* 4th edition. Edited by Fernandes J, Saudubray JM, van den Berghe G, Walter JH. Heidelberg: Springer; 2006
9. Gissen P, Maher ER: **Cargos and genes: insights into vesicular transport from inherited human disease.** *J Med Genet* 2007, **44:**545-555.
10. Johnson JA, Le KL, Palacios E: **Propionic acidemia: case report and review of neurologic sequelae.** *Pediatr Neurol* 2009, **40:**317-320.
11. Sauer SW: **Biochemistry and bioenergetics of glutaryl-CoA dehydrogenase deficiency.** *J Inherit Metab Dis* 2007, **30:**673-680.
12. Debray FG, Lambert M, Mitchell GA: **Disorders of mitochondrial function.** *Curr Opin Pediatr* 2008, **20:**471-482.
13. Phelan JA, Lowe LH, Glasier CM: **Pediatric neurodegenerative white matter processes: leukodystrophies and beyond.** *Pediatr Radiol* 2008, **38:**729-749.
14. Verity C, Winstone AM, Stellitano L, Will R, Nicoll A, Verity C, Winstone AM, Stellitano L, Will R, Nicoll A: **The epidemiology of progressive intellectual and neurological deterioration in childhood.** *Archives of Disease in Childhood* 2010, **95:**361-364.
15. te Water Naude J: **Investigation of progressive developmental delay.** *Current Paediatrics* 2005, **15:**273-279.
16. Enns GM: **Neurologic Damage and Neurocognitive Dysfunction in Urea Cycle Disorders.** *Seminars in Pediatric Neurology* 2008, **15:**132-139.
17. van Spronsen F, Hoeksma M, Reijngoud D-J: **Brain dysfunction in phenylketonuria: Is phenylalanine toxicity the only possible cause?** *Journal of Inherited Metabolic Disease* 2009, **32:**46-51.
18. Wraith JE: **Enzyme replacement therapy with idursulfase in patients with mucopolysaccharidosis type II.** *Acta Paediatr Suppl* 2008, **97:**76-78.
19. Schreiber J, Chapman KA, Summar ML, Mew NA, Sutton VR, Macleod E, Stagni K, Ueda K, Franks J, Island E, et al: **Neurologic considerations in propionic acidemia.** *Mol Genet Metab* 2011.

20. Mancuso M, Orsucci D, Coppede F, Nesti C, Choub A, Siciliano G: **Diagnostic approach to mitochondrial disorders: the need for a reliable biomarker.** *Current Molecular Medicine* 2009, **9:**1095-1107.
21. Wishart DS, Lewis MJ, Morrissey JA, Flegel MD, Jeroncic K, Xiong Y, Cheng D, Eisner R, Gautam B, Tzur D, et al: **The human cerebrospinal fluid metabolome.** *J Chromatogr B Analyt Technol Biomed Life Sci* 2008, **871:**164-173.
22. Kurian MA, Gissen P, Smith M, Heales S, Jr., Clayton PT: **The monoamine neurotransmitter disorders: an expanding range of neurological syndromes.** *Lancet Neurol* 2011, **10:**721-733.
23. Mills PB, Surtees RA, Champion MP, Beesley CE, Dalton N, Scambler PJ, Heales SJ, Briddon A, Scheimberg I, Hoffmann GF, et al: **Neonatal epileptic encephalopathy caused by mutations in the PNPO gene encoding pyridox(am)ine 5'-phosphate oxidase.** *Hum Mol Genet* 2005, **14:**1077-1086.
24. Samuelsson C, Hillered L, Enblad P, Ronne-Engstrom E: **Microdialysis patterns in subarachnoid hemorrhage patients with focus on ischemic events and brain interstitial glutamine levels.** *Acta Neurochir (Wien)* 2009, **151:**437-446; discussion 446.
25. Maurer MH, Berger C, Wolf M, Futterer CD, Feldmann RE, Jr., Schwab S, Kuschinsky W: **The proteome of human brain microdialysate.** *Proteome Sci* 2003, **1:**7.
26. Belli A, Sen J, Petzold A, Russo S, Kitchen N, Smith M, Tavazzi B, Vagnozzi R, Signoretti S, Amorini AM, et al: **Extracellular N-acetylaspartate depletion in traumatic brain injury.** *Journal of Neurochemistry* 2006, **96:**861-869.
27. Frykholm P, Hillered L, LÃ¥ngstrÃ¶m B, Persson L, Valtysson J, Watanabe Y, Enblad P: **Increase of interstitial glycerol reflects the degree of ischaemic brain damage: a PET and microdialysis study in a middle cerebral artery occlusion-reperfusion primate model.** *Journal of Neurology, Neurosurgery & Psychiatry* 2001, **71:**455-461.
28. Wilson M, Davies NP, Brundler MA, McConville C, Grundy RG, Peet AC: **High resolution magic angle spinning 1H NMR of childhood brain and nervous system tumours.** *Mol Cancer* 2009, **8:**6.
29. Wilson M, Davies NP, Grundy RG, Peet AC: **A quantitative comparison of metabolite signals as detected by in vivo MRS with ex vivo 1H HR-MAS for childhood brain tumours.** *NMR Biomed* 2009, **22:**213-219.
30. Pears MR, Cooper JD, Mitchison HM, Mortishire-Smith RJ, Pearce DA, Griffin JL: **High resolution 1H NMR-based metabolomics indicates a neurotransmitter cycling deficit in cerebral tissue from a mouse model of Batten disease.** *J Biol Chem* 2005, **280:**42508-42514.
31. Damadian R: **Tumor detection by nuclear magnetic resonance.** *Science* 1971, **171:**1151-1153.
32. Lauterbur PC: **Image Formation by Induced Local Interactions: Examples Employing Nuclear Magnetic Resonance.** *Nature* 1973, **242:**190-191.
33. Mansfield P, Maudsley AA: **Medical imaging by NMR.** *Br J Radiol* 1977, **50:**188-194.
34. Peet AC, Leach MO, Pinkerton CR, Price P, Williams SR, Grundy RG: **The development of functional imaging in the diagnosis, management and understanding of childhood brain tumours.** *Pediatr Blood Cancer* 2005, **44:**103-113.

35. Gropman A: **Imaging of neurogenetic and neurometabolic disorders of childhood.** *Curr Neurol Neurosci Rep* 2004, **4:**139-146.
36. de Graaf RA: *In vivo NMR spectroscopy: principles and techniques.* 2nd edn. Chichester: John Wiley & Sons Ltd; 2007.
37. Jacobsen NE: *NMR Spectroscopy Explained: Simplified theory, applications and examples for organic chemistry and structrual biology.* Hoboken: John Wiley & Sons Inc.; 2007.
38. Jose da Rocha A, Tulio Braga F, Carlos Martins Maia A, Jr., Jorge da Silva C, Toyama C, Pereira Pinto Gama H, Kok F, Rodrigues Gomes H, Jose da Rocha A, Tulio Braga F, et al: **Lactate detection by MRS in mitochondrial encephalopathy: optimization of technical parameters.** *Journal of Neuroimaging* 2008, **18:**1-8.
39. Bottomley PA: **Spatial localization in NMR spectroscopy in vivo.** *Annals of the New York Academy of Sciences* 1987, **508:**333-348.
40. Frahm J, Bruhn H, Gyngell ML, Merboldt KD, Hanicke W, Sauter R: **Localized high-resolution proton NMR spectroscopy using stimulated echoes: initial applications to human brain in vivo.** *Magnetic Resonance in Medicine* 1989, **9:**79-93.
41. Moonen CT, von Kienlin M, van Zijl PC, Cohen J, Gillen J, Daly P, Wolf G: **Comparison of single-shot localization methods (STEAM and PRESS) for in vivo proton NMR spectroscopy.** *NMR in Biomedicine* 1989, **2:**201-208.
42. Jiru F: **Introduction to post-processing techniques.** *European Journal of Radiology* 2008, **67:**202-217.
43. Provencher SW: **Estimation of metabolite concentrations from localized in vivo proton NMR spectra.** *Magn Reson Med* 1993, **30:**672-679.
44. Provencher SW: **Automatic quantitation of localized in vivo 1H spectra with LCModel.** *NMR Biomed* 2001, **14:**260-264.
45. Davies NP, Wilson M, Natarajan K, Sun Y, MacPherson L, Brundler MA, Arvanitis TN, Grundy RG, Peet AC: **Non-invasive detection of glycine as a biomarker of malignancy in childhood brain tumours using in-vivo 1H MRS at 1.5 tesla confirmed by ex-vivo high-resolution magic-angle spinning NMR.** *NMR Biomed* 2009, **23:**80-87.
46. Ernst T, Kreis R, Ross BD: **Absolute Quantitation of Water and Metabolites in the Human Brain. I. Compartments and Water.** *Journal of Magnetic Resonance, Series B* 1993, **102:**1-8.
47. McRobbie DW, Moore EA, Graves MJ, Prince MR: *MRI: From picture to proton.* 2nd edn. Cambridge: Cambridge University Press; 2007.
48. Bluml S: **In vivo quantitation of cerebral metabolite concentrations using natural abundance 13C MRS at 1.5 T.** *J Magn Reson* 1999, **136:**219-225.
49. Bhakoo KK, Pearce D: **In vitro expression of N-acetyl aspartate by oligodendrocytes: implications for proton magnetic resonance spectroscopy signal in vivo.** *J Neurochem* 2000, **74:**254-262.
50. Griffin JL, Bollard M, Nicholson JK, Bhakoo K, Griffin JL, Bollard M, Nicholson JK, Bhakoo K: **Spectral profiles of cultured neuronal and glial cells derived from HRMAS (1)H NMR spectroscopy.** *NMR in Biomedicine* 2002, **15:**375-384.
51. Goldstein FB: **Biosynthesis of N-acetyl-L-aspartic acid.** *Biochim Biophys Acta* 1959, **33:**583-584.
52. Moffett JR, Ross B, Arun P, Madhavarao CN, Namboodiri AM: **N-Acetylaspartate in the CNS: from neurodiagnostics to neurobiology.** *Prog Neurobiol* 2007, **81:**89-131.

53. Wittsack HJ, Kugel H, Roth B, Heindel W: **Quantitative measurements with localized 1H MR spectroscopy in children with Canavan's disease.** *J Magn Reson Imaging* 1996, **6:**889-893.
54. Wibom R, Lasorsa FM, Tohonen V, Barbaro M, Sterky FH, Kucinski T, Naess K, Jonsson M, Pierri CL, Palmieri F, Wedell A: **AGC1 deficiency associated with global cerebral hypomyelination.** *N Engl J Med* 2009, **361:**489-495.
55. Cecil KM: **MR Spectroscopy of Metabolic Disorders.** *Neuroimaging Clinics of North America* 2006, **16:**87-116.
56. Dezortova M, Hajek M: **(1)H MR spectroscopy in pediatrics.** *Eur J Radiol* 2008, **67:**240-249.
57. Neale JH, Bzdega T, Wroblewska B: **N-Acetylaspartylglutamate: the most abundant peptide neurotransmitter in the mammalian central nervous system.** *J Neurochem* 2000, **75:**443-452.
58. Becker I, Lodder J, Gieselmann V, Eckhardt M: **Molecular characterization of N-acetylaspartylglutamate synthetase.** *J Biol Chem* 2010, **285:**29156-29164.
59. Mochel F, Engelke UF, Barritault J, Yang B, McNeill NH, Thompson JN, Vanderver A, Wolf NI, Willemsen MA, Verheijen FW, et al: **Elevated CSF N-acetylaspartylglutamate in patients with free sialic acid storage diseases.** *Neurology* 2010, **74:**302-305.
60. Wolf NI, Willemsen MA, Engelke UF, van der Knaap MS, Pouwels PJ, Harting I, Zschocke J, Sistermans EA, Rating D, Wevers RA, et al: **Severe hypomyelination associated with increased levels of N-acetylaspartylglutamate in CSF.[see comment].** *Neurology* 2004, **62:**1503-1508.
61. Sartori S, Burlina AB, Salviati L, Trevisson E, Toldo I, Laverda AM, Burlina AP: **Increased level of N-acetylaspartylglutamate (NAAG) in the CSF of a patient with Pelizaeus-Merzbacher-like disease due to mutation in the GJA12 gene.** *European Journal of Paediatric Neurology* 2008, **12:**348-350.
62. Hanefeld FA, Brockmann K, Pouwels PJ, Wilken B, Frahm J, Dechent P, Pouwels PJW: **Quantitative proton MRS of Pelizaeus-Merzbacher disease: evidence of dys- and hypomyelination.[see comment].** *Neurology* 2005, **65:**701-706.
63. Wallimann T, Wyss M, Brdiczka D, Nicolay K, Eppenberger HM: **Intracellular compartmentation, structure and function of creatine kinase isoenzymes in tissues with high and fluctuating energy demands: the 'phosphocreatine circuit' for cellular energy homeostasis.** *Biochem J* 1992, **281 (Pt 1):**21-40.
64. Braissant O, Henry H, Beard E, Uldry J: **Creatine deficiency syndromes and the importance of creatine synthesis in the brain.** *Amino Acids* 2011, **40:**1315-1324.
65. Wallimann T, Tokarska-Schlattner M, Schlattner U: **The creatine kinase system and pleiotropic effects of creatine.** *Amino Acids* 2011, **40:**1271-1296.
66. Stockler S, Schutz PW, Salomons GS: **Cerebral creatine deficiency syndromes: clinical aspects, treatment and pathophysiology.** *Subcell Biochem* 2007, **46:**149-166.
67. Pouwels PJ, Brockmann K, Kruse B, Wilken B, Wick M, Hanefeld F, Frahm J: **Regional age dependence of human brain metabolites from infancy to adulthood as detected by quantitative localized proton MRS.** *Pediatr Res* 1999, **46:**474-485.
68. Glunde K, Bhujwalla ZM, Ronen SM: **Choline metabolism in malignant transformation.** *Nat Rev Cancer* 2011.

69. Andria G, Fowler B, Sebastio G: **Disorders of sulfur amino acid metabolism.** In *Inborn metabolic diseases - diagnosis and treatment.* 4th edition. Edited by Fernandes J, Saudubray JM, van den Berghe G, Walter JH. Heidelberg: Springer; 2006
70. Sajja BR, Wolinsky JS, Narayana PA: **Proton magnetic resonance spectroscopy in multiple sclerosis.** *Neuroimaging Clin N Am* 2009, **19:**45-58.
71. Fisher SK, Novak JE, Agranoff BW: **Inositol and higher inositol phosphates in neural tissues: homeostasis, metabolism and functional significance.** *J Neurochem* 2002, **82:**736-754.
72. Granner DK: **Hormone action and signal transduction.** In *Harper's Illustrated Biochemistry.* 26th edition. Edited by Murray RK, Granner DK, Mayes PA, Rodwell VW. New York: Lange Medical Books/McGraw-Hill; 2003
73. Fenili D, Weng YQ, Aubert I, Nitz M, McLaurin J: **Sodium/myo-Inositol transporters: substrate transport requirements and regional brain expression in the TgCRND8 mouse model of amyloid pathology.** *PLoS ONE [Electronic Resource]* 2011, **6:**e24032.
74. Zwingmann C, Butterworth R, Zwingmann C, Butterworth R: **An update on the role of brain glutamine synthesis and its relation to cell-specific energy metabolism in the hyperammonemic brain: further studies using NMR spectroscopy.** *Neurochemistry International* 2005, **47:**19-30.
75. Kim JP, Lentz MR, Westmoreland SV, Greco JB, Ratai EM, Halpern E, Lackner AA, Masliah E, Gonzalez RG, Kim JP, et al: **Relationships between astrogliosis and 1H MR spectroscopic measures of brain choline/creatine and myo-inositol/creatine in a primate model.** *Ajnr: American Journal of Neuroradiology* 2005, **26:**752-759.
76. Peet AC, Lateef S, MacPherson L, Natarajan K, Sgouros S, Grundy RG: **Short echo time 1 H magnetic resonance spectroscopy of childhood brain tumours.** *Childs Nerv Syst* 2007, **23:**163-169.
77. Griffith HR, Hollander JAd, Stewart CC, Evanochko WT, Buchthal SD, Harrell LE, Zamrini EY, Brockington JC, Marson DC: **Elevated brain scyllo-inositol concentrations in patients with Alzheimer's disease.** *NMR in Biomedicine* 2007, **20:**709-716.
78. Fenili D, Brown M, Rappaport R, McLaurin J: **Properties of scyllo–inositol as a therapeutic treatment of AD-like pathology.** *Journal of Molecular Medicine* 2007, **85:**603-611.
79. Simeone TA, Sanchez RM, Rho JM: **Molecular biology and ontogeny of glutamate receptors in the mammalian central nervous system.** *J Child Neurol* 2004, **19:**343-360; discussion 361.
80. Magistretti PJ: **Brain energy metabolism.** In *From Molecules to Networks: An Introduction to Cellular and Molecular Neuroscience.* Edited by Byrne JH, Roberts JL: Elsevier Inc.; 2004
81. Seidner G, Alvarez MG, Yeh JI, O'Driscoll KR, Klepper J, Stump TS, Wang D, Spinner NB, Birnbaum MJ, De Vivo DC: **GLUT-1 deficiency syndrome caused by haploinsufficiency of the blood-brain barrier hexose carrier.** *Nat Genet* 1998, **18:**188-191.
82. Kayano T, Fukumoto H, Eddy RL, Fan YS, Byers MG, Shows TB, Bell GI: **Evidence for a family of human glucose transporter-like proteins. Sequence and gene localization of a protein expressed in fetal skeletal muscle and other tissues.** *J Biol Chem* 1988, **263:**15245-15248.

83. Mayes PA, Bender DA: **Glycolysis and the oxidation of pyruvate.** In *Harper's Illustrated Biochemistry.* 26th edition. Edited by Murray RK, Granner DK, Mayes PA, Rodwell VW. New York: Lange Medical Books/McGraw-Hill; 2003
84. Harada K, Honmou O, Liu H, Bando M, Houkin K, Kocsis JD: **Magnetic resonance lactate and lipid signals in rat brain after middle cerebral artery occlusion model.** *Brain Res* 2007, **1134:**206-213.
85. van Baalen A, Stephani U, Rohr A: **Increased brain lactate during stroke-like episode in a patient with congenital disorder of glycosylation type Ia.** *Brain Dev* 2009, **31:**183.
86. Prichard J, Rothman D, Novotny E, Petroff O, Kuwabara T, Avison M, Howseman A, Hanstock C, Shulman R: **Lactate rise detected by 1H NMR in human visual cortex during physiologic stimulation.** *Proc Natl Acad Sci U S A* 1991, **88:**5829-5831.
87. Waddell KW, Avison MJ, Joers JM, Gore JC, Waddell KW, Avison MJ, Joers JM, Gore JC: **A practical guide to robust detection of GABA in human brain by J-difference spectroscopy at 3 T using a standard volume coil.** *Magnetic Resonance Imaging* 2007, **25:**1032-1038.
88. Kauppinen RA, Niskanen T, Hakumaki J, Williams SR: **Quantitative analysis of 1H NMR detected proteins in the rat cerebral cortex in vivo and in vitro.** *NMR Biomed* 1993, **6:**242-247.
89. Auer DP, Gossl C, Schirmer T, Czisch M: **Improved analysis of 1H-MR spectra in the presence of mobile lipids.** *Magn Reson Med* 2001, **46:**615-618.
90. Hakumaki JM, Kauppinen RA: **1H NMR visible lipids in the life and death of cells.** *Trends Biochem Sci* 2000, **25:**357-362.
91. Gropman AL, Gropman AL: **Expanding the diagnostic and research toolbox for inborn errors of metabolism: the role of magnetic resonance spectroscopy.** *Molecular Genetics & Metabolism* 2005, **86:**2-9.
92. Hajek M, Dezortova M: **Introduction to clinical in vivo MR spectroscopy.** *Eur J Radiol* 2008, **67:**185-193.
93. Barger AV, Campeau NG, Port JD, Renaud DL: **MRS is the Test of Choice for Detecting and Monitoring Disorders of Creatine Metabolism.** *Pediatric Neurology* 2009, **40:**408-410.
94. Sijens PE, Westerlaan HE, de Groot JC, Boon M, Potze JH, van Spronsen FJ, Lunsing RJ, Oudkerk M: **MR spectroscopy and diffusion tensor imaging of the brain in Sjogren-Larsson syndrome.** *Molecular Genetics & Metabolism* 2009, **98:**367-371.
95. Pirgon O, Aydin K, Atabek ME: **Proton Magnetic Resonance Spectroscopy Findings and Clinical Effects of Montelukast Sodium in a Case With Sjogren-Larsson Syndrome.** *J Child Neurol* 2006, **21:**1092-1095.
96. Nakayama M, Tavora DG, Alvim TC, Araujo AC, Gama RL: **MRI and 1H-MRS findings of three patients with Sjogren-Larsson syndrome.** *Arq Neuropsiquiatr* 2006, **64:**398-401.
97. Willemsen MA, Van Der Graaf M, Van Der Knaap MS, Heerschap A, Van Domburg PH, Gabreels FJ, Rotteveel JJ: **MR imaging and proton MR spectroscopic studies in Sjogren-Larsson syndrome: characterization of the leukoencephalopathy.** *AJNR Am J Neuroradiol* 2004, **25:**649-657.
98. Henneke M, Dreha-Kulaczewski S, Brockmann K, van der Graaf M, Willemsen MA, Engelke U, Dechent P, Heerschap A, Helms G, Wevers RA, Gartner J: **In vivo proton MR spectroscopy findings specific for adenylosuccinate lyase deficiency.** *NMR Biomed* 2010.

99. Mitochondrial Medicine Society's Committee on D, Haas RH, Parikh S, Falk MJ, Saneto RP, Wolf NI, Darin N, Wong LJ, Cohen BH, Naviaux RK, et al: **The in-depth evaluation of suspected mitochondrial disease.** *Molecular Genetics & Metabolism* 2008, **94:**16-37.
100. Worgall S, Kekatpure MV, Heier L, Ballon D, Dyke JP, Shungu D, Mao X, Kosofsky B, Kaplitt MG, Souweidane MM, et al: **Neurological deterioration in late infantile neuronal ceroid lipofuscinosis.** *Neurology* 2007, **69:**521-535.
101. Engelke U, Moolenaar SH, Hoenderop SMGC, Morava E, Van der Graaf M, Heerschap A, Wevers RA: *Handbook of 1H-NMR spectroscopy in inborn errors of metabolism: body fluid NMR spectroscopy and in vivo MR spectroscopy.* 2nd edn. Heilbronn: SPS Publications; 2007.
102. van der Knaap MS, Wevers RA, Struys EA, Verhoeven NM, Pouwels PJ, Engelke UF, Feikema W, Valk J, Jakobs C: **Leukoencephalopathy associated with a disturbance in the metabolism of polyols.** *Ann Neurol* 1999, **46:**925-928.
103. Yalcinkaya C, Dincer A, Gunduz E, Ficicioglu C, Kocer N, Aydin A: **MRI and MRS in HMG-CoA lyase deficiency.** *Pediatr Neurol* 1999, **20:**375-380.
104. Schindeler S, Ghosh-Jerath S, Thompson S, Rocca A, Joy P, Kemp A, Rae C, Green K, Wilcken B, Christodoulou J: **The effects of large neutral amino acid supplements in PKU: an MRS and neuropsychological study.** *Mol Genet Metab* 2007, **91:**48-54.
105. Sener RN: **Maple syrup urine disease: Diffusion MRI, and proton MR spectroscopy findings.** *Computerized Medical Imaging and Graphics* 2007, **31:**106-110.
106. Ethofer T, Seeger U, Klose U, Erb M, Kardatzki B, Kraft E, Landwehrmeyer GB, Grodd W, Storch A: **Proton MR spectroscopy in succinic semialdehyde dehydrogenase deficiency.** *Neurology* 2004, **62:**1016-1018.
107. Engelke UF, Kremer B, Kluijtmans LA, van der Graaf M, Morava E, Loupatty FJ, Wanders RJ, Moskau D, Loss S, van den Bergh E, Wevers RA: **NMR spectroscopic studies on the late onset form of 3-methylglutaconic aciduria type I and other defects in leucine metabolism.** *NMR Biomed* 2006, **19:**271-278.
108. Beckonert O, Keun HC, Ebbels TMD, Bundy J, Holmes E, Lindon JC, Nicholson JK: **Metabolic profiling, metabolomic and metabonomic procedures for NMR spectroscopy of urine, plasma, serum and tissue extracts.** *Nat Protocols* 2007, **2:**2692-2703.
109. Wishart DS, Knox C, Guo AC, Eisner R, Young N, Gautam B, Hau DD, Psychogios N, Dong E, Bouatra S, et al: **HMDB: a knowledgebase for the human metabolome.** *Nucleic Acids Res* 2009, **37:**D603-610.
110. Saneto RP, Friedman SD, Shaw DW: **Neuroimaging of mitochondrial disease.** *Mitochondrion* 2008, **8:**396-413.
111. Barkovich AJ, Good WV, Koch TK, Berg BO: **Mitochondrial disorders: analysis of their clinical and imaging characteristics.** *Ajnr: American Journal of Neuroradiology* 1993, **14:**1119-1137.
112. Chi CS, Lee HF, Tsai CR, Chen WS, Tung JN, Hung HC: **Lactate peak on brain MRS in children with syndromic mitochondrial diseases.** *Journal of the Chinese Medical Association: JCMA* 2011, **74:**305-309.
113. Haas RH, Parikh S, Falk MJ, Saneto RP, Wolf NI, Darin N, Wong LJ, Cohen BH, Naviaux RK: **The in-depth evaluation of suspected mitochondrial disease.** *Mol Genet Metab* 2008, **94:**16-37.

114. Kingsley PB, Shah TC, Woldenberg R: **Identification of diffuse and focal brain lesions by clinical magnetic resonance spectroscopy.** *NMR Biomed* 2006, **19:**435-462.
115. Dinopoulos A, Cecil KM, Schapiro MB, Papadimitriou A, Hadjigeorgiou GM, Wong B, deGrauw T, Egelhoff JC: **Brain MRI and proton MRS findings in infants and children with respiratory chain defects.** *Neuropediatrics* 2005, **36:**290-301.
116. Valanne L, Ketonen L, Majander A, Suomalainen A, Pihko H: **Neuroradiologic findings in children with mitochondrial disorders.** *AJNR Am J Neuroradiol* 1998, **19:**369-377.
117. Boddaert N, Romano S, Funalot B, Rio M, Sarzi E, Lebre AS, Bahi-Buisson N, Valayannopoulos V, Desguerre I, Seidenwurm D, et al: **1H MRS spectroscopy evidence of cerebellar high lactate in mitochondrial respiratory chain deficiency.** *Molecular Genetics & Metabolism* 2008, **93:**85-88.
118. van der Voorn JP, Pouwels PJ, Hart AA, Serrarens J, Willemsen MA, Kremer HP, Barkhof F, van der Knaap MS: **Childhood white matter disorders: quantitative MR imaging and spectroscopy.** *Radiology* 2006, **241:**510-517.
119. Brockmann K, Bjornstad A, Dechent P, Korenke CG, Smeitink J, Trijbels JM, Athanassopoulos S, Villagran R, Skjeldal OH, Wilichowski E, et al: **Succinate in dystrophic white matter: a proton magnetic resonance spectroscopy finding characteristic for complex II deficiency.** *Ann Neurol* 2002, **52:**38-46.
120. Fodor E, Hellerud C, Hulting J, Karlson-Stiber C, Abrahamsson L, Nystrom T, Andersson DE, Sjoholm A: **Glycerol kinase deficiency in adult hypoglycemic acidemia.** *N Engl J Med* 2011, **364:**1781-1782.
121. Davison JE, Hendriksz CJ, Sun Y, Davies NP, Gissen P, Peet AC: **Quantitative in vivo brain magnetic resonance spectroscopic monitoring of neurological involvement in mucopolysaccharidosis type II (Hunter Syndrome).** *J Inherit Metab Dis* 2010, **33:**819.
122. Maxfield FR, Mukherjee S: **The endosomal-lysosomal system.** In *Lysosomal disorders of the brain.* Edited by Platt FM, Walkley SU. Oxford: Oxford University Press; 2004
123. Platt FM, Walkley SU: **Lysosomal defects and storage.** In *Lysosomal disorders of the brain.* Edited by Platt FM, Walkley SU. Oxford: Oxford University Press; 2004
124. Walkley SU: **Pathogenic cascades and brain dysfunction.** In *Lysosomal disorders of the brain.* Edited by Platt FM, Walkley SU. Oxford: Oxford University Press; 2004
125. Winchester BG: **Primary defects in lysosomal enzymes.** In *Lysosomal disorders of the brain.* Edited by Platt FM, Walkley SU. Oxford: Oxford University Press; 2004
126. Wraith JE: **Mucopolysaccharidoses and oligosaccharidoses.** In *Inborn Metabolic Diseases: Diagnosis and Treatment* 4th edition. Edited by Fernandes J, Saudubray JM, van den Berghe G, Walter JH: Springer; 2006
127. Martin R, Beck M, Eng C, Giugliani R, Harmatz P, Munoz V, Muenzer J: **Recognition and diagnosis of mucopolysaccharidosis II (Hunter syndrome).** *Pediatrics* 2008, **121:**e377-386.
128. Wraith JE, Scarpa M, Beck M, Bodamer OA, De Meirleir L, Guffon N, Meldgaard Lund A, Malm G, Van der Ploeg AT, Zeman J: **Mucopolysaccharidosis type II (Hunter syndrome): a clinical review and recommendations for treatment in the era of enzyme replacement therapy.** *Eur J Pediatr* 2008, **167:**267-277.
129. Scarpa M, Almassy Z, Beck M, Bodamer O, Bruce IA, De Meirleir L, Guffon N, Guillen-Navarro E, Hensman P, Jones S, et al: **Mucopolysaccharidosis type II:**

European recommendations for the diagnosis and multidisciplinary management of a rare disease. *Orphanet J Rare Dis* 2011, **6:**72.
130. Jones SA, Almassy Z, Beck M, Burt K, Clarke JT, Giugliani R, Hendriksz C, Kroepfl T, Lavery L, Lin SP, et al: **Mortality and cause of death in mucopolysaccharidosis type II-a historical review based on data from the Hunter Outcome Survey (HOS).** *J Inherit Metab Dis* 2009, **32:**534-543.
131. Holt JB, Poe MD, Escolar ML: **Natural progression of neurological disease in mucopolysaccharidosis type II.** *Pediatrics* 2011, **127:**e1258-1265.
132. Muenzer J, Bodamer O, Burton B, Clarke L, Frenking GS, Giugliani R, Jones S, Rojas MV, Scarpa M, Beck M, Harmatz P: **The role of enzyme replacement therapy in severe Hunter syndrome-an expert panel consensus.** *Eur J Pediatr* 2012, **171:**181-188.
133. Young ID, Harper PS, Newcombe RG, Archer IM: **A clinical and genetic study of Hunter's syndrome. 2. Differences between the mild and severe forms.** *J Med Genet* 1982, **19:**408-411.
134. Holt J, Poe MD, Escolar ML: **Early clinical markers of central nervous system involvement in mucopolysaccharidosis type II.** *J Pediatr* 2011, **159:**320-326 e322.
135. Walkley SU: **Pathogenic cascades in lysosomal disease-Why so complex?** *J Inherit Metab Dis* 2009, **32:**181-189.
136. Hamano K, Hayashi M, Shioda K, Fukatsu R, Mizutani S, Hamano K, Hayashi M, Shioda K, Fukatsu R, Mizutani S: **Mechanisms of neurodegeneration in mucopolysaccharidoses II and IIIB: analysis of human brain tissue.** *Acta Neuropathologica* 2008, **115:**547-559.
137. Muenzer J, Wraith JE, Beck M, Giugliani R, Harmatz P, Eng CM, Vellodi A, Martin R, Ramaswami U, Gucsavas-Calikoglu M, et al: **A phase II/III clinical study of enzyme replacement therapy with idursulfase in mucopolysaccharidosis II (Hunter syndrome).** *Genet Med* 2006, **8:**465-473.
138. Muenzer J, Beck M, Eng CM, Giugliani R, Harmatz P, Martin R, Ramaswami U, Vellodi A, Wraith JE, Cleary M, et al: **Long-term, open-labeled extension study of idursulfase in the treatment of Hunter syndrome.** *Genet Med* 2011, **13:**95-101.
139. da Silva EM, Strufaldi MW, Andriolo RB, Silva LA: **Enzyme replacement therapy with idursulfase for mucopolysaccharidosis type II (Hunter syndrome).** *Cochrane Database Syst Rev* 2011, **11:**CD008185.
140. Glamuzina E, Fettes E, Bainbridge K, Crook V, Finnegan N, Abulhoul L, Vellodi A: **Treatment of mucopolysaccharidosis type II (Hunter syndrome) with idursulfase: the relevance of clinical trial end points.** *J Inherit Metab Dis* 2011, **34:**749-754.
141. Wang RY, Cambray-Forker EJ, Ohanian K, Karlin DS, Covault KK, Schwartz PH, Abdenur JE: **Treatment reduces or stabilizes brain imaging abnormalities in patients with MPS I and II.** *Mol Genet Metab* 2009, **98:**406-411.
142. Abbott NJ, Patabendige AA, Dolman DE, Yusof SR, Begley DJ: **Structure and function of the blood-brain barrier.** *Neurobiol Dis* 2010, **37:**13-25.
143. Calias P, Papisov M, Pan J, Savioli N, Belov V, Huang Y, Lotterhand J, Alessandrini M, Liu N, Fischman AJ, et al: **CNS penetration of intrathecal-lumbar idursulfase in the monkey, dog and mouse: implications for neurological outcomes of lysosomal storage disorder.** *PLoS ONE [Electronic Resource]* 2012, **7:**e30341.
144. Vedolin L, Schwartz IV, Komlos M, Schuch A, Azevedo AC, Vieira T, Maeda FK, Marques da Silva AM, Giugliani R: **Brain MRI in mucopolysaccharidosis: effect of aging and correlation with biochemical findings.** *Neurology* 2007, **69:**917-924.

145. Manara R, Priante E, Grimaldi M, Santoro L, Astarita L, Barone R, Concolino D, Di Rocco M, Donati MA, Fecarotta S, et al: **Brain and spine MRI features of Hunter disease: frequency, natural evolution and response to therapy.** *J Inherit Metab Dis* 2011, **34:**763-780.
146. Vedolin L, Schwartz IV, Komlos M, Schuch A, Puga AC, Pinto LL, Pires AP, Giugliani R: **Correlation of MR imaging and MR spectroscopy findings with cognitive impairment in mucopolysaccharidosis II.** *AJNR Am J Neuroradiol* 2007, **28:**1029-1033.
147. Takahashi Y, Sukegawa K, Aoki M, Ito A, Suzuki K, Sakaguchi H, Watanabe M, Isogai K, Mizuno S, Hoshi H, et al: **Evaluation of accumulated mucopolysaccharides in the brain of patients with mucopolysaccharidoses by (1)H-magnetic resonance spectroscopy before and after bone marrow transplantation.** *Pediatr Res* 2001, **49:**349-355.
148. Northover H, Cowie RA, Wraith JE: **Mucopolysaccharidosis type IVA (Morquio syndrome): a clinical review.** *J Inherit Metab Dis* 1996, **19:**357-365.
149. Tomatsu S, Montano AM, Ohashi A, Gutierrez MA, Oikawa H, Oguma T, Dung VC, Nishioka T, Orii T, Sly WS: **Enzyme replacement therapy in a murine model of Morquio A syndrome.** *Hum Mol Genet* 2008, **17:**815-824.
150. Dvorak-Ewell M, Wendt D, Hague C, Christianson T, Koppaka V, Crippen D, Kakkis E, Vellard M: **Enzyme replacement in a human model of mucopolysaccharidosis IVA in vitro and its biodistribution in the cartilage of wild type mice.** *PLoS ONE [Electronic Resource]* 2011, **5:**e12194.
151. Davison JE, Kearney S, Horton J, Foster K, Peet AC, Hendriksz CJ: **Intellectual and neurological functioning in Morquio syndrome (MPS IVa).** *J Inherit Metab Dis* 2012, **In press**.
152. Shprecher D, Schwalb J, Kurlan R: **Normal pressure hydrocephalus: diagnosis and treatment.** *Curr Neurol Neurosci Rep* 2008, **8:**371-376.
153. Seto T, Kono K, Morimoto K, Inoue Y, Shintaku H, Hattori H, Matsuoka O, Yamano T, Tanaka A: **Brain magnetic resonance imaging in 23 patients with mucopolysaccharidoses and the effect of bone marrow transplantation.** *Ann Neurol* 2001, **50:**79-92.
154. Griffin JL, Shockcor JP: **Metabolic profiles of cancer cells.** *Nat Rev Cancer* 2004, **4:**551-561.
155. Ling W, Regatte RR, Navon G, Jerschow A: **Assessment of glycosaminoglycan concentration in vivo by chemical exchange-dependent saturation transfer (gagCEST).** *Proceedings of the National Academy of Sciences* 2008, **105:**2266-2270.
156. van Zijl PC, Jones CK, Ren J, Malloy CR, Sherry AD: **MRI detection of glycogen in vivo by using chemical exchange saturation transfer imaging (glycoCEST).** *Proc Natl Acad Sci U S A* 2007, **104:**4359-4364.
157. Zhu H, Jones CK, van Zijl PC, Barker PB, Zhou J: **Fast 3D chemical exchange saturation transfer (CEST) imaging of the human brain.** *Magn Reson Med* 2010, **64:**638-644.
158. Davison JE, Davies NP, Wilson M, Sun Y, Chakrapani A, McKiernan PJ, Walter JH, Gissen P, Peet AC: **MR spectroscopy-based brain metabolite profiling in propionic acidaemia: metabolic changes in the basal ganglia during acute decompensation and effect of liver transplantation.** *Orphanet J Rare Dis* 2011, **6:**19.

159. Chapman KA, Summar ML: **Propionic acidemia consensus conference summary.** *Mol Genet Metab* 2011.
160. Childs B, Nyhan WL, Borden M, Bard L, Cooke RE: **Idiopathic hyperglycinemia and hyperglycinuria: a new disorder of amino acid metabolism. I.** *Pediatrics* 1961, **27:**522-538.
161. Pena L, Franks J, Chapman KA, Gropman A, Ah Mew N, Chakrapani A, Island E, Macleod E, Matern D, Smith B, et al: **Natural history of propionic acidemia.** *Mol Genet Metab* 2011.
162. Deodato F, Boenzi S, Santorelli FM, Dionisi-Vici C: **Methylmalonic and propionic aciduria.** *American Journal of Medical Genetics Part C: Seminars in Medical Genetics* 2006, **142C:**104-112.
163. Kraus JP, Spector E, Venezia S, Estes P, Chiang PW, Creadon-Swindell G, Mullerleile S, de Silva L, Barth M, Walter M, et al: **Mutation analysis in 54 propionic acidemia patients.** *J Inherit Metab Dis* 2012, **35:**51-63.
164. Sass JO, Hofmann M, Skladal D, Mayatepek E, Schwahn B, Sperl W: **Propionic acidemia revisited: a workshop report.** *Clin Pediatr (Phila)* 2004, **43:**837-843.
165. Leonard JV: **Stable isotope studies in propionic and methylmalonic acidaemia.** *Eur J Pediatr* 1997, **156 Suppl 1:**S67-69.
166. Scholl-Burgi S, Sass JO, Heinz-Erian P, Amann E, Haberlandt E, Albrecht U, Ertl C, Sigl SB, Lagler F, Rostasy K, Karall D: **Changes in plasma amino acid concentrations with increasing age in patients with propionic acidemia.** *Amino Acids* 2009.
167. Wendel U, Ogier de Baulny H: **Branched-chain organic acidurias/acidemias.** In *Inborn metabolic diseases - diagnosis and treatment.* 4th edition. Edited by Fernandes J, Saudubray JM, van den Berghe G, Walter JH. Heidelberg: Springer; 2006
168. Chapman KA, Gropman A, Macleod E, Stagni K, Summar ML, Ueda K, Mew NA, Franks J, Island E, Matern D, et al: **Acute management of propionic acidemia.** *Mol Genet Metab* 2011.
169. Grunert SC, Mullerleile S, de Silva L, Barth M, Walter M, Walter K, Meissner T, Lindner M, Ensenauer R, Santer R, et al: **Propionic acidemia: neonatal versus selective metabolic screening.** *J Inherit Metab Dis* 2012, **35:**41-49.
170. Sutton VR, Chapman KA, Gropman AL, Macleod E, Stagni K, Summar ML, Ueda K, Mew NA, Franks J, Island E, et al: **Chronic management and health supervision of individuals with propionic acidemia.** *Mol Genet Metab* 2011.
171. Barshes NR, Vanatta JM, Patel AJ, Carter BA, O'Mahony CA, Karpen SJ, Goss JA: **Evaluation and management of patients with propionic acidemia undergoing liver transplantation: a comprehensive review.** *Pediatr Transplant* 2006, **10:**773-781.
172. Vara R, Turner C, Mundy H, Heaton ND, Rela M, Mieli-Vergani G, Champion M, Hadzic N: **Liver transplantation for propionic acidemia in children.** *Liver Transpl* 2011, **17:**661-667.
173. Burlina AP, Baracchini C, Carollo C, Burlina AB: **Propionic acidaemia with basal ganglia stroke: treatment of acute extrapyramidal symptoms with L-DOPA.** *J Inherit Metab Dis* 2001, **24:**596-598.
174. North KN, Korson MS, Gopal YR, Rohr FJ, Brazelton TB, Waisbren SE, Warman ML: **Neonatal-onset propionic acidemia: neurologic and developmental profiles, and implications for management.** *Journal of Pediatrics* 1995, **126:**916-922.

175. Surtees RA, Matthews EE, Leonard JV: **Neurologic outcome of propionic acidemia.** *Pediatr Neurol* 1992, **8:**333-337.
176. Brismar J, Ozand PT: **CT and MR of the brain in disorders of the propionate and methylmalonate metabolism.** *AJNR Am J Neuroradiol* 1994, **15:**1459-1473.
177. Al-Essa M, Bakheet S, Patay Z, Al-Shamsan L, Al-Sonbul A, Al-Watban J, Powe J, Ozand PT: **18Fluoro-2-deoxyglucose (18FDG) PET scan of the brain in propionic acidemia: clinical and MRI correlations.** *Brain & Development* 1999, **21:**312-317.
178. Broomfield A, Gunny R, Prabhakar P, Grunewald S: **Spontaneous rapid resolution of acute Basal Ganglia changes in an untreated infant with propionic acidemia: a clue to pathogenesis?** *Neuropediatrics* 2010, **41:**256-260.
179. Scholl-Burgi S, Haberlandt E, Gotwald T, Albrecht U, Baumgartner Sigl S, Rauchenzauner M, Rostasy K, Karall D: **Stroke-like episodes in propionic acidemia caused by central focal metabolic decompensation.** *Neuropediatrics* 2009, **40:**76-81.
180. Lucke T, Perez-Cerda C, Baumgartner M, Fowler B, Sander S, Sasse M, Scholl S, Ugarte M, Das AM: **Propionic acidemia: unusual course with late onset and fatal outcome.** *Metabolism* 2004, **53:**809-810.
181. Nyhan WL, Bay C, Beyer EW, Mazi M: **Neurologic nonmetabolic presentation of propionic acidemia.** *Arch Neurol* 1999, **56:**1143-1147.
182. Aldamiz-Echevarria Azuar L, Prats Vinas JM, Sanjurjo Crespo P, Prieto Perera JA, Labayru Echeverria MT: **Infantile spasms as the first manifestation of propionic acidemia.** *An Pediatr (Barc)* 2005, **63:**548-550.
183. Kiernan JA: *Barr's The Human Nervous System: An anatomical viewpoint.* 7th edn. Philadelphia: Lippincott-Raven; 1998.
184. Gerfen CR, Surmeier DJ: **Modulation of striatal projection systems by dopamine.** *Annu Rev Neurosci* 2011, **34:**441-466.
185. Hamilton RL, Haas RH, Nyhan WL, Powell HC, Grafe MR: **Neuropathology of propionic acidemia: a report of two patients with basal ganglia lesions.** *J Child Neurol* 1995, **10:**25-30.
186. Steinman L, Clancy RR, Cann H, Urich H: **The neuropathology of propionic acidemia.** *Dev Med Child Neurol* 1983, **25:**87-94.
187. Feliz B, Witt DR, Harris BT: **Propionic acidemia: a neuropathology case report and review of prior cases.** *Arch Pathol Lab Med* 2003, **127:**e325-328.
188. Filipowicz HR, Ernst SL, Ashurst CL, Pasquali M, Longo N: **Metabolic changes associated with hyperammonemia in patients with propionic acidemia.** *Molecular Genetics and Metabolism* 2006, **88:**123-130.
189. Lichter-Konecki U: **Profiling of astrocyte properties in the hyperammonaemic brain: Shedding new light on the pathophysiology of the brain damage in hyperammonaemia.** *Journal of Inherited Metabolic Disease* 2008, **31:**492-502.
190. Coude FX, Sweetman L, Nyhan WL: **Inhibition by propionyl-coenzyme A of N-acetylglutamate synthetase in rat liver mitochondria. A possible explanation for hyperammonemia in propionic and methylmalonic acidemia.** *J Clin Invest* 1979, **64:**1544-1551.
191. Rigo FK, Pasquetti L, Malfatti CR, Fighera MR, Coelho RC, Petri CZ, Mello CF, Rigo FK, Pasquetti L, Malfatti CRM, et al: **Propionic acid induces convulsions and protein carbonylation in rats.** *Neuroscience Letters* 2006, **408:**151-154.
192. Nguyen NH, Morland C, Gonzalez SV, Rise F, Storm-Mathisen J, Gundersen V, Hassel B: **Propionate increases neuronal histone acetylation, but is metabolized**

oxidatively by glia. Relevance for propionic acidemia. *J Neurochem* 2007, **101:**806-814.
193. Kolker S, Sauer SW, Surtees RA, Leonard JV: **The aetiology of neurological complications of organic acidaemias--a role for the blood-brain barrier.** *J Inherit Metab Dis* 2006, **29:**701-704; discussion 705-706.
194. Schwab MA, Sauer SW, Okun JG, Nijtmans LG, Rodenburg RJ, van den Heuvel LP, Drose S, Brandt U, Hoffmann GF, Ter Laak H, et al: **Secondary mitochondrial dysfunction in propionic aciduria: a pathogenic role for endogenous mitochondrial toxins.** *Biochem J* 2006, **398:**107-112.
195. Brunengraber H, Roe CR: **Anaplerotic molecules: current and future.** *J Inherit Metab Dis* 2006, **29:**327-331.
196. Mayes PA, Bender DA: **The Citric Acid Cycle:The Catabolism of Acetyl-CoA.** In *Harper's Illustrated Biochemistry.* 26th edition. Edited by Murray RK, Granner DK, Mayes PA, Rodwell VW. New York: Lange Medical Books/McGraw-Hill; 2003
197. Roe CR, Mochel F, Roe CR, Mochel F: **Anaplerotic diet therapy in inherited metabolic disease: therapeutic potential.** *Journal of Inherited Metabolic Disease* 2006, **29:**332-340.
198. Scholl-Burgi S, Sass JO, Zschocke J, Karall D: **Amino acid metabolism in patients with propionic acidaemia.** *J Inherit Metab Dis* 2012, **35:**65-70.
199. Scholl-Burgi S, Korman SH, Applegarth DA, Karall D, Lillquist Y, Heinz-Erian P, Davidson AG, Haberlandt E, Sass JO: **The relation of cerebrospinal fluid and plasma glycine levels in propionic acidaemia, a 'ketotic hyperglycinaemia'.** *J Inherit Metab Dis* 2008, **31:**395-398.
200. Ierardi-Curto L, Kaplan P, Saitta S, Mazur A, Berry GT: **The glutamine paradox in a neonate with propionic acidaemia and severe hyperammonaemia.** *J Inherit Metab Dis* 2000, **23:**85-86.
201. Bergman AJ, Van der Knaap MS, Smeitink JA, Duran M, Dorland L, Valk J, Poll-The BT: **Magnetic resonance imaging and spectroscopy of the brain in propionic acidemia: clinical and biochemical considerations.** *Pediatr Res* 1996, **40:**404-409.
202. Chemelli AP, Schocke M, Sperl W, Trieb T, Aichner F, Felber S: **Magnetic resonance spectroscopy (MRS) in five patients with treated propionic acidemia.** *J Magn Reson Imaging* 2000, **11:**596-600.
203. Hoffmann GF, Meier-Augenstein W, Stockler S, Surtees R, Rating D, Nyhan WL: **Physiology and pathophysiology of organic acids in cerebrospinal fluid.** *J Inherit Metab Dis* 1993, **16:**648-669.
204. Iles RA, Chalmers RA, Hind AJ: **Methylmalonic aciduria and propionic acidaemia studied by proton nuclear magnetic resonance spectroscopy.** *Clinica Chimica Acta* 1986, **161:**173-189.
205. Davies SE, Iles RA, Stacey TE, de Sousa C, Chalmers RA: **Carnitine therapy and metabolism in the disorders of propionyl-CoA metabolism studied using 1H-NMR spectroscopy.** *Clinica Chimica Acta* 1991, **204:**263-277.
206. Lever M, Slow S: **The clinical significance of betaine, an osmolyte with a key role in methyl group metabolism.** *Clin Biochem* 2010, **43:**732-744.
207. Wenzel A, Fritschy JM, Mohler H, Benke D: **NMDA Receptor Heterogeneity During Postnatal Development of the Rat Brain: Differential Expression of the NR2A, NR2B, and NR2C Subunit Proteins.** *Journal of Neurochemistry* 1997, **68:**469-478.

208. van der Zijden JP, van Eijsden P, de Graaf RA, Dijkhuizen RM, van der Zijden JP, van Eijsden P, de Graaf RA, Dijkhuizen RM: **1H/13C MR spectroscopic imaging of regionally specific metabolic alterations after experimental stroke.** *Brain* 2008, **131:**2209-2219.
209. Wilson M, Reynolds G, Kauppinen RA, Arvanitis TN, Peet AC: **A constrained least-squares approach to the automated quantitation of in vivo (1)H magnetic resonance spectroscopy data.** *Magn Reson Med* 2011, **65:**1-12.
210. Wilson M, Davies NP, Sun Y, Natarajan K, Arvanitis TN, Kauppinen RA, Peet AC: **A comparison between simulated and experimental basis sets for assessing short-TE in vivo (1)H MRS data at 1.5 T.** *NMR Biomed* 2010, **23:**1117-1126.
211. Davies NP, Wilson M, Harris LM, Natarajan K, Lateef S, Macpherson L, Sgouros S, Grundy RG, Arvanitis TN, Peet AC: **Identification and characterisation of childhood cerebellar tumours by in vivo proton MRS.** *NMR Biomed* 2008, **21:**908-918.
212. Maxvold NJ, Smoyer WE, Custer JR, Bunchman TE: **Amino acid loss and nitrogen balance in critically ill children with acute renal failure: a prospective comparison between classic hemofiltration and hemofiltration with dialysis.** *Crit Care Med* 2000, **28:**1161-1165.
213. Perez-Duenas B, De La Osa A, Capdevila A, Navarro-Sastre A, Leist A, Ribes A, Garcia-Cazorla A, Serrano M, Pineda M, Campistol J: **Brain injury in glutaric aciduria type I: the value of functional techniques in magnetic resonance imaging.** *Eur J Paediatr Neurol* 2009, **13:**534-540.
214. Oguz KK, Ozturk A, Cila A: **Diffusion-weighted MR imaging and MR spectroscopy in glutaric aciduria type 1.** *Neuroradiology* 2005, **47:**229-234.
215. Sijens PE, Smit GP, Meiners LC, Oudkerk M, van Spronsen FJ: **Cerebral 1H MR spectroscopy revealing white matter NAA decreases in glutaric aciduria type I.** *Mol Genet Metab* 2006, **88:**285-289.
216. Longo D, Fariello G, Dionisi-Vici C, Cannata V, Boenzi S, Genovese E, Deodato F: **MRI and 1H-MRS findings in early-onset cobalamin C/D defect.** *Neuropediatrics* 2005, **36:**366-372.
217. Takeuchi M, Harada M, Matsuzaki K, Hisaoka S, Nishitani H, Mori K: **Magnetic resonance imaging and spectroscopy in a patient with treated methylmalonic acidemia.** *J Comput Assist Tomogr* 2003, **27:**547-551.
218. Moller HE, Koch HG, Weglage J, Freudenberg F, Ullrich K: **Investigation of the cerebral energy status in patients with glutaric aciduria type I by 31P magnetic resonance spectroscopy.** *Neuropediatrics* 2003, **34:**57-60.
219. Miyazaki T, Ohura T, Kobayashi M, Shigematsu Y, Yamaguchi S, Suzuki Y, Hata I, Aoki Y, Yang X, Minjares C, et al: **Fatal propionic acidemia in mice lacking propionyl-CoA carboxylase and its rescue by postnatal, liver-specific supplementation via a transgene.** *J Biol Chem* 2001, **276:**35995-35999.
220. Hofherr SE, Senac JS, Chen CY, Palmer DJ, Ng P, Barry MA, Hofherr SE, Senac JS, Chen CY, Palmer DJ, et al: **Short-term rescue of neonatal lethality in a mouse model of propionic acidemia by gene therapy.** *Human Gene Therapy* 2009, **20:**169-180.
221. Chandler RJ, Chandrasekaran S, Carrillo-Carrasco N, Senac JS, Hofherr SE, Barry MA, Venditti CP: **Adeno-associated virus serotype 8 gene transfer rescues a neonatal lethal murine model of propionic acidemia.** *Hum Gene Ther* 2011, **22:**477-481.

222. Leonard JV: **Disorders of the urea cycle and related enzymes.** In *Inborn Metabolic Diseases: Diagnosis and Treatment* 4th edition. Edited by Fernandes J, Saudubray JM, van den Berghe G, Walter JH: Springer; 2006
223. Erez A, Nagamani SC, Shchelochkov OA, Premkumar MH, Campeau PM, Chen Y, Garg HK, Li L, Mian A, Bertin TK, et al: **Requirement of argininosuccinate lyase for systemic nitric oxide production.** *Nat Med* 2011, **17:**1619-1626.
224. Gropman AL, Summar M, Leonard JV: **Neurological implications of urea cycle disorders.** *J Inherit Metab Dis* 2007, **30:**865-879.
225. Tuchman M, Lee B, Lichter-Konecki U, Summar ML, Yudkoff M, Cederbaum SD, Kerr DS, Diaz GA, Seashore MR, Lee HS, et al: **Cross-sectional multicenter study of patients with urea cycle disorders in the United States.** *Mol Genet Metab* 2008, **94:**397-402.
226. Kido J, Nakamura K, Mitsubuchi H, Ohura T, Takayanagi M, Matsuo M, Yoshino M, Shigematsu Y, Yorifuji T, Kasahara M, et al: **Long-term outcome and intervention of urea cycle disorders in Japan.** *J Inherit Metab Dis* 2011.
227. Dent CE: **Argininosuccinic aciduria. A new form of mental deficiency due to metabolic causes.** *Proceedings of the Royal Society of Medicine* 1959, **52:**885.
228. Erez A, Nagamani SC, Lee B: **Argininosuccinate lyase deficiency-argininosuccinic aciduria and beyond.** *Am J Med Genet C Semin Med Genet* 2011, **157:**45-53.
229. Grioni D, Furlan F, Corbetta C, Barboni C, Lastrico A, Marzocchi GM, Contri M, Gamba A, Vizziello P, Parini R: **Epilepsy and argininosuccinic aciduria.** *Neuropediatrics* 2011, **42:**97-103.
230. Mori T, Nagai K, Mori M, Nagao M, Imamura M, Iijima M, Kobayashi K, Mori T, Nagai K, Mori M, et al: **Progressive liver fibrosis in late-onset argininosuccinate lyase deficiency.** *Pediatric & Developmental Pathology* 2002, **5:**597-601.
231. Scaglia F, Brunetti-Pierri N, Kleppe S, Marini J, Carter S, Garlick P, Jahoor F, O'Brien W, Lee B: **Clinical consequences of urea cycle enzyme deficiencies and potential links to arginine and nitric oxide metabolism.** *J Nutr* 2004, **134:**2775S-2782S; discussion 2796S-2797S.
232. Brunetti-Pierri N, Erez A, Shchelochkov O, Craigen W, Lee B, Brunetti-Pierri N, Erez A, Shchelochkov O, Craigen W, Lee B: **Systemic hypertension in two patients with ASL deficiency: a result of nitric oxide deficiency?** *Molecular Genetics & Metabolism* 2009, **98:**195-197.
233. Engel K, Vuissoz JM, Eggimann S, Groux M, Berning C, Hu L, Klaus V, Moeslinger D, Mercimek-Mahmutoglu S, Stockler S, et al: **Bacterial expression of mutant argininosuccinate lyase reveals imperfect correlation of in-vitro enzyme activity with clinical phenotype in argininosuccinic aciduria.** *J Inherit Metab Dis* 2012, **35:**133-140.
234. Mercimek-Mahmutoglu S, Moeslinger D, Haberle J, Engel K, Herle M, Strobl MW, Scheibenreiter S, Muehl A, Stockler-Ipsiroglu S: **Long-term outcome of patients with argininosuccinate lyase deficiency diagnosed by newborn screening in Austria.** *Molecular Genetics & Metabolism* 2010, **100:**24-28.
235. Ficicioglu C, Mandell R, Shih VE: **Argininosuccinate lyase deficiency: longterm outcome of 13 patients detected by newborn screening.** *Molecular Genetics & Metabolism* 2009, **98:**273-277.
236. Bindu PS, Sinha S, Taly AB, Chandrasekhar HS, Christopher R, Arunodaya GR, Shetty T: **Extensive cortical magnetic resonance signal change in proximal urea cycle disorder.** *J Child Neurol* 2007, **22:**238-239.

237. Barkovich AJ: *Pediatric neuroimaging.* 4th edn. Philiadelphia: Lippincott Williams & Wilkins; 2005.
238. Aoyagi K, Akiyama K, Shahrzad S, Tomida C, Hirayama A, Nagase S, Takemura K, Koyama A, Ohba S, Narita M: **Formation of guanidinosuccinic acid, a stable nitric oxide mimic, from argininosuccinic acid and nitric oxide-derived free radicals.** *Free Radic Res* 1999, **31:**59-65.
239. Grillo MA, Lanza A, Colombatto S: **Transport of amino acids through the placenta and their role.** *Amino Acids* 2008, **34:**517-523.
240. Brosnan JT, Brosnan ME: **Creatine metabolism and the urea cycle.** *Molecular Genetics and Metabolism* 2010, **100:**S49-S52.
241. Brosnan JT, da Silva RP, Brosnan ME: **The metabolic burden of creatine synthesis.** *Amino Acids* 2011, **40:**1325-1331.
242. Braissant O, Beard E, Torrent C, Henry H: **Dissociation of AGAT, GAMT and SLC6A8 in CNS: relevance to creatine deficiency syndromes.** *Neurobiol Dis* 2010, **37:**423-433.
243. Arias A, Garcia-Villoria J, Ribes A: **Guanidinoacetate and creatine/creatinine levels in controls and patients with urea cycle defects.** *Mol Genet Metab* 2004, **82:**220-223.
244. Roze E, Azuar C, Menuel C, Haberle J, Guillevin R: **Usefulness of magnetic resonance spectroscopy in urea cycle disorders.** *Pediatr Neurol* 2007, **37:**222-225.
245. Braissant O, Cagnon L, Monnet-Tschudi F, Speer O, Wallimann T, Honegger P, Henry H: **Ammonium alters creatine transport and synthesis in a 3D culture of developing brain cells, resulting in secondary cerebral creatine deficiency.** *Eur J Neurosci* 2008, **27:**1673-1685.
246. Sijens PE, Verbruggen KT, Meiners LC, Soorani-Lunsing RJ, Rake JP, Oudkerk M: **1H chemical shift imaging of the brain in guanidino methyltransferase deficiency, a creatine deficiency syndrome; guanidinoacetate accumulation in the gray matter.** *Eur Radiol* 2005, **15:**1923-1926.
247. Sijens PE, Reijngoud DJ, Soorani-Lunsing RJ, Oudkerk M, van Spronsen FJ: **Cerebral 1H MR spectroscopy showing elevation of brain guanidinoacetate in argininosuccinate lyase deficiency.** *Mol Genet Metab* 2006, **88:**100-102.
248. van Spronsen FJ, Reijngoud DJ, Verhoeven NM, Soorani-Lunsing RJ, Jakobs C, Sijens PE: **High cerebral guanidinoacetate and variable creatine concentrations in argininosuccinate synthetase and lyase deficiency: implications for treatment?** *Molecular Genetics & Metabolism* 2006, **89:**274-276.
249. Swamy M, Sirajudeen KN, Chandran G, Swamy M, Sirajudeen KNS, Chandran G: **Nitric oxide (NO), citrulline-NO cycle enzymes, glutamine synthetase, and oxidative status in kainic acid-mediated excitotoxicity in rat brain.** *Drug & Chemical Toxicology* 2009, **32:**326-331.
250. Bizzoco E, Vannucchi MG, Faussone-Pellegrini MS, Bizzoco E, Vannucchi M-G, Faussone-Pellegrini M-S: **Transient ischemia increases neuronal nitric oxide synthase, argininosuccinate synthetase and argininosuccinate lyase co-expression in rat striatal neurons.** *Experimental Neurology* 2007, **204:**252-259.
251. Bizzoco E, Faussone-Pellegrini MS, Vannucchi MG, Bizzoco E, Faussone-Pellegrini MS, Vannucchi MG: **Activated microglia cells express argininosuccinate synthetase and argininosuccinate lyase in the rat brain after transient ischemia.** *Experimental Neurology* 2007, **208:**100-109.

252. Wiesinger H: **Arginine metabolism and the synthesis of nitric oxide in the nervous system.** *Progress in Neurobiology* 2001, **64:**365-391.
253. Pignitter M, Gorren AC, Nedeianu S, Schmidt K, Mayer B: **Inefficient spin trapping of superoxide in the presence of nitric-oxide: implications for studies on nitric-oxide synthase uncoupling.** *Free Radical Biology & Medicine* 2006, **41:**455-463.
254. Newnham T, Hardikar W, Allen K, Wellard RM, Hamilton C, Angus P, Jones R, Boneh A: **Liver transplantation for argininosuccinic aciduria: clinical, biochemical, and metabolic outcome.** *Liver Transpl* 2008, **14:**41-45.
255. Scaglia F, Carter S, O'Brien WE, Lee B: **Effect of alternative pathway therapy on branched chain amino acid metabolism in urea cycle disorder patients.** *Molecular Genetics and Metabolism* 2004, **81:**79-85.
256. Barkovich AJ, Kuzniecky RI: **Gray matter heterotopia.** *Neurology* 2000, **55:**1603-1608.
257. Haase A, Bicker G: **Nitric oxide and cyclic nucleotides are regulators of neuronal migration in an insect embryo.** *Development* 2003, **130:**3977-3987.
258. Tegenge MA, Rockel TD, Fritsche E, Bicker G: **Nitric oxide stimulates human neural progenitor cell migration via cGMP-mediated signal transduction.** *Cellular & Molecular Life Sciences* 2011, **68:**2089-2099.
259. Braissant O, Henry H: **AGAT, GAMT and SLC6A8 distribution in the central nervous system, in relation to creatine deficiency syndromes: A review.** *J Inherit Metab Dis* 2008.
260. Peet AC, Arvanitis TN, Auer DP, Davies NP, Hargrave D, Howe FA, Jaspan T, Leach MO, Macarthur D, MacPherson L, et al: **The value of magnetic resonance spectroscopy in tumour imaging.** *Arch Dis Child* 2008, **93:**725-727.
261. Triulzi F: **Paediatric neuroimaging.** *Neurological Sciences* 2008, **29:**342-345.
262. Sheerin F, Pretorius PM, Briley D, Meagher T: **Differential diagnosis of restricted diffusion confined to the cerebral cortex.** *Clinical Radiology* 2008, **63:**1245-1253.
263. Robertson RL, Glasier CM, Robertson RL, Glasier CM: **Diffusion-weighted imaging of the brain in infants and children.** *Pediatric Radiology* 2007, **37:**749-768.
264. Sener RN: **Diffusion magnetic resonance imaging patterns in metabolic and toxic brain disorders.** *Acta Radiol* 2004, **45:**561-570.
265. Gao Y, Guan WY, Wang J, Zhang YZ, Li YH, Han LS, Gao Y, Guan W-y, Wang J, Zhang Y-z, et al: **Fractional anisotropy for assessment of white matter tracts injury in methylmalonic acidemia.** *Chinese Medical Journal* 2009, **122:**945-949.
266. Yesildag A, Ayata A, Baykal B, Koroglu M, Yildiz H, Oral B, Oktem F, Oyar O: **Magnetic resonance imaging and diffusion-weighted imaging in methylmalonic acidemia.** *Acta Radiologica* 2005, **46:**101-103.
267. Michel SJ, Given CA, 2nd, Robertson WC, Jr., Michel SJ, Given CA, 2nd, Robertson WC, Jr.: **Imaging of the brain, including diffusion-weighted imaging in methylmalonic acidemia.** *Pediatric Radiology* 2004, **34:**580-582.
268. Burlina AP, Manara R, Calderone M, Catuogno S, Burlina AB: **Diffusion-weighted imaging in the assessment of neurological damage in patients with methylmalonic aciduria.** *Journal of Inherited Metabolic Disease* 2003, **26:**417-422.
269. Trinh BC, Melhem ER, Barker PB: **Multi-slice proton MR spectroscopy and diffusion-weighted imaging in methylmalonic acidemia: report of two cases and review of the literature.** *Ajnr: American Journal of Neuroradiology* 2001, **22:**831-833.

270. Duning T, Deppe M, Keller S, Mohammadi S, Schiffbauer H, Marziniak M, Duning T, Deppe M, Keller S, Mohammadi S, et al: **Diffusion tensor imaging in a case of Kearns-Sayre syndrome: striking brainstem involvement as a possible cause of oculomotor symptoms.** *Journal of the Neurological Sciences* 2009, **281:**110-112.
271. Ducreux D, Nasser G, Lacroix C, Adams D, Lasjaunias P, Ducreux D, Nasser G, Lacroix C, Adams D, Lasjaunias P: **MR diffusion tensor imaging, fiber tracking, and single-voxel spectroscopy findings in an unusual MELAS case.** *Ajnr: American Journal of Neuroradiology* 2005, **26:**1840-1844.
272. Brockmann K, Finsterbusch J, Schara U, Wilichowski E, Frahm J, Hanefeld F: **Stroke-like pattern in DTI and MRS of childhood mitochondrial leukoencephalopathy.** *Neuroradiology* 2004, **46:**267-271.
273. Majoie CB, Akkerman EM, Blank C, Barth PG, Poll-The BT, den Heeten GJ, Majoie CB, Akkerman EM, Blank C, Barth PG, Poll-The BT: **Mitochondrial encephalomyopathy: comparison of conventional MR imaging with diffusion-weighted and diffusion tensor imaging: case report.** *Ajnr: American Journal of Neuroradiology* 2002, **23:**813-816.
274. Tzoulis C, Bindoff LA, Tzoulis C, Bindoff LA: **Serial diffusion imaging in a case of mitochondrial encephalomyopathy, lactic acidosis, and stroke-like episodes.** *Stroke* 2009, **40:**e15-17.
275. Timothy J, Geller T, Timothy J, Geller T: **SURF-1 gene mutation associated with leukoencephalopathy in a 2-year-old.** *Journal of Child Neurology* 2009, **24:**1296-1301.
276. Kumakura A, Asada J, Okumura R, Fujisawa I, Hata D, Kumakura A, Asada J, Okumura R, Fujisawa I, Hata D: **Diffusion-weighted imaging in preclinical Leigh syndrome.** *Pediatric Neurology* 2009, **41:**309-311.
277. Fortuna F, Barboni P, Liguori R, Valentino ML, Savini G, Gellera C, Mariotti C, Rizzo G, Tonon C, Manners D, et al: **Visual system involvement in patients with Friedreich's ataxia.** *Brain* 2009, **132:**116-123.
278. Finsterer J: **[MELAS syndrome as a differential diagnosis of ischemic stroke].** *Fortschritte der Neurologie-Psychiatrie* 2009, **77:**25-31.
279. Stoquart-Elsankari S, Lehmann P, Perin B, Gondry-Jouet C, Godefroy O: **MRI and diffusion-weighted imaging followup of a stroke-like event in a patient with MELAS.** *Journal of Neurology* 2008, **255:**1593-1595.
280. Soares-Fernandes JP, Teixeira-Gomes R, Cruz R, Ribeiro M, Magalhaes Z, Rocha JF, Leijser LM, Soares-Fernandes JP, Teixeira-Gomes R, Cruz R, et al: **Neonatal pyruvate dehydrogenase deficiency due to a R302H mutation in the PDHA1 gene: MRI findings.** *Pediatric Radiology* 2008, **38:**559-562.
281. Oishi M, Miki K, Morita A, Fujioka K, Aoki S, Nishino I, Nonaka I, Goto Y, Mizutani T, Oishi M, et al: **Mitochondrial encephalomyopathy associated with diabetes mellitus, cataract, and corpus callosum atrophy.** *Internal Medicine* 2008, **47:**441-444.
282. Niehues SM, Radtke A, Bohner G, Lemke AJ: **[Rare MRI diagnosis of MELAS syndrome].** *Rofo: Fortschritte auf dem Gebiete der Rontgenstrahlen und der Nuklearmedizin* 2008, **180:**346-348.
283. Lee H, Yi HA, Lee SR, Lee SY, Park BR, Lee H, Yi H-A, Lee S-R, Lee S-Y, Park B-R: **Ocular torsion associated with infarction in the territory of the anterior inferior cerebellar artery: frequency, pattern, and a major determinant.** *Journal of the Neurological Sciences* 2008, **269:**18-23.

284. Ito H, Mori K, Harada M, Minato M, Naito E, Takeuchi M, Kuroda Y, Kagami S, Ito H, Mori K, et al: **Serial brain imaging analysis of stroke-like episodes in MELAS.** *Brain & Development* 2008, **30:**483-488.
285. Aygok GA, Marmarou A, Fatouros P, Kettenmann B, Bullock RM, Aygok GA, Marmarou A, Fatouros P, Kettenmann B, Bullock RM: **Assessment of mitochondrial impairment and cerebral blood flow in severe brain injured patients.** *Acta Neurochirurgica - Supplement* 2008, **102:**57-61.
286. Pliss L, Mazurchuk R, Spernyak JA, Patel MS, Pliss L, Mazurchuk R, Spernyak JA, Patel MS: **Brain MR imaging and proton MR spectroscopy in female mice with pyruvate dehydrogenase complex deficiency.** *Neurochemical Research* 2007, **32:**645-654.
287. Chan DW, Lim CC, Tay SK, Choong CT, Phuah HK, Chan DWS, Lim CCT, Tay SKH, Choong C-T, Phuah HK: **Elevated thyroid peroxidase antibodies with encephalopathy in MELAS syndrome.** *Pediatric Neurology* 2007, **36:**414-417.
288. Alemdar M, Iseri P, Selekler M, Budak F, Demirci A, Komsuoglu SS, Alemdar M, Iseri P, Selekler M, Budak F, et al: **MELAS presented with status epilepticus and Anton-Babinski syndrome; value of ADC mapping in MELAS.** *Journal of Neuropsychiatry & Clinical Neurosciences* 2007, **19:**482-483.
289. Sakai Y, Kira R, Torisu H, Ihara K, Yoshiura T, Hara T: **Persistent diffusion abnormalities in the brain stem of three children with mitochondrial diseases.** *Ajnr: American Journal of Neuroradiology* 2006, **27:**1924-1926.
290. Heidenreich JO, Klopstock T, Schirmer T, Saemann P, Mueller-Felber W, Auer DP, Heidenreich JO, Klopstock T, Schirmer T, Saemann P, et al: **Chronic progressive external ophthalmoplegia: MR spectroscopy and MR diffusion studies in the brain.** *AJR American Journal of Roentgenology* 2006, **187:**820-824.
291. Sacher M, Fatterpekar GM, Edelstein S, Sansaricq C, Naidich TP, Sacher M, Fatterpekar GM, Edelstein S, Sansaricq C, Naidich TP: **MRI findings in an atypical case of Kearns-Sayre syndrome: a case report.** *Neuroradiology* 2005, **47:**241-244.
292. Atalar MH, Egilmez H, Bulut S, Icagasioglu D, Atalar MH, Egilmez H, Bulut S, Icagasioglu D: **Magnetic resonance spectroscopy and diffusion-weighted imaging findings in a child with Leigh's disease.** *Pediatrics International* 2005, **47:**601-603.
293. Sener RN: **Diffusion MRI in the postmortem brain: case report.** *Journal of Neuroradiology Journal de Neuroradiologie* 2004, **31:**406-408.
294. Abe K, Yoshimura H, Tanaka H, Fujita N, Hikita T, Sakoda S: **Comparison of conventional and diffusion-weighted MRI and proton MR spectroscopy in patients with mitochondrial encephalomyopathy, lactic acidosis, and stroke-like events.** *Neuroradiology* 2004, **46:**113-117.
295. Wang XY, Noguchi K, Takashima S, Hayashi N, Ogawa S, Seto H: **Serial diffusion-weighted imaging in a patient with MELAS and presumed cytotoxic oedema.** *Neuroradiology* 2003, **45:**640-643.
296. Kolb SJ, Costello F, Lee AG, White M, Wong S, Schwartz ED, Messe SR, Ellenbogen J, Kasner SE, Galetta SL, et al: **Distinguishing ischemic stroke from the stroke-like lesions of MELAS using apparent diffusion coefficient mapping.** *Journal of the Neurological Sciences* 2003, **216:**11-15.
297. Keng WT, Pilz DT, Minns B, FitzPatrick DR: **A3243G mitochondrial mutation associated with polymicrogyria.** *Developmental Medicine & Child Neurology* 2003, **45:**704-708.

298. Flemming K, Ulmer S, Duisberg B, Hahn A, Jansen O, Flemming K, Ulmer S, Duisberg B, Hahn A, Jansen O: **MR spectroscopic findings in a case of Alpers-Huttenlocher syndrome.** *Ajnr: American Journal of Neuroradiology* 2002, **23:**1421-1423.
299. Inglese M, Rovaris M, Bianchi S, La Mantia L, Mancardi GL, Ghezzi A, Montagna P, Salvi F, Filippi M: **Magnetic resonance imaging, magnetisation transfer imaging, and diffusion weighted imaging correlates of optic nerve, brain, and cervical cord damage in Leber's hereditary optic neuropathy.** *Journal of Neurology, Neurosurgery & Psychiatry* 2001, **70:**444-449.
300. Ohshita T, Oka M, Imon Y, Watanabe C, Katayama S, Yamaguchi S, Kajima T, Mimori Y, Nakamura S: **Serial diffusion-weighted imaging in MELAS.** *Neuroradiology* 2000, **42:**651-656.
301. Tzoulis C, Neckelmann G, Mork SJ, Engelsen BE, Viscomi C, Moen G, Ersland L, Zeviani M, Bindoff LA, Tzoulis C, et al: **Localized cerebral energy failure in DNA polymerase gamma-associated encephalopathy syndromes.** *Brain* 2010, **133:**1428-1437.
302. Davison JE, Davies NP, English MW, Philip S, Macpherson LK, Gissen P, Peet AC: **Magnetic resonance spectroscopy in the diagnostic evaluation of brainstem lesions in alexander disease.** *J Child Neurol* 2011, **26:**356-360.
303. Vergara IA, Norambuena T, Ferrada E, Slater AW, Melo F: **StAR: a simple tool for the statistical comparison of ROC curves.** *BMC Bioinformatics* 2008, **9:**265.